FEDERAL UNIVERSITY OF MINAS GERAIS
GRADUATE PROGRAM IN MECHANICAL ENGINEERING

Samuel Marques Barcelos

Feasibility analysis of 1d numerical simulation during the pre-design phase applied to Brazilian regulation to comprehend different scenarios for mild hybrid technology (BSG-12 V)

BELO HORIZONTE
2022

Samuel Marques Barcelos

Feasibility analysis of 1d numerical simulation during the pre-design phase applied to Brazilian regulation to comprehend different scenarios for mild hybrid technology (BSG-12 V)

Dissertação apresentada ao Programa de Pós-Graduação em Engenharia Mecânica, Universidade Federal de Minas Gerais, como requisito parcial à obtenção do título de Mestre em Engenharia Mecânica

Área de concentração: Energia e Sustentabilidade

Orientador: Prof. Dr. José Guilherme Coelho Baeta

BELO HORIZONTE

2022

Barcelos, Samuel Marques.
B242f Feasibility analysis of 1D numerical simulation during the pre-design phase applied to brazilian regulation to comprehend different scenarios for mild hybrid technology (BSG-12 V) [recurso eletrônico] / Samuel Marques Barcelos. - 2022.
1 recurso online (249 f. : il., color.) : pdf.

Orientador: José Guilherme Coelho Baêta.

Dissertação (mestrado) - Universidade Federal de Minas Gerais, Escola de Engenharia.

Apêndices e anexos: f. 182-249.

Bibliografia: f. 175-181.
Exigências do sistema: Adobe Acrobat Reader.

1. Engenharia mecânica - Teses. 2. Simulação (Computadores) - Teses. 3. Automóveis - Consumo de combustíveis - Teses. 4. Motores elétricos - Teses. 5. Veículos elétricos híbridos - Teses. 6.Eficiência energética - Teses. I. Baêta, José Guilherme Coelho. II. Universidade Federal de Minas Gerais. Escola de Engenharia.
III. Título.

CDU: 621 (043)

Ficha catalográfica elaborada pela Bibliotecária Roseli Alves de Oliveira CRB/6 2121
Biblioteca Prof. Mário Werneck, Escola de Engenharia da UFMG.

UNIVERSIDADE FEDERAL DE MINAS GERAIS

ESCOLA DE ENGENHARIA

PROGRAMA DE PÓS-GRADUAÇÃO EM ENGENHARIA MECÂNICA

FOLHA DE APROVAÇÃO

Feasibility analysis of 1d numerical simulation during the pre-design phase applied to Brazilian regulation to comprehend different scenarios for mild hybrid technology (BSG-12 V).

Samuel Marques Barcelos

Dissertação submetida à Banca Examinadora designada pelo Colegiado do Programa de Pós-Graduação em Engenharia Mecânica da Universidade Federal de Minas Gerais, constuída pelos Professores: Dr. José Guilherme Coelho Baêta (Orientador - Departamento de Engenharia Mecânica/UFMG), Dr. Rogério Jorge Amorim (Programa de Pós-graduação em Engenharia Mecânica/PUC-Minas) e Dr. Fabrício José Pacheco Pujatti (Departamento de Engenharia Mecânica/UFMG), como parte dos requisitos necessários à obtenção do título de **"Mestre em Engenharia Mecânica"**, na área de concentração de **"Energia e Sustentabilidade".**

Dissertação aprovada no dia 17 de fevereiro de 2022.

Documento assinado eletronicamente por **Jose Guilherme Coelho Baeta**, **Professor do Magistério Superior**, em 24/02/2022, às 11:12, conforme horário oficial de Brasília, com fundamento no art. 5º do Decreto nº 10.543, de 13 de novembro de 2020.

Documento assinado eletronicamente por **Fabricio Jose Pacheco Pujatti**, **Professor do Magistério Superior**, em 24/02/2022, às 11:23, conforme horário oficial de Brasília, com fundamento no art. 5º do Decreto nº 10.543, de 13 de novembro de 2020.

Documento assinado eletronicamente por **Rogério Jorge Amorim**, **Usuário Externo**, em 25/02/2022, às 09:18, conforme horário oficial de Brasília, com fundamento no art. 5º do Decreto nº 10.543, de 13 de novembro de 2020.

A autenticidade deste documento pode ser conferida no site https://sei.ufmg.br/sei/controlador_externo.php?acao=documento_conferir&id_orgao_acesso_externo=0, informando o código verificador **1271274** e o código CRC **1DB17C0F**.

Á minha família em especial minha avó Dona Maria.

ACKNOWLEDGMENT

Em primeiro lugar agradeço a Deus por ter me dado força, paciência e saúde para conseguir vencer os desafios que surgiram durante esses anos em que me dediquei a esse trabalho.

A toda minha família que sempre me apoiou em todas as minhas dificuldades, me dando todo suporte necessário para que eu pudesse concluir mais essa etapa, em especial minha avó Maria do Carmo Perreira Barcelos e minha mãe Cleia Maria de Barcelos.

Ao professor José Guilherme Coelho Baeta, pela orientação, por todas as oportunidades que me proporcionou e pela paciência, atenção e ensinamentos.

A todos os professores em especial Sérgio Augusto Araújo da Gama Cerqueira, Claudio de Castro Pellegrini, Anderson Baptista Leite, e Lenir de Abreu Júnior que me orientaram e inspiraram ao logo da vida.

A Stellantis ltda, por todos os tipos de incentivo, com ajuda técnica, intelectual e financeira, em especial os engenheiros: Alex Amorim (Stellantis), Charles Pimenta (Stellantis), Daniel Goretti (Stellantis), Igor trevas (Stellantis), Eduardo Xavier (Stellantis) por acreditar no meu potencial e me ajudar na criação e desenvolvimento dessa atividade. Ao CTM-UFMG, por disponibilizar o espaço físico, os equipamentos e ajuda necessários a conclusão dessa atividade.

Um agradecimento especial a todos colegas da Stellantis e amigos, por toda a ajuda que me foi fornecida, em especial aos amigos, Maiza Vasconcelos, Romário Ribeiro, Marco Vinicios, Gustavo Percília, e Tullia Leão. Aos engenheiros, Gabriel Kopte, Nicole Foureaux, Rafael Faria, Pedro Bachir, Felipe Lintz, André Reis, Felipe Augusto, Marcelo Braga, Vitor Crepaldi, Leopoldo Brasil, Lucas Pumputis, Venicio Teixeira, Marcos Estevão e Matheus Ferraz que foram essenciais no desenvolvimento desse trabalho.

Enfim, a todos que estiveram comigo nessa jornada, entendendo os finais de semana de ausência, aos cancelamentos de reuniões de família e encontros com os amigos, o meu mais sincero agradecimento.

A person who never made a mistake never tried anything new

(Albert Einstein)

RESUMO

Impulsionado pelas mudanças climáticas, a busca pela redução de emissões de gases do efeito estufa veem impulsionando a busca por combustíveis alternativos e a comercialização de veículos híbridos (HEVs). O objetivo principal do presente trabalho é analisar o benefício de consumo de combustível das tecnologias BSG quando aplicadas a diferentes arquiteturas de veículos, usando um experimento de fator completo simulado em uma plataforma ADVISOR para avaliar cenários da regulamentação brasileira. Para isso, desenvolve-se um modelo do veículo convencional com os blocos disponibilizados no ADVISOR. O modelo foi validado de forma comparativa com valores gravados de um protótipo real. Após foi possível introduzir os componentes característicos da tecnologia testada (BSG 12 V) para duas categorias diferentes de veículos simuladas; SUV, e hatch. Com os devidos modelos criados e validados, uma série de simulações foram executadas para os ciclos de condução FTP-75, HWFET, e SP, a partir das simulações senários foram criados considerando possíveis benefícios propostos pela lei brasileira para a melhoria da eficiência energética. Os resultados mostraram que a metodologia proposta e robusta para a análise inicial de viabilidade de uma tecnologia de veículo hibrido, além disso, foi possível entender que os maiores benefícios da tecnologia testada são para os ciclos urbano e SP devido a sua característica de repetitivas paradas e desacelerações. Além disso, foi possível identificar que não há grandes diferenças de operação do sistema híbrido quando interagindo com E22 ou E100 como combustível. Em conclusão, o uso de simulação 1D para análise inicial de tecnologias hibridas se mostrou valorosa e eficaz, porém, para maior precisão dos resultados de simulação é de sumária importância testes específicos para o levantamento das incertezas.

Palavras-chave: Simulação, Automóveis, Consumo de combustíveis, Motor elétricos, Veículos híbridos, Eficiência energética.

ABSTRACT

Driven by climate change, the search for the reduction of greenhouse gas emissions has been motivated by the search for alternative fuels and the commercialization of hybrid vehicles (HEVs) today. The main goal of the present work is to analyze the fuel consumption benefit of BSG technologies when applied to different vehicle's architecture, using a full factor experiment that will be simulated on an Advisor platform to assess scenarios of Brazilian regulation. For this, a model of a standard automobile was created using ADVISOR blocks, and the model was validated by comparing recorded values from a prototype. Following that, the characteristic components of the tested technology (BSG 12 V) may be introduced for two different categories of simulated vehicles: SUV and hatchback. Following the creation and validation of the necessary models, a series of simulations for the FTP-75, HWFET, and SP conduction cycles were run based on the scenario simulations, taking into account the potential advantages given by Brazilian law for energy efficiency improvement. The findings revealed that the proposed methodology is reliable for performing an initial feasibility analysis of hybrid vehicle technology. Additionally, it was possible to deduce that the tested technology's best outcomes are for urban and SP cycles because of its characteristic of frequent stops and decelerations. Furthermore, it was observed that there are no significant variations in the hybrid system's operation while using E22 or E100 as a fuel. To summarize, the use of 1D simulation for the first examination of hybrid technologies has proven to be helpful and successful; nevertheless, specialized tests for the assessment of uncertainties are critical for improved accuracy of the simulation findings.

Keywords: Simulation, Vehicle, Fuel consumption, Electric motor, Hybrid vehicle, Energy efficiency.

LIST OF FIGURES

LIST OF TABLES

LIST OF ABBREVIATIONS AND ACRONYMS

AC - Alternating Current

ADVISOR - Advanced Vehicle Simulator

AER - All-Electric range

ANP - Brazilian Oil Agency

BDC - Bottom Dead Center

BEV - Battery Electric Vehicle

BOF - Beginning-of-life

BSG - Belt Starter Generator

BSFC - Brake Specific Fuel Consumption

BMEP - Brake mean effective pressure

CI - Compression ignition

CO - Carbon Monoxide

CO_2 - Carbon dioxide

CO_4 - methane

DC - Direct Current

DI - Direct Injection

E100 - Hydrous ethanol

E22 - Gasoline blended with 22% anhydrous ethanol

EE - Energetic Efficiency

EM - Electric Machines

EOL - End -of-Life

EPS - Electric Power Steering

ESS - Energy Storage System

EU - European Union

EVC - Exhaust Valve Close

EVO - Exhaust Valve Opening

EV - Electric Vehicle

FEAD - Front-end Accessory Drive

fmep - frictional mean effective pressure

FTP-75 - Federal Test Procedure

HC - Hydrocarbon

HESS - Hybrid Energy Storage System

HEV - Hybrid Electric Vehicle

HF - hybridization factor

HVAC - Heating, venting, and air conditioning

HW - Highway

HWFET - Highway Fuel Economy Test Cycle

HVIL - high-voltage interlock loop

ICE - Internal Combustion Engine

IGBTs - Insulated Gate Bipolar Transistors

IM - Induction Machine

IVC - Intake Valve Closing

IVO - Intake Valve Opening

imep - indicated mean effective pressure

IPMSM - Interior Permanent Magnet Synchronous Machine

$LiCoO_2$ - Lithium Cobalt Oxide

LiFePO4 - Lithium Iron Phosphate

LC - Low-pass

Li - Ion - Lithium-ion

LiMnO4 - Lithium Polymer

LVHEV - Low Voltage Hybrid Electric Vehicle

LLNL - Lawrence Livermore National Laboratory

MA - Memetic algorithm

MAPE - mean absolute percentage error)

Mmf - Magnetomotive force

MDIC - Ministry of Industry and Trade

MOSFETs - Metal Oxide Field-Effect Transistors

MP - Mass Particulate

MEP - Mean Effective Pressure

MBT - Maximum Brake Torque

MON - Motor Octane Number

Na-Ni-Cl - Sodium Nickel Chloride

NASA - National Aeronautics And Space Administration

NCA - Lithium Nickel Cobalt and Aluminum

NEDC - New European Driving Cycle

NiMH - Nickel Metal Hybrid

NMC - Lithium Manganese Cobalt

NMHC - non-methane hydrocarbons

NMOG - non-methane organic gas

NREL - National Renewable Energy Laboratory

NOx - nitrogen oxides

NVH - Noise, Vibration, and Harshness

PHEV - Plug-in Hybrid Electric Vehicle

PM - Permanent Magnets

PROCONVE - Programa De Controle da Poluição do Ar para Veículos Automotores

pmep - pumping mean effective pressure

Proalcool - Brazilian Alcohol Program

R&D - Research and development

RCL - Rotor copper losses

RON - Research Octane Number

RMSE - root mean squared error

RTCS - Real-Time Control Strategy

SCL - Stator copper losses

SPMSM - Surface Permanent Magnet Synchronous Machine

SRM - Switched Reluctance Machines

SI - Spark-ignition

SFC - Specific fuel consumption

SUV - Sport Utility Vehicle

TDC - Top Dead Center

THC - Tetra-hidrocarbinol

UC - Ultracapacitor Cell

UDDS - Urban Dynamometer Driving Schedule

WTW - well-to-wheel

WLTC - Worldwide harmonized Light vehicles Test Cycles

WOT - Wide-open throttle

ZEV - zero-emissions vehicles

TABLE CONTENT

1. Introduction

Climate change is caused by the greenhouse effect, induced by the presence of carbon dioxide (CO_2) and other gases, such as methane (CH_4), in the atmosphere. These elements, known as greenhouse gases, trap the Sun's long-wave radiation emitted by the Earth's surface, retaining energy in the atmosphere and causing the average global temperature to increase (EHSANI et al., 2018). According to NASA (2020), the mean surface temperature increased by 1.0 C over the last 115 years (1901-2016). As a consequence, severe weather events such as heatwaves, droughts, heavy rainfall, tornados, and hurricanes have intensified and become more frequent worldwide in the last century. Furthermore, mainly due to the melting of the polar ice caps, the average sea level has risen about 7 to 8 inches since the 1900s, causing the permanent inundation of coastal regions. (WUEBBLES et al., 2016)

Among the human activities that release greenhouse gases, transportation represents a significant part. For instance, the Lawrence Livermore National Laboratory (LLNL) estimated that 21% of the United States energy consumption in 2019 occurred within the transportation sector, where roughly 91% came from petroleum (Lawrence Livermore National Laboratory, 2018). As burning fossil fuels emit CO_2, many nations worldwide established stringent criteria for the transportation sector. The European Union has set bold CO_2 target emissions for the period from 2020 to 2021. The target is 95 g CO_2/km for passenger cars, 26% less than the 2015 target, which was 130 g CO_2/km. The targets for 2025 and 2030 are also set: 80.75 g and 59.38 g CO_2/km for passenger cars and light commercial vehicles, respectively (EUROPEAN PARLIAMENT, 2019).

Due to the global population increase and middle-class growth, the demand for transportation will grow steadily in the coming years. (EXXON MOBIL CORPORATION, 2019). In 2015, the vehicle's global fleet reached 1.3 billion with an upward trend of roughly 4% a year. The Brazilian fleet was increasing by approximately 9% annually until 2013, when it followed the global trend of 4% growth (see Figure 1).

As the vehicle fleet grows, the consumption targets become stricter worldwide, and as climate change progresses, different approaches have been applied to mitigate those issues. Electrification is one of these approaches, and it is based on developing vehicles with electric propulsion to be able to run with different energy sources. The other approach aims to

improve internal combustion engine (ICE) efficiency, fuel consumption, and emissions. Examples of technologies used in this area are variable compression ratio, variable valve timing, variable cam timing, reduction of engine size (known as downsizing), stratified combustion, hybridization of the thermal engine with electric motors, and alternative fuels. (PENHA, 2019)

Figure 1 - Historic vehicle fleet series

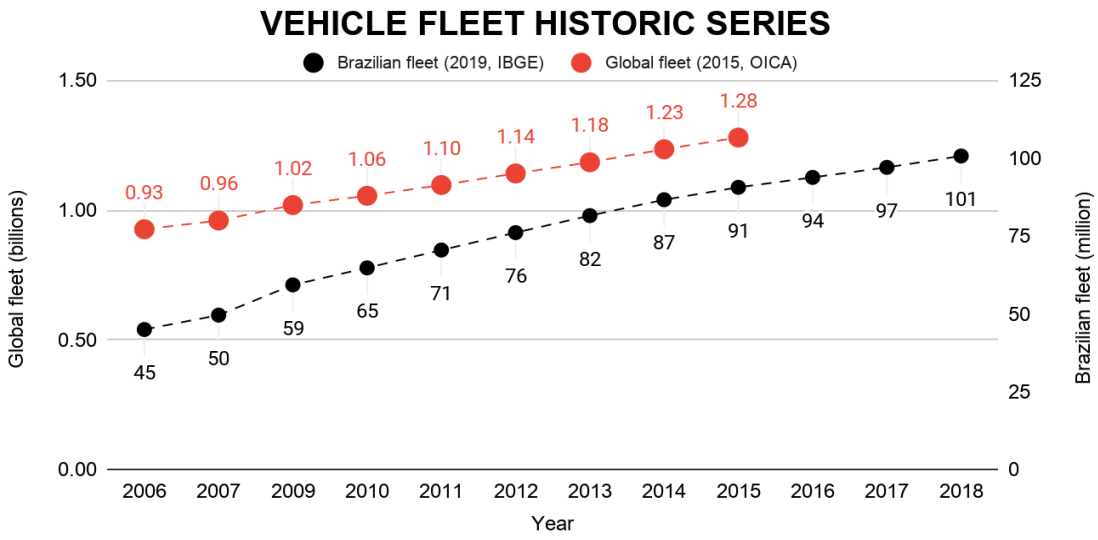

Source: (2019, IBGE)

According to DE SOUZA DIAS et al. (2015), and MALAQUIAS et al.(2019) the replacement of fossil fuels by ethanol would eliminate net CO_2 emissions, considering the whole cycle. The adequate environmental conditions to grow sugarcane cane culture and the experience with ethanol since Brazil launched the Brazilian Alcohol Program (Proalcool) in 1975 consolidated Brazil as one of the world's leading ethanol producers. In 2018 Brazil produced more than 7000 million tonnes, falling only behind the global leader, the United States, with more than 16000 million tonnes. (KOEHLER et al., 2019). Beyond the commercial advantages, ethanol's physicochemical properties make it a more suitable fuel for extreme intake-boosted pressure and efficient engines. Due to its elevated octane rating, knock resistance is increased, while the great latent heat of vaporization gives the charge a cooling effect, ending in a reduction of chamber temperature, and allowing the adoption of high volumetric compression rates and optional ignition timing.

The downsizing concept consists in operating the engine in better efficiency regions, and this can be done by reducing engine displacement and operating at higher loads, which generates less pumping losses at the throttle. However, the higher operating loads lead to elevated auto-ignition risk, mainly when the engine is working with gasoline fuel, due to the low gasoline octane number. This issue is known as Knock. One option to decrease Knock tendency is using ethanol as a unique fuel or blended with gasoline because of ethanol's higher octane number. Then, lower knock tendency allows higher compression ratios and higher intake boost pressure in turbocharged engines. Furthermore, there is a decrease in hydrocarbon emissions because of ethanol oxygen content that improves the combustion in the engine. (PENHA, 2019)

On the other hand, the idea of electric motors as a propulsion system is one trend worldwide. Interestingly, Battery Electric Vehicles (BEV) are considered as zero-emissions vehicles (ZEV), but that analysis does not consider the CO_2 emissions produced by manufacturing BEVs and produced by the electric power plants. For instance, (WU et al., 2017) point out that in some regions of China, full-fleet electrification would not bring benefits in well-to-wheel (WTW) due to coal-fired electricity dependence. The EVs feasibility is linked with the increase of renewable energy production (that meant about 10% in 2017 considering the non-fuel source) which rose to around 30% considering biofuels. In contrast, 33.4% were from coal, 19.9% were from natural gas, 14.2% from nuclear, and 2.9% from oil. (See Figure 2(a)) (IEA, 2020)

Figure 2 - Electricity Generation 2017.

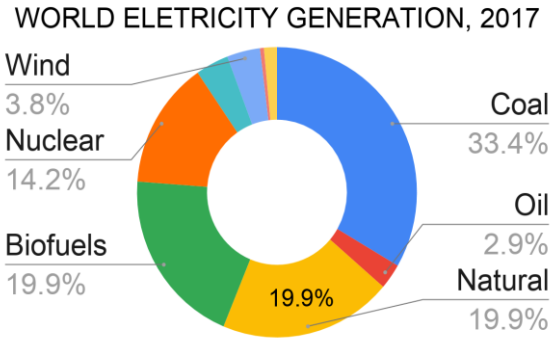

Figure 2(a) World Electricity Generation 2017.

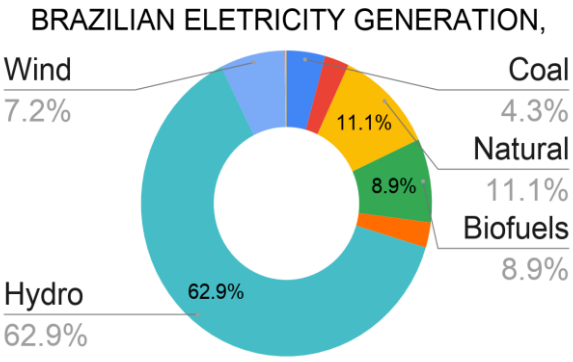

Figure 2(b) - Brazilian Electricity Generation 2017

Source: Prepared by the author based on (IEA, 2020)

In Brazil, full electrification presents additional barriers; according to EXXON MOBIL CORPORATION (2019), Brazil has the highest electricity taxes in the world. The particular circumstance is that 63% of the electric power comes from hydroelectric plants (see Figure 2.b), which generate an attention point, insufficient network due to the growth rate of some country regions, and rainfall index instability are highlighted as reasons for energy supply failures according to IDEC (2018) in a recent study. Also globally, BEVs are facing issues related to their architecture and acceptance, a small range of autonomy, a high technology price mainly due to the elements used to manufacture battery cells, insufficient charging infrastructure, and a small range of vehicle models compared with ICEs. (SLOWIK; LUTSEY, 2018)

According to MALAQUIAS et al. (2019), 2.4% of new auto sales are EVs, which means 0.2% of the global fleet. Furthermore, it is already possible to recognize an increase in sales of HEVs and EVs in some regions of the world. It is estimated that the Electrification market will achieve 28% of the current world fleet in 2052. The electric or hybrid vehicles sold in Brazil rose from 0.15% in 2018 to 0.4% in 2019. This is still a tiny part of the Brazilian market, which is widely dominated by flex-fuel vehicles with 84% of the market share considering all vehicle categories. In addition, 13% were diesel and 2.6% were gasoline. (FEBABRAVE, 2019)

As a reasonable opportunity to increase engine efficiency and decrease pollution, Hybrid Electric Vehicles are associated with ethanol fuel; HEVs include one or more electric machines linked to the ICE and/or to wheels. There are different levels of hybridization, depending on the internal combustion engine size and the electric machine capacity. The Belt Starter Generation (BSG) is a Mild Hybrid; it has functionalities such as start/stop and kinetic energy recovery. Additionally, there is some level of assistance to ICE depending on the electric machine (EM) power. The BSG technology gained increasing importance due to its characteristics of low weight, low delta cost, and fuel economy improvement. (ONORI, 2016)

The first commercial application of BSG was introduced in the EU in 2004 by the PSA group. The Citroen C3 model was produced from 2004 to 2008, and it was supplied with a BSG 12-volt that was capable of automatically stopping the engine when the car was waiting at a red light or stuck in a traffic jam. The system could reduce fuel consumption

between 6% to 10% in combined urban and highway cycles (AGENCE FRANCE-PRESSE, 2004). Because of the low fuel consumption reduction shown by the 12-volt architecture and its limitation on torque assisting, 48-volt architecture interest has grown substantially in recent years, mainly due to its fuel consumption reduction benefit. According to Delphi, a 48-volt architecture system with dual batteries can deliver 70% of the higher-voltage architecture fuel consumption benefits with 30% of the higher-voltage architecture cost. Moreover, it is being estimated that 10% of new vehicles sold in the world in 2025 will be 48-volt architecture. (DELPHI, 2017)

Due to the low delta cost, improvement in fuel consumption, and global market interests, this technology has high potential to become the first level of hybridization produced in the Brazilian market. For this reason, understanding the potential of these technologies when associated with gasoline and ethanol fuels on the overall Brazilian energetic matrix is relevant to automotive companies.

1.1. Main Objective

The main goal of the present work is to analyze the fuel consumption benefit of BSG technologies when applied to different vehicle architectures, using a full factor experiment that will be simulated on an Advisor platform to assess scenarios of Brazilian regulation.

The specific objectives of this work are to:

1) Develop the quasi-static model of BSG configuration using data collected in steady-state tests based on the Advanced Vehicle Simulator (ADVISOR) open-source.
2) Validate the model developed through roller dynamometer data applying the homologation cycle Federal Test Procedure (FTP-75 + HWFET)
3) Simulate the matrix of possible configurations for the FTP-75, HWFET, and real-world driving cycles.
4) Compare the fuel consumption and performance of the HEV simulation.
5) Correlate the fuel economy of the different vehicles configurations and quantify the possible benefits of the current government incentive policy for using this technology.

2. Literature Review

2.1. Hybrid Electric Vehicles

Basically, an HEV is defined as “A vehicle that has two or more energy sources and energy converters” (EHSANI et al., 2018). Usually, the HEV combines the Internal Combustion Engine (ICE) with another energy source, for instance, electric energy. Furthermore, HEVs with more than two powertrains are not common due to their high complexity. The general hybrid drivetrain concept and the possible different power flow routes are presented in Figure 3. In this chart, energy source (1) is ICE, and energy source (2) is battery-electric machine.

Figure 3 - Conceptual illustration of a hybrid electric drivetrain

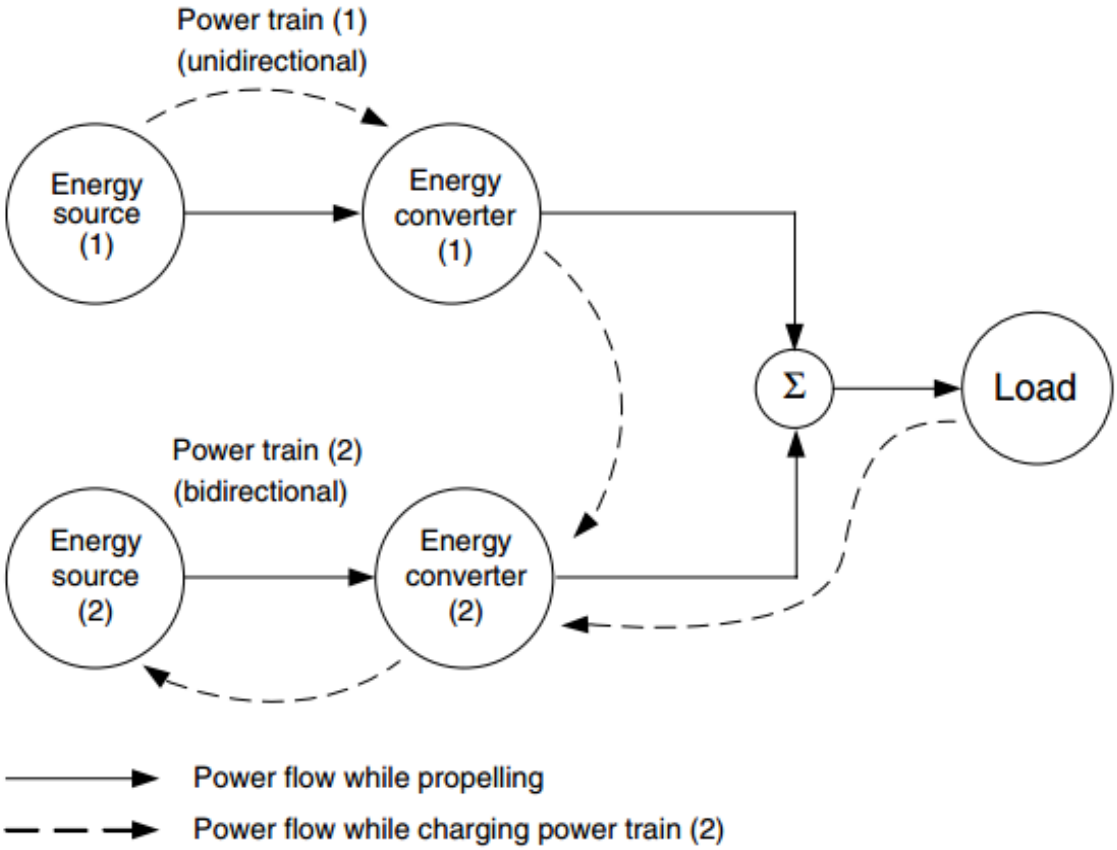

Source: adapted from (EHSANI et al., 2018)

To meet vehicle load requirements, power can flow in many different forms between the energy sources, and each pattern represents a different mode of operation; these modes are summarized in sequence:

- The power to the load came exclusively from the energy source (1) - The ICE mode is mainly used when the batteries are almost depleted, and the ICE operates alone to deliver the power to the load required to drive the vehicle.
- The power to the load came exclusively from the energy source (2) - In the pure electric mode, the electric motor delivers the power to the load required to drive the vehicle. This might happen when there is enough energy in the batteries and the ICE cannot operate effectively, such as at very low speeds.
- The power to the load came from both Energy sources - The hybrid traction mode might be used when a large amount of power is needed, for instance, during sharp acceleration or steep hill climbing.
- Energy source (2) obtains power from regenerative braking - The regenerative braking mode is when kinetic or potential energy is recovered through the electric motor functioning as a generator.
- Energy source (2) obtains power from the energy source (1) - In this mode the batteries are charged by the ICE when the vehicle is at a standstill, coasting, or descending a slight grade.
- Energy source (1) delivers power to load and to an energy source (2) at the same time - This mode happens when the ICE propels the vehicle and charges the batteries at the same time.
- Energy source (1) delivers power to an energy source (2), and the energy source (2) delivers power to load - In this mode, the batteries propel the vehicle while they are being charged by the ICE.
- Energy source (1) delivers power to load, and load delivers power to an energy source (2) - In this mode, the batteries are charged by the ICE while burning fuel.
- Energy source (2) obtains power from the energy source (1) and load at the same time - The batteries are charged by the ICE and the regenerative braking at the same time in this operation mode.

In contrast with the hybrid vehicles' multiple energy sources, a conventional vehicle uses only a chemical source of energy, such as gasoline, diesel, ethanol, or a blending of

these fuels. In addition, conventional vehicles usually operate with an ICE transforming any of those fuels into mechanical energy and heat. Other propulsion sources might come from fuel cells, hydraulic energy, and flywheel. (PENHA, 2019) However, only conventional vehicles and HEVs will be addressed in this work.

An HEV might use less fuel when compared with conventional vehicles for four main reasons:

1. It allows the ICE to shut down during a traffic jam or at a red light.
2. It allows the ICE to operate in the most efficient region.
3. It allows the recovery of part of the vehicle kinetic energy during braking.
4. It allows the ICE to be downsized without compromising the vehicle performance.

As mentioned before, there are many options to operate the HEVs system. Thus, the main challenges of HEVs are: optimizing their operation mode and designing a single powertrain system that incorporates all aspects of driving situations. (EHSANI et al., 2018) Hybrid Electric vehicles can be classified in three main ways: by their powertrain architecture, by their hybridization factor, or even by their technologies.

2.1.1. Classification of HEVs by Powertrain Architectures

The powertrain or powerplant consists of the components set that converts the energy source to power and delivers that to the road surface. Traditionally, the powertrain of HEV's is classified into two types: parallel and series. However, EHSANI et al. (2018) pointed out that the current classification was split into four types: series hybrid, parallel hybrid, series-parallel hybrid, and complex hybrid. The two new categories are the combination of the traditional configurations, series, and parallel hybrid, and will be dealt with in subsection 2.1.1.3.

2.1.1.1. Hybrid Series

The Hybrid Series architecture can be defined as "a drivetrain where two power sources feed a single powertrain (electric motor) that propels the vehicle." This configuration

is primarily an electric vehicle with an onboard energy generator. It must be noted that there is no mechanical connection between the ICE and the wheels on the HEV series. As shown in Figure 4, the more commonly used series hybrid consists of an internal combustion engine operating at an optimal efficiency point running the generator that charges the onboard batteries in a unidirectional energy flow. Furthermore, the electrochemical battery pack is linked by a DC/AC Inverter with the traction motor allowing bidirectional energy flow. Finally, the traction motor (electric motor) is linked to the wheels by the axles.

Figure 4 - Typical layout of a series HEV drivetrain

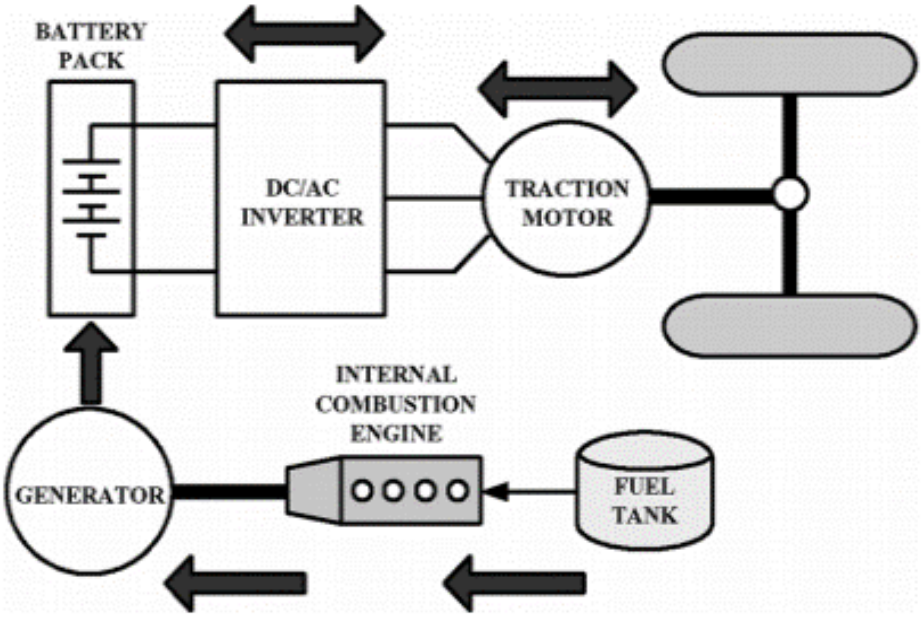

Source: adapted from (EMADI et al., 2005)

The operation modes of the Hybrid series are very wide; the bidirectional characteristic of its inverter and the traction motor that can be controlled either as a motor or a generator allows the Hybrid series to turn off the ICE during braking and recover energy to charge the battery; this mode is called regenerative braking mode. When the batteries are full, the vehicle operates in pure electric mode. On the other hand, when the battery needs supply, the ICE-generator will deliver power either for the batteries or traction power; in this case, the electric machine is reduced in electric transmission and the vehicle operates in pure engine mode. Furthermore, when both ICE and traction motor operate to charge the batteries, the operation mode is known as hybrid battery changing mode. Finally, there is a battery

charging mode where the ICE charges the batteries, and the traction motor does not receive power; this happens when the vehicle is stopped.

Several advantages can be offered by the Series hybrid:

- An ICE can operate at any point in its speed-torque range because it is decoupled from the driven wheels. Therefore, the efficiency can be optimized, and the engine can potentially be operated only within its maximum efficiency regions. Consequently, the emissions of the engine can be greatly improved by optimal design and control.
- As a consequence of the mechanical decoupling afforded by the electrical transmission, simple control strategies can be applied.
- There is no need for complex multigear transmissions as the electric motors have near-ideal torque-speed characteristics.

Nonetheless, series hybrid presents some drawbacks:

- There are two energy conversions: first, the mechanical energy from the engine is converted to electrical energy and stored in the batteries, and then electrical energy is converted to mechanical energy at the traction motor. In addition, the inefficiencies of the traction motor and the generator increase the losses.
- The cost and weight are increased due to the new components added, for instance, the generator, the (DC/AC Inverter), the battery pack, and the traction motor.
- The traction motor must deliver the maximum torque required to drive. For this purpose, the traction motor should be sized for each powerplant; a factor that elevates the research and development (R&D) cost.

The series hybrid drivetrain is usually used in heavy vehicles, such as heavy commercial vehicles, military vehicles, buses, and even locomotives. Some examples of series hybrid drivetrain applications are; the hybrid-electric city buses manufactured by Ebus, ISE Research Thunder-volt, and Electric Vehicles International. The major reason is that large vehicles have enough space for the bulky engine/generator system. (EHSANI; GAO; MILLER, 2007)

2.1.1.2. Hybrid Parallel

According to EMADI et al. (2005), a parallel hybrid drivetrain can be defined as “a drivetrain in which the engine supplies its power mechanically to the wheels, as in a conventional ICE-powered vehicle”. As shown in Figure 5, both the ICE and traction motor are linked mechanically to the wheels through the torque/speed coupling and the transmission system. Furthermore, this mechanical coupling could simply be a single axle, a gearbox, even a pulley-belt unit (BSG), or a sprocket chain. This possibility leaves room for several different configurations.

Figure 5 - Typical layout of a parallel HEV drivetrain

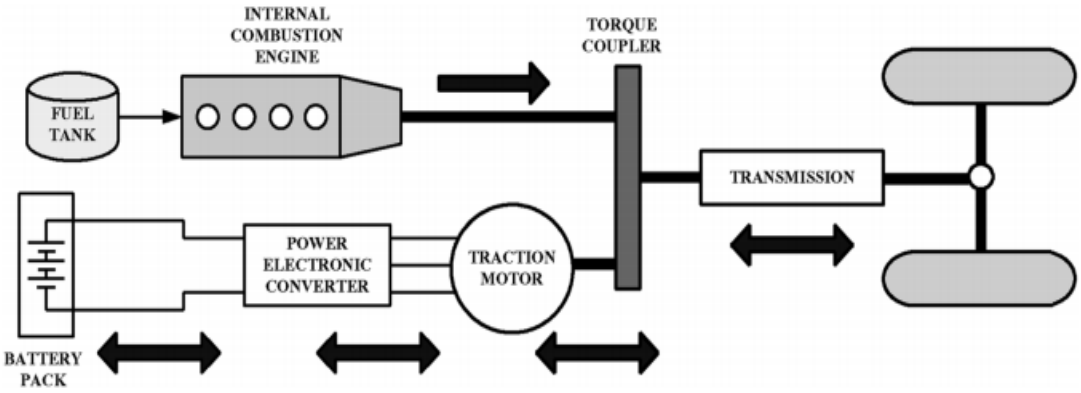

Source: adapted from (EMADI et al., 2005)

The mechanical coupling “Torque Coupler” in Figure 5, between the energy converter's motor and engine and the wheels, maybe a speed coupling, as can be seen in the conceptual Figure 6(a), or a torque coupling as shown in Figure 6(b).

Figure 6 - Torque and speed conceptual coupling with two inputs.

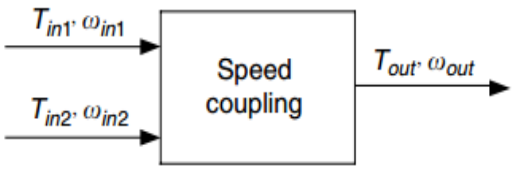

Figure 6(a) - Mechanical speed coupling

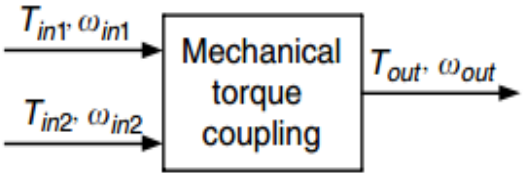

Figure 6(b) - Mechanical torque coupling

Source: adapted from (EHSANI et al., 2018)

2.1.1.2.1. Torque-coupling parallel hybrid electric drivetrains

The torque-coupling parallel hybrid electric drivetrains add the torque of the electric motor and the ICE together or split the engine torque into two parts: battery charge and vehicles propelling. There are torque-coupling variations depending on their mechanical coupling components, their transmission positions, and their different gears. Generally, they can be classified as two-shaft, and one-shaft. Moreover, the tractive requirements, engine characteristics, engine size, motor size, and motor characteristics are some factors that will determine a HEV optimum design

The two-shaft possible designs are shown in Figures 7(a) and 7(b); the two-shaft with two transmissions and the two-shaft in parallel, respectively. The two-shaft with two transmissions configuration can be subdivided into: (i) two-shaft with two multigear transmissions; (ii) two-shaft with a single transmission (marked 1 in Fig. 7(a)) and a multigear transmission (marked 2); (iii) two-shaft with a multigear transmission (marked 1) and a single transmission (marked 2); and (iv) two-shaft with two single transmissions. On the other hand, the two-shaft in parallel Figure 7(b) has no subdivisions.

Figure 7 - Two-shaft designs

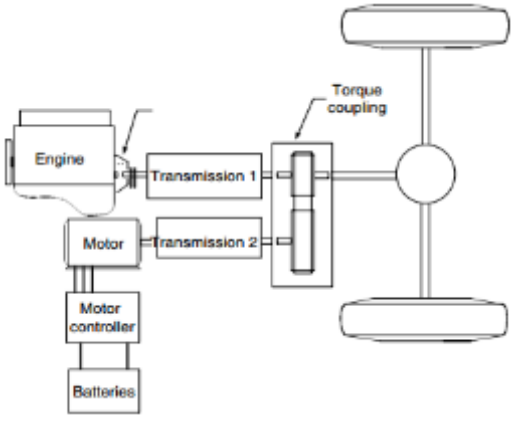

Figure 7(a) - Two axle configuration

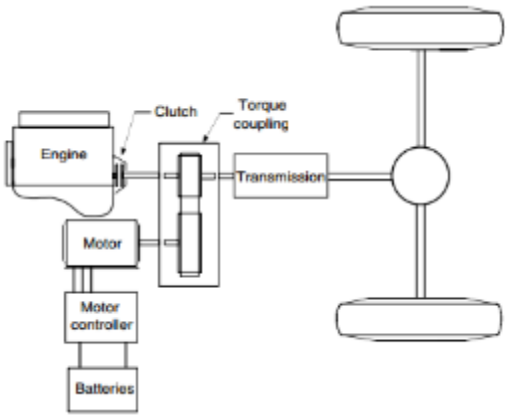

Figure 7(b) - Two-shaft parallel configuration

Source: adapted from (EHSANI et al., 2018)

The overall efficiency of the two multigear transmissions (i) is superior to the others designs, mainly due to its wide range of tractive effort profiles. However, drivetrain is significantly more complex because of its two multigear transmissions. On the other hand,

the configuration with a multigear transmission 2 and the single-gear transmission 1(ii) takes advantage of the high torque characteristic of electric machines at low speeds, while tending to improve engine efficiency. In contrast, the opposite configuration with a multigear transmission 1 and the single-gear transmission 2 (iii) is considered an unfavorable design, because it does not use the advantages of both powertrains. Finally, the two single-gear configuration (iv) results in simple configuration and control, and when the drivetrain is properly designed it would have satisfactory performance and efficiency.

With the transmission located between the torque coupler and the drive shaft, the two-shaft parallel configuration Figure 7(b) would be suitable for passenger cars, when a relatively small engine and electric motor are used.

Figure 8 - Single-shaft designs

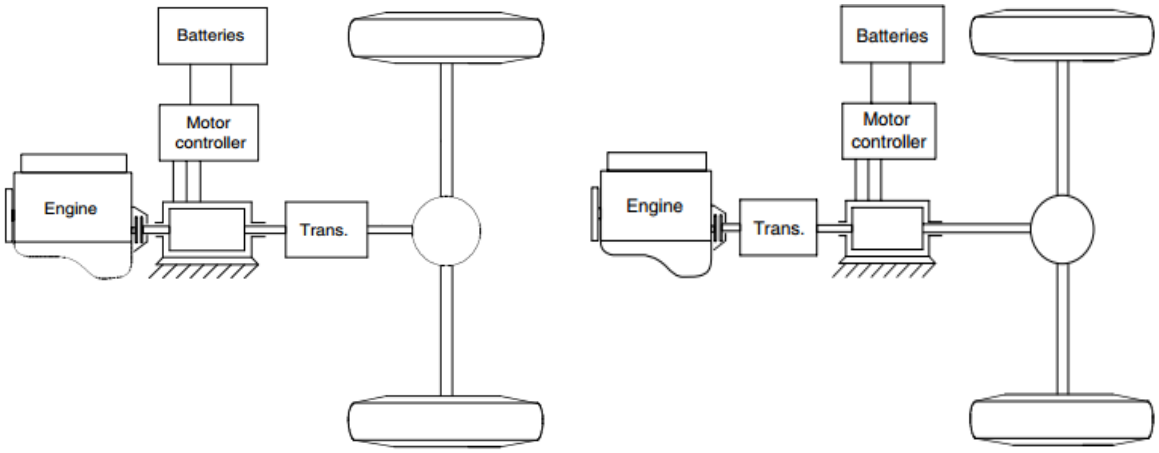

Figure 8(a) - single-shaft “pre-transmission” configuration

Figure 8(b) -single-shaft “post-transmission” configuration

Source: adapted from (EHSANI et al., 2018)

The single-shaft designs are presented in Figures 8(a) and 8(b) and the main difference between them is the position of the motor, in the pre-transmission configuration Figure 8(a) it is ahead of the transmission, while in the post-transmission configuration Figure 8(b) it is behind the transmission. In the pre-transmission configuration both, the motor and engine are modified by the transmission; this configuration is usually applied for a small motor, referred to as a mild-hybrid drivetrain. On the other hand, the post-transmission is widely applied to large electric motors with long and constant power, and the

transmission cannot modify the motor torque as it is linked directly with the driven wheels. It should be noted that the electric motor could not be operated as a generator because the motor is rigidly connected to the driven wheels. Moreover, the transmission can be used to modify the engine operating point to improve the vehicle performance and engine operation efficiency.

Another possible variation of the torque coupling parallel hybrid with two-shaft shown in Figure 7(a) is the torque coupling parallel hybrid drivetrain with separated axle architecture as presented in Figure 9. The engine powers one axle and the other axle is powered by the motor. The principles and gear's possibilities are similar to the two-shaft configuration presented in Figure 7(a). Furthermore, the separate axle architecture presents substantial advantages from the conventional vehicle. First, it keeps the original engine architecture and adds an electric traction system on the other axle which makes the vehicle four-wheel drive, optimizing the traction on slippery roads and reducing the tractive effort on a single tire. On the other hand, the electric machines and components, for instance, the eventual differential gear system, would increase the vehicle weight and they occupy considerable space and potentially may reduce the available passenger and luggage space

Figure 9 - Two-shaft possibility

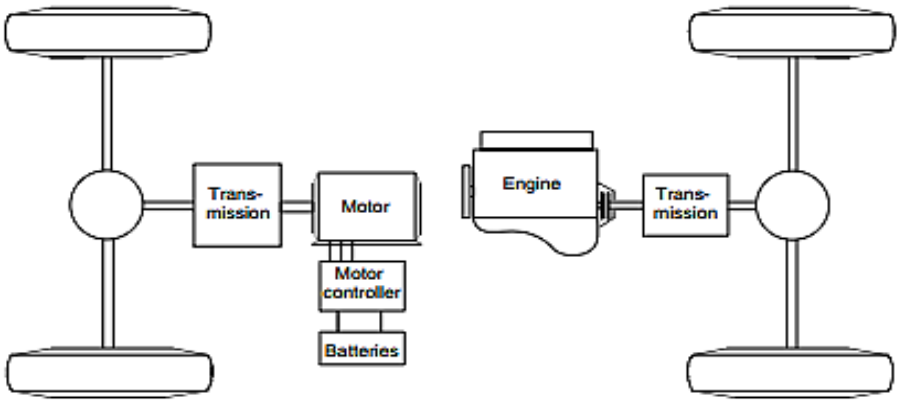

Source: adapted from (EHSANI et al., 2018)

2.1.1.2.2. Speed-coupling parallel hybrid electric drivetrains

Speed-coupling parallel hybrid electric drivetrains couple together the engine and motor at speed, and as in torque-coupling, there are two typical speed-coupling

configurations: the planetary gear unit configuration shown in Figure 10(a) and the electric motor with a floating stator, called a transmotor in this work, is presented in Figure 10(b).

The planetary gear unit consists of a three-port unit, in which the sun gear, the speed, and the ring gear are added together and output through the yoke. As shown in Figure 10(a), the transmission is linked to the engine by a clutch, and it can be used to modify the speed-torque characteristics of the ICE. In addition, the electric motor is linked through a pair of gears where Locks 1 and 2 are used to lock the sun gear and right gear, respectively, to meet the vehicle's different operation modes. The possible operation modes are hybrid traction, engine-alone traction, motor-alone traction, regenerative braking, and battery charging from the engine.

Figure 10 - Speed-coupling parallel hybrid electric drivetrains

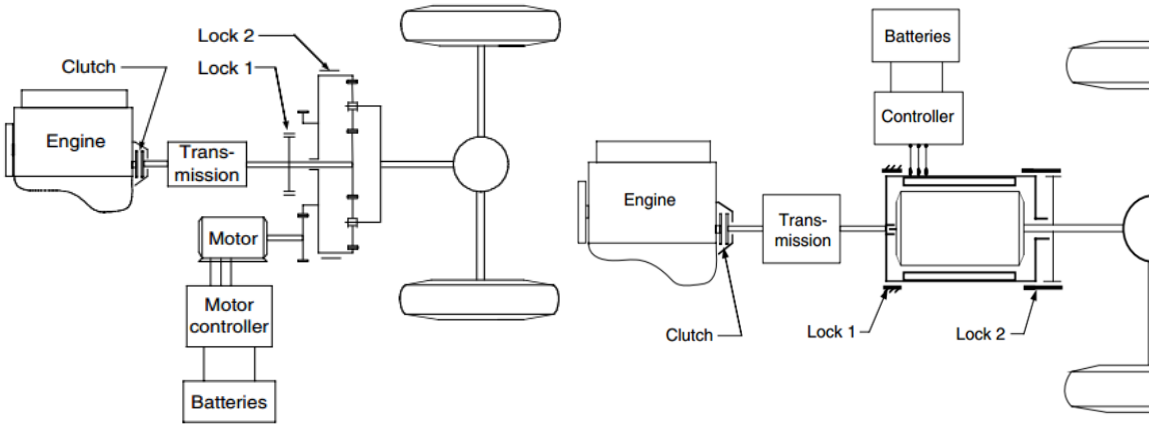

Figure 10(a) - Hybrid electric drivetrain with speed coupling of planetary gear unit

Figure 10(b) -Hybrid electric drivetrain with speed coupling of electric trans motor

Source: adapted from (EHSANI et al., 2018)

Another possibility is presented in Figure 10(b); the transmotor has a structure similar to the planetary gear unit. Lock 2 and 1 are used to lock the stator to the rotor, and the stator to the vehicle frame respectively. This configuration can operate in the same modes as the planetary gear unit.

The hybrid drivetrain with speed coupling presents advantages in powerplants such as the Stirling engine and the gas turbine engine, in which their efficiency is less sensitive to

torque and more sensitive to speed. This is because the speed of the two powertrains is decoupled; thus, the speed of both electric and ICE sides can be chosen freely.

2.1.1.3. Hybrid Parallel series

Finally, it is possible to combine both torque and speed coupling; it is called a Torque-coupling and Speed-coupling parallel hybrid-electric drivetrain. This configuration allows switching between speed coupling and torque coupling to achieve an optimal powertrain performance. The best example of this architecture is the Toyota Prius by the Toyota Motor Company; this drive-plant is schematically shown in Figure 11. A planetary gear is used to couple two electric machines: the small motor or generator (a few kilowatts) and a large motor traction motor (a few to ten kilowatts), to the ICE, and to the wheels. Through this system of operation, a high fuel economy can be achieved using the small motor to adjust the engine speed in order to operate at the optimum speed range.

Figure 11 - Series-parallel hybrid drivetrain by using a planetary gear unit

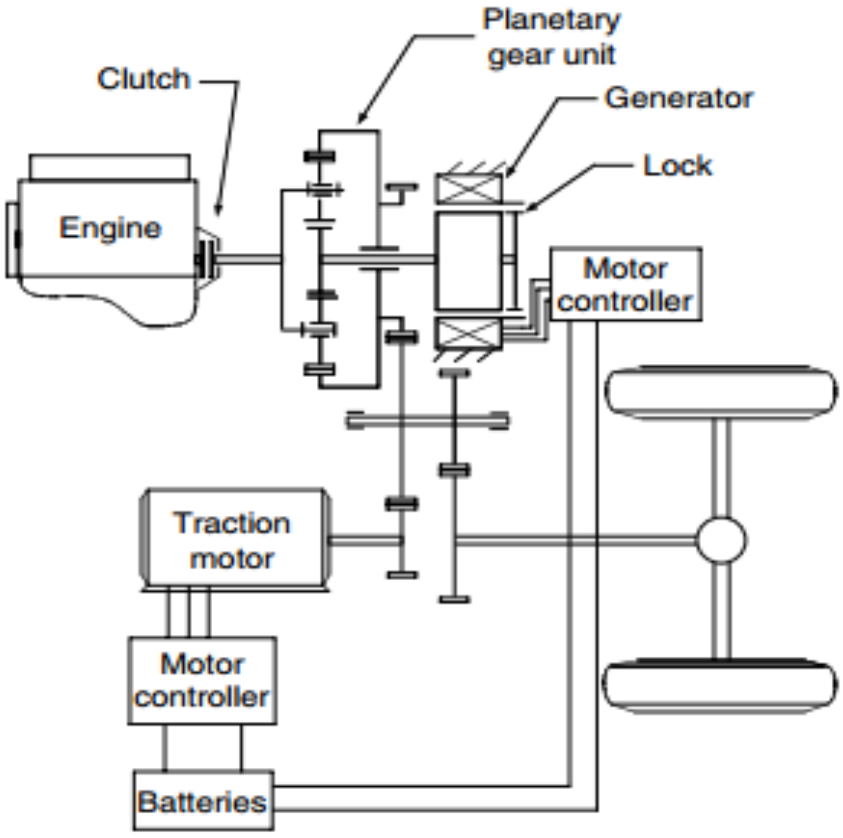

Source: adapted from (EHSANI et al., 2018)

2.1.2. Classification by factor and degree of hybridization

Besides HEVs powertrain architecture, some vehicle characteristics, such as control strategy, rolling friction, vehicle mass, and accessory load are fundamental to extend the fuel economy improvement. With a wide range of factors affecting the fuel economy, a classification method for hybrid vehicles over a standard baseline becomes fundamental. One such method to classify HEVs is the hybridization factor (HF). Essentially, the HF parameter is a ratio between the power of the installed electric motor and the total amount of power delivered by the electric motor and the ICE. The HF is given by equation 1:

$$HF = \frac{P_{electric}}{P_{electric} + P_{ICE}} \quad (1)$$

Where: HF is the hybridization factor unitless; $P_{electric}$ is the electric motor drive power in kW, and P_{ICE} is the power of the internal combustion engine in kW

According to equation 1, a vehicle could be classified as: (i) conventional when HF is equal to zero; (ii) Micro hybrid when HF is more than zero and less than 0.1; (iii) Mild Hybrid when HF is between 0.1 and 0.25; (iv) Full Hybrid when HF is greater than 0.25 and less than 0.5; (v) Plug-in Hybrid when HF is higher than 0.5, less than 1 and, in addition, it has the ability of recharging from the grid; (vi) and finally, electric vehicles when HF reaches 1. (PENHA, 2019)

According to ONORI (2016), a possible classification of today's vehicles in the market can be given based on the electric machine size and internal combustion engine size Furthermore, this classification is proportionally linked with the Hybrid factor as shown in Figure 12. The classification is as follows:

- (i) Conventional vehicles - (HF = 0): In conventional vehicles, the total power request at the wheel is satisfied by the ICE, that is, it is the only source of power. In addition, conventional vehicles do not have any propulsion electric motor.

- (ii) Micro Hybrids ($0 < HF < 0.1$): Stop-start systems reduce fuel consumption and emissions by shutting down the ICE and restarting it while the vehicle is waiting at traffic lights or in a traffic jam. For that reason, stop-start is very advantageous in busy cities, for instance; São Paulo, Belo Horizonte, and New York, where the average hours lost in congestion annually reached 152, 160, and 140, respectively, in 2019. (INRIX, 2020) Moreover, this feature is present in hybrid vehicles and conventional vehicles. Non-electric vehicles with stop-start features are called micro hybrids.
- (iii) Mild HEV ($0.1 < HF < 0.25$): The main characteristic of Mild HEVs is that they do not have an exclusive electric-only mode of propulsion. The electric motor/generator is linked to the ICE in torque coupling parallel architecture as shown in subsection 2.1.1.2.1. Furthermore, the mild hybrids can employ regenerative braking and allow the ICE to be turned off whenever the car is coasting, braking, or stopping. In addition, the motor/generator provides some level of ICE power assist.
- (iv) Full HEVs ($0.25 < HF < 0.5$): In contrast with micro-hybrid and mild HEV, full HEVs are capable of running the vehicle in electric mode only, pure ICE, or a combination of both. To fully attend these operation modes a high-capacity battery pack is required. Moreover, the simple heuristic rules controller system applied to mild and micro vehicles is replaced in full hybrid vehicles energy management strategies to fully exploit the benefits of vehicle hybridization. There are many powertrain architectures, and they were described in subsection 2.1.1
- (v) Plug-in Hybrids ($HF > 0.5$): The main difference between Plug-in Hybrid electric vehicles (PHEVs) and full HEVs is that PHEVs can recharge their batteries from the electric grid. Besides this requirement, according to Penha (2019), a PHEV must still fulfill other requirements: it must have a range in full electric mode operation called all-electric range (AER), and the battery must have a storage capacity of 4kWh or greater. Furthermore, the AER is usually designed to meet the average daily driving requirements of PHEV owners. According to Emadi (2014), it is estimated that in Europe, 50% of trips are less than 10 km (6.25 miles). In the United States, roughly 60% of vehicles are driven less than 50 km (31.25 miles) daily. Moreover, Emadi states that connection to the grid becomes a crucial factor to be taken into

account in hybrid vehicles with plug-in features. For this purpose, the plug-in hybrid electric factor (P_{ihef}) is expressed in equation 2:

$$P_{ihef} = \frac{E_{grid}}{E_{grid} + E_{fuel}} \quad (2)$$

Where: P_{ihef} is the plug-in hybrid electric factor unitless; E_{grid} is the average supplied by the grid in kJ, and E_{fuel} is the energy extracted from the fuel. A P_{ihef}= 1 means that no energy from the fuel is being used and any value between 1 and 0 implies that there is a split of energy supplies. Finally, a P_{ihef}= 0 means that no energy from the grid was required for the propulsion.

- (vi) Electric Vehicles (HF = 1): Electric Vehicles do not have an ICE; hence, their propulsion comes entirely from an electric motor. For that reason, a higher capacity battery pack is required. EVs are recharged from the power grid or a hydrogen fuel cell. Moreover, as pointed out in section 1 (Introduction), the EVs' benefits have to be carefully discussed due to their almost exclusive power grid dependence.

Figure 12 - Spectrum of vehicles technologies

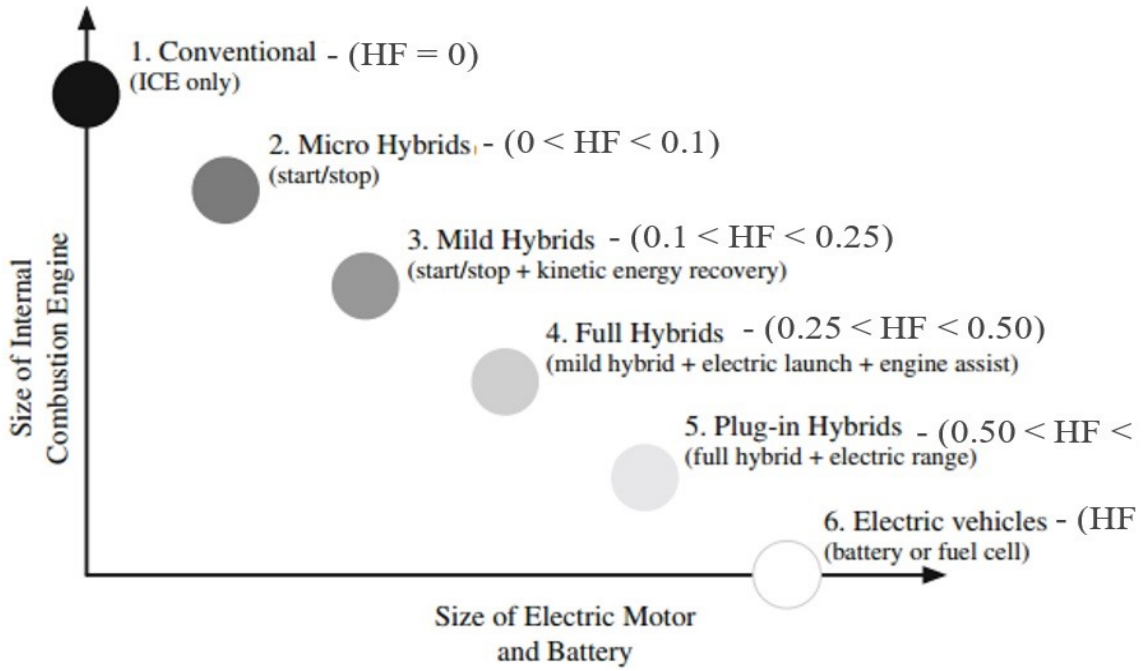

Source: adapted from (ONORI, 2016)

2.1.3. Hybrid classification: focus on Belt Starter Generator (BSG)

As discussed in subsections 2.1.1 and 2.1.2, there are two main ways to classify an HEV: by its powertrain architecture, and by its hybridization degree, respectively. A schematic combination between the level of hybridization (its size of engine and motor) and the powerplant architecture (the way its engine and motor are linked) is presented in Figure 13. It is remarkable to observe that the micro-hybrid and the mild-hybrid are usually designed in a hybrid parallel configuration. However, the full hybrid, fuel cell, and plug-in can be designed in either architectures, series, parallel, or a combination between them, called series-parallel HEVs. This fact can be explained by observing that in mild and micro hybrids, the electric motor is too small to provide enough power to the wheels.

Figure 13 - Vehicle classification and hybridization concept

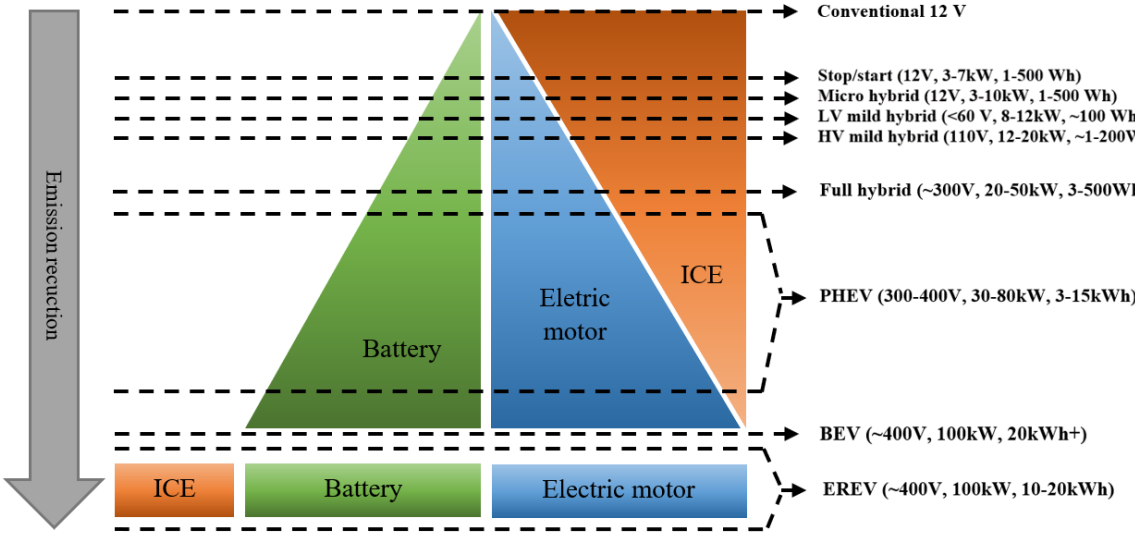

Source: adapted from (BALDIZZONE, 2012)

Although fuel consumption is reduced while the HF or P_{ihef} is increased, hybridization adds a second propulsion system into the ICE-based propulsion system that leads to an additional component cost. Therefore, as the degree of hybridization increases, the system cost rises proportionally. Figure 14 shows the relationship between the cost of fuel economy improvement and the percentage of CO_2 reduction. (EMADI, 2014)

Figure 14 - Best value curve for increasing the degree of hybridization

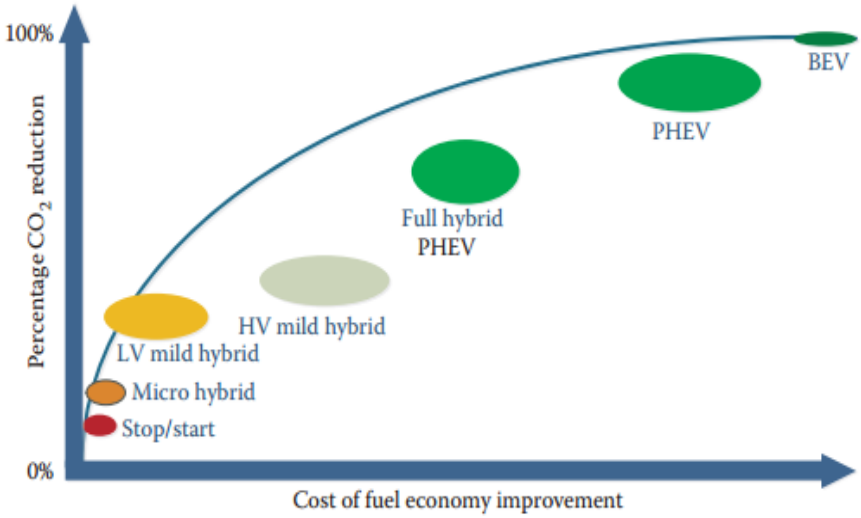

Source: adapted from (EMADI, 2014)

According to EMADI (2014), a High Voltage (HV) is defined as a DC voltage greater than 60 V, and in Figure 14 it can be observed that a higher hybridization degree requires a High Voltage system to meet the large electric power demand required to assist and even fully take over vehicle propulsion. Moreover, an HV system allows ~~a~~ support of vehicle power demands effectively without a commensurate increase in operating electric current.

The additional components and interface connections required for HV systems add a massive burden on the vehicle cost. Furthermore, much additional care is required due to safety and regulatory concerns in an HV system, for instance, special wiring that has unique insulation and orange color, multiple series-connected HV battery modules, high-voltage interlock loop (HVIL), and an additional diagnostic system to monitor all systems. These components and systems are designed to ensure that, in case of collision, the voltage will be reduced to under 60 V in 5 seconds to avoid electric shock.

On the other hand, Low Voltage (LV) systems present an interesting trade-off between implementation cost and fuel consumption improvement. According to EMADI (2014), fuel economy can reach up to 15%. Besides the fuel consumption gain, the LV system has another benefit, since they are easy to integrate to compact class segments (passenger cars) because of their suitable package. This fact can give a large consumer base access to fuel-efficient cars.

Therefore, this thesis is going to focus on mild-hybrid configuration with a low voltage system in a parallel architecture, specifically a Belt Starter Generator (BSG) technology. For this reason, a detailed description of all of the various hybrid systems is out of our scope. For further information, the reader is referred to more specific texts (EHSANI et al., 2018; EHSANI; GAO; MILLER, 2007; EMADI, 2014, 2017; MI; MASRUR; GAO, 2011) (EMADI, 2014, EMADI, 2018).

2.1.3.1. Belt Starter Generator description

The Belt Starter Generator, or BSG, is a mild parallel hybrid technology that raised interest in the last few years due to its characteristics of low delta cost, low weight, and fuel economy improvement. Furthermore, the BSG system should be designed to improve customer driving experience and acceleration transients. The system can minimize vibration and noise, resulting in more comfort during start and stop. In addition, the BSG improves shift and launch quality, it allows torque assist, and finally, when the BSG architecture is 48 Volts, it enables the introduction of 48 Volt auxiliary loads such as electric power steering (EPS), active body control, electric heating, venting, and air conditioning (HVAC), and so on.

The main functional objectives of a BSG system are regenerative braking recuperation; supporting engine stop-start; it provides torque-assist during high torque loads, and last but not least, generates power to support auxiliary loads. They are detailed below.

The first function, the regenerative braking recuperation, works as follows. In conventional vehicles, kinetic energy is released into the air during breaking events in heat and sound form. According to EMADI (2014), the overall economy with regenerative braking can reach 5% to 8% in NEDC and 8% to 12% in the FTP-75 drive cycles. Among various operation methods, two can be highlighted: fully blended, and the overly regenerative braking system. The fully blended is the more challenging one to be developed; however, it improves fuel economy while maintaining a more natural braking feel. On the other hand, the overly regenerative is the most cost-effective methodology. When the driver begins to press the brake pedal, the event is purely regenerative, and almost all of the energy is captured into the energy storage system. After some time braking, the friction from braking begins to

dissipate energy as heat to ensure safety and smooth drivability. In addition, regenerative braking is limited by the battery capacity, peak power limits of the power inverter module, and the motor.

The second function, support engine stop-start, is described as follows: When initiating a vehicle by the “key on” function, usually a dedicated starter turns the engine on. In a conventional BSG application, the starter will continue to crank the engine during “key on” events mainly because of the BSG fault risk when it operates at a low temperature such as -40 C. In contrast, the BSG will turn the engine on in a stop-start event, when the operating temperature is appropriate to the BSG system. During events such as idle, coasting, and deceleration the start/stop event occurs, and the engine is turned off when it is not required to provide propulsion to the vehicle. Furthermore, typical BSG will focus on turning off the engine during idle events due to the higher complexity of control and calibration of the other events.

In the stop-start event, the driver experience and satisfaction should be maximized by reducing engine vibration on shutdown through engine braking and torque management, enhancing restart quality and time. In addition, to fulfill the driver's needs the BSG control system is usually calibrated with at least two profiles of engine start, a smooth auto-start profile that is transparent and seamless to the driver, and an aggressive profile that turns on the engine as fast as possible, no matter the driver's experience. Between these two extreme requirement profiles, the BSG controller interpolates to ensure the most transparent auto-starts.

The next function is to provide torque assist and the main idea of this function is to provide additional torque to the ICE during some events, such as starting, acceleration, and high-grade driving. The power and duration are limited by the voltage of the system, the power rating of the motor, the battery capacity, the thermal limitations of the system, and the torque-speed motor map. Furthermore, the torque assist allows the optimization of the gearshift schedule due to the electric motor contribution according to the driver's requirements, when no gear down is required to meet the request. In addition, the acceleration events might potentially be enhanced by the torque-assist function. Moreover, it yields a substantial improvement in fuel economy by enabling the engine to operate more efficiently.

Finally, generating power to support auxiliary loads works as follows: As the BSG is designed to support the 12 Volt loads and the 48 Volt “if the BSG configuration is 48 V” of the vehicle. The traditional alternator can be removed, which causes a positive impact on cost, integration, and packaging efforts. Basically, in this mode, the motor will be required to provide constant power to supply the battery pack load and the auxiliary loads. Furthermore, due to the high efficiency, the BSG will take advantage of the alternator when it is necessary to generate a large energy amount to supply the auxiliary loads.

2.1.3.2. 12V and 48V Topologies

Subsection 2.1.3.1 discussed the BSG definitions and their functions. This subsection, illustrates the key differences between the possible 12V and 48V topologies (Figure 15) and how they impact fuel economy, ease of integration, and the implementation cost. There are four topologies; P1 topology (marked P1 in Figure 15), P2 topology (marked P2), P3 topology (marked P3), and P4 topology (marked P4). The key differences between them are the packaging, the location of the electric motor installation, and how each one connects to the engine.

Figure 15 - Possible topologies for BSG integration

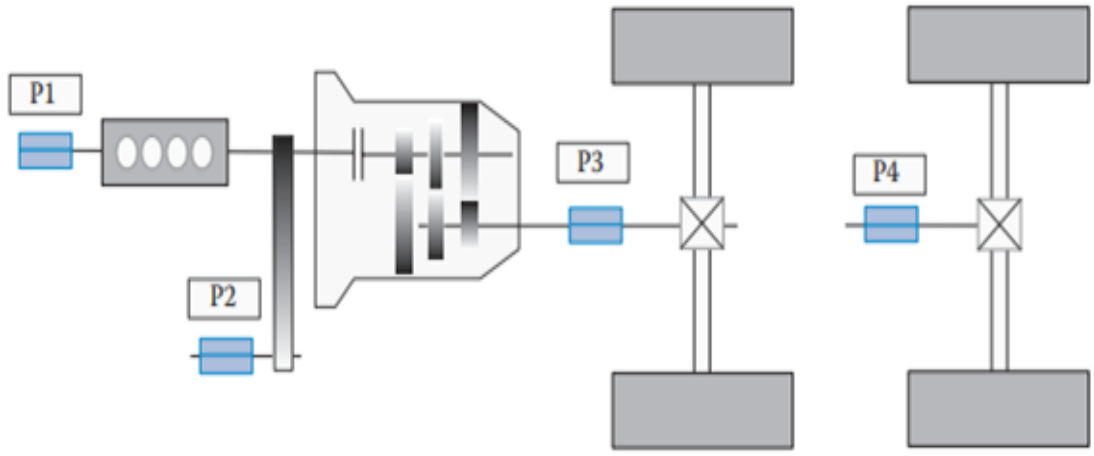

Source: adapted from (EMADI, 2014)

P1 Topology: In this topology, the electric motor is directly integrated into the engine by a front-end accessory drive (FEAD) system, and in most cases can be mounted on the

engine in place of the conventional alternator, the reason for its low integration complexity. Moreover, torque assist, coasting, idle charging, and regenerative braking features are available with P1. However, the engine drag limits the regenerative braking, and an e-clutch system is required for coasting function. Furthermore, the electric motor will always start the ICE in start/stop events, unless low ambient temperature conditions are reached, where a conventional starter is required to start the vehicle.

P2 Topology: The electric motor is linked directly or via a belt to the crankshaft, and it is placed between the transmission and the engine. Furthermore, the P2 topology provides functions such as: torque assist, improved regenerative capacity, idle charging, start/stop, and electric-only drive. The electric-only is dependent on the battery capacity and power of the electric motor. Overall, this topology offers a substantial fuel economy improvement with a medium implementation cost.

P3 Topology: In this topology, the electric motor is linked to the engine through a drive shaft between the transmission and the differential, which can be either via a belt or via mechanical direct coupling. The P3 Topology allows electric-only drive, electric-assist/boost, and regenerative braking features. Furthermore, the clutch is always electrically actuated, and it is possible to perform coasting with manual transmission. This topology is complex to be integrated into an existing drive train.

P4 Topology: The electric motor is installed to the second set of wheels in this configuration, a fact that adds an advantage because the vehicle becomes all-wheel drive during electric assist mode. However, this topology does not allow start/stop or idle charging because the motor is not directly linked to the ICE. On the other hand, P4 provides high regenerative capability, fuel cutoff during coasting, torque assist/boost, and electric-only drive.

As can be seen, the BSG is a P1 topology and uses an electric motor, and in the next section 2.2, the basic theory of these machines and the types of motors used in HEV application specifically for BSG technologies will be addressed.

2.2. Electric Machines

Electric machines (EM) are the core technology for HEVs, EVs, and PHEVs. The EMs are defined as “A device that can convert either mechanical energy to electric energy, or electric energy to mechanical energy.”(STEPHEN J. CHAPMAN, 2003)

According to CHAU, CHAN, and LIU (2008), these machines can be classified into two main groups, the brushed and the brushless, and each one has subgroups, as can be seen in Figure 16. The feasibility of each application depends on many characteristics, for instance, torque density, power density, speed range, efficiency, constant power operation capacity, reliability, and robustness. In addition, comfort characteristics should be observed, such as low acoustic noise and, last but not least, the cost of each EM should be taken into account.

Figure 16 - Classification of the EV Drivers

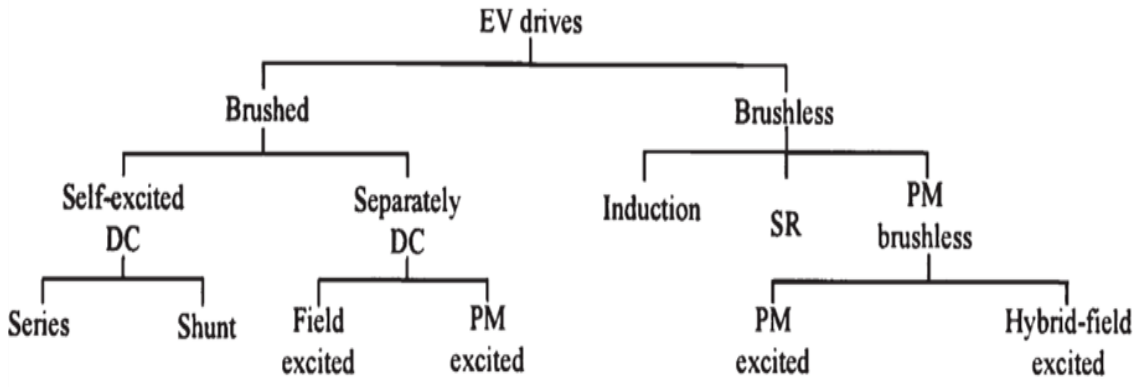

Source: adapted from (CHAU; CHAN; LIU, 2008)

The stator and the rotor are the main parts of an electric machine: the stator remains static and is fixed to the ground, while the rotor is the piece that rotates and connects to the output shaft. An important characteristic of these machines is called the air gap, and this is the distance between the rotor and the stator. In addition, there are two windings: the field winding, which produces a magnetic flux, and the armature winding, which induces a voltage.

Peak power is limited by the maximum temperature that a winding can withstand without degrading its insulation. Furthermore, proper insulation helps to increase the maximum power capability of the machine due to the heat dissipation improvement in the windings. (EMADI, 2014; STEPHEN J. CHAPMAN, 2003) In addition, the size of the electric machines mainly depends on the torque and is not given by the power, since the heat produced is fundamentally dependent on the current and torque. (PENHA, 2019)

An important characteristic of electric machines is called rated torque (nominal torque), and it is the torque that can be delivered continuously without overheating. Even though some electric machines models can deliver long operation over the rated torque, it could dramatically reduce the motor life.

During the electric machine operation, maintaining a constant voltage is desirable, as the variation in load determines the current consumption of the electric machine; nonetheless, the load and the current are not necessarily proportional to each other. Furthermore, the nominal current of the machine is attained only when the electric machine is at rated torque and nominal voltage.

The functionality of operating as a motor or as a generator is very important to EVs, HEVs, and PHEVs, due to the energy recuperation requirement. In contrast to common belief, the operation mode (motor or generator) is not linked with the electric machine direction of rotation, but it is correlated with the interaction of the external forces. If an external force is applied in the direction of rotation, the electric machine is operating as a generator. Contrarily, if an external force is applied contrary to the direction of rotation, it is operating as a motor.

Subsections 2.2.1 and 2.2.2 present the fundamentals of the two main electric machine architectures and their main characteristics. These are the Direct Current Machines (DC), and the Alternator Current Machines (AC). The latter is subdivided into two subsections: 2.2.2.1 and 2.2.2.2 the Synchronous machines (SM), and the Induction Machines (IM), respectively. Finally, 2.2.3 presents the main models used for BSG and their advantages and disadvantages.

2.2.1. Direct Current Machines (DC)

According to Ehsani, Gao, Gay, and Emadi (2018), DC machines are widely applied to many different electric drivetrain projects, mainly due to their technological maturity, control simplicity, adjustable speed, good speed regulation, and frequent starting, braking, and reversing. DC machine architecture has its field windings located on the stator, and its armature windings located in the rotor. Furthermore, the field flux origin of a DC motor affects its torque-speed characteristic. In addition, DC machines can be classified according to their field flux as: separately, series, compound, and shunt excited.

Figure 17 - Classification of DC machines

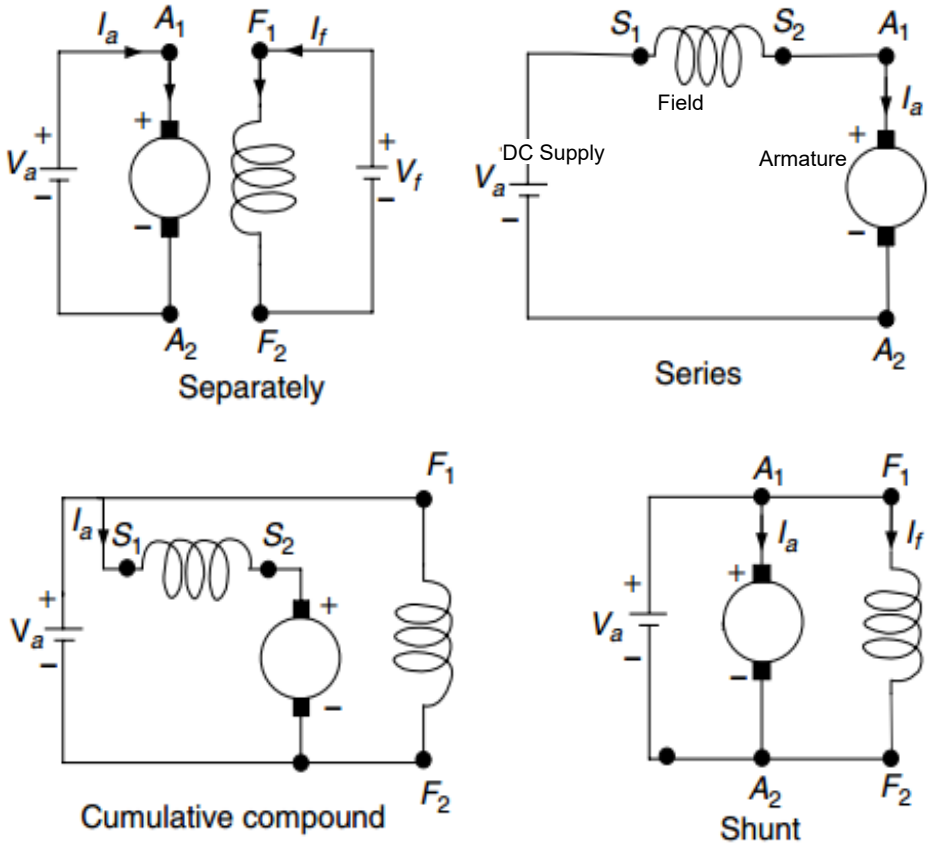

Source: adapted from (CHAU; CHAN; LIU, 2008; EMADI, 2014; STEPHEN J. CHAPMAN, 2003)

As can be seen in Figure 17, in the case of a separately excited motor, the field voltage V_f and the armature Voltage V_a can be controlled independently. Furthermore, DC separately excited requires a small part of a rated current to control a large armature power. In the case of a series motor, the armature current is the same as the field current; consequently, field

flux is a function of armature current. The DC cumulative compound, the magnetomotive force (mmf) of a series field is a function of the armature current and is in the same direction as the mmf of the shunt field. Finally, in the DC shunt excited, the armature and field are connected in a common source in parallel. Therefore, to achieve independent control of field and armature current, a resistance into the appropriate circuit should be applied; however, this methodology is inefficient. An efficient way to obtain a separate control of the current is using a power electronics-based DC-DC converter.

As a result of an EM rotation loop, a constant alternating voltage value is obtained, as can be seen in Figure 19(a). In order to generate a DC output voltage, a commutator is applied. The commutator has two components; two fixed contacts named brushes, and two semicircular conducting segments at the end of the loop wire named commutator segments, as can be seen in Figure 18.

Figure 18 - Sketch of a commutator in DC machines

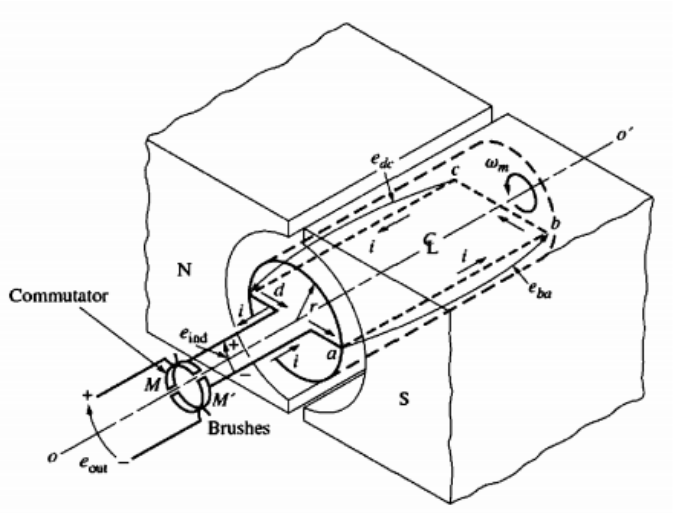

Source: adapted from (STEPHEN J. CHAPMAN, 2003)

According to Chapman (2003), the commutation process is the most critical part of a DC machine, and the fixed contacts are carefully set up in the position where “every time the voltage of the loop switches direction, the contacts also switch connections, and the output of the contacts is always built up in the same way”. This process is named “commutation”, and in Figure 19(b) the result of this process is presented as can be observed the voltage negative part was inverted.

Figure 19 - Process of commutation

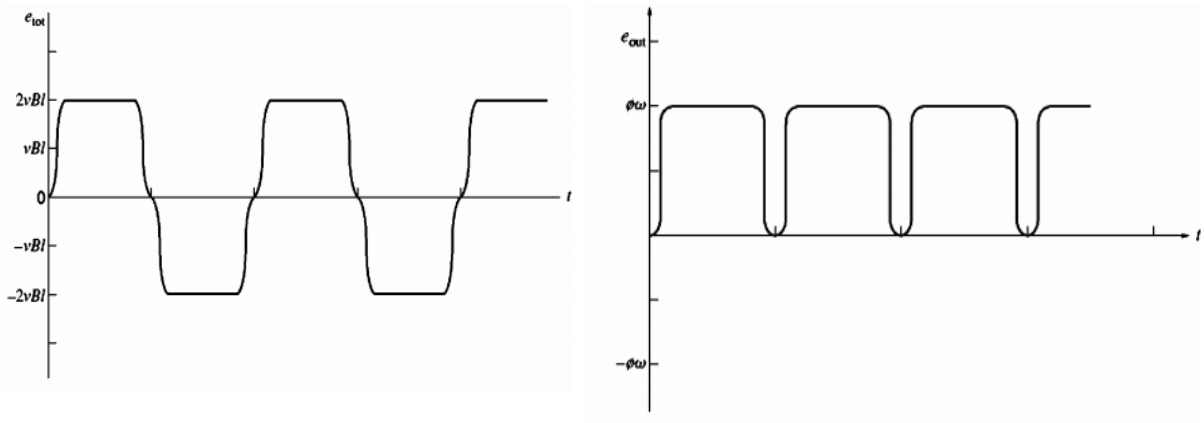

19(a) The output voltage of the loop without a commutator

19(b)The resulting output voltage

Source: adapted from (STEPHEN J. CHAPMAN, 2003)

An aspect to be taken into account with EVs, HEVs, and PHEVs is the losses; in DC machines, five losses can be observed:

1. Electrical or copper losses (I^2 R losses)
2. Brush losses
3. Core losses
4. Mechanical losses
5. Stray load losses

Electrical or copper losses; these are the losses in the field windings and the armature of the machines. The copper losses are given by:

$$Armature\ loss: P_A = I_A^2 R_A \quad (3)$$

$$Field\ loss: P_f = I_F^2 R_f \quad (4)$$

Where: P_A is the armature loss, P_f is the field circuit loss, R_A is the armature resistance, R_f is the field resistance, I_A is the armature current, and I_f is the field current. The winding resistance at normal operating temperature is usually used for this calculation.

Brush Losses; these are the power losses between the computation component brushes and commutator segments, and the losses are given by the equation 5:

$$P_{BD} = V_{BD} I_A \tag{5}$$

Where: P_{BD} is the brush drop loss, V_{BD} is the brush voltage drop, and I_A is the armature current.

Core losses; the hysteresis and eddy current losses that occur in the metal of the motor are the core losses. These losses are proportional to the flux density squared (B^2) and, for the rotor, to the 1.5th power of the rotational speed ($n^{1.5}$)

Mechanical losses; Friction and windage are the basic types of mechanical losses in DC machines, and these are associated with mechanical effects. The windage losses are caused by the friction between the air inside the motor casing and the moving parts of the machine, while the friction losses are the result of the losses at bearings in the machine.

Stray losses (or miscellaneous losses); these are the losses not accounted for by the other losses presented here. No matter how carefully losses are classified, some small energy losses always escape inclusion in one of the above categories. For a common electric machine, a stray loss of 1 percent of full load can usually be considered.

The power diagram in Figure 20 is the most convenient technique to illustrate the power flow of a DC machine. In the generator Figure 20(a) configuration, power input P_{in} enters into the machine, from the P_{in} the stray, mechanical, core, and I^2R losses are subtracted. After that, the remaining power is output in electric power. Furthermore, the electric machine can work as a motor, as shown in Figure 20(b), the most common configuration, where the electric power is converted to mechanical power, as in the case of the generator the same losses are subtracted, and the remaining power is output as mechanical power.

Figure 20 - Power diagrams for the machine

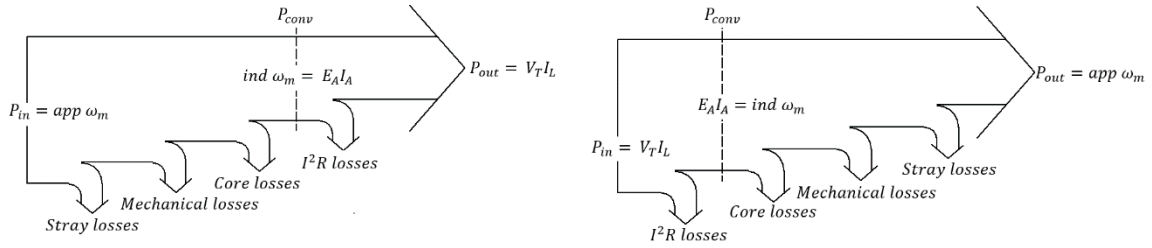

20(a) Generator 20(b) Motor

Source: adapted from (STEPHEN J. CHAPMAN, 2003)

2.2.2. Alternating Current Machines (AC)

AC machine principles are very simple; however, their real construction is somewhat complicated. When operated as generators, these machines are capable of converting mechanical energy to AC electrical energy. Furthermore, when the opposite flow occurs, AC electrical energy is converted into mechanical energy, and the AC machine operates as a motor. In addition, there are two subclasses of AC machines; the Synchronous machines that are going to be discussed in subsection 2.2.2.1, and the Induction machines that will be presented in subsection 2.2.2.2.: (STEPHEN J. CHAPMAN, 2003)

2.2.2.1 Synchronous machines

The field circuit on the AC machine must be supplied by a DC current. For this, there are two approaches to provide the DC current to synchronous machine rotor field windings for their operation: using slip rings and brushes, or using a brushless exciter. The slip rings and brushes approach has lower efficiency because of the voltage drop of the brushes, and their friction. Moreover, the maintenance needed increases considerably, since the slip rings and brushes must be checked regularly. In contrast, rings and brushes are very cost-effective for smaller synchronous machines. On the other hand, since there is no contact between the shaft and the power source in the brushless exciter approach, the motor's maintenance decreases. In scheme Figure 21: "The three-phase output of the exciter generator is rectified to direct current by a three-phase rectifier circuit also mounted on the shaft of the generator,

and is then fed into the main field circuit ". As a consequence, it is possible to control the field current without slip rings and brushes. (STEPHEN J. CHAPMAN, 2003)

Figure 21 - A brushless exciter circuit

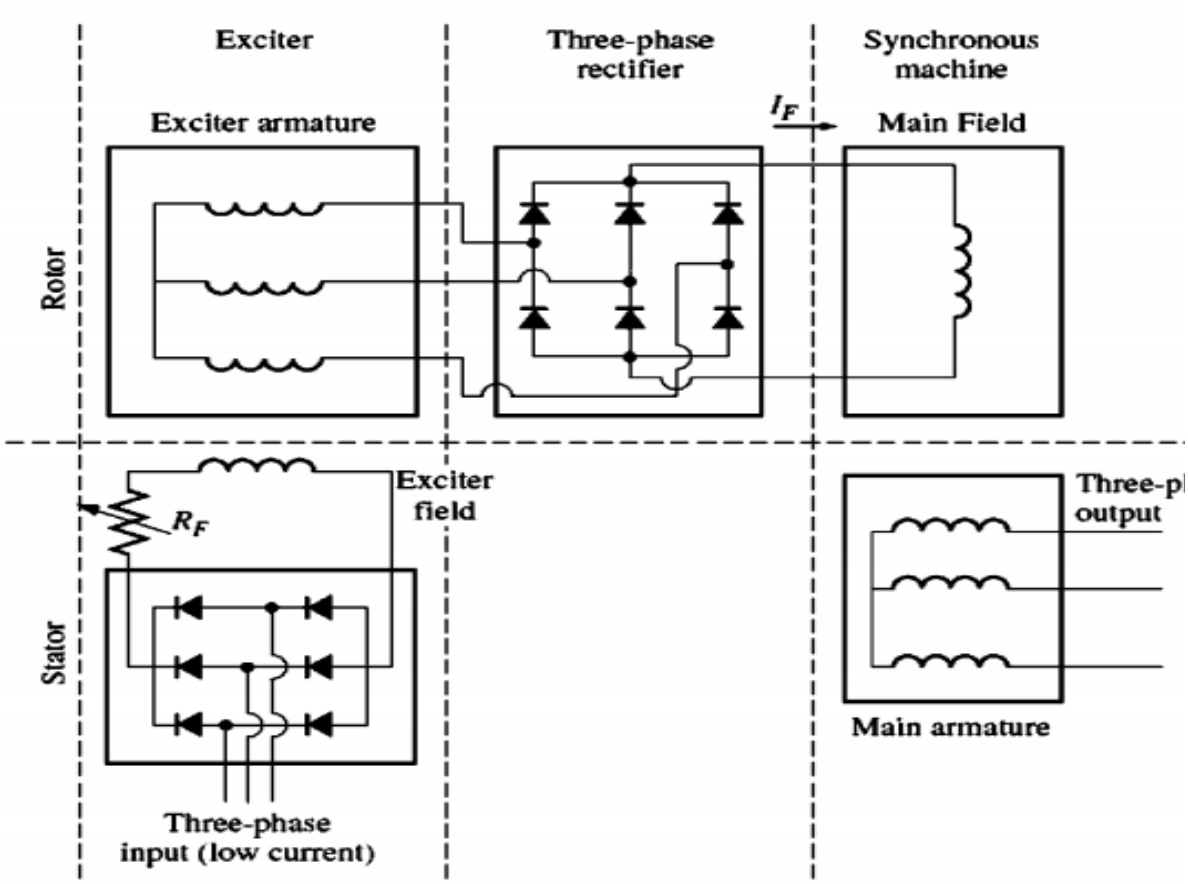

Source: adapted from (STEPHEN J. CHAPMAN, 2003)

To make an AC machine independent of any external power sources, a small pilot exciter can be included in the system, as is shown in Figure 22 that is known as Permanent Magnets (PM) excited. A small pilot is an AC generator with permanent magnets, mounted on the rotor shaft and with a three-phase winding on the stator. As a consequence, no external electric power is required to run the machine as a generator. Furthermore, to deal with possible emergency needs, some machines have both; the slip rings and brushes and the brushless exciter system that are named as Hybrid-field excited in Figure 16.

Figure 22 - A brushless exciter circuit includes a pilot exciter

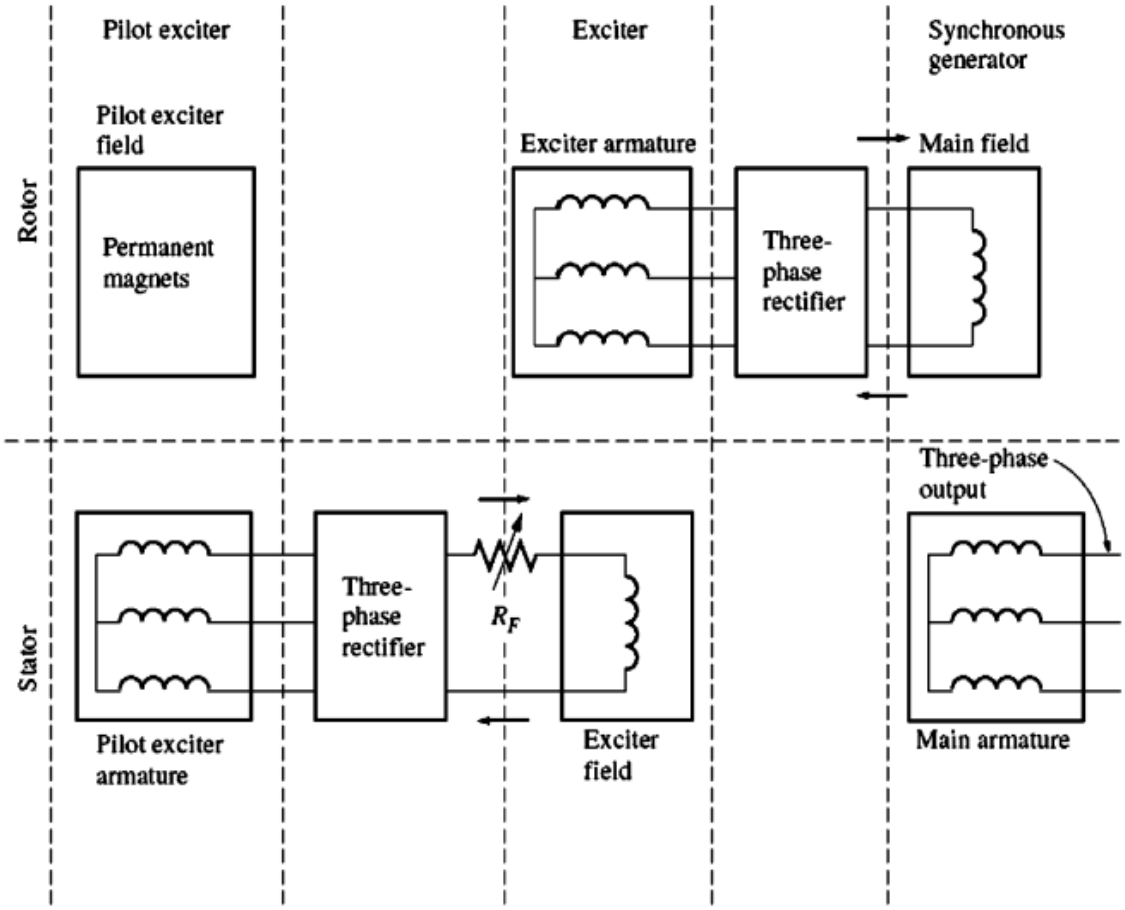

Source: adapted from (STEPHEN J. CHAPMAN, 2003)

To describe the losses of AC machines the same scheme that was applied to DC machines can be used, and in Figure 23 the power diagram is shown. The main difference is that the brush losses do not exist as the AC machines are brushless. Furthermore, the rotor copper losses (RCL) of synchronous machines are the same as DC machines. On the other hand, because of the three-phase synchronous machine characteristic, the stator copper losses (SCL) are given by the equation 6:

$$P_{SCL} = 3I_a^2 R_A \tag{6}$$

Where: P_{SCL} is the stator copper losses; I_a is the current flowing in each armature phase; and R_A is the resistance of each armature phase.

Figure 23 - Power diagrams for the machine

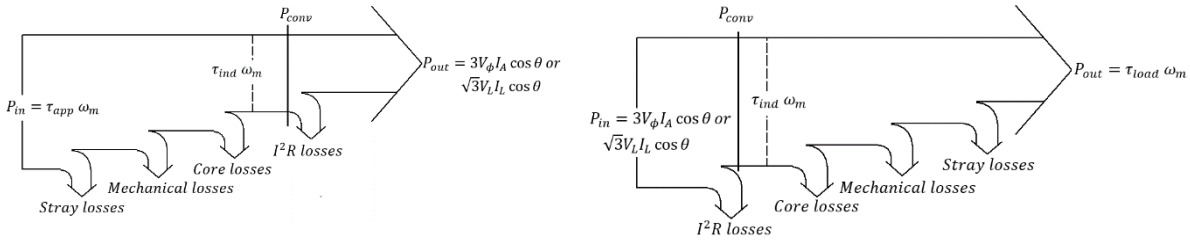

23(a) Generator 23(b) Motor

Source: adapted from (CHAPMAN, 1991)

2.2.2.2 Induction Machines

The main characteristic of an Induction Machine (IM) is the ability to start torque without the field current external supply needs, due to the exclusive amortisseur winding content in these machines. It is called Induction because of the rotor voltage that produces rotor current, and the rotor magnetic field is induced in the rotor windings instead of being physically connected by wires.

Figure 24 - Induction machine rotor construction

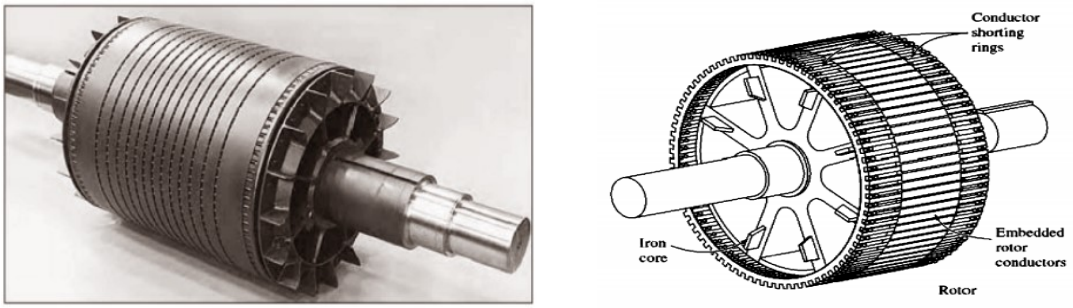

(a) wound rotor (b) Cage rotor

Source: adapted from (STEPHEN J. CHAPMAN, 2003)

The difference between a synchronous machine and an IM is the rotor construction, of which there are two distinct types; the wound rotor and the cage rotor; as shown in Figures 24(a) and 24(b) respectively. The wound rotor is rarely used due to its high cost and high maintenance requirement.

The amortisseur windings are special bars laid into notches carved in the face of a synchronous motor's rotor, and their operating principle is: considering the time zero when the power is first applied the magnetic field B_s is vertical, and as the magnetic field sweeps direction, it induces a voltage in the bars of the amortisseur windings, following the equation 7:

$$e_{ind} = vB\,I \tag{7}$$

Where: the e_{ind} is the induced voltage; v is the velocity of the bar relative to the magnetic field; B is the magnetic flux density vector; and I is the length of the conductor in the magnetic field. The voltage produces a current flow, which results in a winding magnetic field B_w, and as a consequence an induced-torque equation 8:

$$\tau_{ind} = kB_w\,B_s \tag{8}$$

Where: B_s is the stator magnetic field, this torque speeds up the motor progressively. Nonetheless, it will never reach the synchronous speed, which fact is easy to understand, considering that the stator magnetic field is the same as the rotor's speed, and there is no relative motion between B_s and the rotor. Without relative motion, the induced voltage will become zero, so the current flow will be zero, and finally there will not be enough torque in the rotor to keep it turning. Furthermore, the difference between the speed of the magnetic fields η_{sync} and the mechanical shaft speed of the rotor η_m is denoted as slip s, and it is given by the equation 9:

$$s = \frac{\eta_{slip}}{\eta_{sync}} = \frac{\eta_{sync} - \eta_m}{\eta_{sync}} \tag{9}$$

Notice that when the slip is zero, the motor is running at synchronous speed; on the contrary, if s is equal to one, it is stationary. Consequently, the mechanical speed of the rotor can be rewritten in terms of slip as can be seen in equations 10 and 11 respectively:

$$\eta_m = (1 - s)\eta_{sync} \tag{10}$$

$$\omega_m = (1 - s)\omega_{sync} \tag{11}$$

The speed of the magnetic field's rotations is given by:

$$\eta_{sync} = \frac{120\ f_e}{P} \tag{12}$$

Where: P is the machine poles number; η_{sync} is the synchronous speed in rev/min; and f_e is the system frequency in hertz.

The induction motor is similar to the transformer, and it works by inducing voltages and currents in the rotor of the machine. However, unlike the transformers, the frequency of the primary and secondary does not need to be the same, and equation 13 shows the relation between the frequency system f_e in hertz, and the rotor frequency f_r in hertz.

$$f_r = s\ f_e \tag{13}$$

As can be seen, the rotor frequency is directly proportional to the slip. Furthermore, in Figure 25 a diagram is shown of the relationship between the mechanical power output of the IM motor and the electric power input. There are five losses to be taken into account, listed as follows:

1. Stator copper loss (P_{SCL})
2. Core loss (P_{core})
3. Rotor copper loss (P_{RCL})
4. Friction and windage loss (P_{FW})
5. Stray load losses (P_{mins})

Figure 25 - The power-flow diagram of an induction motor

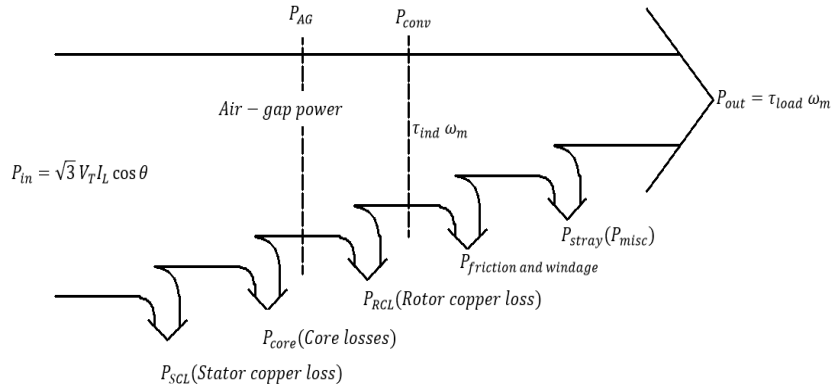

Source: adapted from (STEPHEN J. CHAPMAN, 2003)

The induction motor power P_{in} initial is formed as a three-phase electric voltage and currents. As can be observed in the diagram, the first loss in the initial power is because of the Stator copper loss P_{SCL} and this loss can be calculated by I^2R. Then the hysteresis and eddy currents in the stator are subtracted so that the losses are called Core loss P_{core}. After this, the power remaining is transferred from the stator to the rotor through the air gap between them, and that power is called air-gap power $P_{AG.}$ Part of the P_{AG} power is lost as I^2R losses and are called Rotor copper loss P_{RCL}. Finally, there are some losses such as friction and windage loss P_{FW} to be taken into account, and last but not least, a small part of power is lost without any way to identify it; this power is called Stray load losses P_{mins} and the rest of the power is the output as a mechanical power P_{out} .

2.2.3. Specific BSG machines

According to Baldizzone (2012), the most common machines applied to start-generator machines for BSG application are Switched Reluctance Machines (SRM), Induction Machines (IM), Surface and Interior Permanent Magnet Synchronous Machines (SPMSM and IPMSM). Considering a BSG machine context, the SRMs presents high torque ripples, vibrations and acoustic noise, due to the non-sinusoidal excitation as disadvantages. In contrast, their structure is very robust; the machine cost is low when compared with the other technologies, and its simple construction and the low rotor moment of inertia benefit high-speed operation.

The IM is very well-developed, and its major disadvantage is that at high speeds, the specific torque is relatively low, which fact leads to power capability decreases at high speed. As a consequence, the machine is not capable of providing wide constant power operation; this can be minimized by oversizing the machine and converter ratings or using special control techniques. However, these solutions increase the weight and the cost of the project. On the other hand, IM machines have rugged rotor configuration, low maintenance features, and a wide speed range.

Finally, the permanent magnet machine can present its rotor mounted either on the surface or in the interior, originating two configurations; the Surface and Interior Permanent Magnet Synchronous Machines (SPMSM and IPMSM). Despite its simplicity, the SPMSM presents critical integrity problems, mainly due to the high centrifugal forces at very high speeds. This fact has become a focal point, since BSG applications can hit speeds as high as 20,000 rpm. Furthermore, an extended constant power operation is difficult to achieve due to the electromagnetic characteristics. In addition, it presents problematic packaging because of safety issues caused by the potential existence of high voltage in order to provide high-speed requirements. On the contrary, since the magnets are embedded inside the rotor, the IPMSMs are more robust, and therefore they can achieve higher speeds. Furthermore, the magnets are protected from air gap corrosion and iron dregs. A drawback is that the manufacturing and magnetization processes are more difficult and expensive. Overall, the main advantages of PMSMs are convenient packaging and weight when compared with the other technologies and, because of the absence of field coil losses, their efficiency is high, which leads to a higher torque and power density among the machine typologies considered in this work. The characteristics summary of the machines studied are shown in the Table 1.

Table 1 - Comparison of different machine typologies for BSG application

Electric machine type	IM	SPMSM	IPMSM	SRM
Peak efficiency and compactness		✔	✔	
Low torque ripple and noise	✔	✔	✔	
Easy close loop control	✔	✔	✔	✔
Fewer control sensors	✔			
Wide speed range	✔		✔	✔

Source: adapted from (BALDIZZONE, 2012)

2.3. Electric Energy Storage System (ESS)

Commercial batteries can be dated as early as the end of the 18th century, and since their invention have provided a good solution for energy storage. During most of the twentieth century, the use of automotive batteries was basically limited to: powering electronics, lights, and vehicle starting. In contrast, in the twenty-first century, the electrification of automobiles has been shown as a partially feasible solution to mitigate environmental concerns. As a consequence, the use of batteries for this end has been substantially increasing, as can be seen in Table 2, where many commercial electrified vehicles are presented. (EHSANI; GAO; EMADI, 2017)

Table 2 - Battery Types Used in Selected Electrified Vehicles

Company	Country	Vehicle Model	Battery Type
GM	United States	Chevy-Volt, Spark	Li-ion
		Saturn Vue Hybrid	NiMH
Ford	United States	Escape, Fusion, MKZ HEV	NiMH
		Escape PHEV, and Focus EV	Li-ion
Toyota	Japan	Prius, Lexus	NiMH
		Scion iQ EV, RAV4 EV	Li-ion
Honda	Japan	Civic, Insight	NiMH
		Fit EV	Li-ion
Hyundai	South Korea	Sonata	Li-polymer
Chrysler/Fiat	United States	Fiat 500e	Li-ion
BMW	Germany	X6	NiMH
		Mini E, ActiveE	Li-ion
BYD	China	E6	Li-ion
Daimler Benz	Germany	ML450, S400	NiMH
		Smart EV	Li-ion
Mitsubishi	Japan	iMiEV	Li-ion
Nissan	Japan	Altima	NiMH
		Leaf EV	Li-ion
Tesla	United States	Roadster, Model S, Model X, Model 3, Model Y	Li-ion
Think	Norway	Think EV	Li-ion/SO-NI-CL
Iveco	Italy	Electric Daily	SO-NI-CL

Source: adapted from (EMADI, 2014)

In this context, a large amount of research has been carried out in order to improve the energy density, power density, durability, safety, and affordability, not only for a single battery, but for all storage systems called electrical Energy Storage System (ESS). The critical factors for ESS development are briefly described below: (EMADI, 2014)

1. Safety: Ensure ESS operation is safe, no risk of thermal runaway, or exothermic behavior in the event of a crash or short circuit

2. Cycle life: The number of full charge/discharge cycles until the ESS reaches end-of-life (EOL) condition; the definition of EOL varies with the usage of the ESS. One commonly used EOL condition is a battery remaining capacity at 80% of its beginning-of-life (BOF) capacity
3. Calendar life: The calendar longevity of the ESS when it is in storage (months or years)
4. Energy density: The amount of energy each kilogram or liter of ESS contains (W/L and W/kg)
5. Power density: The amount of power each kilogram or liter of ESS delivers per second (W/L and W/kg)
6. Charge acceptance capacity: The amount of energy the ESS can absorb per second (W/kg and W/kg)
7. Cost: The cost in dollars ($) per kWh

The main battery technologies applied to Energy Storage System ESS are lead-acid, nickel-metal hybrid, lithium-ion, and sodium nickel chloride, and will be shortly discussed in subsection 2.3.1. Furthermore, the discussion regarding ultracapacitor cells solution is presented in subsection 2.3.2. Finally, the main configurations of ESS and its components will be shown in 2.3.3.

2.3.1. Electrochemical Cells (Batteries)

These batteries operate by converting electrical energy into chemical energy through a pair of reduction-oxidation (redox) reactions and vice versa. Basically, in batteries one pole suffers oxidation while the other is reduced. As these reactions take place in different places, the electrons must travel from one pole, known as the cathode, to another called the anode. The electrons' movement can be used to generate work.

The batteries consist of a set of electrochemical cells connected in series, parallel or series-parallel. The general classification of the electrochemical cells electrolytic cells and galvanic cells. The main characteristic of a galvanic cell is that it is a spontaneous redox reaction, and it is known as non-rechargeable. On the other hand, electrolytic cells have non-spontaneous redox. A rechargeable cell works as a galvanic cell when discharged and as an electrolytic cell when charged. (EHSANI et al., 2018)

Table 3 - Comparison of Electrical Energy Storage Technologies

	Lead Acid	**NiMH**	**Li -ion**	**Na-Ni-Cl**
Specific energy (Wh/kg)	30-50	60-120	100-265	100-120
Energy density (Wh/L)	50-80	140-300	250-730	150-180
Specific power (Wh/kg)	75-300	250-1000	250-340	150-200
Power density (W/L)	10-400	80-300	100-210	220-300
Round-trip efficiency (%)	70-80	60-70	85-98	85-90
Self-discharge (%/day)	0.033-0.3	25-30	0.1-0.3	15
Cycle lifetime (cycles)	100-2000	500-1000	400-1200	2500
Power capacity Cost ($/kW)	175-600	150-1500	175-4000	150-300
Energy capacity Cost ($/kW)	150-400	150-1500	500-2500	150-200

Source: adapted from (EMADI, 2014)

In general, the battery characteristics depend directly on the chemical materials used in its construction, and in Table 3 the comparison of the most used battery technologies in the market is presented, as can be verified in Table 2 in section 2.3.

Among the parameters in Table 3, the most commonly used to compare different batteries are the specific energy density and the specific power density. By plotting the values of energy density (in Wh/kg) versus power density (in Wh/kg), a commonly used plot for performance comparison is obtained. This chart is known as a Ragone plot and is presented in Figure 26. (EMADI, 2014)

Figure 26 - Ragone chart

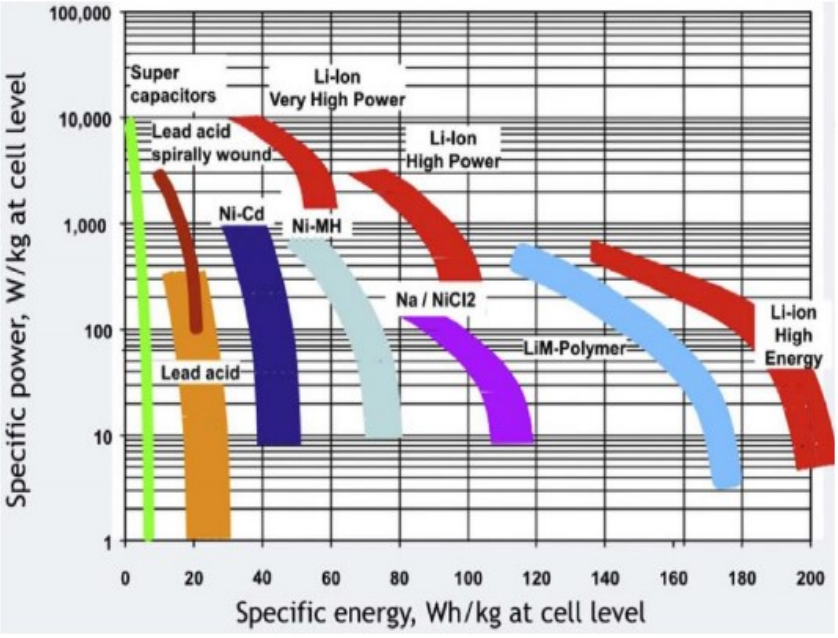

Source: adapted from (EMADI, 2014)

2.3.1.1 Lead-acid

The Lead-acid battery is the most common and mature technology for conventional automotive use, and it is responsible for providing energy for the spark ignition, vehicle starting, lighting, and auxiliary loads. It has the lowest cost (150-400 USD/kWh), good life cycles (100-2000 cycles), and relatively high power capability. On the other hand, this technology has low specific energy (30-50 Wh/kg) and low calendar life. In addition, it is dangerous for human health due to its corrosive sulfuric acid fluid.

EVs and HEVs specific lead-acid batteries have been developed to overcome the disadvantages of this technology. Lead-acid batteries with specific energy over more than 40 Wh/kg, with the possibility of rapid charge (50% capacity in 8 minutes and 100% in less than 30 minutes), competitive cost, high specific power (285 W/kg) are reported in the literature. (EHSANI et al., 2018; EMADI, 2014)

2.3.1.2 Nickel-metal hybrid

As with the Lead-acid battery, the Nickel-metal hybrid type is a mature technology mainly used among hybrid vehicles. As can be observed in Table 2, almost half of the vehicles cited in the Table use Nickel-metal hybrid batteries. Note that the Toyota Prius, the most popular hybrid, uses the Na-Ni-Cl type. On the other hand, this type of battery presents a high self-discharge ranging from 25% to 30% per day. In addition, it has a high cost (150-1500 USD/kWh); however, it is still lower than the Li-ion. Moreover, the Nickel-metal hybrid has an intermediary specific energy (60-120 Wh/kg) and a very good specific power (250-1000 Wh/kg). (EHSANI et al., 2018; EMADI, 2014)

2.3.1.3 Lithium-ion

Lithium-ion batteries present a very high thermodynamic voltage, and as a result, high specific energy (100-265 Wh/kg), and specific power (250-340 Wh/kg). This explains why Lithium-ion technology is considered to be the most promising battery technology. Besides these characteristics, it also presents high Energy density (250-730 Wh/L); and low

self-discharge (0.1-.03 %/day). On the other hand, the worst drawback of Li-ion batteries is the possible catastrophic failure, which can occur in the event of overcharging or over-discharging. In the event of overcharging, the internal pressure can build up, causing cell swelling. In addition, in the event of over-discharging, there is a potential risk of an internal short circuit, leading to a fire. To face these issues, there are common safety features in these batteries, such as thermal interrupts, and external short-circuit interrupting. (EMADI, 2014)

Furthermore, different types of chemistries are applied to Lithium-ion batteries, such as: Lithium-ion Lithium Polymer; Lithium Iron Phosphate; Lithium Manganese Cobalt; Lithium Nickel Cobalt and Aluminum; and Lithium Cobalt Oxide. The main advantages and disadvantages of each Lithium-ion battery type are presented in Table 4.

Table 4 - Comparison of different Lithium-ion battery technologies

Technology	**Advantages**	**Disadvantages**
Lithium Polymer (LiMnO4)	Power density	Calendar life
Lithium Iron Phosphate (LiFePO4)	Safety	Energy density, calendar life
Lithium Manganese Cobalt (NMC)	Power and energy density, cycle, and calendar life	safety
Lithium Nickel Cobalt and Aluminum (NCA)	Power and energy density, cycle, and calendar life	safety
Lithium Cobalt Oxide (LiCoO2)	Power and energy density	safety, cost

Source: adapted from (PENHA, 2019)

2.3.1.4 Sodium nickel chloride

Commercially known as ZEBRA batteries, sodium nickel chloride is a relatively young technology, invented about 25 years ago. Its main characteristic is the molten salt electrolyte, which technology represents an improvement over its older derivative of sodium-sulfur batteries, since sulfur replacement eliminates much of its safety concerns. Moreover, ZEBRA cells operate between 270 ºC and 350 ºC temperature, which characteristic raises the self-discharge (about 15% a day) loss as the high temperature has to be maintained, even in stand-by. To face this possible issue, a special pack design and insulation is employed to deal with the thermal consideration. Even with the special pack design, ZEBRA presents a

relatively low cost (150-300 USD/kWh). Furthermore, ZEBRA batteries have intermediate, specific energy and Energy density, between (100-120 Wh/kg) and (150-180 Wh/kg), respectively. Moreover, the disadvantage of low specific power (150-200 Wh/kg) can be solved by using them together with an ultracapacitor. (EMADI, 2014)

2.3.2. Ultracapacitor Cells

Ultracapacitors (UC), also called Supercapacitors, are characterized by their lower specific energy density and higher specific power density, as can be seen in Table 5. A capacitor is a component that stores energy electrostatically in an electric field. In addition, it consists of two plates separated by a dielectric material. Ultracapacitors are storage components that apply electrostatic-based principles, but with a higher capacitance than conventional capacitors. Furthermore, an ultracapacitor can achieve much higher energy densities when compared with a conventional capacitor, and much higher power densities.

Table 5 - Typical characteristics of ultracapacitor cells (UC)

	Voltage Cell (V)	**Energy density (Wh/kg)**	**Power density (W/kg)**	**Cycle lifetime (Times)**
UC	2.5/2.7	2-20	4000-10.000	Over 1,000,000

Source: adapted from (CAO; EMADI, 2012)

2.3.3. ESSs Configuration and control components

As was previously mentioned, the battery and UC can be used together or separately to provide power to the vehicle. However, additional components are required to control the energy flow, and all components required are known as an energy storage system (ESS). Two ESS configurations are battery-based ESS, and Hybrid ESS (HESS). The battery-based energy storage systems are the most widely used. However, providing the vehicle peak power demand presents several challenges. The common solution for demand issues is to increase the size of the battery, but this causes an increase in the cost and weight of the vehicle. On the other hand, the HESS is a feasible solution to achieve better overall performance. The basic idea of HESS is to combine the UCs with batteries and, as a consequence, take the best

advantage of each energy storage: the high power density of UCs, and the high energy density of batteries. (CAO; EMADI, 2012)

Over the past few decades, different hybrid topologies have been studied. The main types are basic passive parallel; UC/Battery configuration; Battery/UC configuration; cascaded configuration; multiple converter configuration; and multiple input converter configuration. Among them, each one has its characteristics, and in this work, we will focus on the UC/Battery configuration and the Battery/UC configuration.

The Battery/UC configuration in Figure 27: (a) is marked by the battery voltage control, and in this schema, it is possible to maintain the voltage lower or higher than the UC Voltage. Furthermore, the UC is linked directly to the inverter and works as a low-pass filter. In addition, in this configuration, the UC energy is used more effectively because of the control strategy applied to this topology.

By switching the position of the UC and Battery in the Battery/UC configuration, the UC/Battery configuration HESS is shown in Figure 27: (b) uses a bidirectional DC/DC in order to electronically, interface the UC, and a wide range of voltage can be used in the UC. The main disadvantages of these configurations are the size of the bidirectional converter, and the battery voltage cannot be varied because it is connected directly to the DC link. (CAO; EMADI, 2012)

Figure 27 - ESS configurations

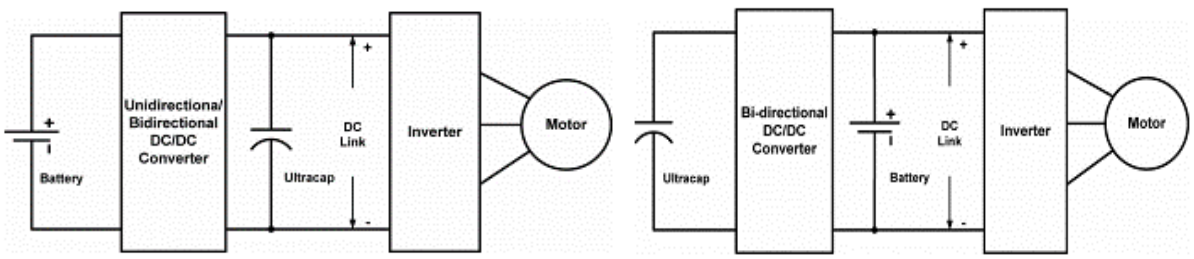

(a) Battery/UC configuration (b)UC/Battery configuration

Source: adapted from (CAO; EMADI, 2012)

As can be seen in Figure 27(a), conventional HESS is mainly formed of five components, the battery and UC already discussed in 2.3.1 and 2.3.2, respectively, the unidirectional/bidirectional DC/DC converter, DC Link, and Inverter. The last three components can be called electronic power converters.

To operate a motor in EVs and HEVs it is necessary to transfer energy from onboard source(s) to the motor. Electronic power systems are the technologies that allow the control of the energy flow and combine the contribution from electronic, magnetic, and electrochemical components. Several different types of components can be used in electronic power systems. Here, a short review of the most widely used is given. (MI; MASRUR; GAO, 2011)

2.3.3.1 Power convertes

The components are commonly classified by their inputs and outputs, as it is possible to switch between direct current (DC) and alternating current (AC), there are four main types of power converters:

- DC-DC converter
- DC-AC inverter
- AC-DC rectifier
- AC-AC cycloconverter

2.3.3.2 Main circuit

Composed of semiconductor devices (diodes and switches) and peripheral circuits, the main circuits are controlled to turn off and turn on at a wide frequency range. Considering the voltage system level, both Metal Oxide Field Effect Transistors MOSFETs and Insulated Gate Bipolar Transistors IGBTs can be used.

2.3.3.3 Filtering circuit

An LC low-pass filter to filter out the high-frequency components of the output voltage and let the low-frequency DC part pass to the load side is usually needed in electronic power converters.

2.4. Internal Combustion Engines

According to HEYWOOD (2018), “the main purpose of internal combustion engines (ICE) is to produce mechanical power from the chemical energy contained in the fuel”. This chapter aims to review the fundamentals of fuels used to supply engines, and ICEs, specifically spark-ignition (SI) engines, usually called Otto engines, the name of the most common operating cycle for this type of engine, though other cycles can be used. The Otto is a reference of Nicolaus August Otto (1832-1891), who introduced the more successful internal combustion engine development in 1876 of the Otto four-stroke, it reached an efficiency of up to 14%, which was a remarkable value for the time. In 1886 Karl Benz and Gottlieb Daimler developed simultaneously and independently light engines with high speed, from which modern gasoline engines originated. Almost 50,000 of these engines had been sold in the United States and Europe by 1890, representing the breakthrough of the internal combustion engine.

Another very well-known engine is called Compression Ignition (CI), and it appeared in 1892 when Rudolf Diesel launched his first model of a CI engine. Its main characteristic is the absence of a spark to initiate the combustion, and the ignition resulted from the high pressure and temperature during the compression. Furthermore, in CI engines combustion occurs at constant pressure. In contrast to CI, SI engines are characterized by spark ignition to initiate the combustion that occurs in a constant volume. Moreover, the SI and CI classifications should be used only as a reference to understand the ICE operation modes, since there are dual models that present both characteristics, spontaneous ignition combustion and spark ignition combustion. Although CI engines are important, they are not going to be deeply discussed in this work. (EM, 2006; BAETA, 2006)

The typical four-stroke SI engine works by the operation of four pistons, and to demonstrate its basic operation, imagine a single piston that is connected by a rod and crank mechanism as shown in Figure 28. Notice that the maximum volume of the cylinder or total volume "V $_t$" in dm^3 is achieved when the piston is at the Bottom Dead Center (BDC). The total volume is the sum of the displacement volume "V $_d$" in dm^3 and the clearance volume "V $_c$" in dm^3. Furthermore, the compression ratio is given by the ratio between these two volumes, and is given by equation 14:

$$r_c = \frac{maximum\ cylinder\ volume}{minimum\ cylinder\ volume} = \frac{V_d + V_c}{V_c} \tag{14}$$

On the other hand, when the piston is at the Top Dead Center (TDC) position, the minimum cylinder volume, that position is called clearance volume "V $_c$"

Figure 28 - Basic geometry of the reciprocating internal combustion engine

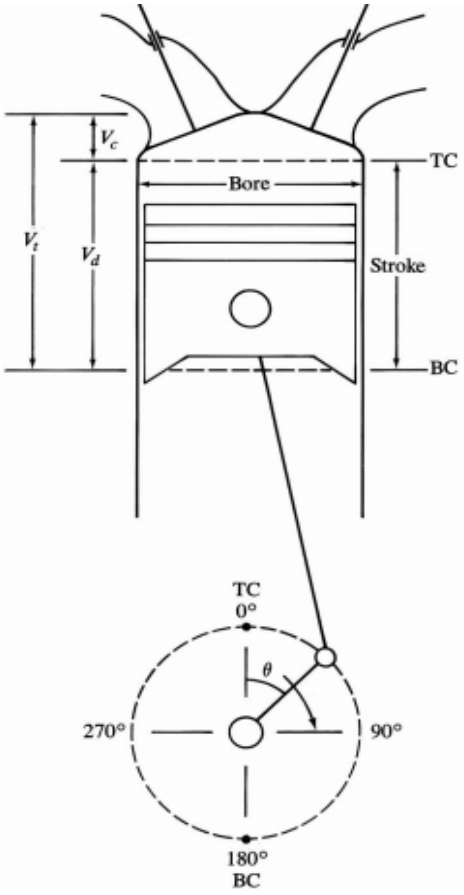

Source: adapted from (HEYWOOD, 2018)

2.4.1. Otto Cycle Engine Fundamentals

The four-stroke cycle is presented in Figure 29. In this cycle, each power stroke requires two crankshaft revolutions. The four phases of the four-stroke cycle are described next:

Figure 29 - The four-stroke operation cycle

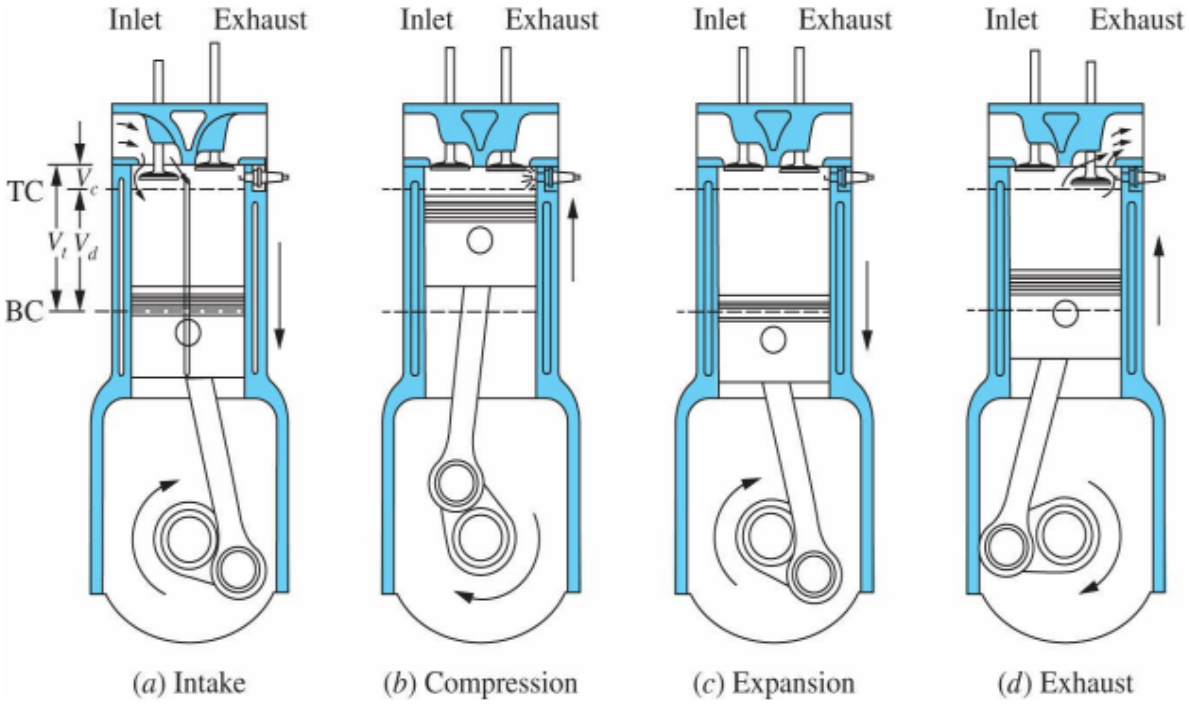

Source: adapted from (HEYWOOD, 2018)

a. In the intake phase, a fresh mixture is drawn into the cylinder, while the piston is displaced from the TDC to the BDC, and during this phase, the inlet valve is maintained open.
b. In the compression stroke, the mixture is compressed due to the piston displacement from the BDC to the TDC while both valves are closed, at the end of the displacement the combustion starts, and the cylinder pressure rises quickly.
c. In the expansion stroke, also called the power stroke, work is generated as a result of the combustion. The piston displaces from the TDC to the BDC because of the high internal pressure and temperature, and as a consequence, the crank is forced to rotate and generate work.

d. In the exhaust stroke, the burned gases are expelled from the cylinder, first by the difference of pressure, and then the piston displacement from the BDC to the TDC. During the process, the exhaust valve remains open to let the gases leave the cylinder.

The four-stroke ideal air cycle PV diagram is shown in Figure 30. To simplify the analysis, several assumptions are applied to the four-stroke process.

Figure 30 - Otto cycle PxV diagram

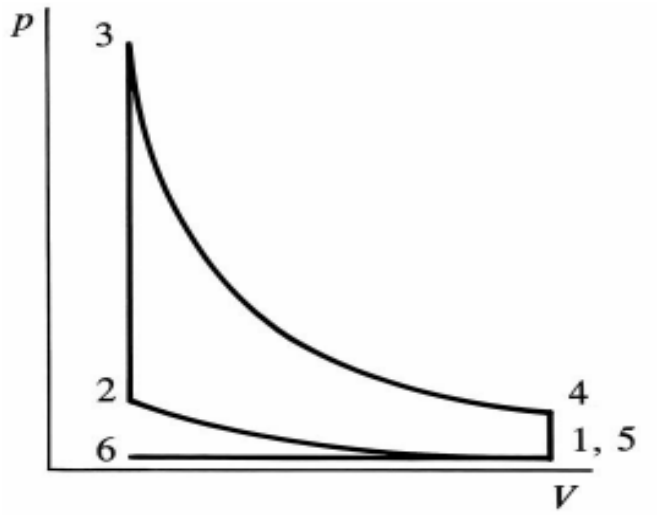

Source: adapted from (HEYWOOD, 2018)

- The compression (1→2) is assumed as isentropic so adiabatic, and reversible.
- The combustion (2→3) is assumed as adiabatic, constant volume combustion, and the combustion is complete ($\eta_c = 1$).
- The Expansion (3→4) is assumed as isentropic so adiabatic, and reversible.
- The Exhaust (4→5→6) and Intake (6→7→1) are assumed as adiabatic, the valve events occur at the BDC and the TDC respectively, velocity effects are negligible, exhaust and intake pressure are constant, and there is no change in cylinder volume as pressure differences across open valves drop to zero. (HEYWOOD, 2018)

In addition, it is considered that the working fluid behaves as a perfect gas. Note that heat is added to the system in the combustion process (2→3), and it will be called: Q_{23}. Furthermore, heat is rejected by the system in part of the exhaust process (4→5), and it will

be called: Q_{45}. In addition, the fluid's specific heats are considered constant and equal to the air. After all assumptions the mass of air that is transferred by the heat are:

$$Q_{23} = m * c_v (T_3 - T_2) \tag{15}$$

$$Q_{45} = m * c_v (T_5 - T_4) \tag{16}$$

Where: Q the heat referent to the sub-index is: m is the mass, c_v is the specific heat at constant volume, and T is the temperature referent to the sub-index.

Therefore, equation 17 gives the efficiency of the Otto cycle:

$$\eta_{Otto} = \frac{W}{Q_{23}} = \frac{Q_{23} + Q_{45}}{Q_{23}} = 1 - \frac{Q_{41}}{Q_{23}} = 1 - \frac{T_4 - T_1}{T_3 - T_2} \tag{17}$$

The isentropic processes compression (1→2) and Expansion (3→4) are represented by equations 18 and 19 respectively:

$$\frac{T_2}{T_1} = \left(\frac{v_1}{v_2}\right)^{k-1} = {r_c}^{k-1} \tag{18}$$

$$\frac{T_3}{T_4} = \left(\frac{v_3}{v_4}\right)^{k-1} = {r_c}^{k-1} \tag{19}$$

Where: v is the volume, r_c is the compression ratio, and k is equal to the $\frac{c_p}{c_v}$, in other words the ratio between the specific heat. Finally, considering $v_1 = v_4$ and $v_2 = v_3$, the Otto's cycle efficiency can be rewritten as equation 20:

$$\eta_{Otto} = 1 - \left(\frac{v_1}{v_2}\right)^{k-1} = 1 - \frac{1}{{r_c}^{k-1}} \tag{20}$$

Note that the four-stroke ideal air cycle overestimates thermal efficiency. In Figure 31 a comparison between the ideal cycle and the real cycle is presented. According to GIACOSA (1986), and HEYWOOD (2018), there are five main differences between them: Heat transfer, Finite combustion time, Valve losses, and Pumping work. They are explained next.

Figure 31 - Comparison between the theory and indicated Otto cycles

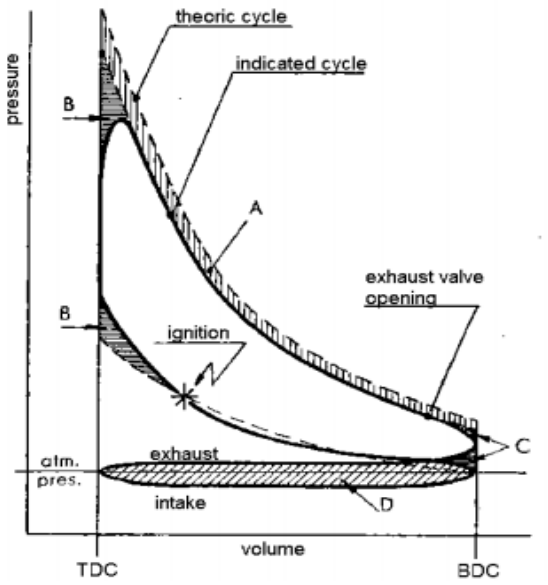

Source: adapted from (GIACOSA, 1986)

1. *Heat losses* - The process of heat loss to the cylinder walls during combustion, and the heat transfer from the burned gases are neglected by the ideal cycle approach. Furthermore, the loss of heat during combustion decreases the peak of pressure in the real cycle, as can be seen in Figure 31 in the higher letter marked as “B”. Due to these heat losses, the efficiency decreases considerably. Moreover, the compression and expansion processes considered adiabatic in the ideal cycle are actually polytrophic processes.
2. *Finite Combustion time* - In an ideal cycle it is assumed that combustion occurs in a constant volume, hence, as it is instantaneous, this fact does not represent reality. For instance, in an SI engine, the combustion typically starts 10 to 40 crank angle degrees before TDC, as is shown in Figure 31 as “ignition”, and is half complete at about 8 after TDC, and is finished 30 to 40 after TDC. Furthermore, the peak pressure occurs between TDC and exhaust blowdown - Usually, in a real cycle, the exhaust valve is

opened 50 degrees before the BDC to reduce cylinder pressure to the manifold pressure before the exhaust process begins, as shown in Figure 31 as “exhaust valve opening”. Consequently, the pumping work is reduced; however, at this time the exhaust gases have high enthalpy, which leads to a decrease in thermal efficiency.

3. *Pumping works* - This is the necessary work to overcome the pressure difference between the interior of the cylinder and the manifold, and it is represented in Figure 31 by letter “D”.

Besides the differences already explained, HEYWOOD (2018) pointed out two further differences; the crevice effects and leakage, which are the gas losses due to high internal pressure. That gas can be lost by engine leakage, but is usually really small in a well-designed and maintained engine. In addition, the other fact is the gas that flows into crevices such as the regions between the pistons. In both cases the cylinder pressure reduces, and as a consequence, the engine efficiency decreases. The other point is incomplete combustion; the chemical energy released in an actual engine is 5% less than the chemical energy of the fuel inducted into it. This happens due to the combustible species contained in the exhaust gases.

Figure 32 - Ignition timing in the indicated Otto cycle

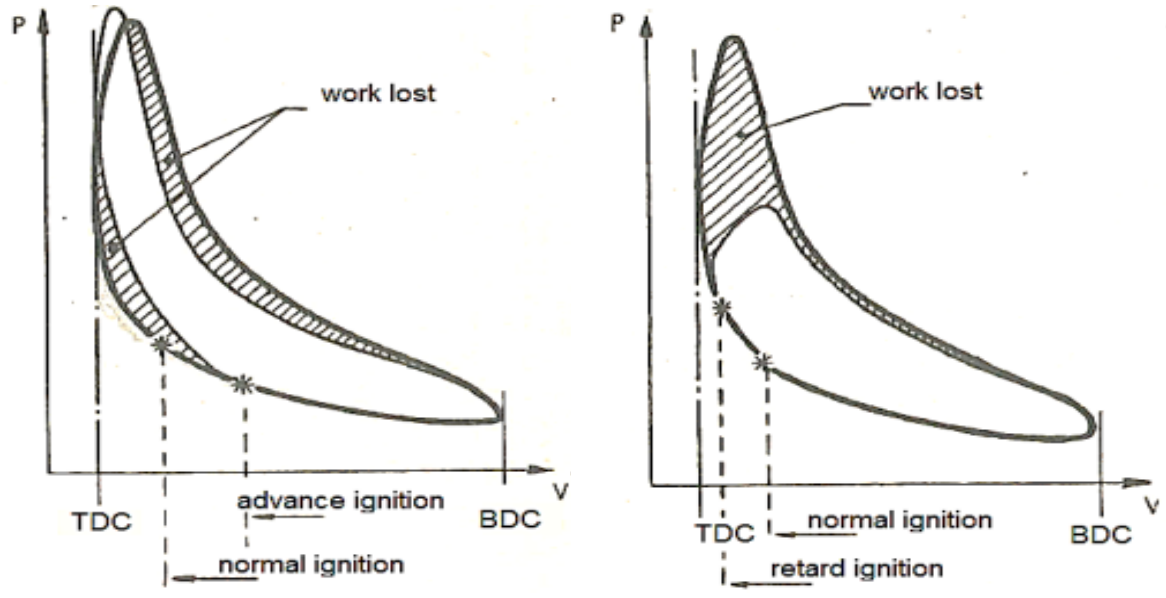

(a) Advanced ignition (b) Retarded ignition

Source: adapted from (GIACOSA, 1986)

Ignition timing is a complicated decision, since if it is not set to the optimum point, net work will be lost. In the case of an early spark, also called advanced ignition, in Figure 32 (a), most of the combustion will be developed before TDC, and as a result, the pressures are higher than normal; consequently, the compression work will increase, and the net work will decrease. On the other hand, a late spark is known as retarded ignition, Figure 32(b), when most of the combustion will occur after TDC, decreasing considerably the net work. This point is determined by empirical experiments.

Concerning the valve losses, the positions of Intake Valve Opening (IVO) and Intake Valve Closing (IVC) are directly proportional to the engine speed; the valve opening (IVO) happens after the piston reaches the top (TDC), and the higher the engine speed, the greater the valve opening advance (IVO). In addition, higher IVC delay should be applied at higher engine speed, and this happens mainly because of the higher fluid inertia during the intake process at higher speeds. Furthermore, the Exhaust Valve Opening (EVO) should be advanced to reduce internal cylinder pressure, as the Exhaust Valve Close (EVC) is usually delayed due to the inertia of the gases. (GIACOSA, 1986)

A pressure curve of a random SI engine operating cycle is shown in Figure 33. The peak pressure is different for each cycle, and in each cylinder because of the combustion process variation. Note the difference between the (dashed lines) without combustion and the (solid line) with combustion; the peak pressure with combustion is much higher than in the combustion profile. To maximize the maximum pressure, the IVO, IVC, EVO, EVC, and the spark timing need to be carefully adjusted.

Figure 33 - Events sequence in an SI engine operating cycle

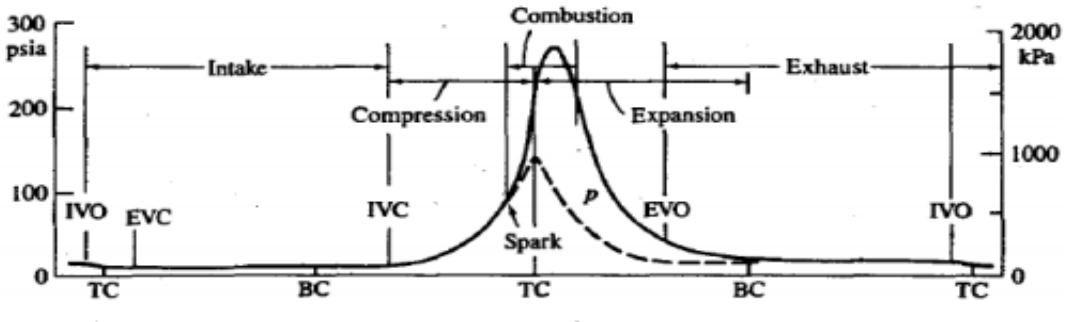

Source: adapted from (GIACOSA, 1986)

The indicated work per cycle is obtained by the p-V curve (Figure 33) integration, and it is given by equation 21. There are two approaches to the indicated work: the gross indicated work per cycle, and the net indicated work per cycle. While the gross work considers only the compression, and combustion, as is indicated in Figure 34 (blue part or region A), the net work takes into account the effects of the compression, combustion, exhaust, and intake processes, and is also indicated in Figure 34 as the summing of the regions (A+B).

Figure 34 - Naturally-aspirated four-stroke cycle engine at part load

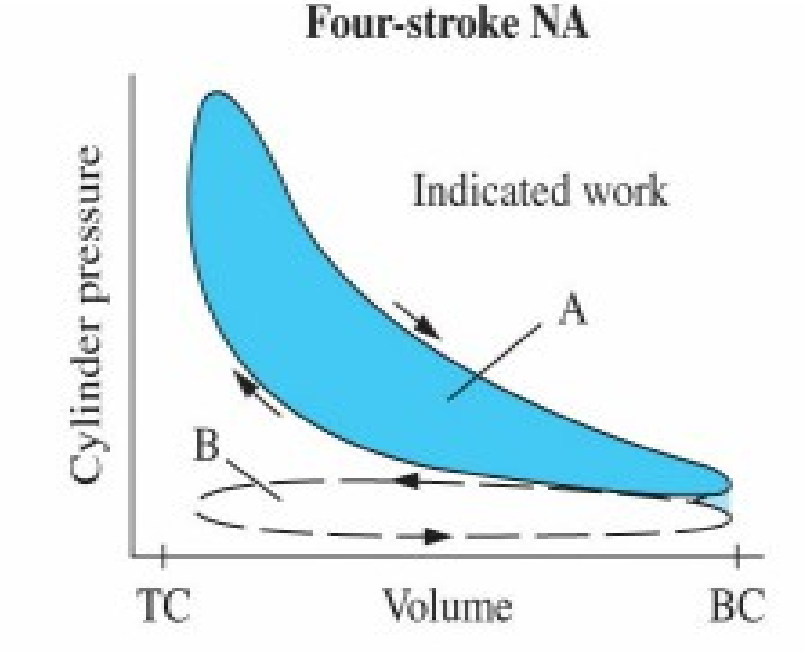

Source: adapted from (HEYWOOD, 2018)

$$W_{c,i} = \int p \, dV \tag{21}$$

The indicated power per cylinder is the rate of work transfer from the gas within the cylinder to the piston, and it is calculated by equation 22:

$$P_i = \frac{W_{c,i} \, N}{2} \tag{22}$$

Where: P_i is the indicated power per cylinder, $W_{c,i}$ is the indicated work per cylinder, and N is the crankshaft rotational speed in rev/s. Note that the indicated power differs from the brake power because it does not take into account the power needed to overcome engine pumping work, essential engine accessories, and engine friction. Furthermore, an alternative to estimate the gross indicated power "P_{gi}" is by equation 23, where P_b is the brake power, and P_f is the power used to overcome friction:

$$P_{gi} = P_b - P_f \tag{23}$$

The friction power P_f is the portion of the work per cylinder used to overcome the friction of the mechanical components of the engine, pistons, and bearings, and to drive the essential engine accessories. On the other hand, the brake power P_b is the usable power delivered by the engine to the load. Furthermore, the ratio between the brake power by the gross indicated power is known as the mechanical efficiency η_m, and it represents the relative importance of engine friction. The mechanical efficiency is presented in equation 24:

$$\eta_m = \frac{P_b}{P_{gi}} = 1 - \frac{P_f}{P_{gi}} \tag{24}$$

An effective engine performance measure is called Mean Effective Pressure (MEP). This measure allows the comparison of different engines independent of their characteristics, for instance, engine size. When mep is calculated from the indicated brake work per cylinder, it is called bmep, and in case mep is calculated with friction work per cylinder, it is known as fmep. Furthermore, the bmep can be expressed in terms of torque as can be seen in equation 25:

$$bmep = \frac{6.28\, n_R T}{V_d} \tag{25}$$

Where: $bmep$ is brake mean effective pressure in kPa, T is torque in Nm, V_d is the displacement volume in dm^3, and n_R is the number of crank revolutions (n_R is equal 2 in case of four-stroke cycles).

Another useful parameter during engine tests is the specific fuel consumption sfc. This is the fuel flow rate per unit power output, and it can measure how efficiently an engine is using the fuel supplied to produce work at a specific operating condition. The sfc is given by equation 26 in g/Wh.h, where m_f is the flow per unit time in g/h, and P is engine Power in kW:

$$sfc = \frac{m_f}{P} \tag{26}$$

Furthermore, the ratio of the work produced per cycle W_c in MJ to the amount of fuel chemical energy supplied per cycle that can be released in the combustion process is known as fuel conversion efficiency η_f unitless, and it is given by:

$$\eta_f = \frac{W_c}{m_f \, Q_{HV}} \tag{27}$$

Where: Q_{HV} is the heating value of a fuel in MJ/kg, and m_f is the mass of fuel injected per cycle in Kg. equation 28 gives the same efficiency in terms of sfc:

$$\eta_f = \frac{3600}{sfc \; (g/kW.h) \; Q_{HV}(MJ/kg)} \tag{28}$$

Due to the incomplete actual combustion process, the energy supplied to the engine per cycle is not fully released as sensible or thermal energy. When adequate air is present in the cylinder to oxidize the fuel completely, the release of fuel energy can reach 95% or more. On the other hand, if there is not enough air in the cylinder to completely oxidize the fuel, a lack of oxygen will prevent this supplied fuel energy from being fully released. For this reason, during an engine test the ratio between the air flow rate m_a , and the fuel mass flow rate are normally measured in order to remain optimal. The air/ fuel ratio known as (A/F) is presented in equation 29. In addition, the inverted ratio is called the Fuel/ air ratio and it is given in equation 30. Finally, a conventional SI engine using gasoline fuel presents a normal operating range $12 \leq A/F \leq 15$ ($0.067 \leq F/A \leq 0.083$):

$$Air/fuel\ ratio\ (A/F) = \frac{m_a}{m_f} \tag{29}$$

$$Fuel/air\ ratio\ (F/A) = \frac{m_f}{m_a} \tag{30}$$

The intake air process has various systems; the air filter, intake duct, throttle plate in a SI engine, intake manifold, intake port, and intake valve. These systems restrict the amount of air that an engine can induct, and as a consequence, the combustion process is affected. Moreover, during tests, a parameter is used to measure the effectiveness of an engine to intake air, which is called volumetric efficiency, and it is given by equation 31:

$$\eta_v = \frac{m_a}{\rho_{a,i}\, V_d} \tag{31}$$

Where: m_a is the mass of air inducted into the cylinder per cycle in Kg, $\rho_{a,i}$ is the inlet air density in Kg/m^3, and V_d is the displacement volume in m^3.

Finally, the power can be obtained in equation 32:

$$P = \frac{\eta_f \eta_v N V_d Q_{HV} \rho_{a,i} (F/A)}{2} \tag{32}$$

Where: η_f is the fuel conversion efficiency unitless, η_v is the volumetric efficiency unitless, N is the engine speed in revolutions per minute, V_d is displaced volume in m^3, $Q_{HV}$is the heating value of the fuel in MJ/kg, $\rho_{a,i}$ is the air density at intake in Kg/m^3, and (F/A) is the air-fuel ratio unitless. Also, the torque τ is given in equation 33:

$$\tau = \frac{\eta_f \eta_v V_d Q_{HV} \rho_{a,i} (F/A)}{4\Pi} \tag{33}$$

2.4.2. Otto Cycle Engines Performance

The engine performance is affected by many different aspects, and some of these are going to be pointed out hereafter. The compression ratio given in equation 14 is the ratio between the total volume of the cylinder and the clearance volume of the cylinder. Several processes are influenced by changes in compression ratio, namely; friction, heat transfer, combustion rate, and combustion stability of the engine**.** In addition, the octane quality of the fuel should be observed as it limits the compression ratio because of knock occurrence. Furthermore, the compression ratio is dependent on valve operation timing.

Figure 35 presents the relation between the gross indicated fuel conversion efficiency and the compression ratio, in relation to different specific heat ratios γ where $= C_p/C_v$, and the different fuel/air equivalence ratio ϕ gives in equation 34:

$$\phi = \frac{(A/F)_{actual}}{(A/F)s} \tag{34}$$

Where: $(A/F)_{actual}$ is the fuel/air ratio for the actual fuel composition, and $(A/F)s$ is the fuel/air ratio for the stoichiometric composition, which is the optimal relation between the air and fuel.

Figure 35 - Gross indicated fuel conversion efficiency as a function of compression ratio

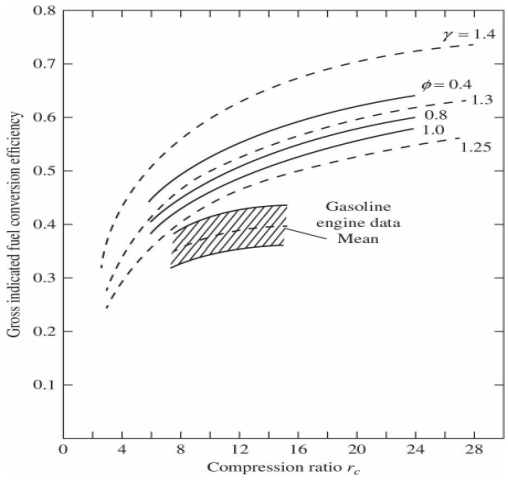

Source: adapted from (HEYWOOD, 2018)

It shows that the fuel conversion efficiency increases as the compression ratio increases. Note that for compression ratios higher than 17, imep and fuel conversion efficiency decrease slightly. Furthermore, HEYWOOD (2018) reports that an extensive SI engine data test shows a different behavior, and as expected, the engine-indicated efficiencies are lower than the ideal-cycle values by some 15%, and the gasoline engine data is shown in Figure 35 named as gasoline engine data mean.

The mean Effective Pressure superficially mentioned before is an important aspect to highlight related to the performance. In Figure 36 the curve is shown for the gross indicated, brake and friction mean effective pressure, imep, bmep, and fmep, respectively. Equation 25 in this section gives the brake mean effective pressure bmep, and represents the engine output work measured by a dynamometer.

Figure 36 - Gross indicated, brake, and friction power and mean effective pressure

3.8-liter six cylinder naturally-aspirated
WOT
Bore = 96.8 mm
Stroke = 86 mm
Rc = 8.7

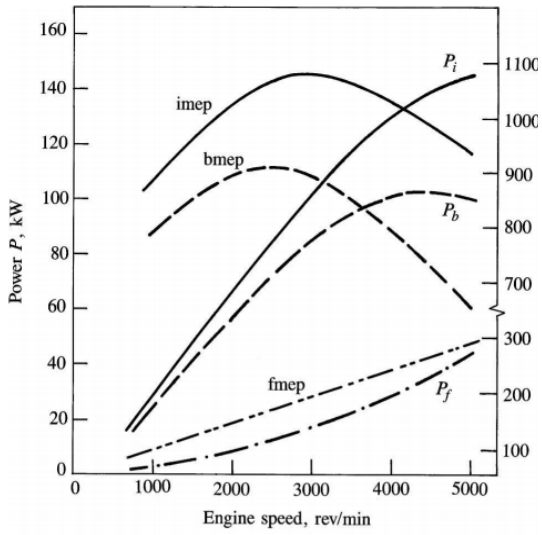

Source: adapted from (HEYWOOD, 2018)

On the other hand, the indicated mean effective pressure (imep) is the work done by the gas on the piston, and similar to the indicated work, the imep can be divided into gross imep and net imep. The main difference is that with net imep, the pumping losses (pmep) are not considered, whereas bmep to peak in gross work, such losses are considered. The gross imep is given in equation 35:

$$gross\ imep\ =\ net\ imep\ +\ pmep \tag{35}$$

Finally, the frictional mean effective pressure (fmep) is the result of a subtraction of an imep by the bmep as given in equation 36:

$$fmep\ =\ imep - bmep \tag{36}$$

Notice that the mechanical efficiency decreases with increasing speed, which causes the bmep to peak at a lower speed than imep.

Figure 37 - Performance map torque/bmep versus engine speed showing contours of constant bsfc

1.6-liter four cylinder naturally-aspirated Spark Ignition Engine

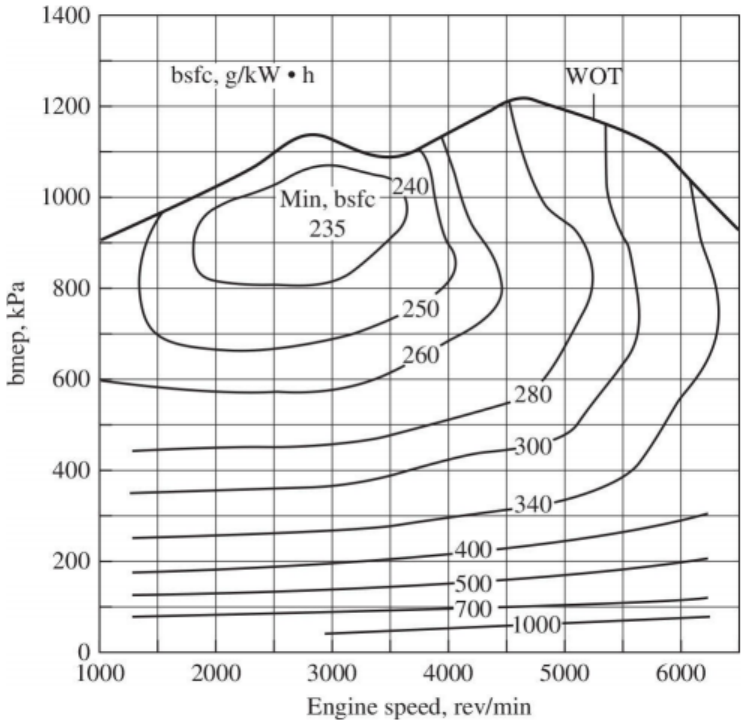

Source: adapted from (HEYWOOD, 2018)

An important way to present the engine operating characteristics is by the parameter-specific fuel consumption SFC previously cited, and it can be calculated by equation 26; the lower the value, the lower will be the fuel consumption. When the SFC is calculated with the brake power it is called BSFC, and it is usually plotted in a contour graph as can be seen in Figure 37. Note that the upper line of the Figure is a wide-open throttle (WOT) performance,

and it is the engine operating limit. Furthermore, the points below the WOT curve define the part-load operating characteristics. In this example, the best BSFC value is 237 g/kW.h and it is located in the upper left quadrant at high bmep, while the BSFC rises significantly in the lower half of the map due to the pumping work increase.

The BSFC is directly related to the fuel/air equivalence ratio given by equation 29. When the ϕ is equal to 1, the engine is running with a stoichiometric mixture and achieves the maximum temperature of the exhaust gas. On the other hand, when the engine is running enriched, in other words with ϕ higher than 1, maximum power is obtained. However, this leads to a high unburnt fuel level and as a consequence, a reduction of fuel conversion efficiency. Finally, when the engine runs lean, with lower than 1, maximum economy is obtained, when the fuel is burnt as much as possible.

Usually, the ideal equivalence ratio is one that gives the minimum BSFC at a required load, in other words, when the engine is running lean. However, as the mixture becomes leaner, the burning process is slower and the cycle-to-cycle pressure fluctuation becomes greater, and as a consequence, the fuel conversion falls as the combustion is incomplete. For this reason, there is a specific fuel/air equivalence ratio for each engine design, depending on compression ratio, quality of the mixture preparation, and combustion chamber design.

Besides the fuel/air equivalence ratio, the variation of spark ignition timing strongly affects the pressure curve. If the ignition is too early in the cycle (marked as 1 in Figure 38 (a)), the amount of work transferred from the piston to the gases in the cylinder at the end of the compression stroke is too large, and as a consequence, the work in the compression phase will be greater than the work done during the expansion stroke. In addition, the pressure could rise enough to generate knock. On the other hand, in the case when the ignition is too late in the cycle (marked as 3 in Figure 38 (a)), the peak cylinder pressure is reduced, and the expansion stroke work transferred from the gas to the piston decreases. Furthermore, there is a considerable chance of combustion being incomplete before the exhaust valve opens, which possibility will generate an overheating of the exhaust valves.

There exists a specific spark ignition timing that gives the maximum engine torque at a fixed speed, mixture composition, and flow rate (marked as 2 in Figure 38(a)), which is named Maximum Brake Torque (MBT), as can be seen in Figure 38 (b). In addition, the

MBT timing depends on the engine speed; in other words, if the engine speed increases, the spark must be advanced because of the increase of the combustion duration, in order to maintain optimum timing.

Figure 38 - Spark time effects in torque and cylinder pressure

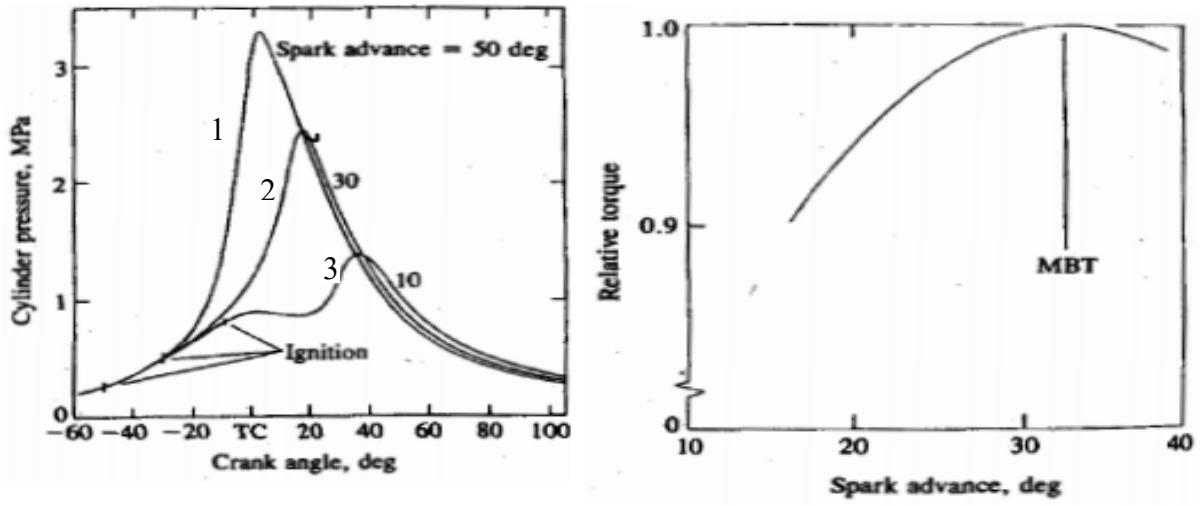

(a) Cylinder pressure vs crank angle (b) MBT

Source: adapted from (GIACOSA, 1986)

2.4.3. Fuel Review

Ethanol fuel is a renewable biofuel mainly derived from sugarcane. According to the Brazilian Oil Agency, ANP, ethanol can replace, partially or totally, fuels derived from oil and natural gas in internal combustion engines, and as a consequence, minimize the environmental impact of human activities on Earth. Table 6 shows the main Basic fuel properties for Gasoline E22, gasoline with 22% of anhydrous Ethanol mixed, and hydrous Ethanol. (ANP, AGÊNCIA NACIONAL DO PETRÓLEO, 2020; MALAQUIAS et al., 2019; OLIVEIRA et al., 2015)

Pure ethanol tolerates a higher compression ratio than gasoline mainly due to its higher Motor Octane Number (MON) and Research Octane Number (RON), as can be seen in Table 6. Furthermore, the combustion time is minimized, so the power output and fuel

conversion efficiency of the engine increase. Moreover, alcohol likewise can work with leaner mixtures than gasoline, leading to lower emissions. Because, in a stoichiometric air/fuel mixture, the energy per kg released during combustion is greater than gasoline. (OLIVEIRA et al., 2015)

Additionally, the volumetric efficiency is improved when pure ethanol fuel is used, because of the greater evaporative cooling effect due to the small amount of fuel that evaporates during the mixture preparation. Finally, pure ethanol can be mixed with gasoline, thus becoming a good additive to improve some characteristics of the gasoline. For instance, Brazilian gasoline has 22% or more of added ethanol in its composition. The presence of ethanol in the gasoline causes a linear increase in the RON, and as a consequence increases knock resistance.

Table 6 - Basic fuel properties

	Gasoline (E22)	Ethanol (E100)
MON	81.8	91.8
RON	97.1	>100
IAD	89.5	-
PCI (MJ/kg)	38.1	24.76

Source: (ANP, AGÊNCIA NACIONAL DO PETRÓLEO, 2020; MALAQUIAS et al., 2019; OLIVEIRA et al., 2015)

Nevertheless, the main disadvantage of blended fuel is the decrease of volatility due to the reduction of ethanol-gasoline miscibility by the presence of water when at low temperatures. As a consequence, the first start at a lower temperature becomes critical. To mitigate this issue, priming agents need to be added to improve the low-temperature vapor pressure and flammability. On the other hand, one of the main characteristics of pure gasoline is its volatility. The volatility influences fuel consumption at cold start, and some improvement of fuel economy at low temperatures can be observed as the volatility increases.

In this work, both fuels (E22 and E100) will be simulated, with the properties presented in Table 6.

2.5. Standard test cycle for fuel consumption

The standard cycles are recommended practice to establish uniform chassis dynamometer test procedures that provide instructions for measuring and calculating fuel economy and exhaust emissions, Furthermore, as was mentioned before in the introduction of this work, each country has its own regulation. In Brazil, the program to reduce emissions was created in 1988, named as *Programa de Controle da Poluição do Ar para Veículos Automotores* (PROCONVE). Moreover, PROCONVE was divided into phases until the present time:

- (L-1 from 1988 until 1991) The first phase was marked by vehicle manufacturing enhancement and soft emission targets.
- (L-2 from 1992 until 1996) The second phase was the focus on in-vehicle technology enhancement, for instance, electronic injection and catalytic converters. Moreover, a substantial target increase can be observed in Table 7.
- (L-3 from 1997 until 2002) The third phase was marked with a substantial restriction on the increase of CO.
- (L-4 from 2003 until 2007) The fourth step was remarkable for the restriction on the increase of the Hydrocarbon (HC) and nitrogen oxides (NOx) limits. Also, non-methane hydrocarbons (NMHC) began to be accounted separately for ethanol and gasoline vehicles.
- (L-5 from 2008 until 2011) The NOx target became more restrictive in the fifth phase as the NMHC, while the CO and HC remained constant.
- (L-6 from 2012 until 2021) The sixth phase was marked with a new CO reduction, as can be seen in Figure 39. Also, the NOx target was reduced again, while HC and NMHC remained constant.

Table 7 - Light and commercial vehicles emission limits for phases L-1 to L-6

	L-1 (1988)	L-2 (1992)	L-3 (1997)	L-4 (2003)	L-5 (2008)	L-6 (2012)
CO [g/km]	24	12	2	2	2	1.3
NOx [g/km]	2	1.4	0.6	0.25	0.12	0.08
HC [g/km]	2.1	1.2	0.3	0.3	0.3	0.3
NMHC [g/km]	1	1	1	0.16	0.05	0.05

Source: adapted from (FIGUEIREDO, 2019)

- (L-7 from 2022 until 2024) The next two phases had not been implemented by the time this work was written. The seventh phase presents new emission targets as can be seen in Table 8. Furthermore, the MHC will be replaced by non-methane organic gas (NMOG), and the Mass Particulate (MP) will be monitored for DI engines.

Table 8 - Vehicle Emission targets Proconve L-7 Otto cycle

Vehicle category	NMOG + NOx	CO	MP
Passenger car	0.080	1.000	0.006
Commercial car	0.140		

Source: adapted from (FIGUEIREDO, 2019)

- (L-8 from 2025 until 2031) The eighth phase is remarkable for the introduction of corporate targets, which is the weighted average for the sales volume of each model. Moreover, as can be seen in Figure 39, the NMOG + NOx targets are to be decreased every two years.

Figure 39 - Proconve L-8 corporative targets

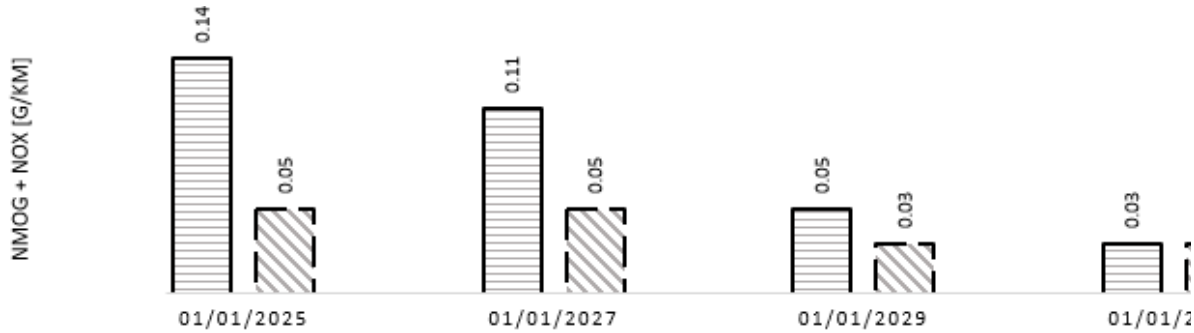

	01/01/2025	01/01/2027	01/01/2029	01/01/2031
Passager Car	0.14	0.11	0.05	0.03
Comercial Car	0.05	0.05	0.03	0.03

Source: adapted from (FIGUEIREDO, 2019)

Also, in this phase, the vehicles would be classified by emission levels as presented in Table 9. Basically, in Brazil, light and commercial vehicles must weigh less than 2800 kg and carry at most twelve passengers. Also, light and commercial vehicles are subdivided into

two vehicle level categories based on mass. Furthermore, each country has its own classification for considering a vehicle as light or commercial. (FIGUEIREDO, 2019)

Table 9 - Vehicle Emission targets Proconve L-8 by vehicle level

Vehicle Level Category		Level	Emission Limits (in g/km) NMOG + NOx	CO	MP
Light and commercial vehicles with mass higher than 1700 kg		140	0.14	1	0.006
		110	0.11		
	Light and commercial vehicles with mass under 1700 kg	80	0.08	1	0.006
		70	0.07		
		60	0.06	0.6	0.004
		50	0.05		
		40	0.04	0.5	0.004
		30	0.03	0.5	0.003
		20	0.02	0.4	0.002
		0	N/A	N/A	N/A

Source: adapted from (FIGUEIREDO, 2019)

2.5.1. Rota 2030 - Classification and calculation of targets

The program ROTA 2030 was created by the Brazilian federal government in partnership with the MDIC (Ministry of Industry and Trade) to set vehicle commercialization requirements in the Brazilian market by the bill 13.755/2008. This law presents incentives to improve vehicle Energetic Efficiency (EE), besides the energetic efficiency targets for each category. Moreover, EE is defined as the level of energy consumption *(in megajoules per kilometer MJ/Km)* measured in the combined cycle of FTP-75 and HWFET calculated by the equation 49 described in subsection 2.5.3.

Furthermore, the incentive is given by overreaching the targets, considering the relation vehicle weight vs EE, as can be seen in Figure 40, the vehicle weight and the EE are calculated by the average of vehicles sold or imported in each category from December 2022 to December 2026. Three categories are defined in this bill:

- Category 1 - Covering light passage cars, light commercial, and compact sports cars (small SUV) that use ethanol, gasoline, flex, diesel engine, or hybrid vehicles without external charge with weight range between 0 and 1564 *(in kg)*.

- Category 2 - Covering large SUVs and off-road 4x4s that have a limited attach angle with a weight higher than 1564 *(in kg)*.
- Category 3 - Covering pickups, heavy off-road 4x4s, and cargo vehicles with a weight higher than 1564 *(in kg)*.

Figure 40 - Incentive by category

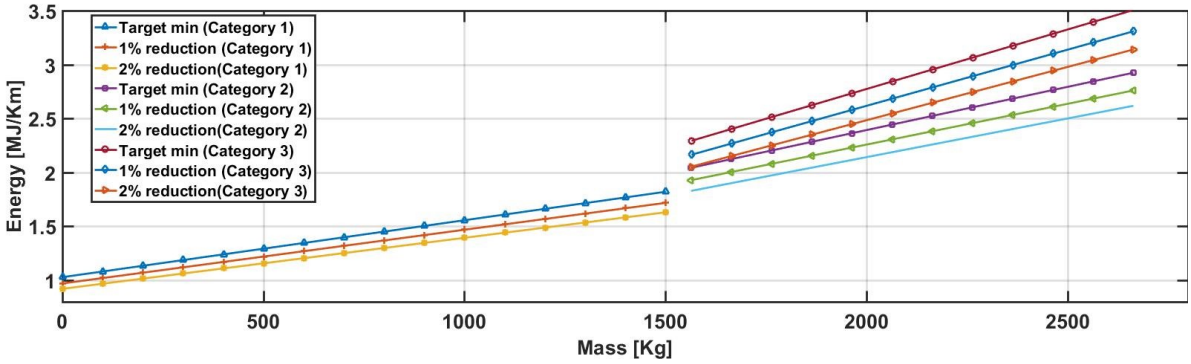

Furthermore, for each of those categories, an incentive of 1% or 2% tax reduction was defined, depending on the EE reduction. Moreover, the equations are plotted in Figure 40. Also, a minimal relation between ethanol (E100) and E22 must be 69.3%, as an additional reduction factor will be added when the relation is higher, following equation 37:

$$Reduction\ Factor\ CE\ (\%) = \left(\frac{\frac{Mj}{km}\ of\ E22}{\frac{Mj}{km}\ of\ E100} - 1\right)41.6 \quad (37)$$

Table 10 - off-cycle technologies reduction

Technologies	Incentive in [MJ/km]
Stop-Start	0.0227
Active Grill Shutter	0.0049
Gear Shift Indicator	0.0134
TPMS	0.0134
Stop-Start - Light Commercial	0.0439
High-efficiency lighting system	00079
Variable A/C compressor	0.04
Active aerodynamic	Until 0.0268
Thermal management technologies	Until 0.0363
Mild Hybrid	0.06

In addition to the incentives already cited, there are some additional benefits called off-cycle conditions. As can be seen in Table 10, these reductions are related to some technologies that should be implemented in the vehicle limited by 0.0936 MJ/km; in other words, the maximum reduction for off-cycle conditions is 0.0936 MJ/km.

Note that the biggest incentive is to be a mild hybrid, and to consider a hybrid system as a mild hybrid in the Rota 2030, the braking energy recovery capacity has to be between 15% and 65%, calculated according to USA EPA regulation §40 CFR 600.116-12. The first step is to determine the road load power $P_{roadload}$ in kW using equation 38:

$$P_{roadload} = -(\frac{V_{m/s} \,.\, (A + (B \,.\, V_{m/s}) + (C \,.\, {V_{m/s}}^2))}{1000}) \tag{38}$$

Where: A, B and C are the vehicle dynamometer road load coefficients in N, (N/m)/s, and $(N/m^2)/s^2$, respectively, and $V_{m/s}$ is the vehicle speed in m/s. The next step is to determine the applied deceleration power at each sampling point time, P_{accel} in kW using equation 39, and the sampling frequency must be 10HZ to follow the standard:

$$P_{accel} = -(\frac{ETW \,.\, V_t \,.\, (\frac{V_t - V_{t-1}}{0.1}))}{1000}) \tag{39}$$

Where: ETW is the vehicle weight, in Kg and V_t is the vehicle speed at each time sampling. Finally, it is possible to determine the braking power P_{brake} in kW subtracting road load power from the deceleration power, as in equation 40:

$$P_{brake} = P_{accel} - P_{roadload} \tag{40}$$

The theoretically total braking energy E_{brake} in kWh will be the absolute sum of all P_{brake} time sampling divided by 1000 to convert, then the next step is to calculate the energy recovered by a hybrid electric vehicle when tested on the FTP-75 (see the cycle in next

subsection). For this, the battery electrical current I_t in Amps must be measured as the voltage in V, then the current flowing into the battery E_t in kW is calculated with equation 41:

$$E_t = \frac{(V_{nominal} \,.\, I_t)}{36000} \tag{41}$$

The nominal voltage can be calculated by equation 42:

$$V_{nominal} = \frac{(V_s \,.\, V_F)}{2} \tag{42}$$

Where: the V_s is the battery voltage measured at the start of the FTP-75 test, and V_F is the battery voltage at the conclusion for the FTP-75 test. The total energy recovered $E_{rec}\ in\ kWh$ is the sum of all time stamps E_t divided by 1000 to convert watt-hours to kilowatt-hours.

Finally, the percentage of braking energy recovered by a hybrid system relative to the total available energy is determined by equation 43:

$$Energy\ Recovered\ \% = \frac{E_{rec}}{E_{brake}}\ x\ 100 \tag{43}$$

2.5.2 FTP-75, and HWFET

The Federal Test Procedure FTP-75 is a cycle used for light-duty vehicles certification in the United States, and the test is a variant of the EPA Urban Dynamometer Driving Schedule (UDDS). Furthermore, Figure 41 shows the speed trace of the FTP-75 cycle, and as can be seen, the cycle count has four phases: from 0 sec to 505 sec is the cold start transient phase, from 506 sec to 1372 sec is the stabilized phase, the hot soak limited at most 600 seconds or 10 minutes with one minute as tolerance, and finally, the first phase is repeated in the Hot start transient phase. Moreover, the test procedure is described in the standard NBR6601. Also, the speed trace in km/h based on time in sec is presented in ANNEX A. (ABNT, 2012; DISELNET, 2020; FIGUEIREDO, 2019)

Figure 41 - US EPA Urban Dynamometer Driving Schedule (FTP-75)

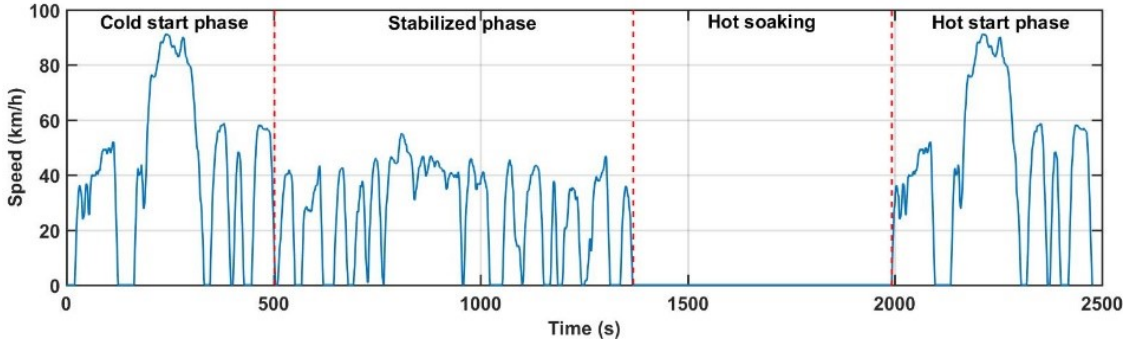

Furthermore, the FTP-75 relevant characteristics were listed in Table 11, where the number of stops in this cycle and the total stopping time can be highlighted:

Table 11 - FTP-75 relevant properties

Characteristic	Value	Unit
Total distance traveled	17.77	km
Total time	1874	s
Deceleration time	655	s
Acceleration time	739	s
Stopping time (Velocity =0)	335	s
Number of stops	23	-
Maximum speed	91.2	Km/h
Mean speed	34.14	Km/h

Source: adapted from (FIGUEIREDO, 2019)

The EPA Highway Fuel Economy Test Cycle (HWFET) is shown in Figure 42 and its speed trace in km/h based on time in sec is presented in ANNEX B. The test is run twice: once for preconditioning the vehicle, and the second run is for measuring fuel economy. Furthermore, the Brazilian test standard is NBR7040.

Figure 42 - EPA Highway Fuel Economy Test Cycle (HWFET)

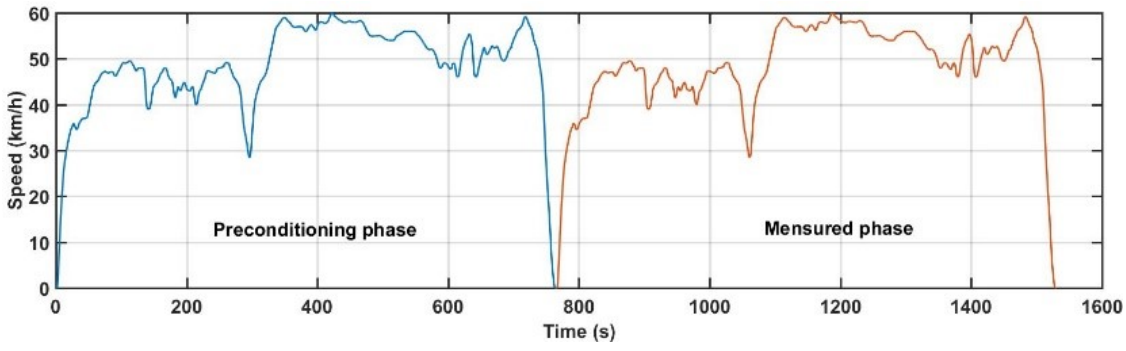

Also, the relevant properties are shown in Table 12. Note that the number of stops and the stopping time were not listed due to their highway characteristics, and the main characteristic of this cycle is the high mean speed:

Table 12 - HW relevant properties

Characteristic	Value	Unit
Total distance traveled	16.5	km
Total time	765	s
Deceleration time	210	s
Acceleration time	264	s
Maximum speed	96.3	Km/h
Mean speed	77.8	Km/h

Source: adapted from (FIGUEIREDO, 2019)

2.5.3. Fuel Consumption calculation and efficiency energetic calculation

The carbon balance method is applied to determine the final fuel consumption for both cycles FTP-75, and HWFET. To calculate the FTP-75 carbon balance, the mass sum of THC, CO and CO_2 *(in g/km)* is considered during the cold, stabilized, and hot phases, as is presented in equation 44:

$$Y_{WA} = 0.43\left(\frac{Y_{COLD} + Y_{STAB}}{d_{COLD} + d_{STAB}}\right) + 0.57\left(\frac{Y_{HOT} + Y_{STAB}}{d_{HOT} + d_{STAB}}\right) \quad (44)$$

Where: Y_{WA} is the weighted average of gas in g/km, Y is the amount of gas in g in the specific phase, and d is the distance in km of each phase, considering that the subscribed COLD, STAB, and HOT are cold phase, stabilized phase, and hot phase, respectively. After calculating equation 44 for each element THC, CO and CO2, the fuel consumption can be calculated by equation 45:

$$C = \left(\frac{[(0.8656\, m_{THC}) + (0.4288\, m_{CO}) + (0.2729\, m_{CO2})]}{(6.4487\ \%V_{gas}) + (4.1102\ \%V_{ETOH})}\right) 100 \quad (45)$$

Where: C is the fuel consumption in l/100km, m is the mass in g/km emitted during the FTP-75 cycle for each gas considered, $\%V_{gas}$ is the percentage volume of gasoline used, and $\%V_{ETOH}$ is the percentage volume of ethanol used. Equation 45 can be applied to determine

the fuel consumption for the highway cycle, and the only difference is that it is not necessary to calculate the weighted average of gas, since the HWFET has only one phase. Furthermore, considering that the fuel consumption in l/100km was already calculated for each phase, and the distance of each phase is known, the weighted fuel consumption (C_{Urb}) in l/100km can be calculated by equation 46:

$$C_{Urb} = 0.43\left(\frac{C_{COLD}\,D_{COLD} + C_{STAB}\,D_{STAB}}{D_{COLD} + D_{STAB}}\right) + 0.57\left(\frac{C_{HOT}\,D_{HOT} + C_{STAB}\,D_{STAB}}{D_{HOT} + D_{STAB}}\right) \quad (46)$$

Where: C is the fuel consumption, and D is the distance *(in km)* for the phases subscribed as COLD, STAB, and HOT.

Furthermore, with the fuel consumption calculated the fuel autonomy for urban (FTP-75) and highway (HWFET) can be computed by equation 47:

$$A_i = \frac{100}{C_i} \quad (47)$$

Where: A_i is the fuel autonomy in km/l, and C_i is the fuel consumption in l/100km. Moreover, the combined fuel consumption can be calculated by equation 48:

$$C_{comb} = \frac{1}{\left(\frac{0.55}{A_{Urb}}\right) + \left(\frac{0.45}{A_{Hw}}\right)} \quad (48)$$

Where: C_{comb} is the fuel consumption combined in km/l, A_{Urb} and A_{Hw} are the fuel autonomy in km/l for urban, and highway cycles respectively.

Furthermore, to calculate the reduction factor equation 37, the fuel consumption must be converted from km/l into MJ/km, and for that purpose the energy content in each fuel must be considered. 1 liter of ethanol has 20.06 MJ, while 1 liter of gasoline (E22) has 28.99 MJ.

Moreover, each fuel energy content must be divided by the fuel consumption obtained with equation 48. Finally, to calculate the MJ/km Mixed (E100 and E22) the arithmetical average should be calculated as shown in equation 49:

$$FC_{cycle} = \frac{C_{E100} + C_{E22}}{2} \quad (49)$$

2.5.4. Real Driving cycle

The real-world driving cycle used in this work is the SP cycle, the main characteristic of which is the high level of traffic found in São Paulo city, with several stops and engine restarts; figure 43 shows the route with the streets and the start and end of the test. The speed trace figure 44 was recorded with an onboard acquisition system; also, the water and air temperatures, gearshift, pedal position, and instantaneous fuel consumption were calculated at the frequency of 10 Hz.(FIGUEIREDO; CAMPOS; PUJATTI, 2020a)

Figure 43 - SP Dynamometer Driving Schedule

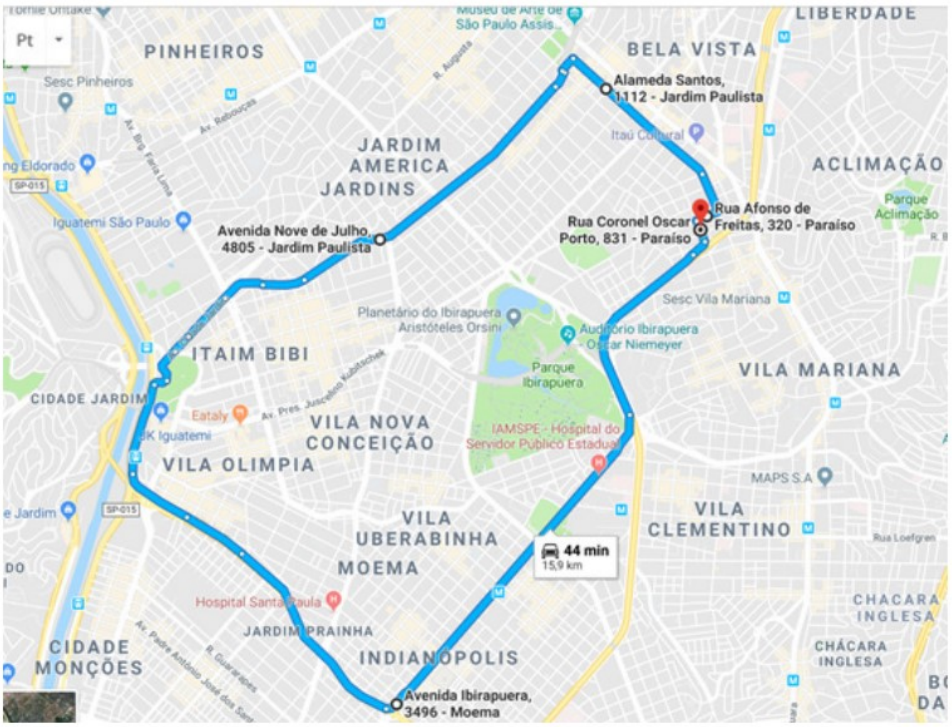

Source: (FIGUEIREDO; CAMPOS; PUJATTI, 2020b)

The main characteristic of the SP cycle is the number of stops; there are 35 stops during the circuit, the speed is very low averaging 18 km/h, and the distance is 15.7 km. The test Cycle (SP) speed trace in km/h is presented in ANNEX C based on time in a sec.

Figure 44 - SP Dynamometer Driving Schedule

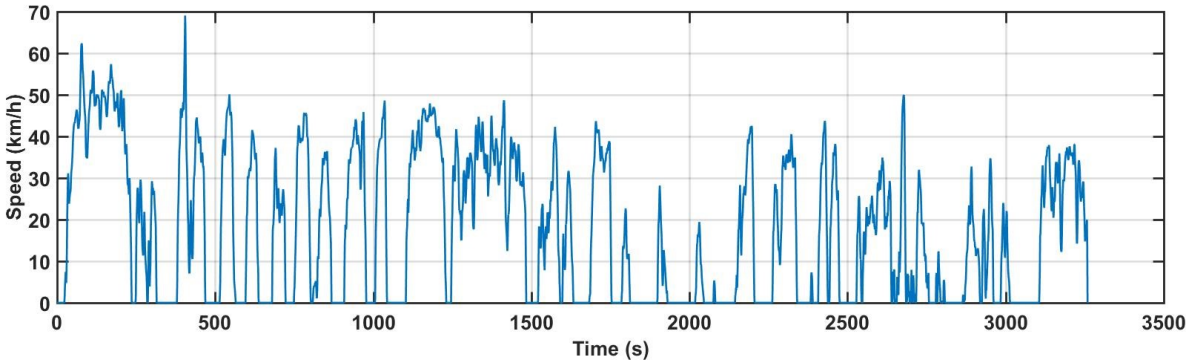

Source: Prepared by the author

Table 13 - SP cycle relevant proprieties.

Characteristic	Value	Unit
Total distance traveled	15.704	km
Total time	3259	s
Stopping time (Velocity =0)	1227	s
Deceleration time	1018	s
Acceleration time	1041	s
Maximum speed	69.06	Km/h
Mean speed	17.3	Km/h

Source: adapted from (FIGUEIREDO; CAMPOS; PUJATTI, 2020a)

2.6 Advisor model description

Advisor is an open-source software developed by NREL that has a large library to deal with conventional and Hybrid vehicle simulations. Among Advisor capabilities that stand out are: gear ratios optimization to reduce fuel consumption, assessing relative tailpipe emissions produced over several cycles, evaluating energy management strategy for hybrid vehicles, and estimating the vehicle's fuel economy that does not exist yet. Besides the

Advisor's flexibility, most of the Advisor components models are quasi-static; they use data collected in steady-state, in other words, empirical tests. For instance, the specific fuel consumption can be recorded at various constant speeds and load points to simulate the overall fuel consumption through a driving cycle, which characteristic raises the main Advisor drawback; the quasi-static assumption. Consequently, the transient behaviors cannot be well predicted. For example, physical vibrations and electric field oscillations. Finally, the Advisor is widely used in the literature, as can be seen in the following documents: (CHEN et al., 2014; FIGUEIREDO, 2019; GAO; MI; EMADI, 2007; HUMPHRIES, 2015; MALIKOPOULOS; FILIPI; ASSANIS, 2006; SILVA, 2017)

Two drivetrains were considered in this work as shown in Figure 45: the conventional drivetrain is shown in Figure 45(a), and the Parallel Starter/ Alternator Drivetrain (HEV P1f) is shown in Figure 45(b). The traditional vehicle architecture is composed of a fuel converter (engine), clutch, gearbox, final drive, and wheel. The parallel starter-alternator drivetrain architecture is already in P1 configuration following the classification in subsection 2.1.3.2, and besides the components already cited in the conventional drivetrain, it still has an energy storage system (battery), torque coupler, and electric motor.

Figure 45 - Drivetrain models

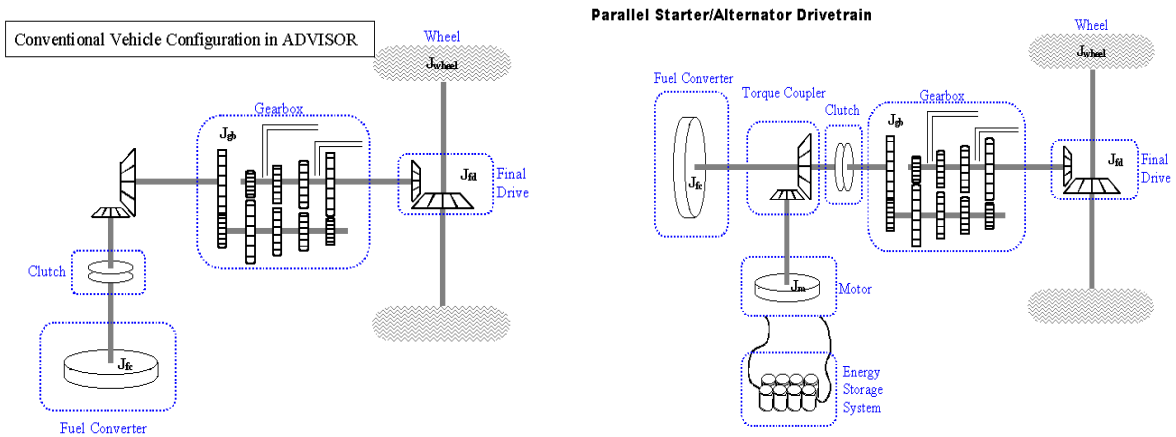

(a) Conventional drivetrain model (b) Hybrid parallel Starter/ Alternator model

Source: adapted from the Advisor manual

The drivetrain architectures were modeled using the MATLAB®/Simulink® environment using the Advisor library, to better understand the Advisor implementation, the Advisor name library objects are written between single quotation marks (‘’), and the

subsystem inside of a library object is written underline, the names assigned by the author are written between double quotation marks (“”), the Advisor variable names are written in *italic*, and, the block’s input and output names are written in **bold**.

The conventional vehicle (CONV) mode is present in the block diagram in Figure 46. The primary components of this assembly are the ‘wheel and axle front/rear <wh>’, the ‘2 axle→ 1 driveline converter’, the ‘final drive <fd>’, the ‘gearbox <gb>’, the ‘clutch <cl>’, and the ‘fuel converter <fc>’. Additionally, it still contains four subassemblies, which are: the ‘Mechanical Accessory <acc>’, the ‘<vc>conv’, the ‘vehicle <veh>’, and finally, the ‘drive cycle <cyc>’. Furthermore, the HEV P1f diagram is shown in Figure 47, and besides the main assemble already presented on the conventional vehicle, the hybrid configuration still has the ‘electric assist control strategy <cs>’, the ‘torque coupler <tc>’, the ‘motor controller <mc>’, the ‘electric acc loads <acc>’, the ‘power bus <pb>’, and the energy storage <ess>.

Figure 46 - Conventional vehicle block diagram

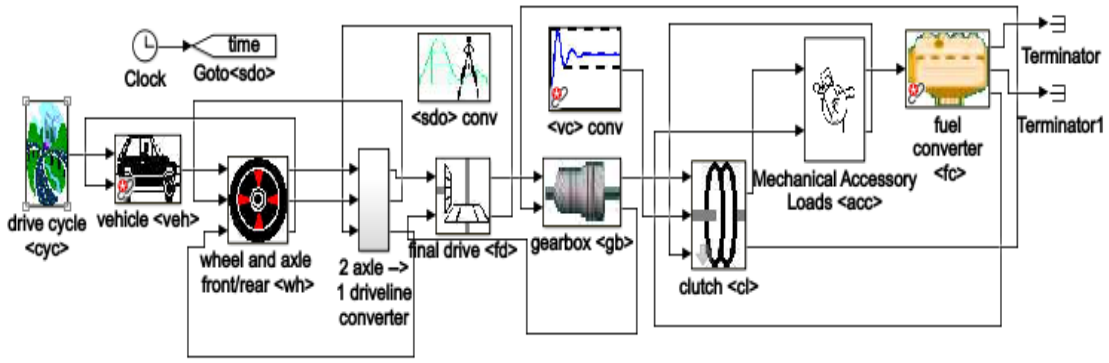

Figure 47 - HEV vehicle block diagram

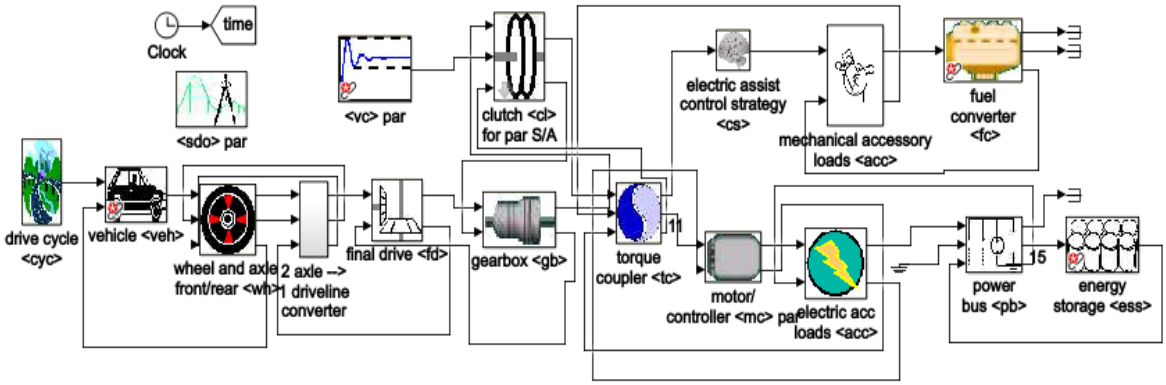

Source : Prepared by the author based on Advisor Manual

Furthermore, the Advisor's principle of work is known as the hybrid backward/forward approach; the backward-facing is used to provide the velocity vehicle required profile initially assuming that the speed profile is met, then the forward-facing handles the component performance limits. Therefore, the forward-facing ensures that no component limits are extrapolated to reach the speed vehicle trace (NREL, 2003). In the next subsection, the specific models are going to be assessed.

2.6.1 Drive cycle subassembly and Vehicle model assembly

In drive cycle subassembly the required vehicle speed versus time trace is imputed to the simulation. For instance, the cycles used in that work are presented in ANNEX A, ANNEX B, and ANNEX C and were further discussed in subsection 2.5.2, and 2.5.4. Moreover, the cycle is smoothed to guarantee simulation stability. Finally, the required speed is sent to the vehicle assembly. The complete drive cycle model and vehicle model are in ANNEX D and ANNEX E respectively.

The approach used to model the vehicle in Advisor software is a classic longitudinal vehicle dynamic equation, and it is shown in equation 50, where $\sum F$ is the sum of forces in N, m is the vehicle mass in kg, and a is acceleration in m/s2:

$$\sum F = ma \tag{50}$$

The Simulink® implementation can be seen in Figure 48 and, the sum of the forces is made in block Sum1, it represents the total force to move the vehicle forward. The sum of forces has four components, rolling resistance named in the Simulink model as rolling resistance force (i), aerodynamic force in the force required to overcome aerodynamic drag (ii), grade force in the model force required to ascend (iii), and tractive force in the model force required to accelerate (iv).

Figure 48 - vehicle block diagram

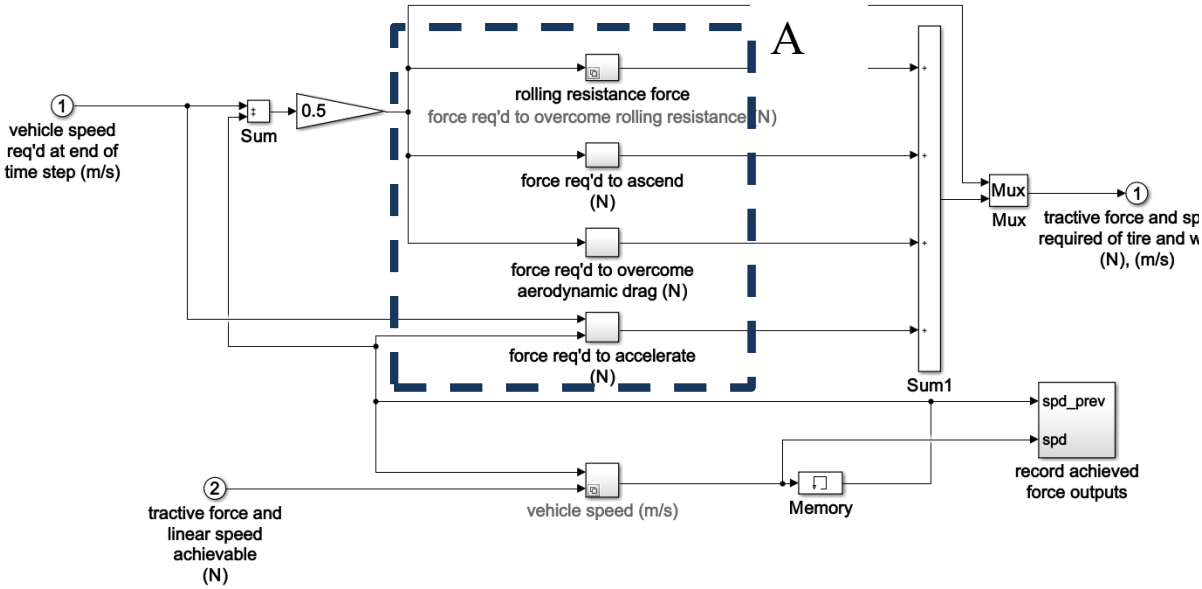

Source: adapted from the Advisor Help

(i) The rolling resistance force (F_{roll}) is a dissipative force that acts on the vehicles from the tires, and it is modeled by equation 51:

$$F_{roll} = C_{roll}(v_{veh}, P_{tire}, \dots) M_{veh} g \cos\delta \tag{51}$$

Where: g is the gravity acceleration *veh_gravity* in the Advisor variables in this work it will be considered 9.81 m/s^2, δ is the road angle *grade*, M_{veh} is the vehicle mass current veh mass and is composed of two parts *veh_mass* which is the vehicle mass considering the test mass, fluids and passengers, and the *veh_cargo_mass*, which is the weight of the external cargo, the total mass used can be found in section 3.1 in Table 16. Finally, the C_{roll} is the rolling resistance coefficient and it has two components, while one varies linearly with speed C_{r1} named in advisor as *wh_2nd_rrc* unitless, the other is a constant C_{r0} *vh_1st_rrc* in s/m, equation 52. (NREL, 2003)

$$C_{roll} = C_{r0} + C_{r1} v_{veh} \tag{52}$$

The rolling coefficients can be empirically measured by the test called coast down, where the vehicle is accelerated up to 110 km/h in a flat track, and then, the vehicle drive is

disengaged. The vehicle slows down due to the resistance forces, and the speed and time are recorded every 10 km/h delta speed until the vehicle reaches 30 km/h. Moreover, the standard ABNT NBR 10312 defines the other characteristics of this test, for instance, vehicle mass, road characteristics, environmental conditions, etc. Also, this test is a prerequisite of the standard NBR 6601. (FIGUEIREDO, 2019):

$$F = F_0 + F_1 + F_2 v^2 \tag{53}$$

Finally, the resistive force F in N is presented in equation 53, where F_0 is the tire rolling resistance in N, the F_2 is the aerodynamic resistance in N/ (km/h) ^{2}, and v is the vehicle speed in Km/h. The correlation between equations 53 and 52 will be done by a full grid optimization shown in subsection 3.6.1.

(ii) The aerodynamic drag force (F_{aero}) is proportional to the velocity squared, and it is presented in equation 54:

$$F_{aero} = \frac{1}{2}\rho_{air} A_f C_d v_{veh}^2 \tag{54}$$

Where: ρ_{air} is the air density in this work it will be considered 1.25 kg/m^3 at normal conditions; in the Simulink model the variable is *veh_air_density*, A_f is the vehicle frontal area *veh_FA* in m^2, C_d is the aerodynamic drag coefficient *veh_CD* unitless, and v_{veh}^2 is the vehicle speed squared, the vehicle speed is named as **average vehicle speed over time step (m/s)** on the model. The aerodynamic drag coefficient and the frontal area are dependent on the vehicle geometry.

(iii) Equation 55 is the grade force(F_{grade}), which represents the force necessary to overcome a hill. Therefore, the bigger the slope, the greater the force needed due to the effect of gravity. In this current work this component can be disregarded because the cycles tested do not have slopes:

$$F_{grade} = M_{veh} g \sin\delta \tag{55}$$

Where: $M_{veh}$the vehicle mass in kg, g is is the gravity acceleration in m/s2, and δ is the road slope angle.

(iv) Finally, the tractive force F_{trac} is responsible to accelerate the vehicle, as can be seen in equation 56:

$$F_{trac} = M_{veh} \frac{d_{v_{veh}}}{dt} \tag{56}$$

Where: M_{veh} is the vehicle mass in kg, $\frac{d_{v_{veh}}}{dt}$ is the vehicle acceleration in m/s2. Note that dt is the difference between the current time and the previous time, and $d_{v_{veh}}$ is the difference between the current speed vehicle and the previous speed vehicle. By the sum of those four components, the total force is calculated in equation 57:

$$\sum F = F_{trac} - F_{aero} - F_{grade} - F_{roll} \tag{57}$$

Furthermore, dashed block A in Figure 48 is shown the equation 57 modeled on the vehicle block when applied for the actual vehicle speed requested by the cycle. In addition, to ensure that the speed calculated for the step time is achievable, the same equations are applied on the subsystem record achieved force outputs given the **tractive force and linear speed achievable** from the 'wheel and axle front/read' model that will be assessed in the next pages. Finally, if no drivetrain ran up against its performance limit during the time step, the current speed is the requested speed, otherwise, the previous vehicle speed will be repeated.

2.6.2 Wheel and axle, 2 axle 1 driveline converter, and final drive models

The main function of the 'wheel and axle front/rear <wh>' assemble is to transmit torque and speed requests from the vehicle block to the final drive, taking into account the

losses of inertia and friction, subsystems loss (Nm), and effect of inertia (Nm) respectively. Also, a tire slip is modeled on the tire slip model (m/s). The complete wheel and axle model is in ANNEX F.

The effects of friction in the axle bearing are addressed in terms of vehicle mass in the look-up Table for **wheel & axle bearing drag.** Furthermore, the axle inertia is calculated on the 'effect of inertial' block, the axle speed is turned into axle acceleration by the derivation, then the axle acceleration is multiplied by the wheel axle assembly rotational $wh\_inertia(J_{wh})$, and at the end, the **inertia torque** is calculated in newton meter Nm. Moreover, the tire slip model guarantees that the traction will be limited by the tire slip coefficient, otherwise the maximum traction possible without slip will be selected. (NREL, 2003) In this work, for all vehicle configurations, the Advisor default curve for light vehicles was considered.

Another important task of the 'wheel and axle front/rear <wh>' assemble is converting linear vehicle speed into the angular speed of wheels and vice versa. After that, the torque request in the wheels is calculated, to do that the tire characteristics are used.

The main purpose of the 'final drive<fd> is transmitting torque and speed requests to the 'gearbox <gb>, Furthermore, the 'final drive<fd>' transmits speed and torque back to the 'wheel and axle front/rear <wh>'. In the 'final drive<fd>' losses from friction and inertia were considered, the subsystems, 'loss', and 'effect of inertia', respectively. Also, the reduction ratio is computed by multiplying the *fd_ratio* to the torque, and the speed by the inverse of the reduction ratio. Finally, the final drive outputted the torque and speed required and available.

2.6.3 Gearbox, and clutch models

The main role of the 'gearbox<gb>' is transmitting torque from the 'final drive <fd>' to the clutch <cl>' with different gear ratios. The Advisor model accounts for the effect of torque multiplication and speed reduction via the gear ratios **gb_ratio**. Also, the rotational inertia loss and the friction of the turning gears loss are computed. The gearbox control is commanded by the gearbox controller interface and pre-TX parallel gearbox control for the

CONV and HEV P1, respectively. For the purpose of this work, the gearbox control boxes were modified to follow a specific sequence determined by the vehicle gear shifting indicator collected during a real bench test, and the gear change sequences used for each cycle and vehicle can be found in ANNEX G.

The torque requested into the gearbox $\tau_{req,into}$ in Nm can be calculated by equation 58, where $\tau_{req,out}$ in Nm is the torque requested outside of the gearbox, $gear$ unitless is the current gear ratio *gear_ratio*, J_{wh} unitless is the torque requested to accelerate rotational inertia and it is the output of the effect of inertia subsystem, and τ_{loss} unitless is the torque loss due to friction output of the Loss subsystem. For this work, the inertial was disregarded due to the lack of information; however, the gearbox losses were considered constant at 4%.

$$\tau_{req,into} = \frac{\tau_{req,out}}{gear\, J_{wh} \tau_{loss}} \tag{58}$$

The gear output subsystem enters on the 'clutch <cl>' assembly, and the main objective of this component is to determine whether the clutch should be fully disengaged, fully engaged, or even slipping-transmitting, where the two sides of the clutch spin at different speeds. The **clutch state** is an input of this block, it came from the 'clutch control', it is important to point out that there are two different clutch controls, one for the CONV vehicle model, and the other for the HEV P1f.

The HEV P1 clutch control differs from the conventional configuration by the logic path to engage or disengage the engine during the stop-start events. The conventional clutch control strategy is already based on the torque **gb_trq_in_r**, speed **gb_spd_in_r,** and gear **shifting**; essentially, the clutch is disengaged if the gear is changing, idem upshift or downshift, and, in case no positive torque is required of the engine. Furthermore, the clutch is slipping in case of a positive torque requirement, and the speed required of the engine is less than the current engine speed, and in the previous time step, the clutch was not completely engaged. Finally, the clutch is engaged if it is not disengaged or slipping.

The idle event is considered in this strategy too; the variable *vc_idle_bool* indicated when the engine is running idle, or not. Also, the idle can be indicated by the *vc_idle_spd* when the **gb_spd_in_r** is less than the *vc_idle_spd* and the engine is idling. The complete gearbox model is in ANNEX H.

2.6.4 Torque coupler model

The 'torque couple <tc>' assembly is exclusive to the hybrid vehicle model due to its main hole. The assembly combines two torque sources into a unique final torque. Fundamentally, the torque coupling receives the torque and speed request from the downstream drivetrain and processes it to apportion requests between the combustion engine and the electric motor. Further discussion regarding the torque coupling can be found in the literature review of the Hybrid Parallel of this work, subsection 2.1.1.2. In addition, the reduction ratio between the energy sources is considered, as the friction loss of the FEAD can be computed.

The reduction ratio between both sources of torque is considered by a factor *tc_mc_to_fc_ratio*, which is physically the relation between the electric motor pulley diameter and the engine pulley diameter. The reduction ratio is designed to avoid running it at dangerous electric machine speeds above its maximum. For instance, the current reduction ratios are in the range of 2.3~3.2 for a gasoline engine with 6000 rpm, depending on the maximum allowed speed of the electric machine. The complete gearbox model is in ANNEX I. (BALDIZZONE, 2012; NREL, 2003)

2.6.5 Electric Motor model

The Electric Motor model is exclusive to the hybrid vehicle mode also; this assembly is called 'motor/ controller <mc>par', and its main role is converting the torque and speed request into motor power requested limited by the electric motor limits. Moreover, the effects of inertia are considered in the effect of inertia (in Nm); besides that, a thermal model is implemented. However, in this work, no temperature variation was taken as an assumption. The subsystem diagram is shown in Figure 49.

Figure 49 - Motor controller assemble diagram

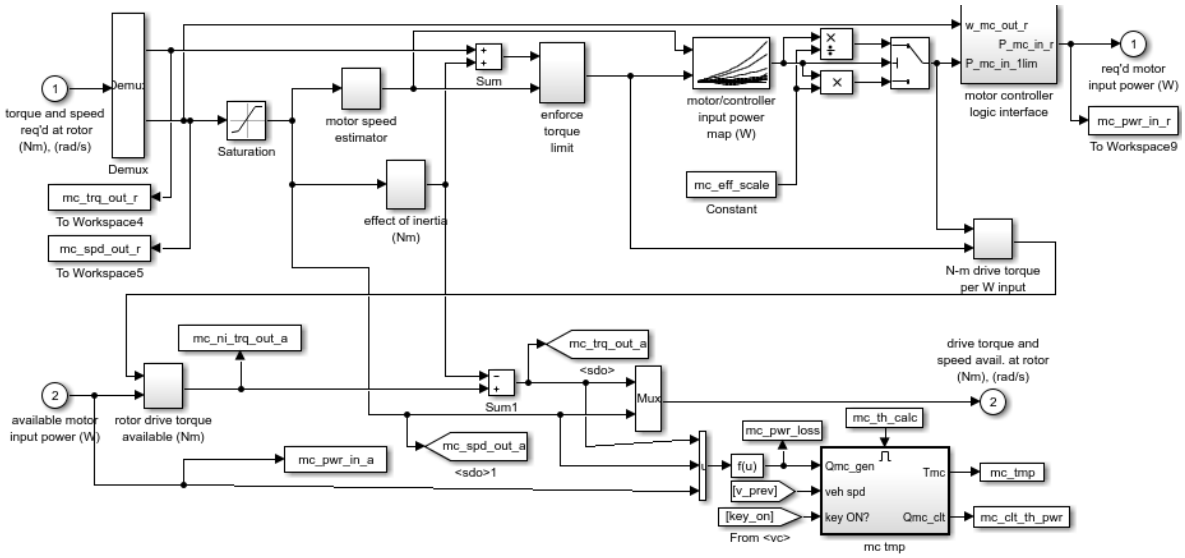

Source: adapted from the Advisor Help

The **limited motor torque** and the **limited motor speed** enter on the motor/controller input power map (W) that outputs the power needed from the electric motor. Next in line, the motor controller logic interface is accessed to ensure that the motor shuts down when it is not needed, for instance, during a gear shifting event. Also, the logic limits the maximum motor's current to the motor/controller. The maximum power is calculated by multiplying the *mc_max_crrnt* maximum current by the **bus voltage;** then, the power requested is compared with the maximum power and the minimum value pass forward, besides that, a gear **shifting** status is used to turn off the motor when it is necessary. Finally, the **requested motor input power (W)** is outputted.

A parallel calculation is done to quantify the **drive torque and speed available at the rotor**. The speed and power enter on the N-m drive torque per W input, where the ratio of requested rotor torque to requested electrical input power is determined. Then, the rotor drive torque available (Nm) subsystem calculates the actual rotor torque given the actual motor input power and the ratio (requested rotor torque)/ (requested input power), the requested input power is zero when the ratio has the value inf, which does not represent the reality, since the rotor torque would be the motor spin-loss when there is zero input power. However, this assumption does not affect the fuel economy, because this simplification occurs just when the requested input power is zero. Finally, the rotor drive torque available

is summed to the effect of inertia to become the **drive torque and speed avail. at rotor.** Furthermore, the complete electric motor model is in ANNEX J.

2.6.6 Electric-assist Control strategy

The 'electric-assist control strategy<cs>' goal is to maintain the battery's state of charge SOC between limits while regenerating the energy and providing torque assist. Figure 50 (a) shows the engine operating status in relation to torque and speed, when SOC is greater than the lowest desired battery state of charge *cs_lo_soc*, and Figure 50 (b) presented the opposite, in other words, when the SOC is less than the lowest desired battery state of charge cs_lo_soc.

Figure 50 - Strategy SOC dependency

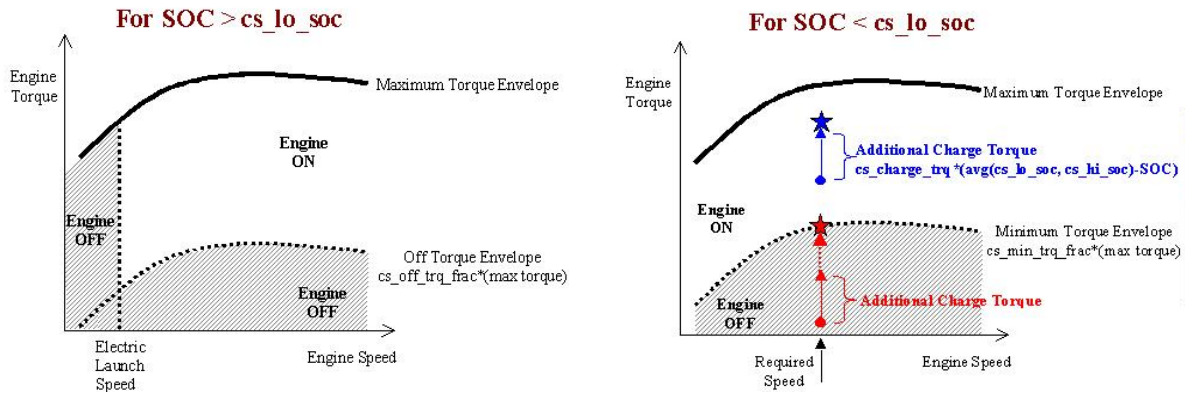

(a) SOC more than the minimum soc (b) SOC less than the minimum soc

Source: adapted from the Advisor Simulink model

In the case of SOC greater than the *cs_lo_soc* Figure 50(a), three important variables should be pointed out; *cs_electric_lauch_spd*, *cs_off_trq_frac*, and *cs_electric_decel_spd*. The *cs_electric_lauch_spd* is called electric launch speed, and is a vehicle speed value where below the vehicle operates as a ZEV (Zero Emissions Vehicle). The second variable to be pointed to is *cs_off_trq_frac* and it is a maximum engine torque fraction where the engine will be turned off and the vehicle will operate as a ZEV. Both functions need an electric mode function to be used; therefore, in this work, both variables were set to zero, as far as the

models treated in this work do not present the pure electric mode. Last but not least, the *cs_electric_decel_spd* is a variation of the electric launch speed strategy, but it just turns off the combustion engine in deceleration events.

The generation strategy when the SOC is less than minimum SOC is shown in Figure 50(b), and there are two cases, in red is the case when additional charge torque is required to charge the battery and the actual torque is too low, and the strategy brings the torque to the lower limit of torque as marked with a red star. Moreover, the second case marked in blue is when the operation point is required torque plus charge torque, the additional torque required is calculated by equation 59:

$$\tau_{add} = \tau_{chage\ torque} \left(\frac{\left(\frac{SOC_{min} + SOC_{max}}{2} \right) - SOC}{\left(\frac{SOC_{max} - SOC_{min}}{2} \right)} \right) \tag{59}$$

Where: $\tau_{chage\ torque}$ is the torque factor in Nm request to charge the batteries *cs_charge_trq*, SOC_{max} and SOC_{min} unitless are the maximum and minimum normalized state of charge respectively, and SOC unitless is the current state of charge. Therefore the additional torque is proportional to the difference between SOC and the average of maximum SOC and Minimum SOC. The subsystem chg trq req'd calculates the additional torque. Forward, the current torque is summed with the additional torque, then the maximum between the torque summed and the minimum torque block output minimum trq (Nm) in the case where the torque is less than the minimum torque envelope, and finally there is a switch that accounts for when the engine is turned on or not by a flag called *ess_on.*

Moreover, equation 59 is used to account for the torque assist when the SOC is more than the minimum state of charge *cs_lo_soc*, in which case the sign is negative, and the proportional value of electric motor torque is deducted from the combustion engine torque, which essentially generates fuel consumption reduction. The complete electric assist control strategy is presented in ANNEX K.

2.6.7 Electric acc loads and Mechanical accessory loads.

The mechanical and electric loads are dedicated auxiliary load systems, and the main difference between them is the source of energy, while the mechanical accessory subsystem gets energy from the spinning shaft, and an electrical source is required for the electrical loads. Both models contain a backward model and a forward model; in the forward model, the subtraction of power or torque by power generated upstream is sent to the auxiliary loads, and the remaining power moves forward on the powertrain. Furthermore, in the backward mode, the extra torque or power requested from the accessory loads is accounted for by modifying torque or power (NREL, 2003).

There is a large list of 14V electric auxiliary loads covered by the modes; for instance, heated seats, rear defrost, radio, rear wipers, front wipers, turn signals, front HVAC, rear HVAC, engine (ignition system), external lights, radiator cooling fan, brake lights, and starter. All these components generated a considerable energy expenditure; however, during the test that will be run on this work, most of these components will be turned off due to the standard recommendations. Besides this, there are two variables to add any different load, the *acc_mech_pwr*, and *acc_elec_pwr* the mechanical and electrical load, respectively. The Electric acc loads and Mechanical accessory loads models are presented in ANNEX L (ABNT, 2012; NREL, 2003)

2.6.8 Energy storage

The main goal of the ‘energy storage <ess>’ is accumulating energy, and even though batteries seem to be simple to model, their thermally-dependent electrochemical processes increase considerably the complexity of the model. Besides this, the electrical behavior of a battery is a nonlinear function. The model used in this work is called the Rint Model; essentially, this subsystem present in the Advisor library accepts a power request, usually from the power bus, and returns available power output from the battery, battery SOC, and the battery current and voltage. Moreover, positive power is discharged by the convention of this approach. ANNEX M contains the entire Energy Storage Model.

Furthermore, the Rint Model is in the function of the remaining charge in the storage in the battery pack. Furthermore, the battery pack equivalent circuit is considered a perfect open circuit voltage source in a series with internal resistance. The coulombic efficiency affects the battery charging, which is also limited by the battery voltage. Besides the voltage limitation, the battery is also limited by the components that are connected to the battery; for instance, the electric motor, generator, etc.

Already, in the subsystem pack Voc, Rint the VOC, and Rint of the battery pack are computed given the current **SOC (prev)** unitless, and the battery temperature named **mod tmp (C)** in C. The VOC and Rint are accounted for by surfaces named, **VOC (V)** in Volts for voltage opening circuit, **Rdis** in ohms for discharge internal resistance, and **Rchg** in ohms for charge internal resistance. These look-up Tables are experimentally measured. Furthermore, after interpolating the VOC, it is multiplied by the *ess_module_num* which is the number of modules in a pack assumed to be strung in series, the output is the **pack open-circuit voltage** and **pack resistance**. Besides this, a switch is used to determine whenever the battery is charging or discharging, based on the power requested signal.

After calculating the open-circuit voltage and the internal resistance of the pack, the limit power subsystem is accessed to prevent overpowering. Three limits are considered over this subsystem, the state of charge, the motor controller's minimum allowable voltage, and the equivalent circuit parameters, the SOC has limited the power request to zero if an attempt is made when the battery pack is empty. Moreover, the maximum power available is limited by three parameters; the voltage allowed in motor/controller *mc_min_voltages*, the energy storage system minimum operation voltage *ess_min_volts*, and the maximum voltage available calculated by **Voc**/2. The maximum value among these is selected as a bus voltage V_{bus} to be used, and finally, the maximum power is limited by equation 60.

$$P = V_{bus}\left(\frac{V_{oc} - V_{bus}}{R}\right) \tag{60}$$

Where: P in W is the maximum power, V_{oc} in Volts is open-circuit voltage, R is the internal resistance, and V_{bus} in Volts is the bus voltage. Finally, the minimum from the power required **Pbty** and the power limited is selected to be the output **Pbty, limited.**

In parallel, the quadratic equation for current is solved on the computer current subsystem, where the equation definition based on Kirchhoff's voltage law is solved, and the output of this subsystem is the current of the battery *ess_current*. Finally, the SOC is determined by the SOC algorithm subsystem, where the SOC is calculated to consider the coulombic efficiency in dependence of battery temperature modeled in ANNEX N, and the maximum capacity *max cap*. In the subsystem is calculated the initial SOC in Ah by using equation 61 where the initial SOC, *ess_init_soc*, is multiplied by the maximum capacity used:

$$SOC = (1 - ess\_init\_soc)\, Max\ capacity\ used \tag{61}$$

Then, the initial SOC in Ah is used as an initial condition to integrate the SOC in time. Finally, the SOC normalized is calculated by equation 62, where SOC is the status of charge, $Max\ Capacity$ in Ah is the maximum capacity of the battery, and $Ah\ used$ is the integrated SOC in Ah.

$$SOC = \left(\frac{Max\ Capacity - Ah\ used}{Max\ Capacity}\right) \tag{62}$$

2.6.9 Fuel converter (Engine)

A fossil power source for the vehicle is simulated on the fuel converter assemble, the operation point is determined given a requested speed and torque from others assemble, and take into account inertial losses and accessory loads. Furthermore, the engine controller determines the engine speed if the clutch is disengaged, and limits the operation point to the engine boundaries. After determination, the operation point of the fuel use and emissions for each time step can be accounted for by using empirical maps in relation to speed and load. In the current work, we didn't assess emissions.

The 'fuel converter <fc>' implementation is composed of four subsystems, the engine controller interface, the engine torque, the engine speed estimator, and the fuel use and EO

emis Configurable subsystem. Moreover, the engine on (parallel hybrid) is called by the interface engine controller interface, this subsystem assesses the engine speed requested **fc_spd_out_r**, and output the speed command; essentially, that is the same input speed but in case of speed less than the idle, the output will become the idle speed **vc_idle_spd**.

Then, the final operation speed is calculated by the 'engine speed estimator', if the request is to increase the speed (spin-up), and the clutch is disengaged the engine speed is less than the commanded speed. On the other hand, if the speed is commanded to decrease (spin down), the engine speed is calculated by integrating the ratio of closed-throttle torque to engine inertia for time. Furthermore, in the case of the engage clutch and trace being missed on the current time step, the previous actual engine speed is used in the current time step. Finally, if the clutch is engaging and the current trace is present, the engine speed is equal to the speed command, respecting the engine's maximum speed limits.

With the speed operation point defined, the torque operation point is calculated on engine torque; if the clutch is engaged the requested torque **fc_trq_out_r** plus the effect of inertial *fc_inertia* is taken as an output torque **map torque (Nm),** if it respects the engine's maximum torque limits. Otherwise, the minimum between the maximum torque and the maximum requested torque is taken. In case the engine is spinning up, the maximum value between the actual torque and the torque required to accelerate the motor T closed throttle is taken; if the engine is spinning down, the T_closed throttle is taken. Also, the **torque to shaft (Nm)** is calculated by subtracting from the map torque the effect of inertia.

Finally, with the speed and torque calculated, the fuel use and EO emis Configurable Subsystem is assessed; the more relevant subsystem is the HOT engine maps where the fuel used is determined on the map f**uel (g/s)** indexed by torque and speed. Also, emissions are determined, but this will not be used in this current work. Furthermore, the fuel used is corrected considering the engine temperature model. Essentially, the temperature calculated by the model is used to define if the engine is cold or not; in the case of the hot engine, the fuel used is map-based; otherwise, a correction is applied in the map's output. The correlation used for this depends on coolant temperature calculated in the thermal model, and was developed by NREL using hot and cold engine data collected. It was assumed that the engine is always hot in this work, since we only have a hot engine map. The full fuel converter is contained in ANNEX O. (NREL, 2003)

2.7 Validations and Statistics index review

To validate the models used in this work, two indexes were applied to measure the prediction quality. The primary is the RMSE (root mean squared error):

$$RMSE = \frac{\sqrt{\sum_{k=1}^{N}(y(k) - \hat{y}(k))^2}}{\sqrt{\sum_{k=1}^{N}(y(k) - \bar{y}(k))^2}} \tag{63}$$

Where: $\hat{y}(k)$ is the simulated signal, $\bar{y}(k)$ is the average of the measured signal, and $y(k)$ is the measured signal calculated in the identification window. Furthermore, when the RMSE values are less than one unit, it implies a high performance of the model considering the standard measure, the average. The second index used was the MAPE (mean absolute percentage error)

$$MAPE = \frac{1}{N}, \sum_{K=1}^{N} \sqrt{\left|\frac{y(k) - \bar{y}(k)}{y(k)}\right|^2} \tag{64}$$

The analysis of the MAPE index is straightforward. The lower the value, the better the prediction of the model; however, when $(y(k))$ is equal to zero, division by zero occurs.

Furthermore, during the validation analysis in this study, a statistical tool called Box Plot was used; this is a valuable visual approach to displaying data. The box plot in Figure 51 shows the maximum, minimum, upper, and lower quartiles (75th percentile and 25th percentile, respectively), as well as the median (the 50th percentile). In addition, from the box's ends to the minimum and maximum values, a dashed line (whiskers) stretches. Finally, outliers are shown by a red + sign. A number is considered an outlier if it exceeds 1.5 times the interquartile range, which is the distance between the bottom and top of each box.

Figure 51 - Compare Random Data from Different Distributions example

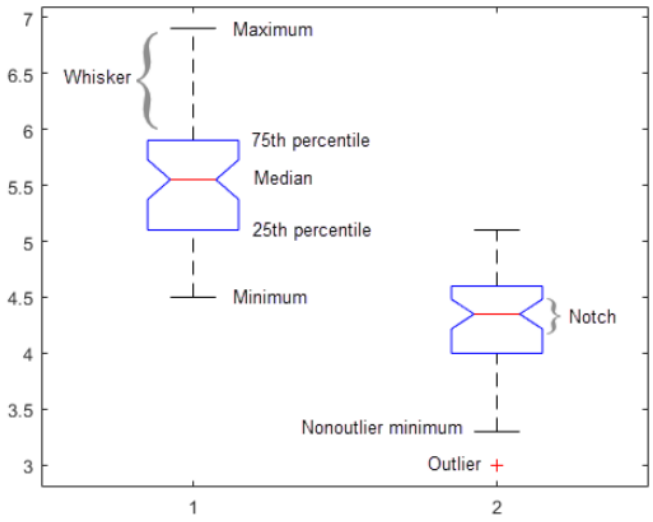

Source: Adapted from Matlab manual

2.8. State-of-the-art review

Recent advances in Hybrid Electric Vehicle research using belt starter generation (BSG) will be summarized in this section.

According to CLUETT (2007), BSG technology can bring various hybridization benefits with a very cost-effective route, mainly because of the possibility for reuse of the vehicle conventional 12V architecture in BSG applications. He studied the impact of BSG technology in an emergent market, and it was concluded that this technology is very suitable for emerging markets due to its low cost and easy implementation. Unfortunately, quantitative data was not provided by this paper.

Opposite, BALDIZZONE (2012) aims in his dissertation at modeling the BSG system and simulating the performance characteristics during engine start events, as the second goal in his work. The fuel-saving was estimated for different cycles (UDDS, HWFET), and finally, a parallel HEV proof of concept vehicle was built. Regarding the consumption analysis, a remarkable reduction in fuel consumption of the BSG application was found when compared with the conventional vehicle. For instance, the UDDS city cycle reached between

1.5 to 2.2 l/km (10-25%) of fuel reduction; on the other hand, in the HWFET highway cycle, gains between 0.4 to 0.6 l/km (8-9%) were found. The benefit is highest for the city cycle because the fuel-saving comes mostly from the stop-start and regenerative braking functionalities, and the city cycle is characterized by its repeated stops and braking opportunities. Finally, the stop-start model performance was evaluated, and it showed satisfactory results by observing the effect of electric motor torque on noise and vibration harshness (NVH) performance.

Despite the good results achieved by the BALDIZZONE (2012) study, his work considered a high voltage system between 115V-220V. Consequently, it has a high cost of implementation due to the high impact on conventional vehicle architecture. On the other hand, STEFFAN, HOFMANN, and GERINGER (2015) analyzed the application of a BSG with a 48V system in an ultra-light vehicle prototype, which had only 600 kg curb weight. Also, in this research the 12V BSG system was considered, named as mild-hybrid. The micro-hybrid concept reached 7.8% in the NEDC cycle when compared with a common stop-start configuration. Moreover, to evaluate the likely benefits of a 48V system, simulations were run in WLTC and NEDC cycles, where CO_2 reductions of -6.6% and -17.9%, respectively, were found.

Furthermore, ZO, NAN and PENG (2019) also reports substantial fuel savings for a 48V system, which achieved about 15%. The simulations were made using commercial software AVL Cruise® vehicle system models. Moreover, it was pointed out that the continuous battery capacity increase does not mean an improvement of the fuel-saving effect. In addition, DE OLIVEIRA (2019) investigated the 48V BSG system in a P3 topology installed in a light vehicle. A fuel-saving of between 8% and 12% was identified when compared with the vehicle base. In this case, the well-known commercial software GT-Suite® was used to simulate the vehicle configurations.

Besides commercial software to estimate fuel consumption, the ADVISOR is an open-source software option based on the MATLAB/SIMULINK® programming environment. ADVISOR was developed by the National Renewable Energy Laboratory's advanced vehicle simulator. In (WIPKE et al., 1999) the authors explain the combined backward/forward mathematical model behind ADVISOR. Moreover, in the same paper, the

NREL team evaluated some model quality parameters such as accuracy, speed, flexibility, availability, and ease of use. For this work, the energy accuracy is the main characteristic to be considered, for the US06 cycle the prediction of energy was around 1.9% of accuracy, which is a good result, as this cycle has active extreme conditions, and a lot of ADVISOR assumptions have to be used. On the other hand, for typical cycles such as UDDS and HWFET, the energy predictions can reach 0.02%.

Likewise SENGER, MERKLE, and NELSON (1998) validated ADVISOR by modeling an HEV with series configuration, and comparing the following factors: energy consumption, fuel efficiency, and electrical energy management strategy, with a prototype for several test procedures. Furthermore, uncertainties in measured data and the discrepancies between actual and predicted behavior were discussed. Finally, the ADVISOR weaknesses and strengths were pointed out, and some of these characteristics will be summarized hereafter.

The uncertainties regarding the model were listed. First, high compatibility between the vehicle and simulator regarding control strategy is required. Second, the engine and electric motor efficiency maps need to be reasonably accurate. Third, special attention should be given to the extremely high loads caused by hard acceleration, due to the limited torque capacity of the engines. And last, as ADVISOR considers a quasi-steady assumption, the transient events cannot be accurately described by the model, despite the time step size, and this fact introduces some error. For this reason, the engine model is the most important transient aspect to be observed, as it is extremely nonlinear and cannot be well modeled by quasi-steady assumptions. Unfortunately, the current ADVISOR version does not have any estimation of engine transient behavior; this issue could be faced with nonlinear modeling techniques, such as a neural network.

Despite the uncertainties of the ADVISOR simulator, it has been used for many applications. CHEN et al. (2014) used ADVISOR to simulate three city hybrid bus configurations (series, parallel, and series-parallel) in order to investigate the advantages and disadvantages of each configuration during the pre-concept phase. In conclusion, ADVISOR appeared helpful for the decision-taken phase of the HEV project; mainly, to determine the

optimal HEV configuration for the city Hybrid bus design. In this case, the best configuration was a series-parallel HEV system with an engine at the rear and an electric motor at the front.

ADVISOR has also been used to simulate control strategies, and CHENG, LAI, and TEH (2017) proposed in their study an appropriate control strategy using a memetic algorithm (MA). The model was evaluated by using ADVISOR as a simulator tool running the UDDS drive cycle. The conclusion was that the MA can increase fuel economy by around 3% to 4% when compared with the parallel HEV base. Also, JOHNSON, WIPKE, and RAUSEN (2000) applied ADVISOR to simulate a Real-Time Control Strategy (RTCS) to demonstrate the advantages and flexibility of this control methodology. The RTCS reduced the PM emission by 13%, NOx emissions by 23%, and fuel economy when compared with a PNGV-type baseline parallel HEV (42 kW engine and a 32-kW motor).

Table 14 - State-of-the-art summary

Paper reference	Electric Architecture	Vehicle	Driving cycle	Engine type	Fuel economy Improvement
(BALDIZZONE, 2012)	(115 V-270V)	PoC	(UDDS, HWFET)	SI gasoline, V6, aspirated, 3.6 L	UDDS: 10-25% HWFET: 8-9%
(STEFFAN; HOFMANN; GERINGER, 2015)	12 V	CULT (600 kg)	NEDC	DI , GNG(compressed natural gas), 3cyl, turbocharged engine, 0.658 L	NEDC: 7.8% (Co2 reduction)
(STEFFAN; HOFMANN; GERINGER, 2015)	48 V	CULT (600 kg)	(NEDC, WLTP)		NEDC: -17.9% (Co2 reduction) WLTP: -6.6%(Co2 reduction)
(ZO; NAN; PENG, 2019)	48 V		NEDC		NEDC: 15% fuel saving
(DE OLIVEIRA, 2019)	48 V	FIAT UNO	FTP + HW	PFI FLEX, aspirated, 1.332 L	FTP + HW: 8% -12% fuel saving
(GUPTA et al., 2020)	48 V	Not cited	Real cycle developed by the author	TSI, turbocharged DOHC I-4 1.8 L (VW EA888)	RC: 10-25%
(CHENG; LAI; TEH, 2017)	12 V	Not cited	UDDS	41 KW Spark Ignition; Geo 1.0 L	3-4%
(JOHNSON; WIPKE; RAUSEN, 2000)		PNGV-type (1028 kg)	(FTP,HWFET,NEDC, WLTP)	42 kW CIDI engine (scaled from Volkswagen 67 kW 1.9 L Turbo Diesel engine, data from ORNL)	As the comparison was between two HEV it will not be present..

Source: Prepared by the author

Finally, MARKEL and WIPKE (2001) applied ADVISOR to investigate an electric utility grid-connected, energy management strategy for a parallel HEV, and to determine the components' sizes using ADVISOR. In SUV indicated in the conclusion, a double of the fuel economy was found when compared with the conventional base, while the performance constraints remained. Moreover, the all-electric range capability of 20 miles has been indicated as a better final vehicle design target, which requires a large energy storage system, and so significant incremental cost is associated. Table 14 summarizes the state-of-the-art results:

3 Methodology

In this section, the methodology will be presented. To assess the BSG technology's impact on the Brazilian market, two factors were considered in this work: the vehicle subsegments and engine size.

The subsegments selection was driven by the market growth of the subsegments in 2019, according to Fenabrave. As can be seen in Figure 52, the chosen subsegments Hatch and SUV indicated in Table 15 represent 59.5 percent of light vehicles registered in Brazil in 2019. Furthermore, bill Nº 9.557 predicts a decrease from 1% to 2% of the vehicles' federal tax, depending on the global fleet energy efficiency reduction. Moreover, both subsegments' characteristics are presented in subsection 3.1. (FEBABRAVE, 2019; REPÚBLICA, 2018).

Figure 52 - Percentage Evolution by Subsegments

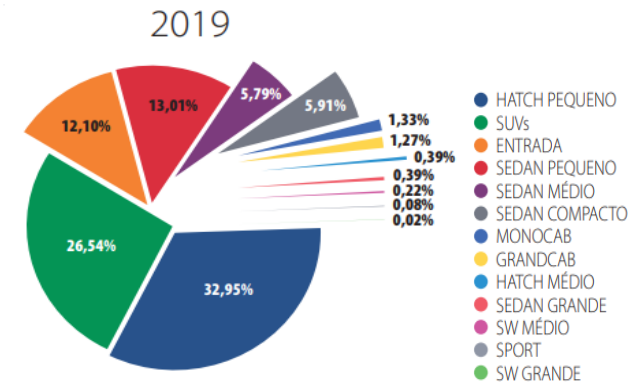

Source: adapted from the Fenabrave report 2019

Besides that, the combustion engine was the second factor, and the choice was driven by the availability of data to feed the model. For the hatch subsegment, a 1.4-liter well-known engine was considered. In the case of SUVs, a 1.8-liter engine was used. More information regarding the engines used can be found in section 3.2. Finally, Table 15 shows the matrix of vehicle configuration. Note that there are two configurations for each subsegment, one base line indicated by a BL at the beginning of the name, and another Hybrid marked with 12V at the end. The BL is the vehicle without any electric system, while the 12V count with the BSG 12 V is implemented. The base configuration was duplicated with the acronyms E22 and E100, indicating both fuels used in this work, totaling eight vehicle models.

Table 15 - Configuration selected

Vehicle name	Subsegments	Engine
BL_H_1.4_E22 BL_H_1.4_E100 H_1.4_E22_12V H_1.4_E100_12V	Hatch	1.4
BL_SUV_1.8_E22 BL_SUV_1.8_E100 SUV_1.8_E22_12V SUV_1.8_E100_12V	SUV	1.8

12V electric architecture was chosen due to its low implementation cost, easy control strategy, and relative fuel consumption benefit as discussed in subsection 2.1.3 of this work. The batteries and electric motor were selected by marked analyses. The battery considered was a lithium-ion manufactured by the A123 Company, while the electric motor was a permanent magnet claw pole synchronous type. The characterization of the battery and electric motor can be found in sections 3.3 and 3.4 respectively.

To evaluate the benefits of the BSG 12V technology two standard driving cycles (FTP-75, and HWFET) discussed in subsection 2.5.2 and a real-world driving cycle called herein the SP cycle subsection 2.5.4 were simulated using the ADVISOR platform already presented in section 2.6. Furthermore, many assumptions and data have been adopted. The values used to populate the vehicle model described in subsection 2.6.1 can be found in section 3.1 in the general vehicle characteristics Table 16. Furthermore, the vehicle model validation was provided in subsection 3.6.1 where the coast-downs and their parameters were calibrated to consider a real data test.

In Tables 17 and 18, the tire characteristics and gearbox characteristics respectively in section 3.1 provide data for the “Wheel and axle, 2 axle 1 driveline converter, and final drive models” and “Gearbox, and clutch models” presented in the subsections 2.6.2 and 2.6.3 respectively. At this point it is important to mention that no losses were considered for the wheel, axle, and final drive models, while for the gearbox and clutch, the losses considered were constant at 4% and 1% respectively. Furthermore, the gear shifts were considered fixed based on real tests. Furthermore, the sequence used for each cycle and vehicle can be found in ANNEX G. The engine model described in subsection 2.6.9 is fed by the maps shown in item 3.2 of this chapter and late in subsection 3.6.2, the model output is confronted with the real acquisitions to ensure that the fuel economy estimate is reasonable.

The hybrid system technology was implemented, and with two sources of energy the torque coupler model is needed. This mode was presented in subsection 2.6.4; the loss of the FEAD was not considered and the ratio between the electric motor and engine was determined by parametrization study. The next component modeled was the electric motor, subsection 3.6.5, and the values and maps needed for the model are presented in section 3.3. Furthermore, the hybrid control model was presented in subsection 2.6.6, and to take the best advantage of the hybrid technology, some parameters were calibrated by parametrization in subsection 3.6.3. For the electric loads modeled in subsection 2.6.7, a constant current value of 20A during the operation of the vehicle was used. Finally, the energy storage system is fully described in subsection 2.6.8 and the maps and data used during the simulations are in section 3.4. Moreover, the validation of the hybrid system was made qualitatively in subsection 3.6.3 as there is no real data on the vehicle configurations with the hybrid system. Finally, with the model validated, the simulation route is described in section 3.5.

3.1 Vehicle characterization

The FIAT Uno Sporting 1.4 flex and the JEEP Renegade Sport 1.8 flex were chosen to represent the hatch and SUV categories, respectively. However, some variables were changed from the vehicle reference for this work; for example, the SUV's mass was increased by 79 kg to achieve category 2 (Figure 40 of this work). Furthermore, the reference materials used in this study are open to the public and can be accessed in ANNEX P and Q Aside from that, several factors were looked up in the following sources: (VRUM, 2021a, 2021b) Table 16 shows a summary of the model's general vehicle characteristics. Note that the Advisor variable names were indexed in the Table.

Table 16 - General vehicle characteristics

Variable name	**Mass**	**Frontal area**	**Aerodynamic drag coefficient**
Advisor Variable name	veh mass	veh_FA	veh_CD
Unit	(kg)	(m^2)	(-)
Hatch_1.4	1017@ 1153(std A @)	2.13	0.37
SUV_1.8	1395@ 1600(std A @)	2.61	0.36

Tire characteristics are an important piece of the torque calculation, and in Table 17 is shown the main properties of the used tires. The radius is the design overall ratio from the European Tire and Rim Technical Organization (ETRTO) standard manual.

Table 17 - Tire characteristics

Variable name		**radius**
Advisor Variable name	**Tire**	wh_radius
Unit		m^2
Hatch_1.4	185/60 R15 88H	0.3015
SUV_1.8	215/65 R16	0.343

In addition, the technical documents in ANNEX P and Q gave the gearbox ratios, which are summarized in Table 18. As can be observed, most of the gear ratios are the same, except for the second, last, and gear reduction. These adjustments must be made to overcome the grade requirement and optimize fuel savings due to the Sport Utility Vehicle's increased weight (SUV).

Table 18 - Gearbox characteristics

Variable name	**1ª Gear**	**2ª Gear**	**3ª Gear**	**4ª Gear**	**5ª Gear**	**Ré**	**gear reduction**
Advisor Variable name			gb_ratio			N/A	fd_ratio
Hatch_1.4	4.273	2.216	1.520	1.029	0.872	3.909	4.067
SUV_1.8	4.273	2.316	1.520	1.156	0.872	3.909	4.200

3.2 Engine selection

The FCA Fiat Chrysler Automaker's Fully Integrated Robotized Engine (Fire 1.4) and e-Torque 1.8 engines were chosen to power the automobiles simulated in this study. They're both SI combustion engines, with four cylinders in series and two and four valves on each cylinder, respectively. They're both aspirated and have an electro-hydraulic valve command. Furthermore, both engines can run on any combination of gasoline and ethanol, including the E22 and E100 fuels employed in this study. Table 19 lists the general characteristics of both engines. In addition, both engines are depicted in Figure 53.

Furthermore, as mentioned in subsection 2.6.9, the specific fuel consumption and maximum torque curve are model inputs; these maps and curves were acquired by the Stellantis laboratory in Betim MG while running with E100 and E22 experimentally and are shown in Figures 54 and 55 for the Fire 1.4, and 56 and 57 for the e-Torque 1.8. In addition, to protect Stellantis' intellectual property, the fuel maps were displayed normalized from 0% to 100% in terms of maximum torque.

Figure 53 - Engines used

(a) Fire 1.4 8V EVO

(b) 1.8 E-TorQ EVO FLEX

Source:(MOTOR GERAIS, 2010; QUATRO RODAS, 2018)

Table 19 - Internal Combustion Engine general characteristics

Name (unitless)	Fire 1.4 8V EVO	1.8 E-TorQ EVO FLEX
Manufacturer (unitless)	FCA	FCA
Suction system (unitless)	Naturally aspirated	Naturally aspirated
Injection system(unitless)	sequential phased multipoint	sequential phased multipoint
Fuel (unitless)	Flex (E22 and E100)	Flex (E22 and E100)
Bore (in mm)	72	80.5
Stroke (in mm)	84	85.8
Compression ratio (unitless)	12.35: 1	12.5: 1
Displacement volume (cm^3)	1368	1747
Number of Valves (unitless)	8 valves (4 of intake, and 4 of exhaust)	16 valves (8 of intake, and 8 of exhaust)
Maximum Power (in Kw, and Cv@ rpm)	64.8/88.0 @ 5750 (with E100) 62.6/85.0 @ 5750 (with E22)	97.1/132 @ 5250 (with E100) 95.6/130 @ 5250 (with E22)
Maximum torque(in Nm, and Kgm@ rpm)	122.6/12.5 @ 3500(with E100) 121.6/12.4 @ 3500 (with E22)	187.2/19.1 @ 3750(with E100) 182.3/168.6 @ 3750 (with E22)

Figure 54 - Fire 1.4 8V EVO Specific fuel consumption (in g/kWh)

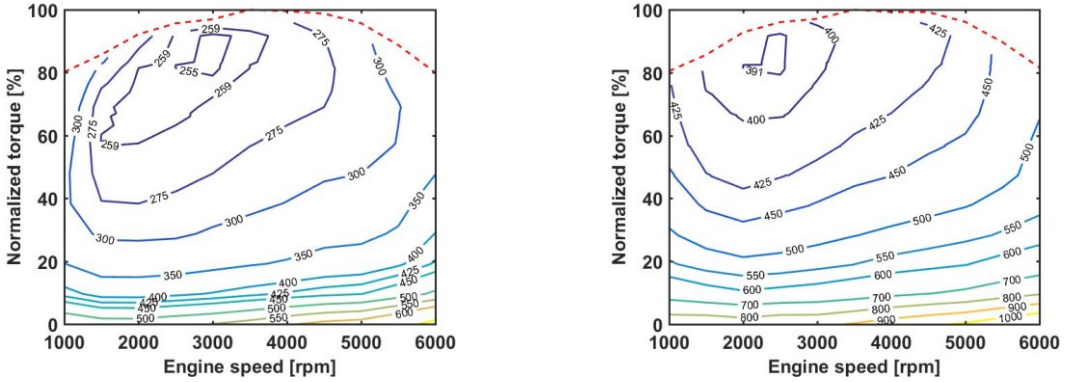

(a) Map with E22 (b) Map with E100

Source: adapted from (FIGUEIREDO, 2019)

Figure 55 - Fire 1.4 8V EVO maximum normalized torque curve

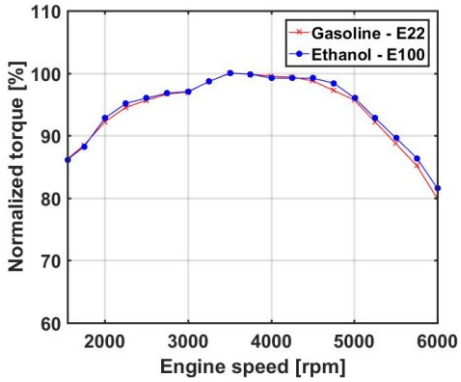

Source: adapted from (FIGUEIREDO, 2019)

Figure 56 - e-Torque 1.8 Specific fuel consumption (in g/kWh)

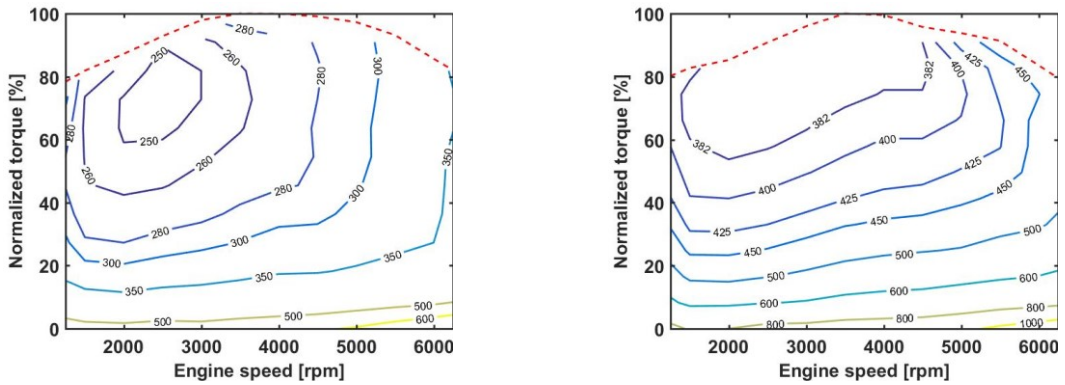

(a) Map with E22 (b) Map with E100

Figure 57 - e-Torque 1.8 maximum normalized torque curve

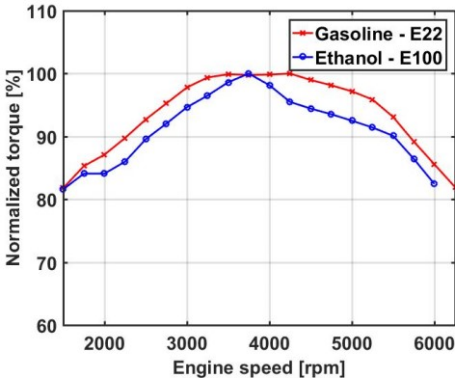

3.3 Electric motor selection

The electric machine used in this work is the permanent magnet claw pole synchronous 12V model, and a further discussion can be found in section 2.2; the main advantage of PM machines are; peak efficiency, compactness, low torque ripple and noise, easy close loop control, and wide speed range. In addition, an example of this type of machine is illustrated in Figure 58, and its main proprieties are listed in Table 20. (FERLITO, 2018)

Figure 58 - Example of electric machine Valeo i-StARS

Source: adapted from (FERLITO, 2018; DE OLIVEIRA, 2019)

Table 20 - Electric Machine Types Characteristics Used

BSG	12 V - motoring	12 V - Generating
Technology	Synchronous claw poles inner magnets	
Peak Power (KW @ rpm)	1.5 @ 1800	4.5 @ 4000
Start Torque (Nm)	50	
Max. Speed (rpm)	18000	18000
Mass (kg)	7.5	
Rotor inertia (Kg*m^2)	0.00385	
Max. Voltage (Vdc)	16	
Max. Current (Arms)	337	289
Max. Temperature (C)	100	

Figure 59 - 12 V Motor efficiency map

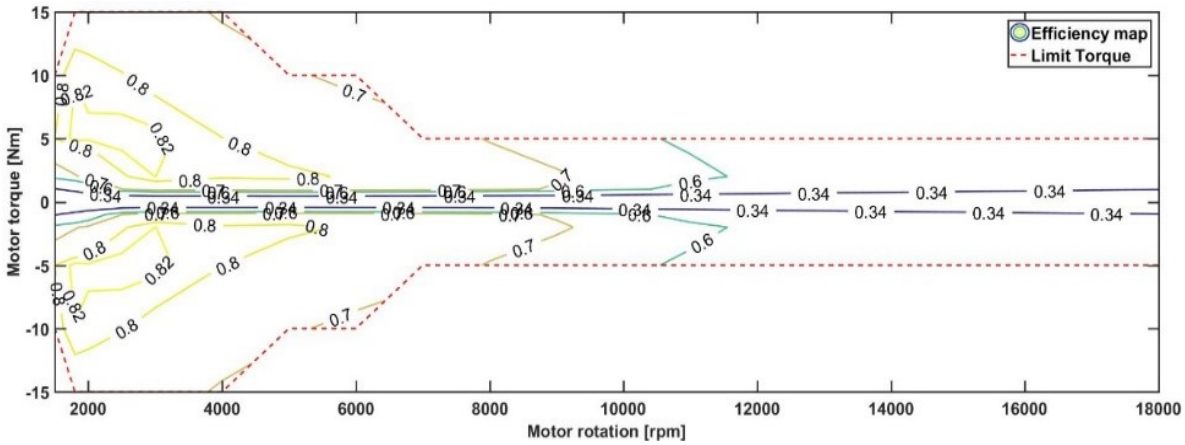

Aside from the rotor inertia already mentioned in Table 20, electromechanical efficiency, as well as torque restrictions when operating as a motor and a generator machine, are necessary to meet the model requirement given in subsection 2.6.5. As a result, the efficiencies are depicted in Figure 59. In addition, positive torque denotes motor operation, whereas negative torque denotes generating (regen) operation. Finally, the bounds are torque limitations for motor and generator operation machines that follow the same signal protocol.

3.4 Battery selection

The 12V battery for the ESS was constructed using a lithium-ion technology cell manufactured by the A123 Company. Furthermore, the significance of this technology, as well as its benefits and drawbacks, were examined in this work's subsection 2.3.1. The energy storage model was also defined in subsection 2.6.8. The Voltage Open Circuit (VOC), as well as the internal resistance of Charge (Rchg) and Discharge (Rdis), were necessary to feed this model. Figure 60 depicts the Voc, whereas Figures 61(a) and 61(b) depict the Rchg and Rdis, respectively. It should be noted that no temperature change on Voc was anticipated (LEE et al., 2018a)

As may be seen in Figure 61, the internal resistance changes significantly with temperature. As a result, three temperature levels were used, with the temperatures between them linearly interpolated.

Figure 60 - Open Circuit Voltage (Voc) of A123 System Lithium-ion Battery Cell at 23°C

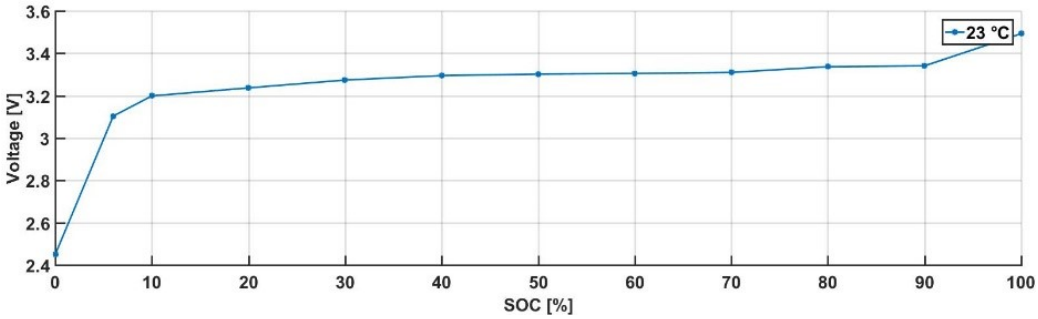

Source: adapted from (LEE et al., 2018b)

Figure 61 - Internal Resistance of A123 System Lithium-ion Battery Cell

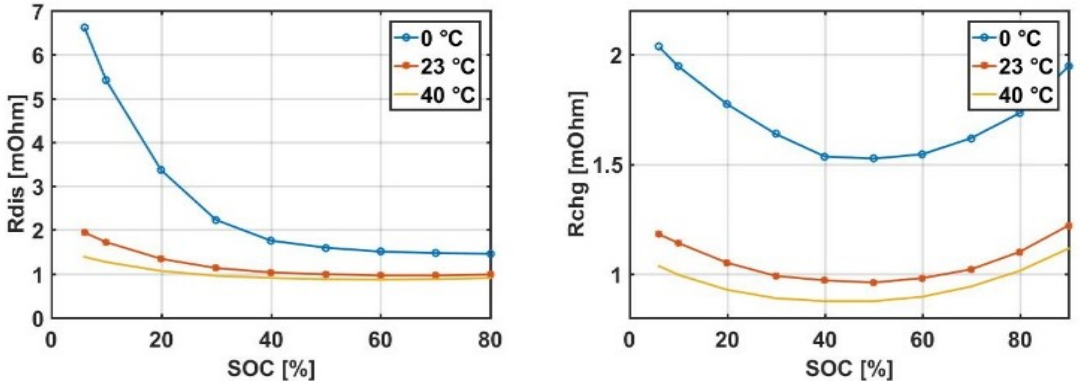

(a) Discharge internal resistance (b) Charge internal resistance

Table 21 - Battery Pack general characteristics

Name configuration	12 V
Pack Configuration (unitless)	4s1p
Manufacturer (unitless)	A123
Technology (unitless)	A123 Systems, LiFePO
Rated Capacity (in Ah)	8
Energy Capacity (in Wh)	105
Mass (in Kg)	3.5 kg
SOC Range (in %)	Determinate by optimization
SOC Operation Windows (in %)	30 - 80
Nominal Voltage (in V)	13.2
Maximum Voltage (in V)	15
Max Discharge Current (during 10s in A)	450
Max Charge Current (during 10s in A)	340

As previously noted, the lithium-ion cells utilized in this study were arranged in 4 series and 1 parallel (4s1p) arrangements to provide a 12 V battery, as shown in Table 21. Furthermore, the SOC Range is a significant feature; as shown in Table 21, the range is between 30 and 80 percent of SOC to safeguard the battery from overheating. Also, a SOC operation window must be determined; for example, in Figure 61, a range of 40% to 60% would reduce resistance in both directions, charge, and discharge; however, this variable is adjusted to minimize the delta SOC and maximize fuel consumption. Finally, the coulombic efficiency was taken from literature for similar battery models and was 0.99. (MI; MASRUR; GAO, 2011)

3.5 Simulations made and analysis methodology

The primary purpose of this research is to estimate the fuel-saving potential of two different vehicle categories when equipped with BSG 12V mild hybrid systems. Initially, the four base line vehicles with both fuels considered in this work, E22 and E100, were simulated, and below is the vehicle configuration list with a short description:

- BL_ H_1.4_E22 (Baseline, hatch, engine 1.4, E22 fuel)
- BL_ H_1.4_E100 (Baseline, hatch, engine 1.4, E100 fuel)
- BL_SUV_1.8_E22 (Base line, SUV, engine 1.8, E122 fuel)
- BL_SUV_1.8_E100 (Base line, SUV, engine 1.8, E100 fuel)

Note that the configuration name follows the order: the first acronyms BL mean base line, and when no is shown, this means that the configuration has a hybrid system active; the second acronym is the category and can be SUV or hatch; next is the engine capacity, and lastly, the fuel. The above settings were simulated and used to validate the model comparing with the real data in subsection 3.6.2 to calculate the benefits of the hybrid system in chapter 4. Then four new models with hybrid systems were created and listed below. Note that the logic of the names is the same as the base line, but now without BL acronyms; in addition, at the end, 12 V was added to reinforce that this configuration is a hybrid system

- H_1.4_E22_12V (hatch, engine 1.4, E22 fuel, BSG 12V configuration)
- SUV_1.8_E22_12V (SUV, engine 1.8, E22 fuel, BSG 12V configuration)
- H_1.4_E100_12V (hatch, engine 1.4, E100 fuel, BSG 12V configuration)
- SUV_1.8_E100_12V (SUV, engine 1.8, E100 fuel, BSG 12V configuration)

Moreover, for hybrid systems there are four operating modes, as can be seen in Table 22, and to simplify the notation, the combination of operating cases will be presented as follows: case 1 is the case where (conventional S&S) was turned on and the engine turned off at 0 km/h; case 2 is the case where the mild hybrid function was active beyond the S&S; and cases 3 and 4 are the cases where the engine is turned off before the vehicle speed reaches 0, 10 km/h for case 3, and 20 km/h for case 4. Note that it will be denotated case 0 for the baseline simulations, in other words, without any hybrid modes, for instance.

Therefore, in the case of the hybrid system, the four configurations mentioned are simulated four times for each operation in Table 22, resulting in 16 simulations for the hybrid configuration which, when added to the four baseline simulations, totals twenty simulations.

Table 22 - Fuel consumption study cases

Functions cases	S&S conv at 0 [km/h]	Mild hybrid	Advanced S&S at 10 [km/h]	Advanced S&S at 20 [km/h]
case 1	✔			
case 2	✔	✔		
case 3	✔	✔	✔	
case 4	✔	✔		✔

Furthermore, the 20 simulations must be repeated for each cycle; the urban (FTP-75) and highway (HWFET) cycles described in subsection 2.5.2, and the real driving cycle called here SP presented in subsection 2.5.4. In the end, 60 simulations were evaluated in this work. Table 23 shows the simulation schedule example for FTP -75, and the same scheme was used for the other two cycles.

Table 23 - FTP-75 simulation schedule

FTP-75	
SUV_1.8_E100	case 1
	case 2
	case 3
	case 4
SUV_1.8_E22	case 1
	case 2
	case 3
	case 4
H_1.4_E100	case 1
	case 2
	case 3
	case 4
H_1.4_E22	case 1
	case 2
	case 3
	case 4
BL_SUV_1.8_E100	case 0
BL_SUV_1.8_E22	case 0
BL_ H_1.4_E100	case 0
BL_ H_1.4_E22	case 0

3.6 Model Validation

There are three subsections in the model validation section. The coast down cycle is used to validate the resistive forces discussed in subsection 3.6.1. In addition, some adjustments were made as needed. The second step was fuel consumption validation in subsection 3.6.2, which involved simulating both baselines without hybrid components and comparing the results to real collected data from Stellantis Group. The hybrid operation modes defined in section 2.6 are validated, discussed, and detailed in subsection 3.6.3.

3.6.1 Coast Down adjust and validation

As was briefly mentioned, the first validating step consists of the coast-down adjustment, and an optimization process to minimize the error between the measured coast down was used, the blue circles in Figure 62 (a), and 62 (b) for hatch and SUV respectively, and the coast down Advisor's simulation. The coefficients F_0 and F_2 equation 53 in this work were regressed from the optimized curves and are shown in Table 24.

Figure 62 - Comparison between the coast down tested and the optimized

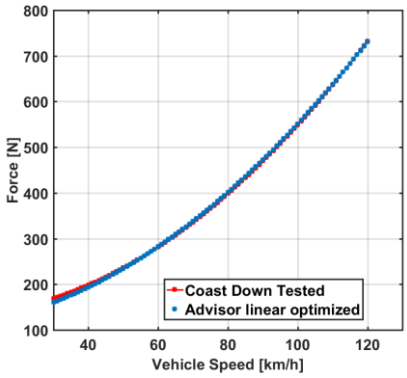

(a) Baseline Hatch category, RMSE = 0.0011

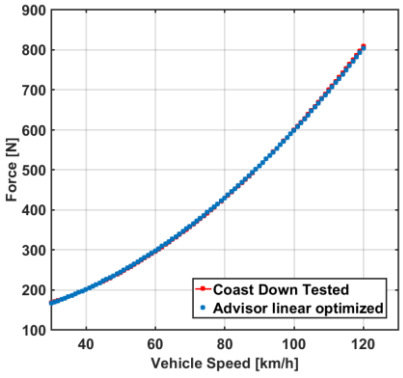

(b) Baseline SUV category, RMSE = 0.0205

Table 24 - Coast Down coefficients tested

Coefficient	F_0 (N)	F_2 (N/(km/h)2)
Hatch_1.4	131.5	0.041
SUV_1.8	123.95	0.047

The objective function equation 65 was evaluated to adjust the rolling coefficients from equation 52 in this work. In Figures 62 (a), and (b) is presented the comparison between the coast down tested and the result optimization, as can be seen by the RMSE, there is a high level of correlation between them.

Decision Variables:

$$C_{r0}$$
$$C_{r1}$$

Objective Function:

$$\min \sum (F(v_{veh}) - C(v_{veh}))^2 \quad (65)$$

Where: (66)

$$F(v_{veh}) = F_0 + F_1 + F_2 {v_{veh}}^2 \quad (67)$$

$$C(v_{veh}) = (C_{r0} + C_{r1} v_{veh}) + F_{aero}(v_{veh}) \quad (68)$$

$$F_{aero} = \frac{1}{2} \rho_{air} A_f C_d v_{veh}^2 \quad (69)$$

Constraints:

$$30 Km/h \leq v_{veh} \leq 120\ km/h \quad (70)$$

$$0.0095 \leq C_{r0} \leq 0.0105 \quad (71)$$

$$0{,}00019 \leq C_{r1} \leq 0{,}00021 \quad (72)$$

$$F_1 = 0 \quad (73)$$

Finally, the rolling coefficients were updated in the Advisor model Table 25, and the simulated cycle presented in the ADVISOR library named CYC_COAST was run, in Figures 63 and 64, the red line with filled circles are shown the simulated cycle added 10% to follow the Brazilian standard for the hatch and SUV configurations, respectively, and this 10 % added force recommendation was assessed in subsection 2.6.1. Furthermore, both cases presented a very good correlation.

Table 25 - Coast Down coefficients adjusted for Advisor

Coefficient	C_{r0}(unitless)	C_{r1}(s/m)
Hatch_1.4	0.0097	2.0720e-04
SUV_1.8	0.0086	7.4745e-05

Figure 63 - Baseline Hatch comparison between real resistive force and simulated plus 10%

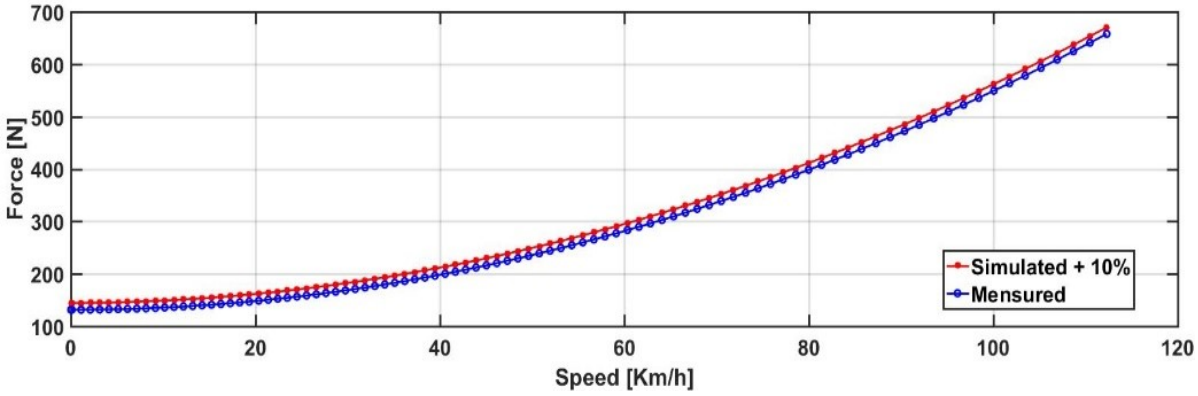

Figure 64 - Baseline SUV comparison between real resistive force and simulated plus 10%

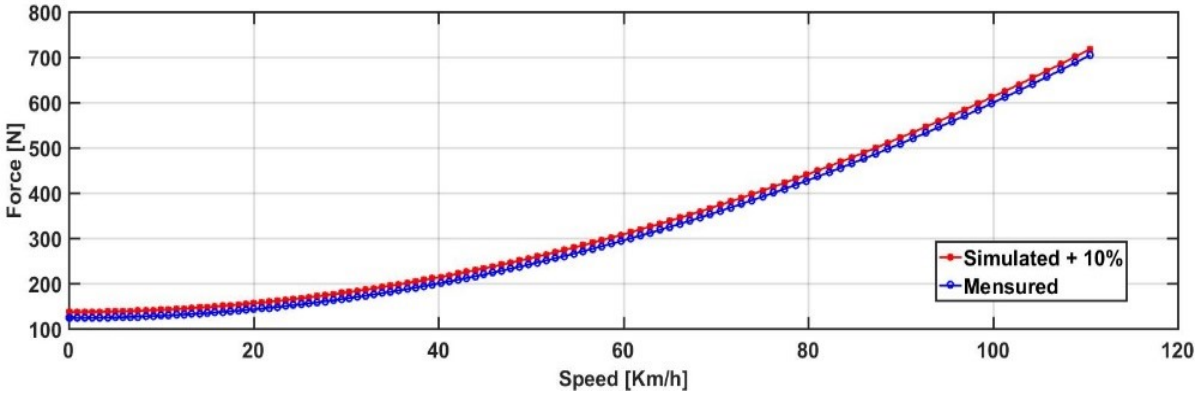

3.6.2 Baseline Fuel consumption validation and correlation

The next validation step was the Baseline fuel consumption comparison analysis, here are presented in detail two baseline models the BL_ H_1.4_E22 and BL_ H_1.4_E100; the test data for this work come from the literature reference (FIGUEIREDO, 2019). The model baselines BL_SUV_1.8_E22 and BL_SUV_1.8_E100 were also validated; however, the results were presented in two summary Tables 28, and 29, respectively, as far as the test data is not public and detailed analysis is not recommended due to company propriety rights.

In addition, for each fuel, five variables were evaluated: vehicle speed, which is the target mission cycle, or the speed profile that the vehicle should follow during the cycles, engine speed, and torque, which were used to access the empirical fuel consumption map to compute the instantaneous fuel consumption for each time step over the cycle, and finally, fuel consumption accumulated, which is the total amount of fuel used over the cycle.

The first graph shows a box plot of the errors across the FTP-75 cycle for E22 fuel Figure 65, and as can be observed, all variables monitored had a minimal error, except for a few outliers generated by noise during the gear change transition.

Figure 65 - Box plot of errors over the FTP-75

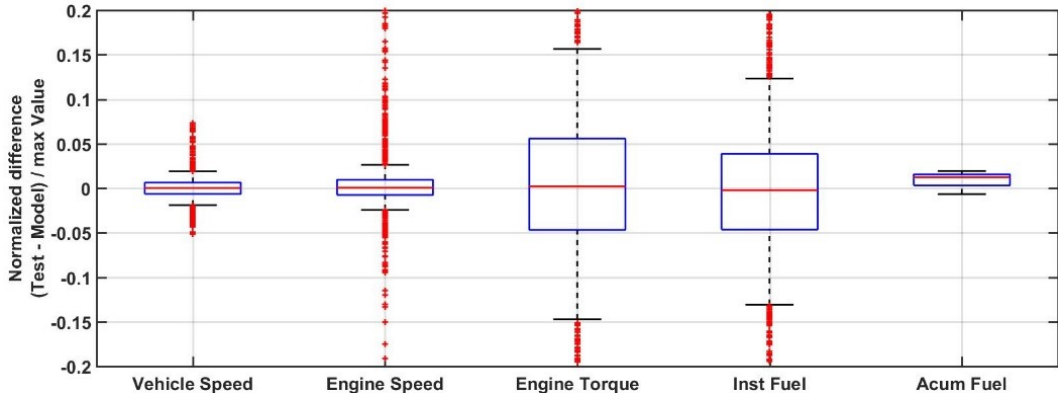

Figure 66 considers only the vehicle speed variable, and it presents a good prediction with a low RMSE and MAPE. Moreover, it is possible to see some outliers. However, this is a result of human interference, since the test is driven manually. Note that most of the outliers are during the gear shift which is hard standardized.

Figure 66 - Comparison of the vehicle speed, and error over the FTP 75 with E22, and comparison of speed tested and speed model. RMSE = 0.0454, MAPE = 0.1860, maximum difference error = 6.77 km/h

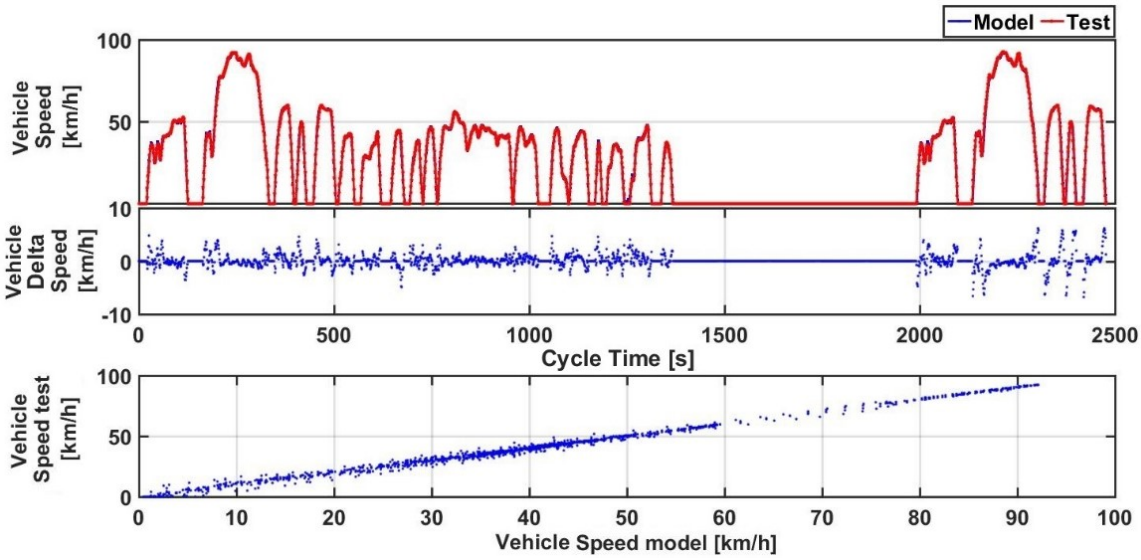

Regarding the engine speed, as in last the case, a high-quality prediction was identified; however, as can be seen in Figure 67, there is one unique attention point where the model follows a different behavior during one accelerating and deaccelerating event. That error did not affect the final fuel consumption result but is responsible for the high maximum difference error. On the other hand, the correlation still presents low RMSE and MAPE.

Figure 67 - Comparison of the engine speed, and error over the FTP 75 with E22, and comparison of speed tested and speed model. RMSE = 0.2623, MAPE = 0.0636, maximum difference error = 1943 rpm

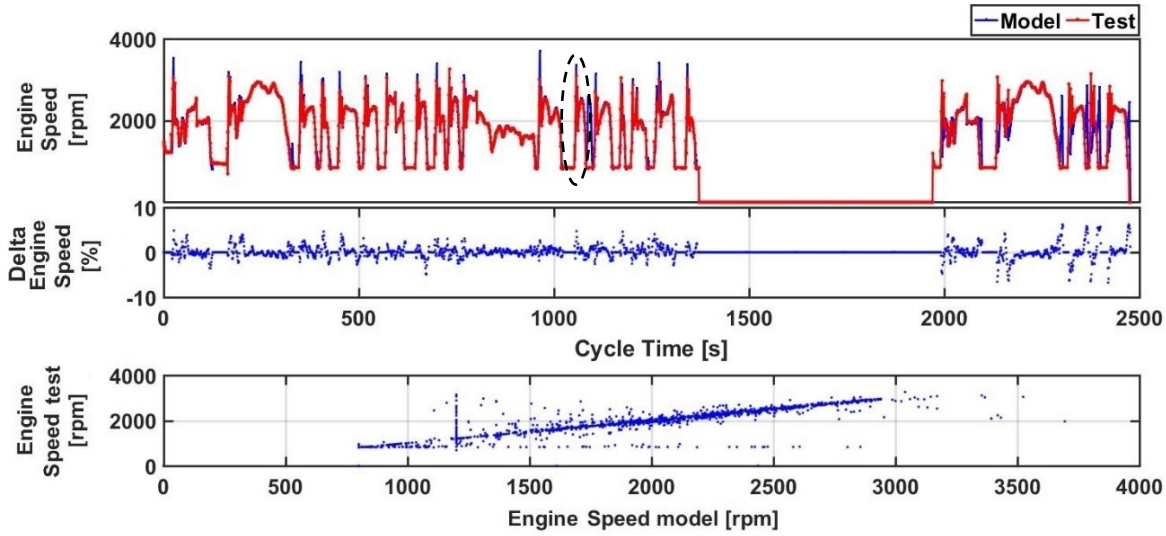

The engine torque represents an attention point in terms of validation, insofar as it presents a high MAPE rounding 8.5, mainly because of the elevated dispersion of errors during the gear shift event, as can be seen in Figure 68. On the other hand, the RMSE is reasonable. Nevertheless, the instantaneous fuel consumption presented a reasonable correlation, as can be seen in Figure 69 of this work. Therefore, there is room for improvement in terms of torque simulation. However, at that moment it did not represent a risk for the simulation because the dispersion did not make an impact on the specific fuel consumption over the cycle. Furthermore, the instantaneous fuel consumption presents two outliers, as are shown in the circles. The first one is related to the cold phase where the consumption is higher than the modeled in this work, and the second looks like an error during the data recording. Again, these isolated outliers did not affect the final result considerably.

Figure 68 - Comparison of the engine torque, and error over the FTP 75 with E22, and comparison of torque tested and torque model. RMSE = 0.4224, MAPE = 8.5325 maximum difference error = 54.73 Nm

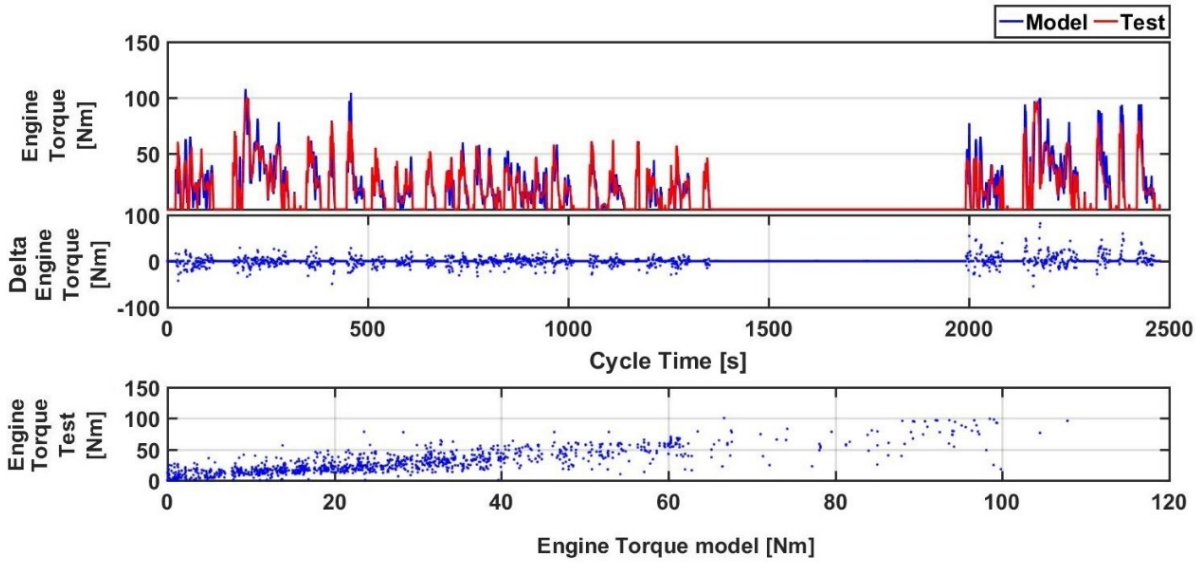

Finally, the accumulated fuel consumption for E22 over the FTP-75 cycle is presented in Figure 70, and as can be inferred, the final result is highly correlated; the RMSE and MAPE are very low, and the maximum difference error was 0.0234. In terms of urban fuel consumption, using equation 47 of this work the autonomy measured was 14.949 km/l and the autonomy simulated was 14.833 km/l; consequently, the simulation is 0.78% over than the measurement.

Figure 69 - Comparison of the instantaneous fuel consumption, and error over the FTP 75 with E22, and comparison of instantaneous fuel consumption tested and instantaneous fuel consumption model. RMSE = 0.4833, MAPE = 0.3275 , maximum difference error = 0.9552 l/s

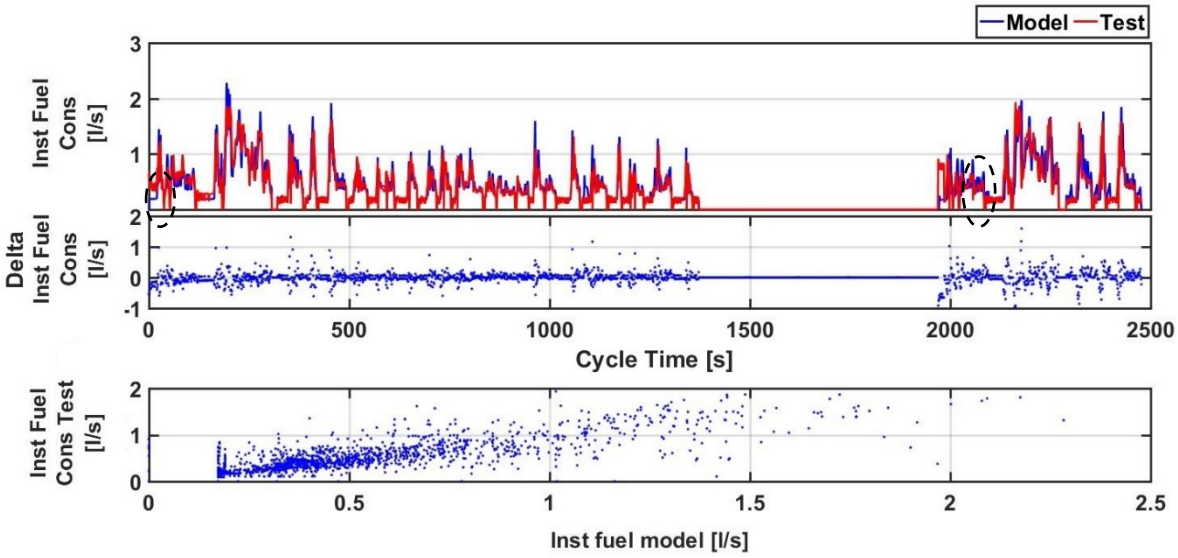

Figure 70 - Comparison of the accumulated fuel consumption, and error over the FTP 75 with E22, and comparison of accumulated fuel consumption tested and accumulated fuel consumption model. RMSE = 0.0421, MAPE = 0.0077 , maximum difference error = 0.0234 l

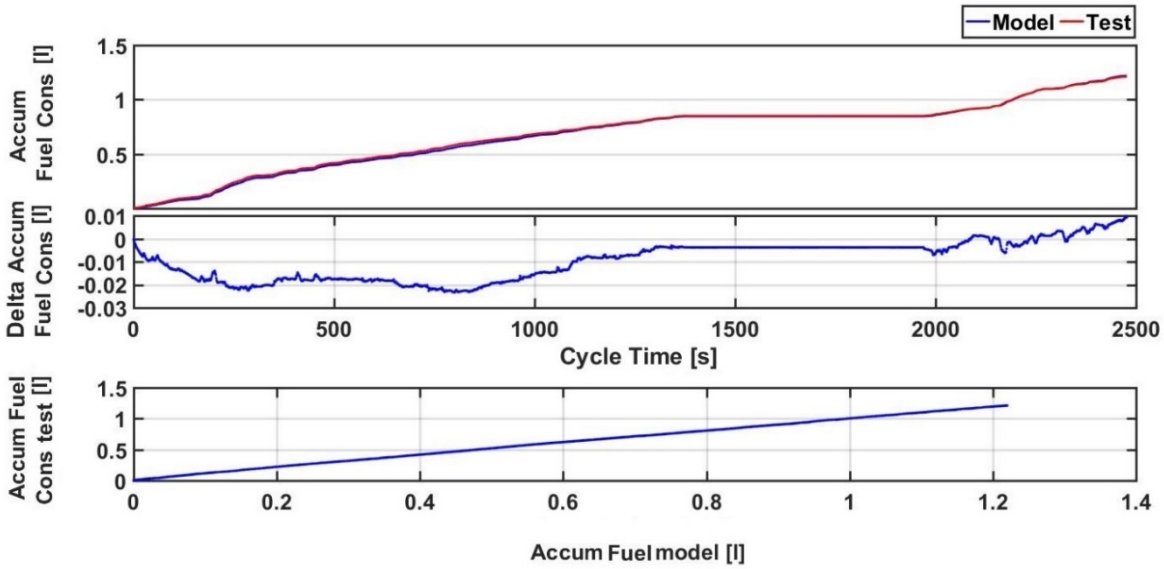

Figure 71 showed the box plot of the errors over the cycle HWFET for E22 fuel, and like the FTP-75, the results are highly correlated. Therefore, from here will be pointed only a few details over the HWFET cycle.

Figure 71 - Box plot of errors over the HWFET

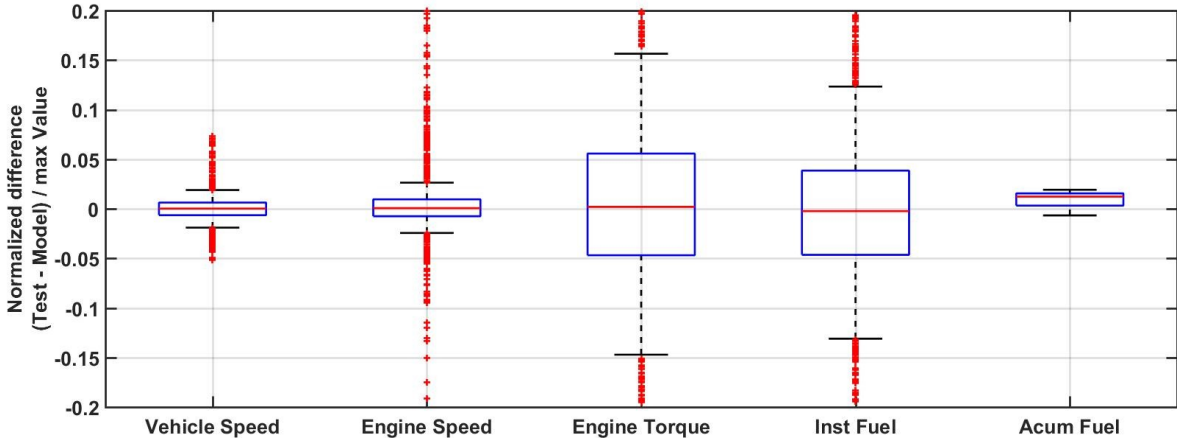

Regarding the vehicle speed and engine speed, the base statistics show a very good correlation; however, there are small differences in Figure 72 during the shift changes, probably because of different step times between the test and the model.

Figure 72 - Comparison of the vehicle speed, and error over the HWFET with E22, and comparison of speed tested and speed model. RMSE = 0.0295, MAPE = 6.2266e-04, maximum difference error = 2.7712 km/h

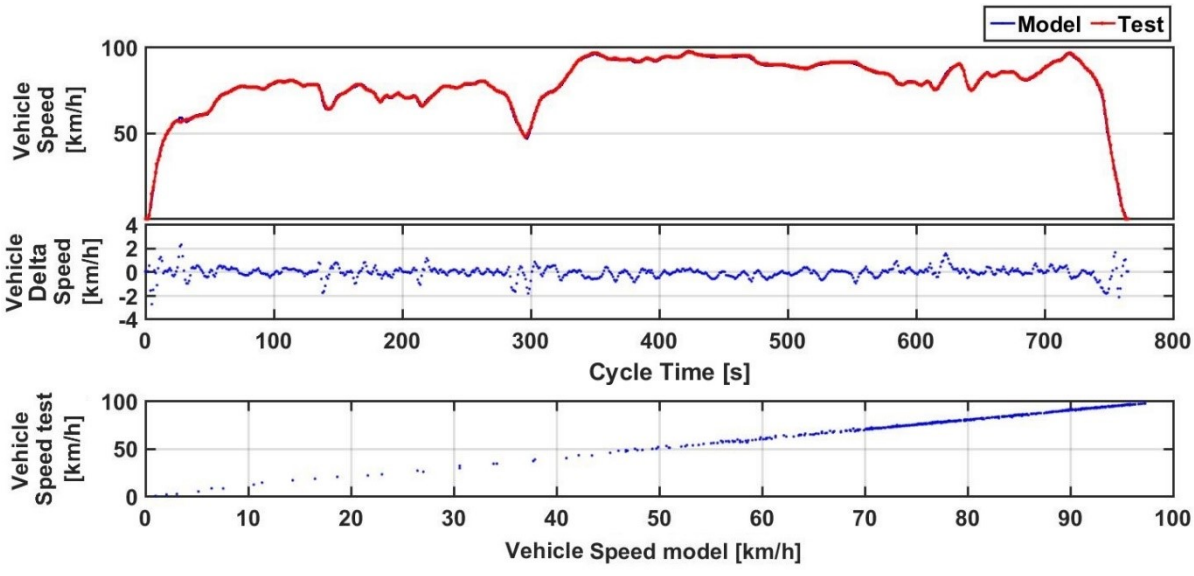

Figure 73 - Comparison of the engine speed, and error over the HWFET with E22, and comparison of speed tested and speed model. RMSE = 0.1042, MAPE = 6.5988e-04, maximum difference error = 572 rpm

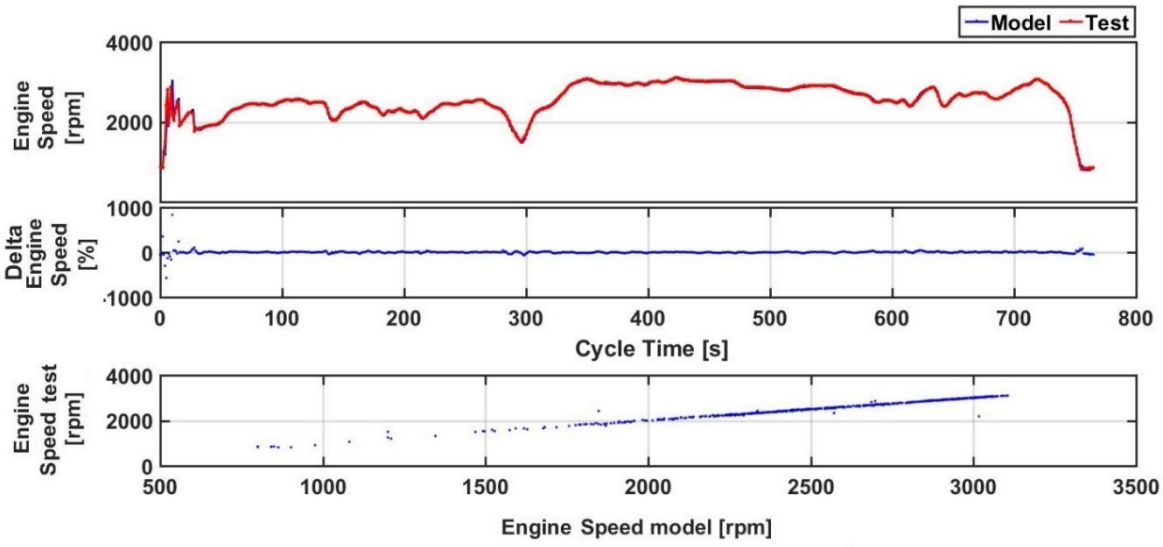

In Figure 74 is shown the engine torque, and like the FTP-75, the MAPE is relatively high when compared with the other variables; however, it is better than the FTP-75. Moreover, this difference did not considerably affect the instantaneous fuel consumption Figure 75.

Figure 74 - Comparison of the engine torque, and error over the HWFET with E22, and comparison of torque tested and torque model. RMSE = 0.3666, MAPE = 1.6963, maximum difference error = 37.30 Nm

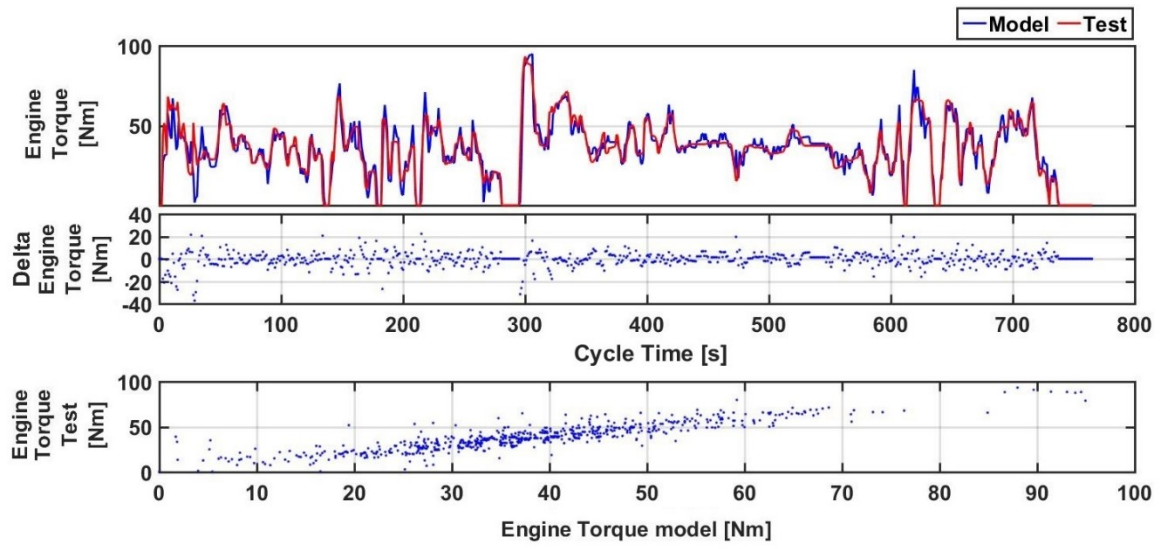

Figure 75 - Comparison of the instantaneous fuel consumption, and error over the HWFET with E22, and comparison of instantaneous fuel consumption tested and instantaneous fuel consumption model. RMSE = 0.3584, MAPE = 0.0480, maximum difference error = 0.499 l/s

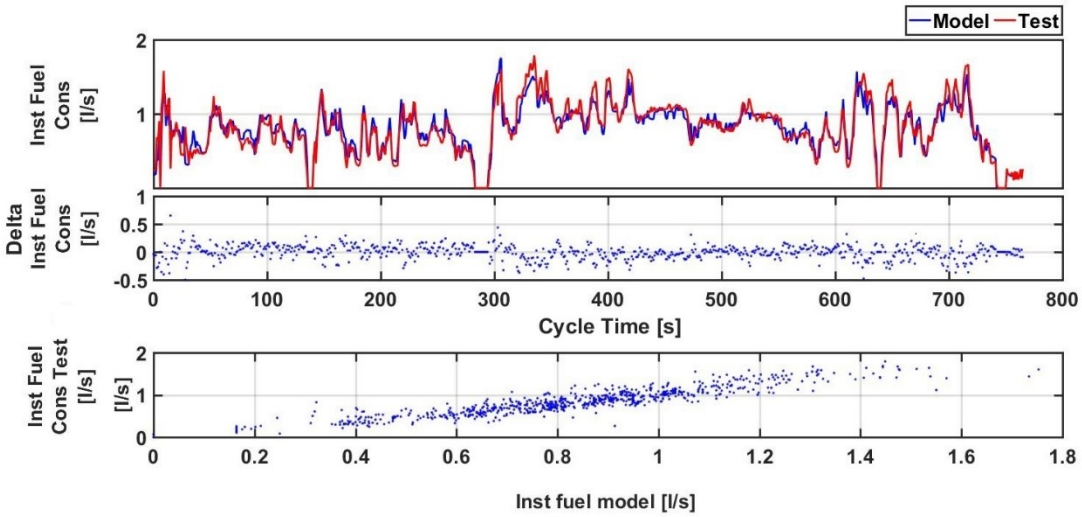

Figure 76 presents the accumulated fuel consumption for E22 over the HWFET cycle, and as can be seen, the final result is highly correlated. The RMSE and MAPE are very low, and the maximum difference error was 0.0079, in terms of autonomy equation 47 of this work, the measurement was 19.206 km/l, and the simulation was 19.370 km/l, consequently, the simulated is 0.89% more than the measured.

Figure 76 - Comparison of the accumulated fuel consumption, and error over the HWFET with E22, and comparison of accumulated fuel consumption tested and accumulated fuel consumption model. RMSE = 0.0223, MAPE = 0.0019, maximum difference error = 0.0079

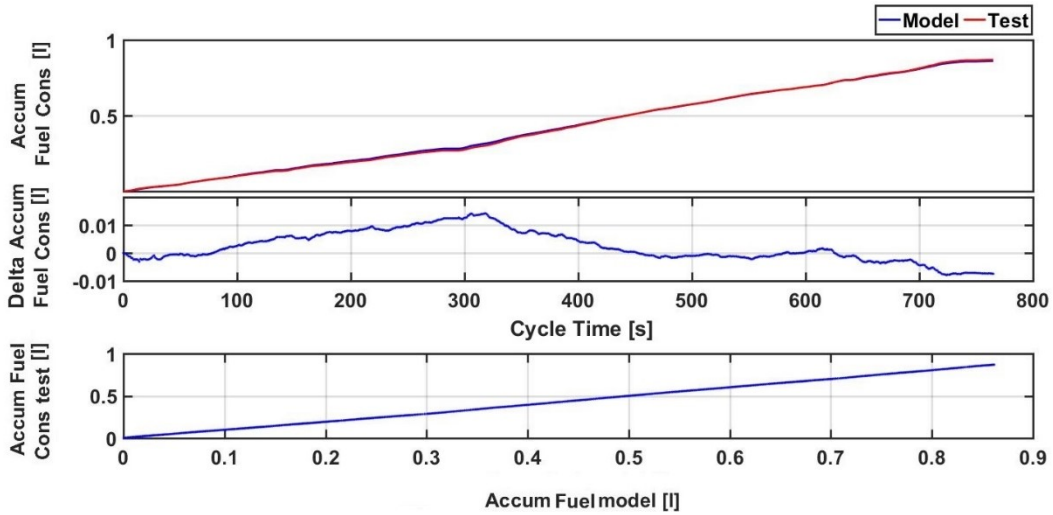

The summarizing of the baseline BL_H_1.4_E22 is presented in Table 26, from now, as was cited before the summary of the validation for the other baselines, “BL_H_1.4_E100”, “BL_SUV_1.8_E22”, and “BL_SUV_1.8_E100” were presented in Tables 27, 28, and 29, respectively.

Table 26 - Summarizing the baseline BL_H_1.4_E22 comparison with test data

	FTP-75			HWFET		
	RMSE	**MAPE**	**MAX DIFF**	**RMSE**	**MAPE**	**MAX DIFF**
Speed	0.0454	0.1860	6.7728	0.0295	6.2266e-04	2.7712
RPM	0.2623	0.0636	1.9430e+03	0.1042	6.5988e-04	572.1512
Torque	0.4224	**8.5325****	54.7397	0.3666	**1.6963****	37.3080
Fuel Inst	0.4833	0.3275	0.9552	0.3584	0.0480	0.4999
Fuel Used	0.0421	0.0077	0.0234	0.0223	0.0019	0.0079

Table 27 - Summarizing the baseline BL_H_1.4_E100 comparison with test data

	FTP-75			HWFET		
	RMSE	**MAPE**	**MAX DIFF**	**RMSE**	**MAPE**	**MAX DIFF**
Speed	0.0610	0.0805	9.1170	0.0611	0.0049	6.1328
RPM	0.3423	0.0705	1.9515e+03	0.2105	0.0020	1.0785e+03
Torque	0.4570	**57.8958 ****	72.4552	0.4013	**3.0749 ****	36.4584
Fuel Inst	0.4732	0.5648	1.5135	0.3776	0.0507	0.8547
Fuel Used	0.0508	0.0126	0.0516	0.0455	0.0062	0.0058

Table 28 - Summarizing the baseline BL_SUV_1.8_E22_ comparison with test data

	FTP-75			HWFET		
	RMSE	**MAPE**	**MAX DIFF**	**RMSE**	**MAPE**	**MAX DIFF**
Speed	0.0445	0.0930	6.1820	0.0563	0.0012	6.0973
RPM	0.3780	0.3445	1824	0.5335	0.0593	1.0341e+03
Torque	0.3819	**93.9348 ****	81.3500	0.5879	**1.0055****	76.1895
Fuel Inst	0.4014	0.4582	1.3808	0.6561	0.6063	1.3042
Fuel Used	0.0451	0.0017	0.0079	0.0354	0.0013	0.0276

Table 29 - Summarizing the baseline BL_SUV_1.8_E100 comparison with test data

	FTP-75			HWFET		
	RMSE	**MAPE**	**MAX DIFF**	**RMSE**	**MAPE**	**MAX DIFF**
Speed	0.0929	0.1617	9.8246	0.0555	0.0014	5.0923
RPM	0.4956	0.1865	2030	0.2688	0.0093	1479
Torque	0.4972	1.2832	50.5465	0.4648	0.0601	43.9918
Fuel Inst	0.4523	0.2010	2.2545	0.4488	0.1156	1.0776
Fuel Used	0.0376	0.0065	0.0278	0.0262	0.0053	0.0079

In BL_H_1.4_E100, BL_SUV_1.8_E22, and BL_SUV_1.8_E100, there are some attention points marked with a double asterisk on the torque. These outliers could be generated due to some sensor problem, or even error in the torque calculation, as the engine torque is not a direct measurement, but a calculation in the engine computer unit; however, there is no impact on the fuel consumption. As the main proposal of this work is to measure the delta fuel consumption between the technologies, these differences were not deeply assessed.

Also, the final fuel autonomy perceptual difference for the baselines in Table 30 was summarized. When the diff value is positive and the arrow up means that the model result value is over, then the test data value is in terms of autonomy, otherwise, the opposite is true. In general, the results represent reality well. The model was capable of reproducing the vehicle behaviors and, considering that the hybrid technology benefit will be compared between simulations, the technology delta gain will not be affected by these discrepancies, but only the absolute autonomy will be affected. Note that all autonomy validation differences are between (+/-) 1% of the difference.

Table 30 - Summarizing the final consumption accumulated over the cycles FTP-75 and HWFET.

[km/l]	FTP-75			HWFET		
	Test	Model	Diff	Test	Model	Diff
BL_H_1.4_E22	**14.949**	**14.833**	**- 0.78 % ↓**	**19.206**	**19.370**	**+ 0.89 % ↑**
BL_H_1.4_E100	**10.021**	**10.125**	**+1.02 % ↑**	**12.816**	**12.765**	**- 0.39 % ↓**
BL_SUV_1.8_E22	**12.959**	**12.854**	**- 0.81 % ↓**	**14.327**	**14.599**	**+0.91 % ↑**
BL_SUV_1.8_E100	**9.802**	**9.870**	**+ 0.68 % ↑**	**10.743**	**10.677**	**- 0.62 % ↓**

The operating points for FTP-75 and HWFET are displayed over the efficiency map for the two baseline vehicles, 1.4 and 1.8, in Figure 77. These graphs will be used to show how the BSG effect affects the engine and, as a result, the specific fuel consumption. Due to inaccuracies in gear change transition, there are few outliers in the SUV categories 77(b) and 77(d), FTP-75 and HWFET, respectively.

Figure 77 - Comparison of the baseline BL_H_1.4_E22 operating points and BL_SUV_1.8_E22 obtained with simulations of the conventional vehicles.

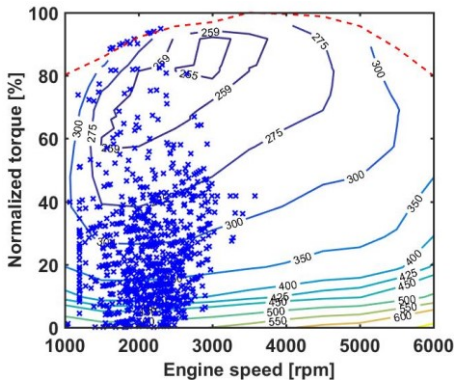

(a) FTP-75 Cycle for BL_H_1.4_E22

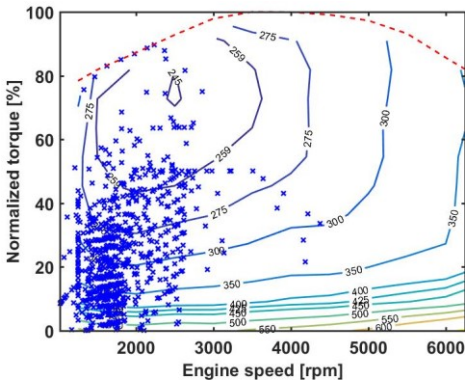

(b) FTP-75 Cycle for BL_SUV_1.8_E22

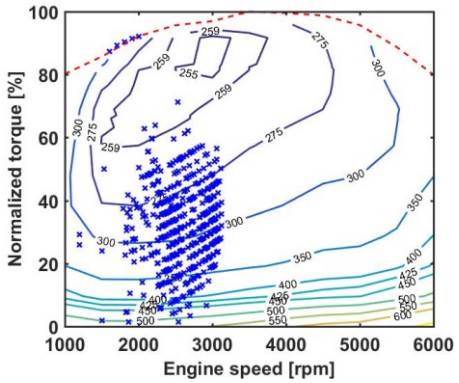

(c) HWFET Cycle for BL_H_1.4_E22

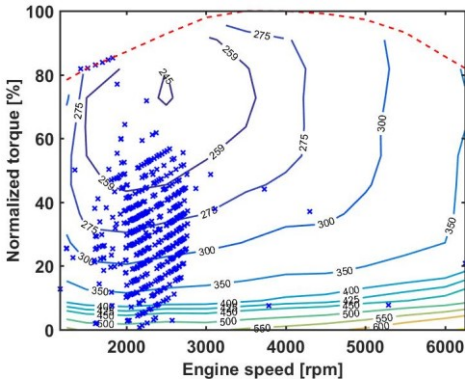

(d) HWFET Cycle for BL_SUV_1.8_E22

3.6.3 Validation and analysis of the hybrid system

In this work, three main hybrid functions will be considered: conventional stop-start (S&S), mild hybrid (which includes regenerative braking and torque-assist), and advanced stop-start (where the engine is turned off during deceleration before the vehicle speed reaches zero). In this work, two shut down engine speeds of 10 km/h and 20 km/h were considered.

In case 1, as can be seen in Figure 78, where the cycle FTP-75 is shown, the engine is correctly shut off. As a result, the advantage of the S&S function appears to be realistic. Furthermore, the maximum stop occurrences on the FTP-75 cycle were determined as 23 engines shutting down. In addition, the FTP-75 was chosen to verify the hybrid system due to a large number of S&S events, as all of the functionality examined here is primarily dependent on regeneration during deceleration and engine shut down occurrences

Figure 78 - Vehicle speed and engine speed comparison between case 0 and case 1

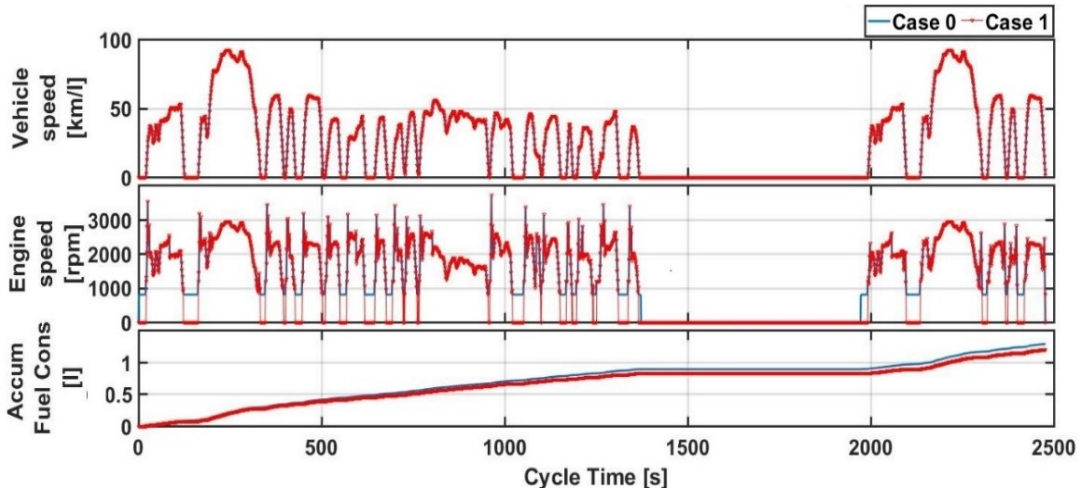

In case 2 the mild hybrid is enabled, and as was cited, there are two main functions: the regenerative brake named hereafter (regen), and the torque assist. The regen occurs during the deceleration phase when part of the energy is used to stop the vehicle flow from the wheel to the battery by increasing the engine brake. Moreover, the regeneration efficiency in this configuration is low when compared with other architectures, because the electric generator is mounted on the front end accessory drive (FEAD); therefore, there is a large energy loss through the energy transmission from the tire to the battery, as can be seen in Figure 79 for a hypothetic deceleration event during the FTP-75 cycle.

The wh/axle dissipation, which is the loss through the axle and friction brakes, the loss at the motor, which occurs due to friction at the engine and engine pumping, and lastly the energy loss due to the wire transmission and battery heating in the storage system were all evaluated in this study (battery storage). Note that the FEAD's loss was ignored at the time. Section 2.1 contains more information regarding the regeneration function.

Figure 79 - Regeneration losses example during a deceleration event over the FTP-75 Cycle

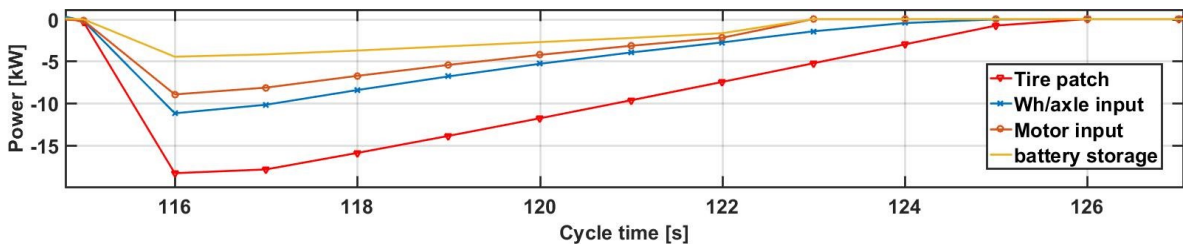

Furthermore, the capability of regeneration is related to the concept of the mild hybrid vehicle, which was described in subsection 2.5.1 and defined by equations 38,39,40,41,42 and 43. If the brake energy recovery capacity of the hybrid vehicle is between 15% and 65 percent, it is categorized as mild. Following the equations mentioned, Table 31 reported the energy recovered value for the two-vehicle categories and fuel used in this study. This is why, in this study, we are categorizing the BSG 12V technology as a mild hybrid, even though other classifications, such as the one stated in subsection 2.1.2, classify it as a micro-hybrid.

Table 31 - Energy recovered calculation

Categories	**Energy Recovered %**
Hatch_1.4_E100 - Hatch_1.4_E22	16.6 % - 16.5%
SUV_1.8_E100 - SUV_1.8_E22	16.9% - 16.8%

The storage system and electric motor restrictions, as discussed in sections 3.3 and 3.4, are two more important considerations. The current, voltage, and operation temperature restrictions are the most important. Throughout the cycles simulated in this study, both current and voltage were kept within their respective ranges. Furthermore, the SOC was kept within the 3.4 section's literature range. The current and voltage variations during the FTP-75 cycle, for example, are represented in Figure 80. All the cases were subjected to the same investigation.

Figure 80 - ESS current and voltage limits

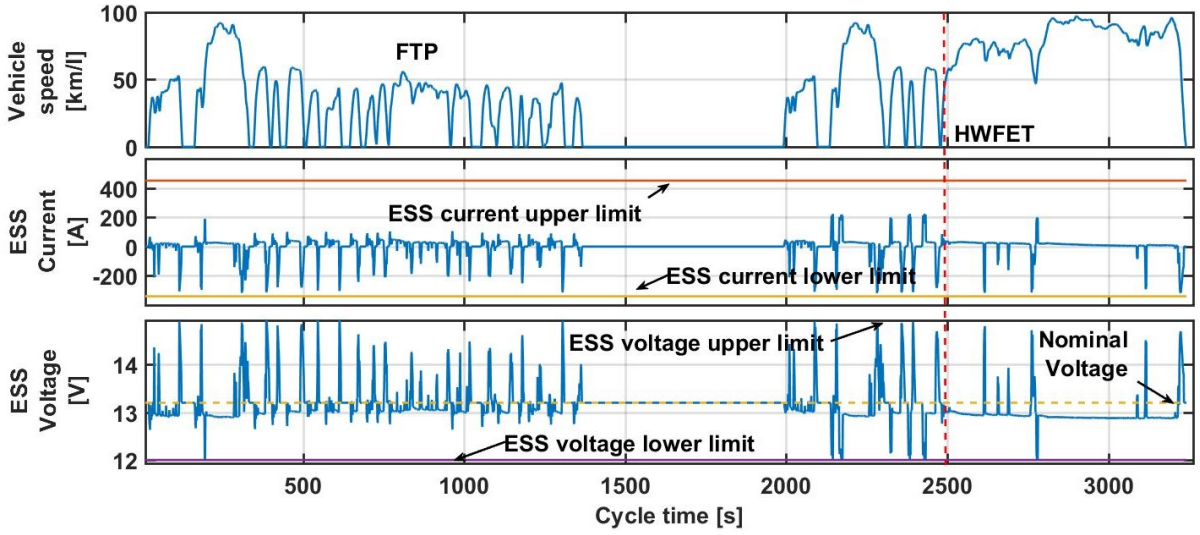

Figure 81 - NEC tolerance example

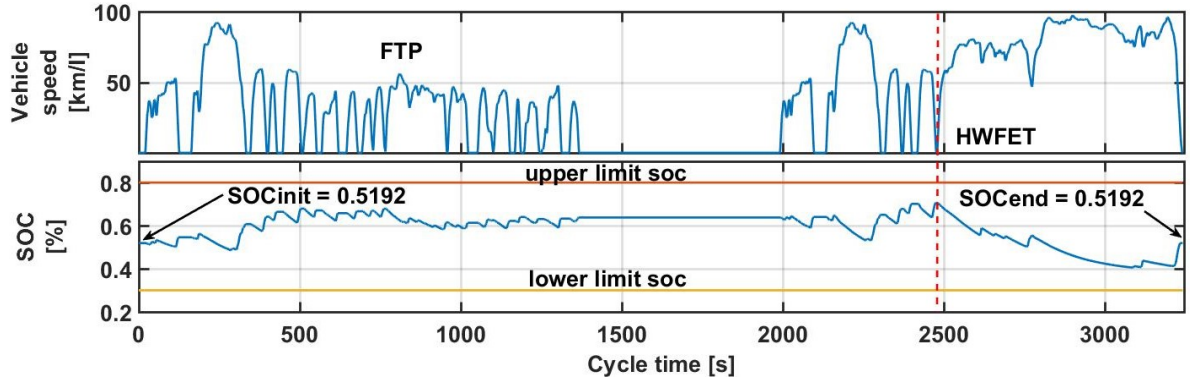

Also, the net energy change (NEC) tolerance was respected. In other words, the net energy balance between the beginning and the end of the test (FPT-75 plus HWFET) was not over 1%. To calculate this, the electrical energy used is divided by the total fuel energy used. The initial state of charge (SOCinit) was optimized to meet the NEC criteria, and as can be seen in Figure 81, the final SOC was the same computing NEC equal to zero, and this optimization was repeated for all simulations.

Figure 82 depicts two instances of mild hybrid functionalities: regeneration, which was previously described, and torque assist, which will be evaluated here. As can be seen, torque assist events occur when the current is positive and there is positive acceleration or even a continuous torque request.

Figure 82 - Example of torque assist and regeneration events over the FTP-75 cycle

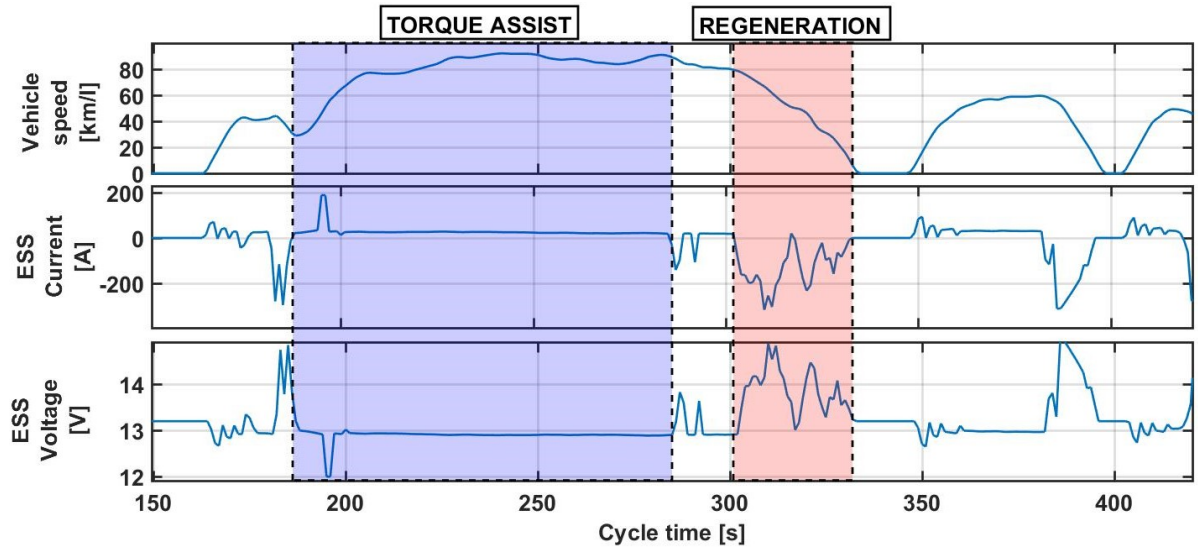

Figure 83 illustrates the torque assist function, from which it can be seen that the fuel consumption gain is provided by a proportionate reduction in torque requested from the engine, based on SOC equation 59 subsection 2.6.6. As a result, the amount of fuel required to complete the cycles decreases, increasing autonomy. On the other hand, because some of the torque came from the electric motor, the specific engine fuel consumption decreased, as shown in Figure 84, which compares case 1 without mild hybrid features enabled to case 2 with them.

Figure 83 - Torque assist detailed

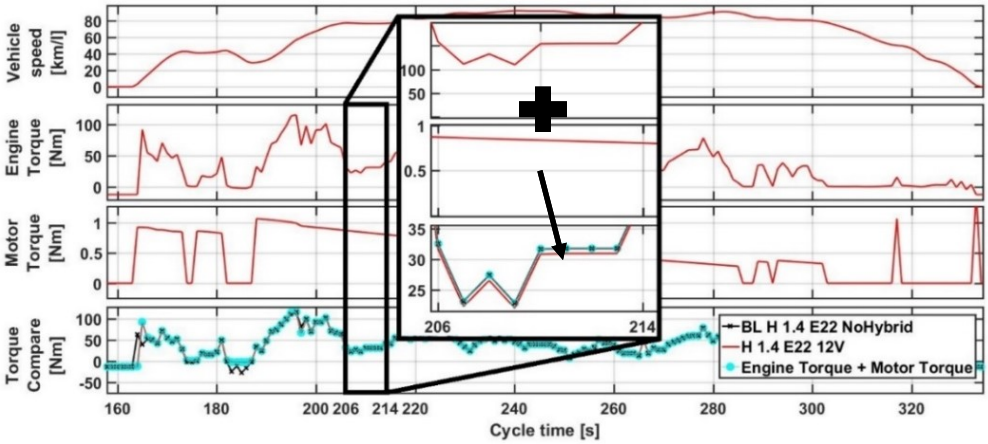

Furthermore, the zoom-in Figure 83 reveals that the total of engine and motor torque equals the baseline torque. In other words, the torque provided to the vehicle remains the same. Note that the Motor Torque signal has been inverted to make it easier to comprehend, although it is negative in the strategy.

Figure 84 - Example of the engine operate points comparison for case 1 and case 2 over the FTP-75 cycle

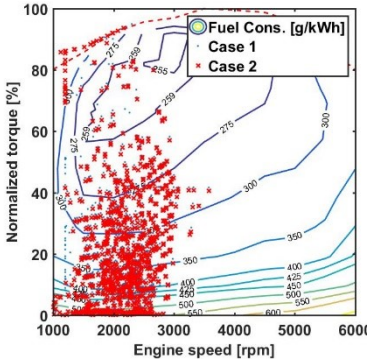

Furthermore, the values for the $\tau_{chage\ torque}$ torque factor in equation 59 were selected by parametrization. Table 32 shows the factor for each category, and the parametric study was developed using a tool in the Advisor where the torque factor was varied from 0 Nm to 2 Nm within 0.1 Nm of increment, then the fuel consumption and the delta SOC were normalized, and as can be seen in Figure 85 for both hatch and SUV, the best peak of autonomy was when the torque factor was 0.5 Nm. At this torque level, there is not any delta SOC.

Table 32 - Torque factor parametrized

Coefficient	$\tau_{\text{chage torque}}$
Hatch_1.4	0.5 Nm
SUV_1.8	0.5 Nm

Figure 85 - Torque factor parametrization results

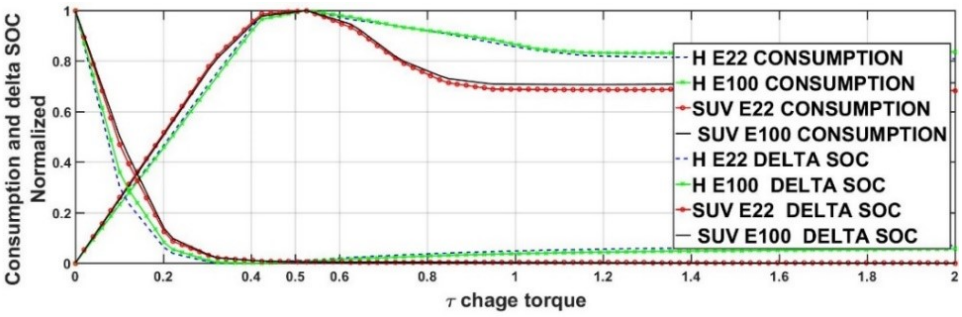

Figure 86 shows an example of motor operations points over the FPT-75 cycle, and it is clear that the cloud of operation points during the torque-assist events positive part of the graphic is less than 1 Nm, as can be seen on the zoom due to the low torque factor, which is expected, given that the electric motor used has a low continuous torque capability of 1.5 KW, but some points over 1 Nm can nonetheless be observed due to the engine starter during the S&S. Another point to be observed is that the amount of energy available to be used is low when compared with other BSG architectures due to the loss characteristic of P1f; in other words, to keep the balance of energy, not much energy can go out during the torque assist.

In the negative half of the graph, regarding the regenerative braking operation points, the strategy tries to recover as much as possible while staying within the minimum torque

curve. Due to the S&S advance at 20 km/h that released the clutch, there is a low-density zone when the motor rotation is less than 2000 rpm in case 4, designated as the blue circles.

Figure 86 - Example of operating points for all cases over the FTP-75 cycle.

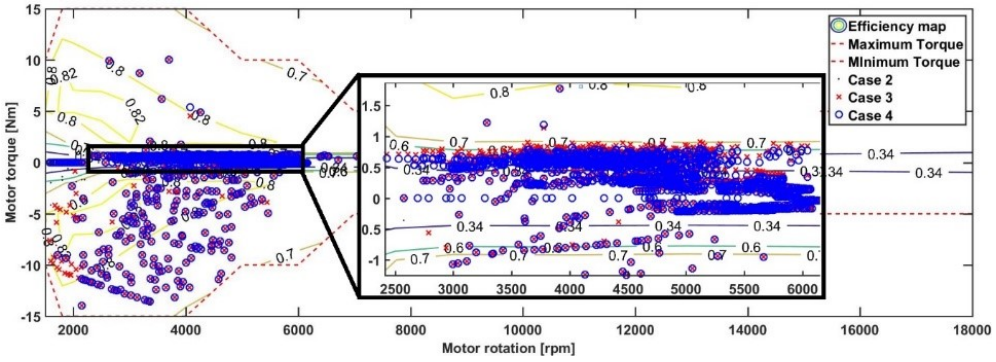

The reduction ratio between the sources of torque can be seen by comparing the engine speed displayed in Figure 84 with the motor rotation plotted in Figure 86. And to determine the ideal reduction ratio, a parametrization procedure identical to the torque factor was utilized in this study, which was equal to 2 for both categories.

The stop-start advance was added to cases 3 and 4, which turns off the engine when it reaches 10 km/h and 20 km/h, respectively, during the deceleration phase, resulting in a reduction in fuel consumption. It is worth noting that the clutch should be kept close to the engine in these cases to take full advantage of the regeneration. The clutch, however, is disengaged in the actual strategy. Figures 87 and 88 demonstrate how both instances turn off at 10 km/h and 20 km/h, respectively.

Figure 87 - Example of advanced S&S at 10 km/h + regen S&S (case 3) compared with the baseline (case 0)

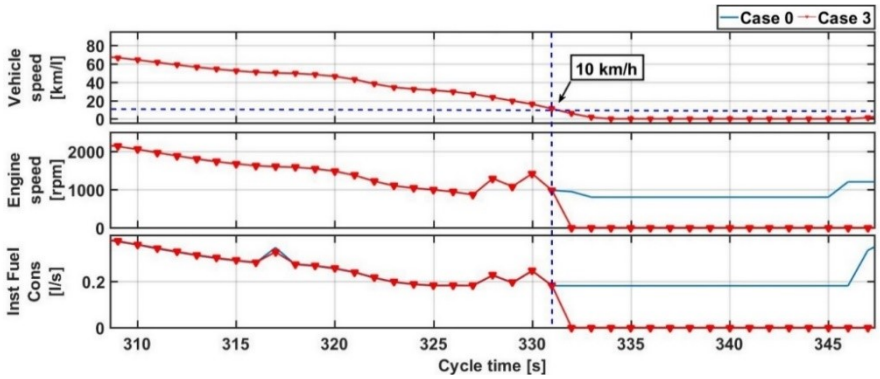

Figure 88 - Example of advanced S&S at 20 km/h + regen S&S (case 4) compared with the baseline (case 0)

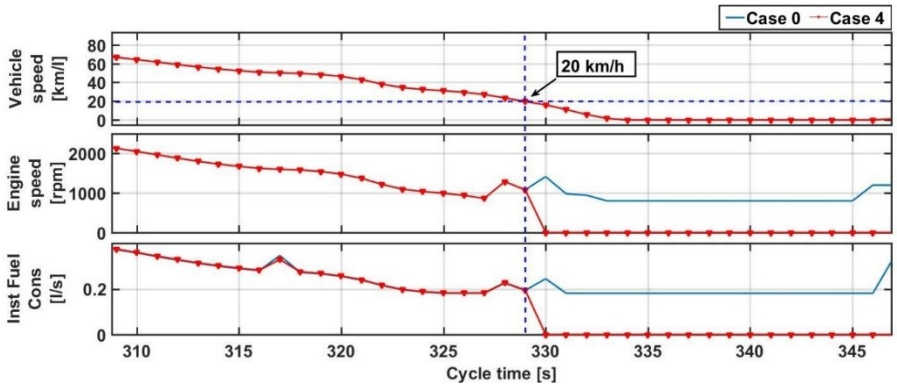

4 Analysis of Results

This chapter presents the results, analysis, and application of the different mild hybrid configurations developed in this work. Section 4.1 deals with the fuel consumption results and analysis. In section 4.2, the results were applied to the Brazilian regulation to assess benefits opportunities generates by the incentives. Finally, in the state-of-the-art comparison section 4.3, results reached in this work were compared with the literature state-of-the-art review section 2.8.

4.1 Fuel consumption analysis: results and discussion

The autonomy analysis results for one of the configurations listed in Table 15 will be presented in subsection 4.3.1 as examples; specifically, the configuration H_1.4_E22_12V and its base line BL_H_1.4_E22. Furthermore, the outcomes will be compared in subsection 4.3.2. In addition, in subsection 4.3.3 an energy balance will be presented in order to support the fuel consumption results. Finally, the findings will be summarized in 4.3.4.

4.1.1 FTP-75, HWFET, and real drive (SP) simulation results.

The fuel autonomy results will be presented in three main summarizing Tables for each configuration of Table 15. The first Table category was named *"configuration name + absolute fuel autonomy results",* for example, Table 33, and are presenting the fuel autonomy

over the three cycles assessed in this work in km/l; the cycles used are FTP-75, HWFET, and real driving cycle (SP), respectively. Furthermore, the autonomy for each cycle was estimated using equations 46 and 47 for FTP-75, HWFET, and SP. The cycle SP was treated as a single-phase similar to the HWFET, and the computer autonomy was combined using equation 48 and it is named in Table 33 COMB. Moreover, the absolute variation between each case of Table 22 to case 0 (conventional vehicle) was calculated for each cycle. The calculation Abs. line in Table 33 shows how the Abs. variation was computed in the same way that the calculation percent line Table 33 shows how the percent variation was computed.

Table 33 - H_1.4_E22_12V absolute fuel autonomy results

[Km/l]	case 0	case 1	case 2	case 3	case 4
FTP	14.8318	15.9556	16.1190	16.1576	16.3380
	calculation abs	**case 1 - case 0**	**case 2 - case 0**	**case 3 - case 0**	**case 4 - case 0**
	Abs. variation→	1.124	1.287	1.326	1.506
	calculation %	**(case 1 - case 0) / case 0**	**(case 2 - case 0) / case 0**	**(case 3 - case 0) / case 0**	**(case 4 - case 0) / case 0**
	% variation→	7.58%	8.68%	8.94%	10.16%
HW	19.3671	19.4138	19.4792	19.4777	19.4662
	Abs. variation→	0.047	0.112	0.111	0.099
	% variation→	0.24%	0.58%	0.57%	0.51%
COMB	16.5788	17.3460	17.4755	17.4999	17.6116
	Abs. variation→	0.767	0.897	0.921	1.033
	% variation→	4.63%	5.41%	5.56%	6.23%
SP	10.7642	13.3621	13.9100	14.0581	14.7209
	Abs. variation→	2.598	3.146	3.294	3.957
	% variation→	24.13%	29.22%	30.60%	36.76%

The *"configuration name + relative fuel autonomy results"* Tables, as seen in Table 34 for H 1.4 E22 12V, are essentially the same calculation as Table 33, but now concerning the previous case given the relative benefit of each hybrid function, S&S (case 1), S&S + mild hybrid (case 2), mild hybrid + advanced S&S at 10 km/h (case 3), and mild hybrid + advanced S&S at 20 km/h (case 4).

Table 34 - H_1.4_E22_12V relative fuel autonomy results

[Km/l]		case 1 - case 0	case 2 - case 1	case 3 - case 2	case 4 - case 1
FTP	**Abs. variation→**	1.124	0.163	0.039	0.180
	% variation→	7.58%	1.10%	0.26%	1.22%
HW	**Abs. variation→**	0.047	0.065	-0.002	-0.011
	% variation→	0.24%	0.34%	-0.01%	-0.06%
COMB	**Abs. variation→**	0.767	0.129	0.024	0.112
	% variation→	4.63%	0.78%	0.15%	0.67%
SP	**Abs. variation→**	2.598	0.548	0.148	0.663
	% variation→	24.13%	5.09%	1.38%	6.16%

Finally, the SOC behaviors Table was given, which were named as *"configuration name +SOC delta",* for example, Table 35, to guarantee that no battery energy was utilized to increase fuel autonomy. There are initial and final SOCs for each cycle, as well as the percent delta, which is the difference between SOC Initial and SOC Final. The FTP-75 frequently finishes with more charge than the beginning state, but this charge is utilized in the HWFET (HW) cycle owing to a Brazilian law that requires the FTP-75 and HWFET to be completed in order. The percent delta in the SP cycle is already zero, indicating that the battery will end up in the same charge condition.

Table 35 - H_1.4_E22_12V SOC delta

[%]		case 2	case 3	case 4
FTP	**SOC Initial →**	40%	40%	40%
	SOC Final →	53%	53%	51%
	% Delta→	-13%	-13%	-11%
HW	**SOC Initial →**	53%	53%	51%
	SOC Final →	40%	40%	40%
	% Delta→	13%	13%	11%
COMB	**SOC Initial →**	40%	40%	40%
	SOC Final →	40%	40%	40%
	% Delta→	0%	0%	0%
SP	**SOC Initial →**	69%	69%	63%
	SOC Final →	69%	69%	63%
	% Delta→	0%	0%	0%

Moreover, for each vehicle configuration in Table 15, the engine operation points were plotted against the specific fuel consumption engine map presented in section 3.2, as can be seen for H_1.4_E22_12V. in Figures 89, 91, and 93 for FTP -75, HWFET, and SP respectively as an example. Note that there are four graphics for each cycle: the first is the comparison between the base line case 0 and case 1 of Table 22; the second is case 1 compared with case 2; the next is case 2 with case 3; and last is case 3 with case 4. Also, a histogram of engine torque, engine speed, and specific fuel consumption was charted in Figures 90, 92, and 94 for each operation case and the base line. Furthermore, the motor operation points were plotted over the motor efficiency map shown in section 3.3 for each cycle in Figures 95, 97, and 99. Finally, the motor speed and engine torque histogram for the electric motor was presented in Figures 96, 98, and 100. As for the fuel consumption results Tables, only the H_1.4_E22_12V was shown here to save space as the results are very close and there is a summary subsection. Moreover, the other graphics can be found in Appendices A, B and C, following the same logic and order presented here for each vehicle configuration.

Figure 89 - Comparison of the engine operating points among the cases over the FTP-75 cycle for H_1.4_E22_12V

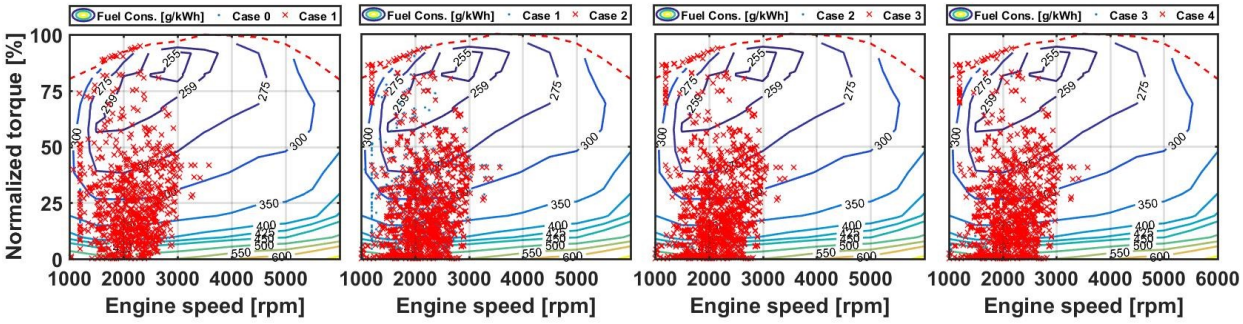

Figure 90 - Histogram of engine torque, engine speed, and engine specific fuel consumption over the FTP-75 cycle for H_1.4_E22_12V

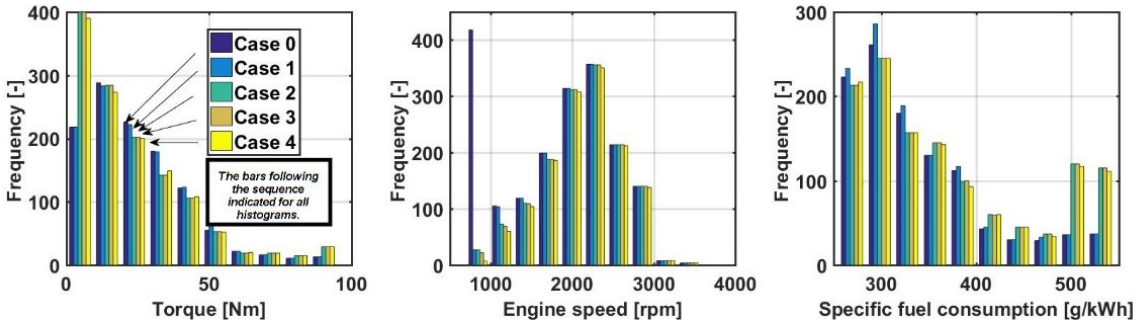

Figure 91 - Comparison of the engine operating points among the cases over the HWFET cycle for H_1.4_E22_12V

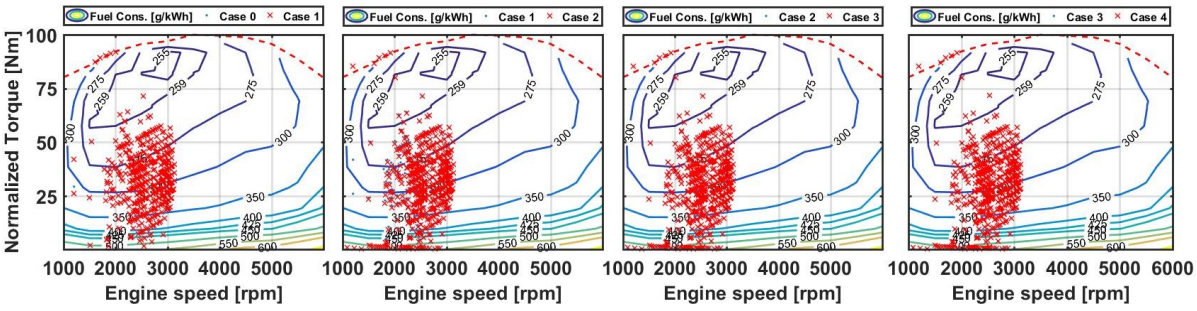

Figure 92 - Histogram of engine torque, engine speed, and engine specific fuel consumption over the HWFET cycle for H_1.4_E22_12V

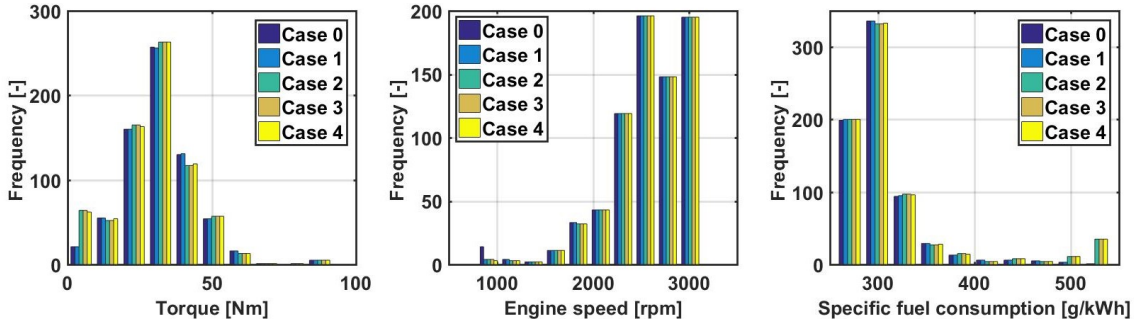

Figure 93 - Comparison of the engine operating points among the cases over the SP cycle for H_1.4_E22_12V

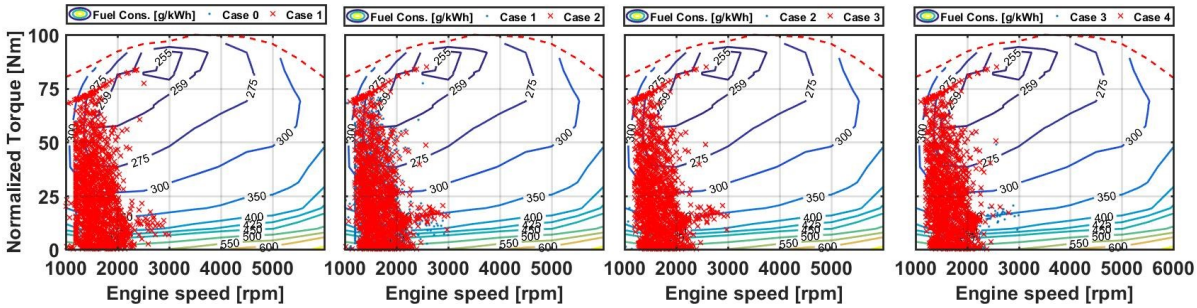

Figure 94 - Histogram of engine torque, engine speed and engine specific fuel consumption over the SP for H_1.4_E22_12V

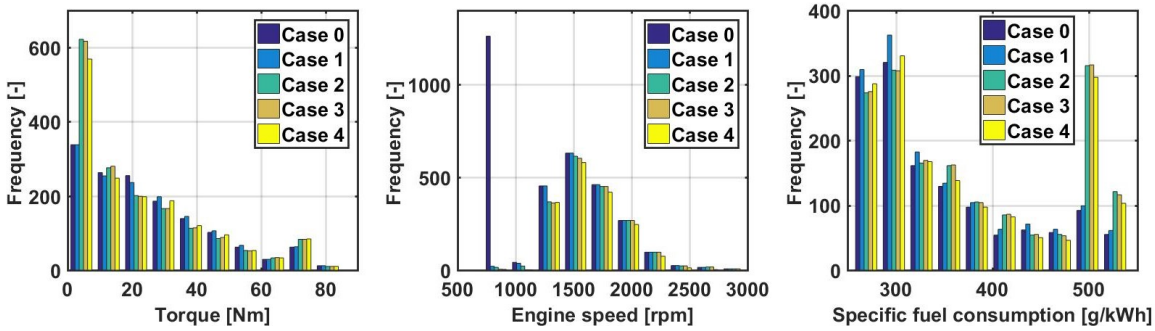

Figure 95 - Comparison of the motor operating points among the cases over the FTP-75 cycle for H_1.4_E22_12V

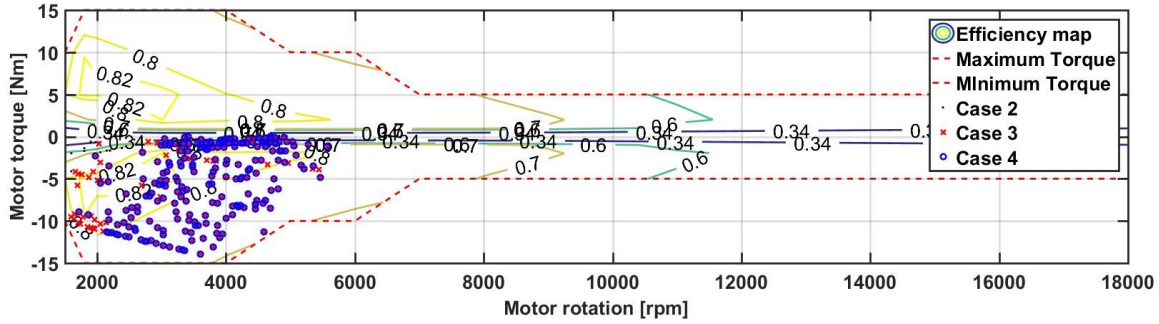

Figure 96 - Histogram of motor torque, motor speed, and specific fuel consumption over the FTP-75 cycle for H_1.4_E22_12V

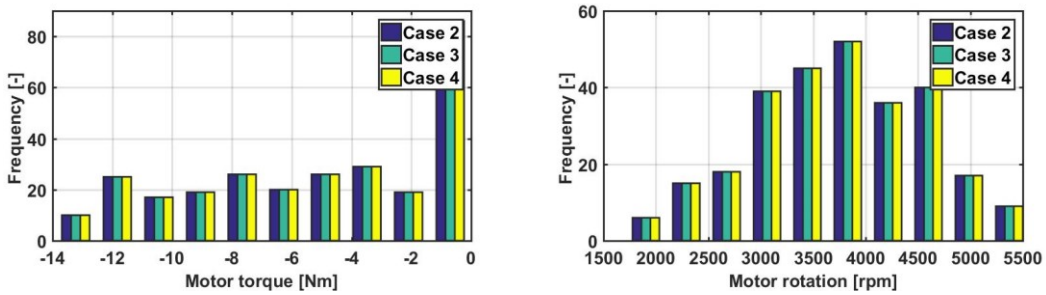

Figure 97 - Comparison of the motor operating points among the cases over the HWFET cycle for H_1.4_E22_12V

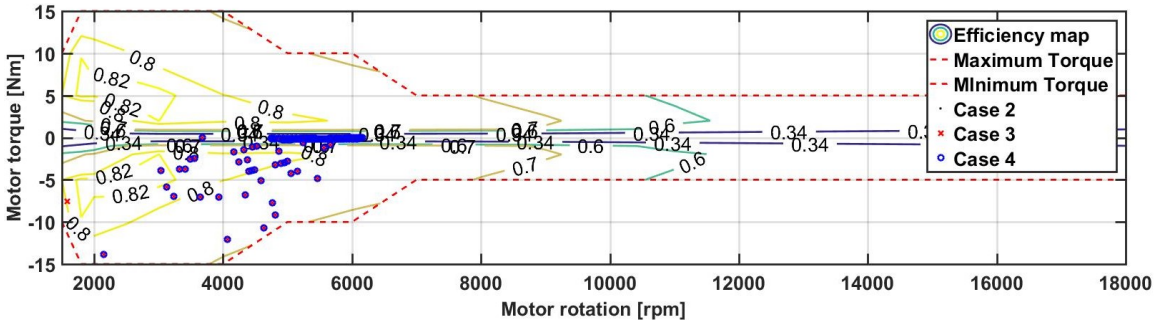

Figure 98 - Histogram of motor torque, motor speed and specific fuel consumption over the HWFET cycle for H_1.4_E22_12V

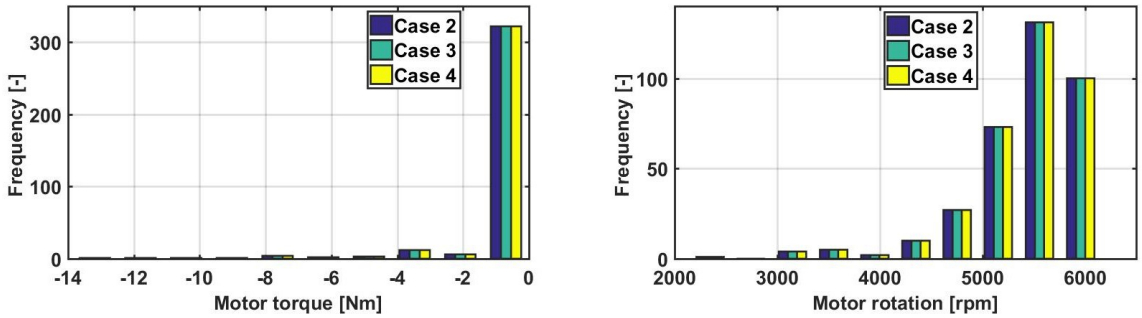

Figure 99 - Comparison of the motor operating points among the cases over the SP cycle for H_1.4_E22_12V

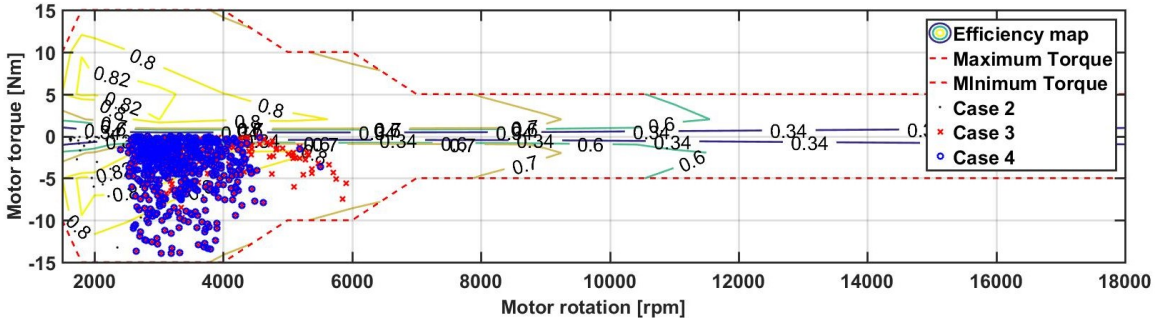

Figure 100 - Histogram of motor torque, motor speed and specific fuel consumption over the SP cycle for H_1.4_E22_12V

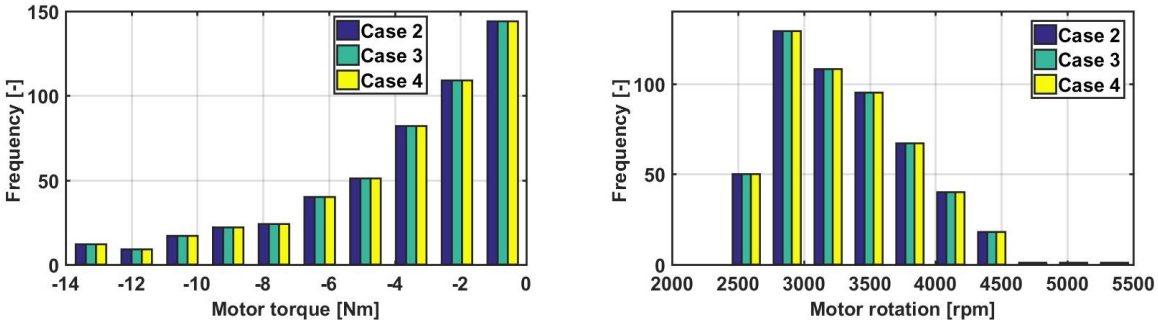

4.1.2 Comparison of the simulation results obtained

In this subsection, the results obtained and previously shown will be analyzed and compared. The different hybrid operation cases presented in Table 22 will be put side by side for each cycle to observe similarities and differences.

As can be seen in the last subsection, statistics of engine speed histograms shown in the middle of Figures 90,92, and 94, the frequency around the idling speed (800 rpm in both categories) became nearly zero, suggesting engine turn off in idle occurrences, with no change in the rest of the operations points. As shown in Figure 101, the discrepancy in fuel consumption Figures between the SUV and hatch categories can be attributed to different specific fuel consumption and, as a result, different fuel rates.

Figure 101 - Fuel flux rate for all vehicles models

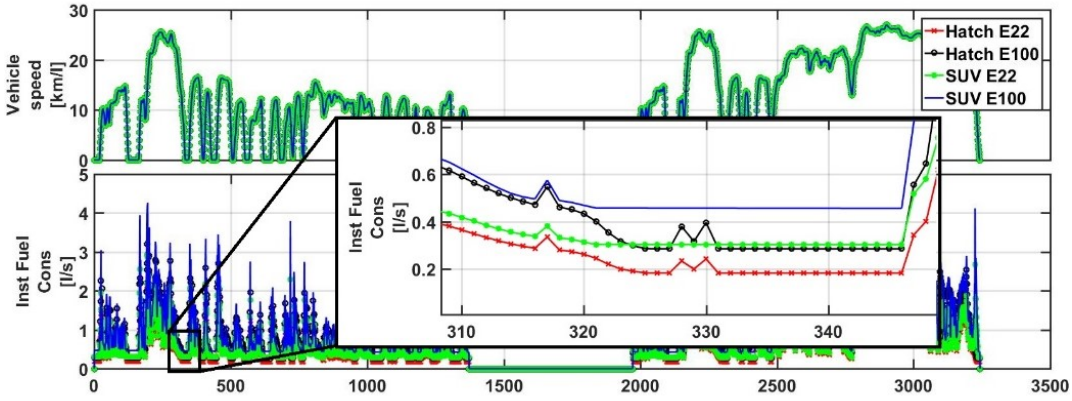

It is also worth mentioning that the large autonomy gain in the SP cycle should be carefully evaluated. Because some occurrences, as seen in the zoom in Figure 102, are likely to affect the vehicle's drivability. In this event, the engine is turned off during a trip-out occurrence when the automobile does not come to a complete stop.

As can be seen in the histogram, Figures 94, the major region of operation for the SP cycle is at low engine torque and engine speed which increases the number of operation points in the high fuel consumption map region. Thus, the autonomy is minor when compared to the other cycles tested here, the results in fuel consumption has a maximum autonomy of 7.996 km/l for SUVs and 10.7642 km/l for hatch utilizing E22 in both circumstances. Furthermore, with all hybrid functions turned on, it gained around 36 % for a hatch and 44 % for an SUV. Note that only one example result is presented in subsection 4.1.1; the rest of the results that support this analysis are in Appendices A, B and C to save space.

Figure 102 - Engine turn off in SP cycle for case 4.

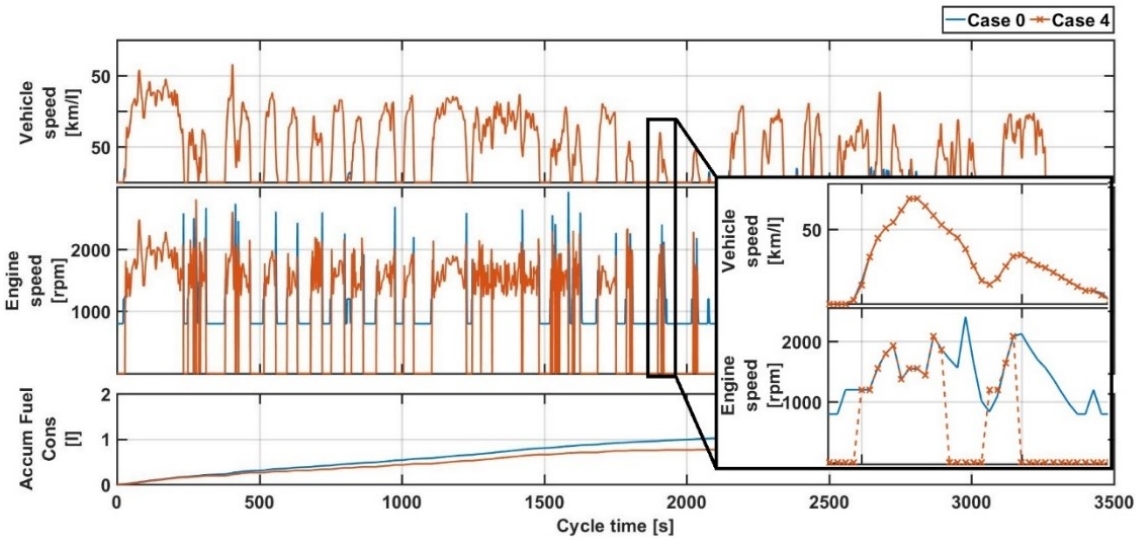

Furthermore, it can be shown that the SP cycle gained the most from mild hybrid technology, with a greater result of 6.81 % for SUVs with ethanol. A similar tendency can be seen in the other SP Tables due to the large number of regeneration possibilities afforded by this cycle.

In general, the performance of the mild-hybrid configuration (case 2) can be considered reasonable; the operations points plotted in Figures 89, 91, and 93-second graphics show that because the energy storage during the regeneration phase some operation points go down due to the lower torque request than when the vehicles loads are generated by the engine; note that the operation points go to the worst fuel consumption region, but the decrease in the fuel used pays off. It is also worth noting that the torque-assist feature was not enabled throughout this project since applying the energy recovered to the auxiliary loads is more efficient.

The best FTP-75 cycle performance was in the SUV category with E100, with a gain of 2.41%, while the hatch category with E100 came close. On the other hand, for both categories with E22, the gain of the mild hybrid function was reduced by roughly 1%. That difference can be assigned to the different fuel consumption regions of operation depending on the fuel, and the fact that the benefit came from the use of the energy regenerated to

provide auxiliary loads instead of generating it by the engine different operation points is deleted.

In terms of the achievement of the mild hybrid functions (case 2) with the HWFET cycle, some improvement was achieved, but only because of the energy storage in the FTP-75 cycle to attain the zero balance of energy when considering (FTP-75 + HW), as shown in Table 35. Furthermore, case 1, case 3, and case 4 did not show considerable improvement. Because these setups are heavily reliant on the Stop-Start (S&S) function and the cycle only has one stop.

Last but not least the advanced S&S at 10 and 20 km/h (case 3 and case 4 respectively) functionality can be observed in the histograms Figures 90, 92, and 94 where the engine speed frequency goes down in the last to bars case 3 and 4, showing that some operation points removed, in other works became zero. Furthermore, in the electric motor histograms Figures 96, 98, and 100 can be inferred a decrease of regeneration in the motor torque in cases 3 and 4, note that in the negative region the last two bars are lower the first one, that happens because in the strategy the clutch is disengaged when the S&S is operating losing that regeneration opportunities.

Regarding fuel autonomy, the difference between cases 2 and 3 is insignificant. Since a portion of the benefit projected in case 3 is lost due to the reduction in regeneration opportunities. As a result, shutting off the engine at 10 km/h still provides a little benefit for the technique presented in this work. In case 4, on the other hand, the gain is already worthwhile. The maximum benefit of the S&S advance was 1.34 percent in the hatch category with E100 during the FTP-75 cycle.

Overall, the simulation results are realistic, and the large number of data presented in this study in subsection 4.1.1 and the Appendices A, B, and C, and the valuable validation in paragraph 3.6.2 was able to demonstrate a great deal of confidence.

4.1.3 Balance of energy

In this subsection, the balance of energy of the simulations will be assessed to auxiliary the fuel consumption analysis and to increase the simulation's accuracy. Furthermore, one balance of energy was made for each vehicle configuration in Table 15; however, to save space, as the cases were very close, only the hatch categories (BL_H_1.4_E22, BL_H_1.4_E100, H_1.4_E22_12V, and H_1.4_E100_12V) were presented and analyzed in this subsection. The balance of energy Tables of the SUV category are in Appendices D, and E. Furthermore, for each configuration the balance for FTP-75 and HWFET cycles was made, considering that "power" refers to energy leaving the system, or energy utilized to power the vehicle. When energy is flowing into the system, it is called "regen." The following list of balance of energy was presented in this work.

H_1.4_E22_12V energy balance over the FTP-75 for power in kW
H_1.4_E22_12V energy balance over the FTP-75 for regen in kW
H_1.4_E22_12V energy balance over the HWFET for power in kW
H_1.4_E22_12V energy balance over the HWFET for regen in kW
H_1.4_E100_12V energy balance over the FTP-75 for power in kW
H_1.4_E100_12V energy balance over the FTP-75 for regen in kW
H_1.4_E100_12V energy balance over the HWFET for power in kW
H_1.4_E100_12V energy balance over the HWFET for regen in kW

Each line in the Power Tables 36, and 38 represents a distinct subsystem, and each column represents: the energy that enters the subsystem "In" in kW; the energy that leaves the subsystem "Out" in kW; the energy lost in the subsystem "loss" in kW; and the efficiency "eff" in %. Furthermore, there are three lines that are not sub-systems; the first line is "Fuel," which is the energy of the fuel that enters the system. Note that the value is in the "Output" column, which means that the energy that leaves the fuel enters the "fuel convert" subsystem. Moreover, the "Aero" and "Rolling" lines represent energy lost by the system because of aerodynamic resistance and rolling resistance, respectively. Each sub-column represents one of the cases in Table 22 plus the case 0, which is the conventional vehicle; in other words, the baseline: BL_H_1.4_E22 and BL_H_1.4_E100.

The energy balance for the FTP-75 cycle with gasoline (E22) for H 1.4 E22 12V configuration for power and regen operation are shown in Tables 36 and 37, respectively. While the energy balance for the HWFET cycle with the logic was presented in Tables 38 and 39.

Table 36 - H_1.4_E22_12V energy balance over the FTP-75 for power *(in kW)*

FTP E22 hatch	In_Power [kW]					out_Power [kW]					loss_Power [kW]					eff_Power [%]				
	Case 0	Case 1	Case 2	Case 3	Case 4	Case 0	Case 1	Case 2	Case 3	Case 4	Case 0	Case 1	Case 2	Case 3	Case 4	Case 0	Case 1	Case 2	Case 3	Case 4
Fuel						35087	32624	32287	32216	31872										
Fuel Converter	35087	32624	32287	32216	31872	7770	7770	7626	7622	7633	27317	24854	24661	24594	24239	0.22	0.24	0.24	0.24	0.24
Clutch	7288	7288	7331	7331	7331	7213	7213	7271	7271	7271	76	76	60	60	60	0.99	0.99	0.99	0.99	0.99
Torque Coupling			7331	7331	7331			7331	7331	7331								1	1	1
Energy Storage			577	575	531			462	461	430			52	52	49			0.91	0.91	0.9
Energy Stored			63	62	51															
Gearbox	7213	7213	7271	7271	7271	6924	6924	6980	6980	6980	289	289	291	291	291	0.96	0.96	0.96	0.96	0.96
Final Drive	6924	6924	6980	6980	6980	6924	6924	6980	6980	6980						1	1	1	1	1
Wheel/Axle	6924	6924	6980	6980	6980	6924	6924	6980	6980	6980						1	1	1	1	1
Aux Loads	790	625	603	598	579						790	625	603	598	579					
Aero											2336	2336	2335	2335	2335					
Rolling											2254	2254	2268	2268	2268					

Table 37 - H_1.4_E22_12V energy balance over the FTP-75 for regen *(in kW)*

FTP E22 hatch	In_Regen [kW]					out_Regen [kW]					loss_Regen [kW]					eff_Regen [%]				
	Case 0	Case 1	Case 2	Case 3	Case 4	Case 0	Case 1	Case 2	Case 3	Case 4	Case 0	Case 1	Case 2	Case 3	Case 4	Case 0	Case 1	Case 2	Case 3	Case 4
Clutch	734	734	849	846	789	734	734	849	846	789						1	1	1	1	1
Torque Coupling			849	846	789			849	846	789								1	1	1
Motor/Controller			849	846	789			577	575	531			272	271	258			0.68	0.68	0.67
Gearbox	764	764	885	882	822	734	734	849	846	789			35	35	33	0.96	0.96	0.96	0.96	0.96
Final Drive	764	764	885	882	822	764	764	885	882	822						1	1	1	1	1
Wheel/Axle	2332	2332	2355	2355	2355	2332	2332	2355	2355	2355						1	1	1	1	1
Braking											1568	1568	1471	1474	1534					

Table 38 - H_1.4_E22_12V energy balance over the HWFET for power *(in kW)*

HW E22 hatch	In_Power [kW]					out_Power [kW]					loss_Power [kW]					eff_Power [%]				
	Case 0	Case 1	Case 2	Case 3	Case 4	Case 0	Case 1	Case 2	Case 3	Case 4	Case 0	Case 1	Case 2	Case 3	Case 4	Case 0	Case 1	Case 2	Case 3	Case 4
Fuel						25283	25220	25202	25202	25195										
Fuel Converter	25283	25220	25202	25202	25195	7452	7452	7457	7457	7457	17831	17769	17745	17745	17738	0.29	0.3	0.3	0.3	0.3
Clutch	7157	7157	7180	7180	7180	7154	7154	7179	7179	7179	3	3	1	1	1	1	1	1	1	1
Torque Coupling			7180	7180	7180	0	0	7180	7180	7180								1	1	1
Energy Storage			108	108	107	0	0	156	156	156			11	11	11			0.9	0.9	0.9
Energy Stored			-59	-59	-60															
Gearbox	7154	7154	7179	7179	7179	6868	6868	6892	6892	6892	286	286	287	287	287	0.96	0.96	0.96	0.96	0.96
Final Drive	6868	6868	6892	6892	6892	6868	6868	6892	6892	6892						1	1	1	1	1
Wheel/Axle	6868	6868	6892	6892	6892	6868	6868	6892	6892	6892						1	1	1	1	1
Aux Loads	322	318	317	317	317						322	318	317	317	317					
Aero											4157	4157	4157	4157	4157					
Rolling											2093.5	2093.5	2111.5	2111.5	2111.5					

Table 39 - H_1.4_E22_12V energy balance over the HWFET for regen *(in kW)*

HW E22 hatch	In_Regen [kW]					out_Regen [kW]					loss_Regen [kW]					eff_Regen [%]				
	Case 0	Case 1	Case 2	Case 3	Case 4	Case 0	Case 1	Case 2	Case 3	Case 4	Case 0	Case 1	Case 2	Case 3	Case 4	Case 0	Case 1	Case 2	Case 3	Case 4
Clutch	169	169	167	167	165	169	169	167	167	165						1	1	1	1	1
Torque Coupling			167	167	165			167	167	165								1	1	1
Motor/Controller			193	193	191			108	108	107			84	84	84			0.56	0.56	0.56
Gearbox	176	176	174	174	172	169	169	167	167	165			7	7	7	0.96	0.96	0.96	0.96	0.96
Final Drive	176	176	174	174	172	176	176	174	174	172						1	1	1	1	1
Wheel/Axle	404	404	409	409	409	404	404	409	409	409						1	1	1	1	1
Braking											228	228	236	236	237					

The energy balance for the FTP-75 cycle with ethanol (E100) for H 1.4 E100 12V configuration for power and regen operation are shown in Tables 40 and 41, respectively. While the energy balance for the HWFET cycle with the logic was presented in Tables 42 and 43.

Table 40 - H_1.4_E100_12V energy balance over the FTP-75 for power *(in kW)*

	In_Power [kW]					out_Power [kW]					loss_Power [kW]					eff_Power [%]				
FTP E100 hatch	Case 0	Case 1	Case 2	Case 3	Case 4	Case 0	Case 1	Case 2	Case 3	Case 4	Case 0	Case 1	Case 2	Case 3	Case 4	Case 0	Case 1	Case 2	Case 3	Case 4
Fuel						35147	32594	31753	31684	31323										
Fuel Converter	35147	32594	31753	31684	31323	7585	7585	7438	7435	7446	27562	25010	24314	24249	23876	0.22	0.23	0.23	0.23	0.24
Clutch	7104	7104	7153	7153	7153	7023	7023	7089	7089	7089	81	81	64	64	64	0.99	0.99	0.99	0.99	0.99
Torque Coupling			7153	7153	7153			7153	7153	7153								1	1	1
Energy Storage			560	557	511			456	455	424			51	51	48			0.91	0.91	0.9
Energy Stored			53	52	40															
Gearbox	7023	7023	7089	7089	7089	6742	6742	6806	6806	6806	281	281	284	284	284	0.96	0.96	0.96	0.96	0.96
Final Drive	6742	6742	6806	6806	6806	6742	6742	6806	6806	6806						1	1	1	1	1
Wheel/Axle	6742	6742	6806	6806	6806	6742	6742	6806	6806	6806						1	1	1	1	1
Aux Loads	790	622	596	592	573						790	622	596	592	573					
Aero											2336	2336	2335	2335	2335					
Rolling											2254	2254	2268	2268	2268					

Table 41 - H_1.4_E100_12V energy balance over the FTP-75 for regen *(in kW)*

	In_Regen [kW]					out_Regen [kW]					loss_Regen [kW]					eff_Regen [%]				
FTP E100 hatch	Case 0	Case 1	Case 2	Case 3	Case 4	Case 0	Case 1	Case 2	Case 3	Case 4	Case 0	Case 1	Case 2	Case 3	Case 4	Case 0	Case 1	Case 2	Case 3	Case 4
Clutch	704	704	821	818	758	704	704	821	818	758						1	1	1	1	1
Torque Coupling			821	818	758			821	818	758								1	1	1
Motor/Controller			821	818	758			560	557	511			261	261	246			0.68	0.68	0.67
Gearbox	733	733	855	852	789	704	704	821	818	758			34	34	32	0.96	0.96	0.96	0.96	0.96
Final Drive	733	733	855	852	789	733	733	855	852	789						1	1	1	1	1
Wheel/Axle	2280	2280	2303	2303	2303	2281	2281	2303	2303	2303						1	1	1	1	1
Braking											1547	1547	1448	1451	1514					

Table 42 - H_1.4_E100_12V energy balance over the HWFET for power *(in kW)*

	In_Power [kW]					out_Power [kW]					loss_Power [kW]					eff_Power [%]				
HW E100 hatch	Case 0	Case 1	Case 2	Case 3	Case 4	Case 0	Case 1	Case 2	Case 3	Case 4	Case 0	Case 1	Case 2	Case 3	Case 4	Case 0	Case 1	Case 2	Case 3	Case 4
Fuel						24784	24741	24705	24690	24660										
Fuel Converter	24784	24741	24705	24690	24660	7003	7003	7006	7005	7004	17782	17738	17699	17685	17656	0.28	0.28	0.28	0.28	0.28
Clutch	6708	6708	6731	6731	6731	6705	6705	6729	6729	6729	3	3	2	2	2	1	1	1	1	1
Torque Coupling			6731	6731	6731			6731	6731	6731								1	1	1
Energy Storage			111	110	108			156	156	156			11	11	11			0.91	0.91	0.9
Energy Stored			-57	-57	-59															
Gearbox	6705	6705	6729	6729	6729	6437	6437	6460	6460	6460	268	268	269	269	269	0.96	0.96	0.96	0.96	0.96
Final Drive	6437	6437	6460	6460	6460	6437	6437	6460	6460	6460						1	1	1	1	1
Wheel/Axle	6437	6437	6460	6460	6460	6437	6437	6460	6460	6460						1	1	1	1	1
Aux Loads	322	318	317	317	317						322	319	318	317	317					
Aero											4157	4157	4157	4157	4157					
Rolling											2066	2066	2084	2084	2084					

Table 43 - H_1.4_E100_12V energy balance over the HWFET for regen *(in kW)*

	In_Regen [kW]					out_Regen [kW]					loss_Regen [kW]					eff_Regen [%]				
HW E100 hatch	Case 0	Case 1	Case 2	Case 3	Case 4	Case 0	Case 1	Case 2	Case 3	Case 4	Case 0	Case 1	Case 2	Case 3	Case 4	Case 0	Case 1	Case 2	Case 3	Case 4
Clutch	169	169	169	168	166	169	169	169	168	166						1	1	1	1	1
Torque Coupling			169	168	166			169	168	166								1	1	1
Motor/Controller	191	191	192	191	189	107	107	111	110	108			81	81	81	0.56	0.56	0.58	0.58	0.57
Gearbox	176	176	176	175	173	169	169	169	168	166			7	7	7	0.96	0.96	0.96	0.96	0.96
Final Drive	176	176	176	175	173	176	176	176	175	173						1	1	1	1	1
Wheel/Axle	400	400	405	405	405	400	400	405	405	405						1	1	1	1	1
Braking											260	260	400	400	400					

The following analyses concern the "Power" flow, including Tables 36, 38, 40, and 42. The subsystems and columns names are between double quotes: “ ”. As a reminder, these analyses are additions to the other vehicle configurations in Table 15.

The energy from the fuel is shown in the column "out Power" in a line called "fuel." Note that there is a tiny difference between the fuels E22 and E100, as shown in Tables 36 and 40, where E22 is 35087 kW, and E100 is 35147 kW, a difference of 0.17%. These discrepancies can be explained by tiny instabilities during the computation calculation, as certain locations are subject to interpolation and are influenced by the gear shift. Furthermore, when comparing cases 0 and 1, there is a significant reduction in fuel consumption; this behavior is the major mechanism of this work's gain in fuel consumption, and it is the consequence of the S&S, as well. Also, in cases 2, 3, and 4, there will be a reduction in the amount of fuel used. In addition, in case 2, the auxiliary energy provided by the hybrid system rather than the engine saves gasoline.

The subsystem “fuel convert” is presented in the following line, and as can be observed, this subsystem has the biggest loss in the system, with roughly 70% to 80% of the energy lost due to the combustion process; nonetheless, the findings are generally consistent. The efficiency of the HWFET cycle is higher than the FTP-75 cycle because of the higher load operation point area. The FTP-75 has an increase in case 2, which is related to a reduction in operating points in the low load

The “clutch” subsystem, on the other hand, has a 100% efficiency, and as can be seen in the energy balance Tables, there is no variation in loss from the conventional model case 1 and case 2 to the hybrid.

The following two subsystems are linked to the hybrid mode cases 2, 3, and 4, “torque coupling, and “energy storage”; the torque coupling efficiency of the subsystem was determined to be 100%. Energy storage deals with energy flow into the battery, which has a global efficiency of roughly 91 percent. The losses come from the columbium effect and wire transmission. Energy is stored in the Energy Stored after the cycle, and as can be seen, the energy in the FTP-75 cycle is positive, while the HWFET is negative by the same amount to maintain the energy balance between the start and conclusion of the cycle

The “gearbox” is the next subsystem and gets energy directly from the clutch subsystem in conventional cases (cases 0 and 1) and the torque coupling in hybrid cases (cases 2, 3, and 4) and discounts the efficiency evaluated in the gear shift the efficiency was rated at 96% in this work. Final Drive and Wheel/Axles, the following two subsystems, were not affected by any losses in this model.

Finally, in the “Aux Loads”, “Aero”, and “Rolling” subsystems, the energy value to provide auxiliary loads, overcome aerodynamic forces, and overcome rolling resistance is presented. Note that, despite using a constant consumption value of 20A, the final value is different for each case, because in the current technique, when the vehicle is shut off at a stop, the loads are also zero. Furthermore, due to the applied efficiency and cycle size, the load value is larger than 20A

The following analyses concern the "Regen" flow, including Tables 37, 39, 41, and 43. The subsystems and columns names are going to be between double quote “”;

The “clutch”, “torque coupling”, “final drive”, and “well/axles” have all 100% efficiency and were simply demonstrated to confirm appropriate behavior. The same 0.96 percent efficiency of the power Tables for gear is used.

The “Motor controller” subsystem shows the value of regenerated energy, using the efficiency of the electric motor shown in the map in Figure 59. And as can be seen, the efficiency is from 56% to 68%. Note that the energy that goes out of the electric motor is the same that enters in the battery “Energy Storage”, see Tables 37, 39, 41, and 43. It is important to mention that this energy is used to maintain the vehicle load in this work. In some cases, more energy than the amount needed by the vehicle is recovered, and in these cases, to account for the benefit, the energy was converted into a reduction of fuel consumption, considering the same efficiency as a conventional alternator.

.

4.1.4 Summary of the fuel consumption results

The simulation showed that a BSG technology delivers a remarkable increase of vehicle autonomy, in other words, a reduction in fuel consumption with respect to a baseline vehicle. It was demonstrated that the overall BSG features obtaining fuel-saving around 10.15% - 13.05% on city cycle (FTP-75), 0.38% - 1.15% on highway cycle (HWFET), 6% - 7.5% on combined cycle (FTP-75 + HWFET) and, 36% - 44% on cycle SP.

Most of the saving on FTP-75 and SP is related to the cut of fuel during idle with stop-start (case 1), the second place was the mild hybrid with stop-start at 0 km/h functionalities (case 2), followed by the mild hybrid with stop-start advanced at 20 km/h, in the last place is the mild hybrid with stop-start at 10 km/h, the overall results can be seen in the Figures 103,104, and 105.

In the case of an HWFET cycle, the gains are limited by the cycle characteristics, in this case, a very low improvement in stop-start can be observed of around 0.24%. The benefit accounted for the mild hybrid is related to the charge stored in the FTP-75 cycle to ensure that the SOC between the beginnings of the test would be the same at the end, considering the combination of FTP-75 and HWFET.

As can be seen in charts 103, and 104, no significant differences between the fuels used in this work (E22 and E100) were found in case 1, case 3, and case 4. These functionalities depend directly on idle events. cases 3 and 4 presents almost the same fuel-saving for both hatch and SUV categories, despite the fact they have different specific fuel consumption maps, on the other hand, the SUV presents more fuel-saving than a hatch in case 1, due to the higher specific fuel consumption of the idle speed in relation to the hatch.

case 2 (mild hybrid) shows a relative difference between the fuels in both categories with the same tendency, with ethanol saving more fuel due to its higher specific fuel consumption. Because the regenerative system is the same for both fuels, no differences in energy recovered are expected in the same cycle, but when this energy is used to keep the auxiliary load running, different specific fuel consumption is assessed, resulting in different improvements.

Figure 103 - Fuel-saving delta among the cases for FTP-75, HWFET, and Combined cycles for Hatch category

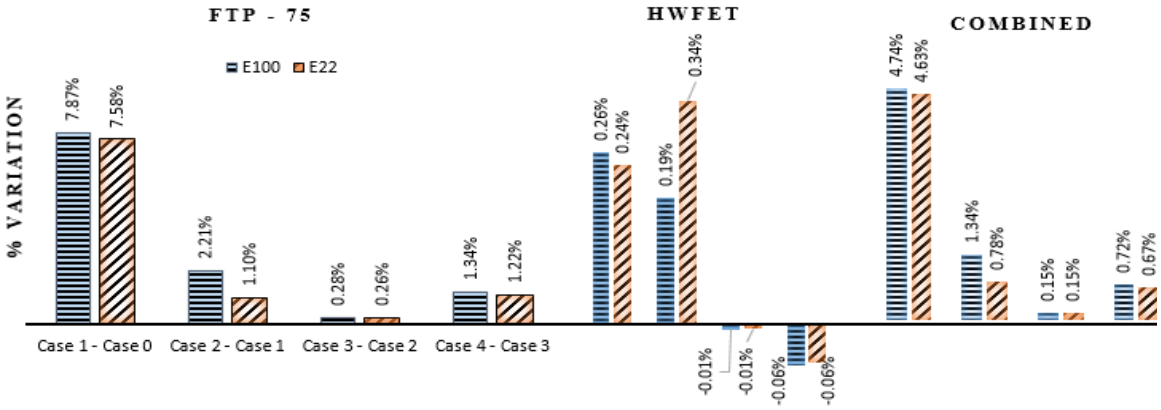

Figure 104 - Fuel-saving delta among the cases for FTP-75, HWFET, and Combined cycles for SUV category

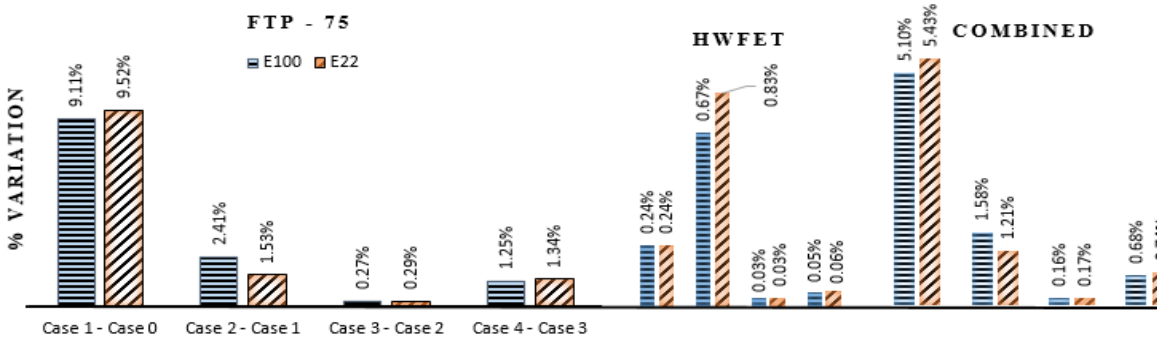

Figure 105 - Fuel-saving delta among the cases for SP cycle for SUV and Hatch categories

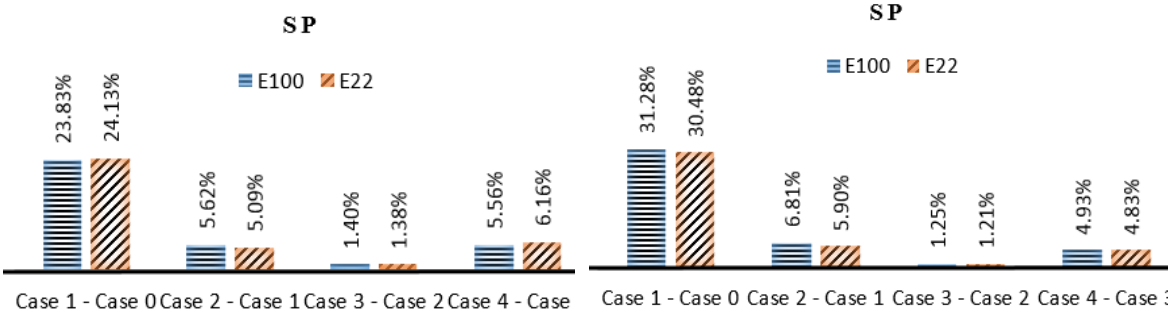

(a) – Hatch

(b) - SUV

Furthermore, it is important to remember that vehicle autonomy is highly dependent on the controls system, motor-generator power, and battery capacity, which are directly related to the amount of regenerative braking that can be achieved, and calibration (where a lot of effort is put into determining the best controls for fuel economy).

4.2 Correlation with the Brazilian regulation

Some benefits are predicted in Brazilian regulation if fuel consumption is improved; this topic was thoroughly discussed in subsection 2.5.1. To account for the potential of the technologies simulated in this work, autonomy (in Km/l) was converted to autonomy (in MJ/km) as recommended in subsection 2.5.3. The findings converted for FTP-75, HWFET, and COMB for E22 and E100 are provided in Tables 44 and 45, respectively for hatch configuration. Tables 46 and 47 show the same findings for the SUV category.

Table 44 - H_1.4_E22_12V autonomy result in MJ/km

[MJ/km]	**case 0**	**case 1**	**case 2**	**case 3**	**case 4**
FTP	1.9546	1.8169	1.7985	1.7942	1.7744
	calculation abs	**case 1 - case 0**	**case 2 - case 0**	**case 3 - case 0**	**case 4 - case 0**
	Abs. variation→	-0.138	-0.156	-0.160	-0.180
	calculation %	**(case 1 - case 0) / case 0**	**(case 2 - case 0) / case 0**	**(case 3 - case 0) / case 0**	**(case 4 - case 0) / case 0**
	% variation→	-7.04%	-7.99%	-8.21%	-9.22%
HW	1.4969	1.4933	1.4883	1.4884	1.4892
	Abs. variation→	-0.004	-0.009	-0.009	-0.008
	% variation→	-0.24%	-0.58%	-0.57%	-0.51%
COMB	1.7486	1.6713	1.6589	1.6566	1.6461
	Abs. variation→	-0.077	-0.090	-0.092	-0.103
	% variation→	-4.42%	-5.13%	-5.26%	-5.86%

Table 45 - H_1.4_E100_12V autonomy result in MJ/km

[MJ/km]	**case 0**	**case 1**	**case 2**	**case 3**	**case 4**
FTP	1.9839	1.8392	1.8023	1.7977	1.7761
	Abs. variation→	-0.145	-0.182	-0.186	-0.208
	% variation→	-7.30%	-9.16%	-9.39%	-10.47%
HW	1.5736	1.5696	1.5666	1.5667	1.5677
	Abs. variation→	-0.004	-0.007	-0.007	-0.006
	% variation→	-0.26%	-0.45%	-0.44%	-0.38%
COMB	1.7995	1.7180	1.6964	1.6939	1.6825
	Abs. variation→	-0.081	-0.103	-0.106	-0.117
	% variation→	-4.53%	-5.73%	-5.86%	-6.50%

Table 46 - SUV_1.8_E22_12V autonomy result in MJ/km

[MJ/km]	case 0	case 1	case 2	case 3	case 4
FTP	2.2553	2.0593	2.0309	2.0256	2.0016
	Abs. variation→	-0.196	-0.224	-0.230	-0.254
	% variation→	-8.69%	-9.95%	-10.19%	-11.25%
HW	1.9858	1.9811	1.9649	1.9643	1.9632
	Abs. variation→	-0.005	-0.021	-0.021	-0.023
	% variation→	-0.24%	-1.05%	-1.08%	-1.14%
COMB	2.1340	2.0241	2.0012	1.9980	1.9843
	Abs. variation→	-0.110	-0.133	-0.136	-0.150
	% variation→	-5.15%	-0.91%	-0.93%	-1.03%

Table 47 - SUV_1.8_E100_12V autonomy result in MJ/km

[MJ/km]	case 0	case 1	case 2	case 3	case 4
FTP	2.0352	1.8653	1.8250	1.8205	1.8003
	Abs. variation→	-0.170	-0.210	-0.215	-0.235
	% variation→	-8.35%	-10.33%	-10.55%	-11.54%
HW	1.8814	1.8770	1.8645	1.8639	1.8629
	Abs. variation→	-0.004	-0.017	-0.018	-0.019
	% variation→	-0.24%	-0.90%	-0.93%	-0.98%
COMB	1.9662	1.8707	1.8430	1.8403	1.8287
	Abs. variation→	-0.095	-0.123	-0.126	-0.138
	% variation→	-4.86%	-6.27%	-6.41%	-6.99%

Furthermore, the Mj/km Mixed (E100 and E22) was calculated using equation 49 of this work for both categories in Table 48.

Table 48 - Mixed (E100 and E22) fuel consumption in MJ/km without additional reductions

Category\[MJ/km]	**case 0**	**case 1**	**case 2**	**case 3**	**case 4**
Hatch	1.7740	1.6947	1.6776	1.6753	1.6643
SUV	2.0501	1.9474	1.9221	1.9191	1.9065

Figure 106 depicts the fuel usage in MJ/km (see Table 48) plotted according to the Brazilian regulation's incentive restrictions, as explained in subsection 2.5.1, and without off-cycle credits. The hatch category simulated in this study did not even reach the minimum target; however, the SUV category has exceeded the target since its baseline (case 0) and was capable of activating the 1% reduction target in mild hybrid, advanced S&S at 10 [km/h], and advanced S&S at 20 [km/h], case 2, case 3, and case 4, respectively. The fuel savings in the standard S&S (case 1) detail reached the board line of a 1% decrease, as can be seen in the SUV mixed (E100 and E22) detail.

Figure 106 - Energetic Efficiency in MJ/km cases over the benefits targets by category without E100 reduction factor and off-cycle conditions.

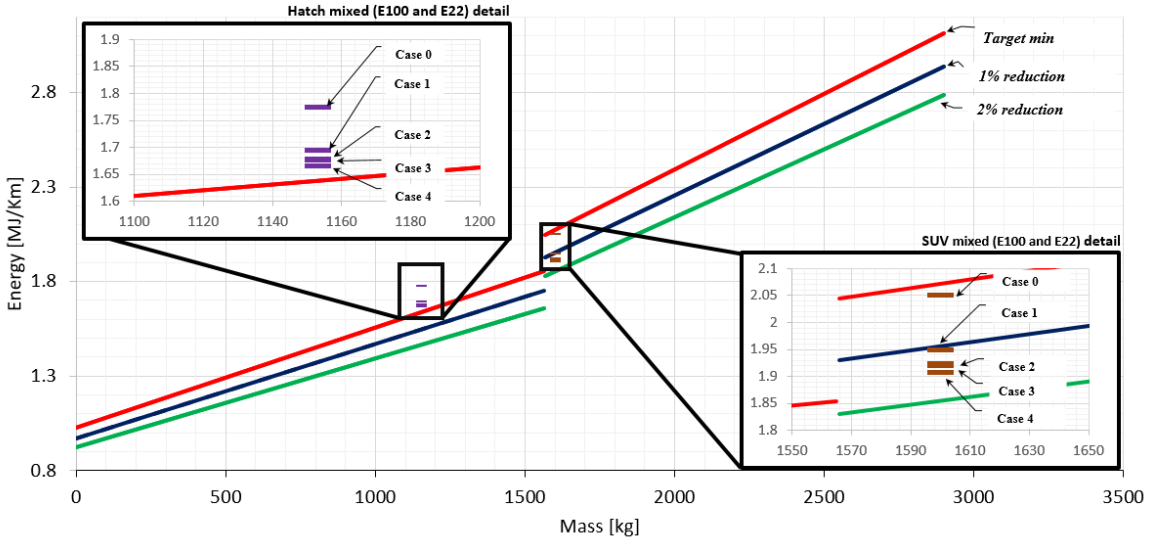

In addition, the E100 reduction factor is a motivator to reduce the performance gap between E100 and E22. The E100 reduction factor was determined using equation 37 and presented in Table 49, and the fuel ratio between E100 and E22 is shown in Table 50. Only fuel ratios greater than 69.27 can use the E100 reduction factor. As can be observed in Table 50, the hatch category is below the target, thus no E100 reduction factor was applied; however, the SUV fuel ratio is over the target, so the reduction was applied, as can be seen by comparing the SUV line Tables 49 and 48.

Table 49 - E100 reduction factor calculation

Category\[MJ/Km]	case 0	case 1	case 2	case 3	case 4
Hatch	1.7740	1.6947	1.6776	1.6753	1.6643
SUV	1.9373	1.8410	1.8134	1.8107	1.7990

Table 50 - Fuel ratio calculation

Category\[%]	case 0	case 1	case 2	case 3	case 4
Hatch	67.34%	67.41%	67.77%	67.77%	67.80%
SUV	75.21%	74.98%	75.25%	75.24%	75.20%

Finally, the off-cycle benefit can be applied; for this work, the maximum value of 0.0936 MJ/km will be used in all circumstances, regardless of the technologies employed to achieve that value, as the value derives from a package of technologies described in Table 10 of this work. The final values of mixed fuel consumption in MJ/km after applying the E100 reduction factor and off-cycle conditions are displayed in Table 51. For the hatch and SUV categories, the results were plotted in Figure 107.

Table 51 - Mixed (E100 and E22) fuel consumption in MJ/km with additional reductions

Category\[MJ/km]	case 0	case 1	case 2	case 3	case 4
Hatch	1.7740	1.6947	1.6776	1.6753	1.6643
SUV	2.0501	1.9474	1.9221	1.9191	1.9065

Figure 107 - Energetic Efficiency in MJ/km cases over the benefits targets by category with E100 reduction factor and off-cycle conditions.

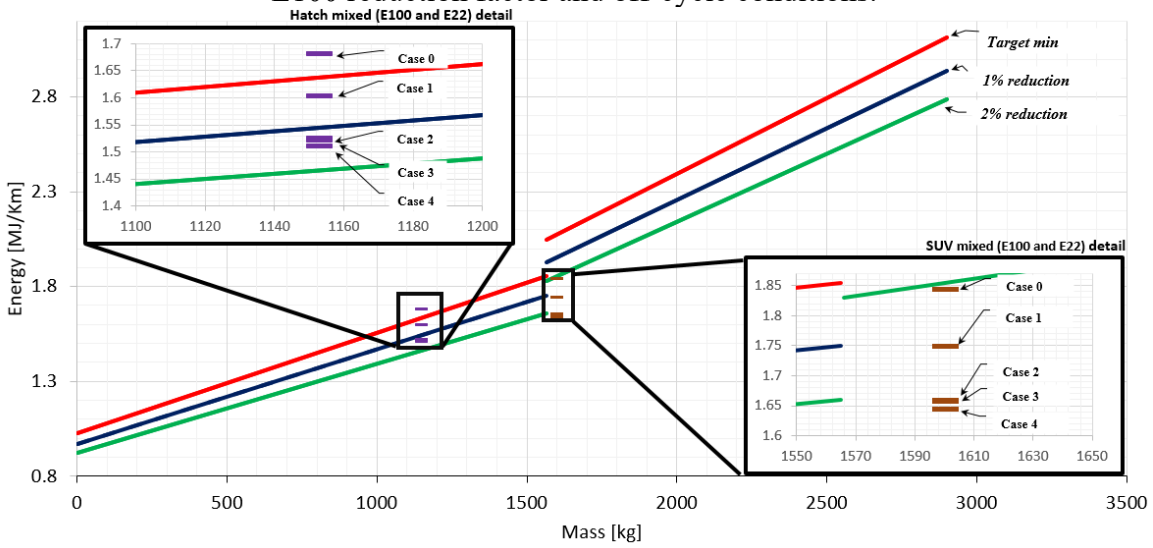

Figure 107 shows that in case 0, without any BSG technology or even conventional S&S, the energetic efficiency is already lower than the 2% reduction target for the SUV category. The high ratio performance between E100 and E22 exhibited by this category was responsible for the SUV result. The hatch, on the other hand, had poor fuel efficiency between E100 and E22, thus the E100 reduction factor was not used. Furthermore, the hatch

in case 0 did not reach the target minimum; however, the aim was met when the conventional S&S (case 1) was added, but no benefit was achieved. Finally, when the mild-hybrid technology was used in cases 2, 3, and 4, the one percent reduction was active.

As can be seen in this subsection, the simulation was effective to trace different scenarios of benefits considering the implementation of new technologies; in this work BSG 12 V over two different categories Hatch and SUV. Regarding the specific results presented, it is important to remember that any simulation is very sensitive to the inputs and uncertainties that were not determined in this work due to the lack of data recorded information used.

Taking into account the last commentary, it is clear that the better result of the BSG implementation was in the SUV category when compared with the hatch. This outcome can be explained by the best SUV baseline (case 0) and the E100 reduction factor. Additionally, the delta between case 0 and case 4 were 0.1097 MJ/km and 0.1383 MJ/km for hatch and SUV, respectively.

4.3 State-of-the-art comparison

Considering section 4.2 where the BSG technology's benefits for the Brazilian market are highlighted, this work corroborates with the reference CLUETT, 2007) regarding the importance of this technology for growing markets due to its low cost and easy implementation.

Regarding the conventional model validation when compared with FIGUEIREDO (2019), the model validation results were improved, as can be seen in Table 30, while in the reference, the difference between the test and the model for the hatch category was between 0.6 % - 4.9% of delta. For the current work, this value reached between 0.39% - 1.02%, and this fact corroborates with the advanced vehicle simulation (ADVISOR) team expectation, as was reported by WIPKE et al.(1999). On the other hand, as was pointed out by SENGER; MERKLE and NELSON (1998), some strange behavior was identified during transient events; for instance, the gear shift, vehicle restart, and during some hard acceleration.

Concerning the hybrid system validation, some uncertainties were identified. However, due to the lack of sensor information, it was difficult to identify those, but when compared with DE OLIVEIRA (2019), the hybrid fuel consumption can be validated, as both works have the same vehicle configuration. In the reference, the fuel-saving was between 8% and 12% for 12V and 48V architectures, respectively, while in this present work, between 6% and 7.5% for 12V architecture for hatch and SUV was obtained, respectively. Still comparing the fuel-saving improvement, CHENG, LAI and THE (2017) stays between 3% and 4 %. However, the lesser benefit for the last work can be explained by the different vehicle types. Finally, when comparing the fuel-saving obtained in this work with BALDIZZONE (2012), STEFFAN, HOFMANN, and GERINGER (2015), ZO, NAN; and PENG (2019), and GUPTA et al. (2020), which are all 48 V architecture, in all references the system improvement was higher; however, in this work, the electrical architecture chosen was 12V due to the cost-benefit.

As reported by MARKEL; and WIPKE (2001), CHENG, LAI, and TEH (2017), JOHNSON, WIPKE, and RAUSEN (2000), and CHEN et al. (2014), the ADVISOR model showed great flexibility in relation to the operation and modification to achieve the objective of this work; however, the ADVISOR proved to be very sensitive during interpolation events, indicating room for improvement in this area. Moreover, the documentation is another negative point, as the simulation model ADVISOR is an open-source created in 1999, and its documentation has not been updated since then.

5 Conclusion

The proposed methodology was appropriate for achieving the work's objectives, and the basic simulation software (ADVISOR) was effective in simulating the fuel savings of automobiles that do not exist in real life. The literature review provided a solid foundation for the project's growth. Finally, the proposed vehicles were developed, validated, and simulated, with the fuel-saving findings utilized to forecast BSG technology benefits for Brazilian regulations.

The model validation findings were acceptable. The discrepancy between the data tested and the data simulated was less than 1.02 % in the worst case, but certain attention spots on engine torque were detected. However, no action was performed because these points did not influence the final autonomy. Consequently, the ADVISOR proved to be a good solution for simulating fuel savings.

Regarding the fuel-saving, it was demonstrated that the overall BSG features obtaining fuel-saving around 10.15% to 13.05% in the city cycle (FTP-75), 0.38% to 1.15% in the highway cycle (HWFET), 6% to 7.5% in the combined cycle (FTP-75 + HWFET) and, 36% - 44% in the SP cycle. Furthermore, the BSG showed up more suitable for the city cycle (FTP-75) and (SP), as most of the fuel-saving comes from the stop-start and mild hybrid functionalities, while these cycles are characterized by repeated stops and braking opportunities. On the contrary, the highway cycle has long periods with no stops and high speed.

Finally, the methodology demonstrates that it is capable of tracing alternative scenarios for the project decision-making phase for Brazilian regulations with a high level of confidence. Furthermore, given the correct information, a confidence interval can be created, improving the quality of the prediction. In terms of the vehicle configurations studied in this study, the hatch achieves 1% tax savings using BSG 12V technology, whereas the SUV does not require this technology to achieve a 2% reduction, owing to its high reduction factor related to the relation between E100 and E22. Furthermore, it is important to remember that fuel-saving is highly dependent on the controls system, calibration, motor-generator power, and battery capacity.

6 Recommendations

From the results obtained in this work and the analysis it is possible to suggest the following recommendations:

- Survey of uncertainties for the test recorded during the validation phase to determine the simulation's confirmability.
- Simulate other electric architectures with different topologies for BSG integration.
- Survey the real friction and inertia of the engine, transmission, and electric motor. Also, there is room for improvement in belt friction determination, as in this work a constant loss value was used.
- Create a logic based on artificial intelligence to optimize the use of the recovery energy.
- Introduce drivability constraints to make regenerative braking, electric assist, and stop-start more realistic.
- Build a prototype vehicle to test with an in-chassis dynamometer to validate the potential fuel-saving simulated.

7 References

ABNT - ASSOCIAÇÃO BRASILEIRA DE NORMAS TÉCNICAS. **ABNT NBR 6601**: Veículos rodoviários automotores leves - Determinação de hidrocarbonetos, monóxido de carbono, óxidos de nitrogênio, dióxido de carbono e material particulado no gás de escapamento. Rio de Janeiro: ABNT, 2012.

ABNT - ASSOCIAÇÃO BRASILEIRA DE NORMAS TÉCNICAS. **ABNT NBR 7024**: Veículos rodoviários automotores leves - Medição do consumo de combustível - Método de ensaio. Rio de Janeiro: ABNT, 2012.

ABNT - ASSOCIAÇÃO BRASILEIRA DE NORMAS TÉCNICAS. **ABNT NBR 10312**: Veículos rodoviários automotores leves - Determinação da resistência ao deslocamento por desaceleração livre em pista de rolamento e simulação em dinamômetro. Rio de Janeiro: ABNT, 2019.

AGENCE FRANCE-PRESSE. **Peugeot Citroen to offer car with "stop and start" engine.** Disponível em: <https://www.spacedaily.com/2004/040907151848.lbjwimun.html>. Acesso em: 13 jun. 2021.

ANP, AGÊNCIA NACIONAL DO PETRÓLEO, ANP Nº 807, DE 23.01.2020 - DOU 24.01.2020 - RETIFICADA DOU 27.01.2020. Disponível em: <http://legislacao.anp.gov.br/?path=legislacao-anp/resol-anp/2020/janeiro&item=ranp-807-2020>. Acesso em: 5 dez. 2020.

BAETA, J. G. C. **Metodologia experimental para a maximização do desempenho de um motor multicombustível turboalimentado sem prejuízo à eficiência energética global**. Tese de doutorado, Universidade Federal de Minas Gerais, Belo Horizonte, 2006.

BALDIZZONE, S. **Performance and Fuel Economy Analysis of a Mild Hybrid Vehicle Equipped with Belt Starter Generator**. Dissertação de mestrado, University of Windsor, Canada, 2012.

CAO, J.; EMADI, A. A new battery/ultracapacitor hybrid energy storage system for electric,

hybrid, and plug-in hybrid electric vehicles. **IEEE Transactions on Power Electronics**, v. 27, n. 1, p. 122-132, 2012.

CHAU, K. T.; CHAN, C. C.; LIU, C. Overview of permanent-magnet brushless drives for electric and hybrid electric vehicles. **IEEE Transactions on Industrial Electronics**, v. 55, n. 6, p. 2246-2257, 2008.

CHEN, D. et al. Research on simulation of the hybrid electric vehicle based on software ADVISOR. **Sensors & Transducers**, v. 171, n. 5, p. 68, 2014.

CHEN, D. et al. Research on simulation of the hybrid electric vehicle based on software ADVISOR. **Sensors & Transducers**, v. 171, n. 5, p. 68, 2014.

CHENG, Y. H.; LAI, C. M.; TEH, J. Memetic algorithm for fuel economy and low emissions parallel hybrid electric vehicles. **Proceedings - 2017 IEEE 8th International Conference on Awareness Science and Technology, iCAST 2017**, v. 2018-Janua, n. iCAST, p. 219-222, 2017.

CLUETT, I. Application of Low-Cost Belt Starter-Generator Hybrid Technology in Emerging Markets. **SAE Technical Papers**, v. 2007-Janua, n. January, 2007.

DE OLIVEIRA, M. F. Análise comparativa de simulação numérica 1D e criação de um conceito veículo elétrico híbrido para redução do consumo de combustível segundo a norma NBR6601 US FTP75. Dissertação de mestrado, Universidade Federal de Minas Gerais, Belo Horizonte, 2019.

DE SOUZA DIAS, M. O. et al. Sugarcane processing for ethanol and sugar in Brazil. **Environmental Development**, v. 15, p. 35-51, 2015.

DELPHI. **Delphi 48-volt technology will be in new cars by 2017**. Disponível em: <https://www.freep.com/story/money/cars/2016/04/13/delphi-48-volt-technology-new-cars-2017/82949374/>. Acesso em: 31 jan. 2022.

DISELNET. **FTP-75**. Disponível em: <https://dieselnet.com/standards/cycles/ftp75.php>.

Acesso em: 31 jan. 2022.

EHSANI, M. et al. **Modern Electric, Hybrid Electric, and Fuel Cell Vehicles**. CRC Press; 2018.

EHSANI, M.; GAO, Y.; MILLER, J. M. Hybrid electric vehicles: Architecture and motor drives. **Proceedings of the IEEE**, v. 95, n. 4, p. 719-728, 2007.

EMADI, A. et al. Topological overview of hybrid electric and fuel cell vehicular power system architectures and configurations. **IEEE Transactions on Vehicular Technology**, v. 54, n. 3, p. 763-770, 2005.

EMADI, A. **Advanced Electric Drive Vehicles**. CRC Press, 2014.

EMADI, A. **Handbook of automotive power electronics and motor drives**. CRC Press, 2005.

EUROPEAN PARLIAMENT. DIRECTIVE (EU) 2019/633 OF THE EUROPEAN PARLIAMENT AND OF THE COUNCIL of 17 April 2019. **official journal of the European Union**, v. 15, n. 6, p. 851-867, 2019.

FEBABRAVE. **Anuário 2019**. São Paulo, 2019. Disponível em: <http://www.fenabrave.org.br/anuarios/Anuario2019.pdf>.

FIGUEIREDO, E. F. **CONTRIBUIÇÃO PARA MELHORIA DA CORRELAÇÃO ENTRE DADOS SIMULADOS E REAIS DE AUTONOMIA DE UM VEÍCULO FLEX FUEL**. Dissertação de mestrado, Universidade Federal de Minas Gerais, Belo Horizonte, 2019.

FERLITO, G. **Adaptation of low cost hybrid architecture to a general purpose platform**. Dissertação de mestrado, POLITECNICO DI TORINO, Italy, 2018.

FIGUEIREDO, E. F.; CAMPOS, C. H. F.; PUJATTI, F. J. P. **Stop & Start technology influence on Brazilian urban off-cycle - Simulated versus experimental data**

analysisSAE International , , 2020a. Disponível em: <https://doi.org/10.4271/2019-36-0286>

GAO, D. W.; MI, C.; EMADI, A. Modeling and Simulation of Electric and Hybrid Vehicles. **Proceedings of the IEEE**, v. 95, n. 4, p. 729-745, 2007.

GIACOSA, D. Motores Endotérmicos-3ªedição. **Editorial Dossat, DL**, 1986.

GUPTA, S. et al. Estimation of Fuel Economy on Real-World Routes for Next-Generation Connected and Automated Hybrid Powertrains. **SAE Technical Papers**, v. 2020-April, n. April, p. 1-12, 2020.

HEYWOOD, John B. **Internal Combustion Engine Fundamentals**. McGraw-Hill Education, 2018.

HUMPHRIES, K. **Simulation and Optimization of Electric and Hybrid Vehicles with Two-Speed Transmissions**. McGill University (Canada), 2015.

IEA. **Data & Statistics - IEA**. Disponível em: <https://www.iea.org/data-and-statistics>. Acesso em: 31 jan. 2022.

INRIX. **Scorecard - INRIXINRIX**. Disponível em: <https://inrix.com/scorecard/>. Acesso em: 31 jan. 2022.

JOHNSON, V. H.; WIPKE, K. B.; RAUSEN, D. J. **HEV Control Strategy for Real-Time Optimization of Fuel Economy and Emissions**. SAE Technical Paper, 2000.

KOEHLER, N. et al. 2019 Ethanol Industry Outlook: Powered With Renewed Energy. **Renewable Fuels Association**, 2019.

LAWRENCE LIVERMORE NATIONAL LABORATORY. **U.S. Energy Flow Diagram 2018**. Disponível em: <https://flowcharts.llnl.gov/content/assets/docs/2018_United-States_Energy.pdf>. Acesso em: 31 jan. 2022.

LEE, S. et al. Modeling and Validation of 48V Mild Hybrid Lithium-Ion Battery Pack. **SAE International Journal of Alternative Powertrains**, v. 7, n. 3, 2018a.

LEE, S. et al. Modeling and Controls Development of 48 v Mild Hybrid Electric Vehicles. **SAE Technical Papers**, v. 2018- April, p. 1-15, 2018b.

MALAQUIAS, A. C. T. et al. The misleading total replacement of internal combustion engines by electric motors and a study of the Brazilian ethanol importance for the sustainable future of mobility: a review. **Journal of the Brazilian Society of Mechanical Sciences and Engineering**, v. 41, n. 12, 2019.

MALIKOPOULOS, A.; FILIPI, Z.; ASSANIS, D. Simulation of an Integrated Starter Alternator (ISA) system for the HMMWV. **SAE Technical Papers**, n. April, 2006.

MARKEL, T.; WIPKE, K. Modeling grid-connected hybrid electric vehicles using ADVISOR. **Proceedings of the Annual Battery Conference on Applications and Advances**, n. January, p. 23-29, 2001.

MI, C.; MASRUR, M. A.; GAO, D. W. **Hybrid Electric Vehicles: Principles and Applications with Practical Perspectives**. Wiley, 2011.

MOTOR GERAIS. **Motores 1.0 e 1.4 Fire Evo poluem e consomem menos**. Disponível em: <http://motorgerais.blogspot.com/2010/05/novos-motores-10-e-14-fire-evo-poluem-e.html>. Acesso em: 31 jan. 2022.

NASA. **Global Climate Change**. Disponível em: <https://climate.nasa.gov/>. Acesso em: 31 jan. 2022.

NREL. **Advanced vehicle simulator documentation.** Disponível em: <http://adv-vehicle-sim.sourceforge.net/>. Acesso em: 31 jan. 2022.

OLIVEIRA, M. et al. Sugarcane processing for ethanol and sugar in Brazil. **Environmental Development**, v. 15, p. 35-51, 2015.

ONORI, S. **Hybrid Electric Vehicles Energy Management Strategies**. Springer, 2016.

PENHA, E. J. V. **SIMULATION OF A SERIES HYBRID ELECTRIC VEHICLE POWERED BY BRAZILIAN HYDRATED ETHANOL ENGINE**. Dissertação de mestrado, Universidade Federal de Minas Gerais, Belo Horizonte, 2019.

QUATRO RODAS. **Motor 1.8 E.torQ usado por Fiat e Jeep será aposentado até 2020**. Disponível em: <https://quatrorodas.abril.com.br/noticias/motor-1-8-e-torq-usado-por-fiat-e-jeep-sera-aposentado-ate-2020/>. Acesso em: 31 jan. 2022.

REPÚBLICA, P. DA. DECRETO Nº 9.442, DE 5 DE JULHO DE 2018. . 2018.

SENGER, R. D.; MERKLE, M. A.; NELSON, D. J. Validation of ADVISOR as a simulation tool for a series hybrid electric vehicle. **SAE Technical Papers**, 1998.

SILVA, R. Á. **Avaliação da Hibridização de um Veículo Nacional Compacto Utilizando a Arquitetura Paralela de Eixos Separados .** Dissertação de mestrado, Universidade Federal de Minas Gerais, Belo Horizonte, 2017.

SLOWIK, P.; LUTSEY, N. The Continued Transition to Electric Vehicles in US Cities. **ICCT white paper**, 2018.

STEFFAN, R.; HOFMANN, P.; GERINGER, B. Potentials of a 48 Volt Belt-Starter-Generator in the Powertrain of an Ultra-Light Vehicle. **SAE Technical Papers**, 2015.

STEPHEN J. CHAPMAN. **Electric Machinery Fundamentals**. McGraw-Hill, 2003

VRUM. **Jeep Renegade Longitude 1.8 4x2**. Disponível em: <https://estadodeminas.vrum.com.br/fichatecnica/jeep/renegade/2018/017035-6>. Acesso em: 31 jan. 2022.

VRUM. **Fiat UNO SPORTING 1.4 EVO FIRE**. Disponível em: <https://estadodeminas.vrum.com.br/fichatecnica/fiat/uno/2015/001341-2>. Acesso em: 31 jan. 2022.

WIPKE, K. et al. **Advisor 2.0: A Second-Generation Advanced Vehicle Simulator for Systems Analysis**. National Renewable Energy Lab., Golden, CO (US), 1999.

WU, Y. et al. On-road vehicle emissions and their control in China: A review and outlook. **Science of the Total Environment**, v. 574, n. January, p. 332-349, 2017.

WUEBBLES, D. J. et al. Highlights of the U.S. Global Change Research Program Climate Science Special Report. **Fourth National Climate Assessment**, p. 10-34, 2016.

ZO, H.; NAN, J.; PENG, F. Simulation Research on Fuel Consumption Reduction Strategy of 48V Micro Hybrid Electric Vehicles. **DEStech Transactions on Environment, Energy and Earth Sciences**, n. iceee, 2019.

APPENDIX A – FUEL CONSUMPTION RESULTS FOR H_1.4_E100_12V

The autonomy Table's results for H_1.4_E100_12V are shown in Tables 01, 02, and 03. The charts were plotted in Figures 01, 02, 03, 04, 05, 06, 07, 08, 09, 10, 11, and 12

Table 01 - H_1.4_E100_12V absolute fuel autonomy results

[Km/l]	case 0	case 1	case 2	case 3	case 4
FTP	10.125	10.922	11.146	11.174	11.310
	Abs. variation→	0.797	1.021	1.049	1.185
	% variation→	7.87%	10.08%	10.36%	11.70%
HW	12.765	12.798	12.823	12.822	12.814
	Abs. variation→	0.033	0.057	0.056	0.048
	% variation→	0.26%	0.45%	0.44%	0.38%
COMB	11.164	11.694	11.843	11.860	11.940
	Abs. variation→	0.529	0.678	0.696	0.776
	% variation→	4.74%	6.08%	6.23%	6.95%
SP	7.696	9.530	9.963	10.071	10.499
	Abs. variation→	1.834	2.267	2.374	2.802
	% variation→	23.83%	29.45%	30.85%	36.41%

Table 02 - H_1.4_E100_12V relative fuel autonomy results

[Km/l]		case 1 - case 0	case 2 - case 1	case 3 - case 2	case 4 - case 1
FTP	**Abs. variation→**	0.797	0.224	0.028	0.136
	% variation→	7.87%	2.21%	0.28%	1.34%
HW	**Abs. variation→**	0.033	0.024	-0.001	-0.008
	% variation→	0.26%	0.19%	-0.01%	-0.06%
COMB	**Abs. variation→**	0.529	0.149	0.017	0.081
	% variation→	4.74%	1.34%	0.15%	0.72%
SP	**Abs. variation→**	1.834	0.433	0.108	0.428
	% variation→	23.83%	5.62%	1.40%	5.56%

Table 03 - H_1.4_E100_12V SOC delta

[%]		case 2	case 3	case 4
FTP	**SOC Initial →**	41%	41%	40%
	SOC Final →	53%	53%	51%
	% Delta→	-13%	-13%	-11%
HW	**SOC Initial →**	53%	53%	51%
	SOC Final →	41%	41%	40%
	% Delta→	13%	13%	11%
COMB	**SOC Initial →**	41%	41%	40%
	SOC Final →	41%	41%	40%
	% Delta→	0%	0%	0%
SP	**SOC Initial →**	43%	43%	41%
	SOC Final →	43%	43%	41%
	% Delta→	0%	0%	0%

Figure 01 - Comparison of the engine operating points among the cases over the FTP-75 cycle for H_1.4_E100_12V

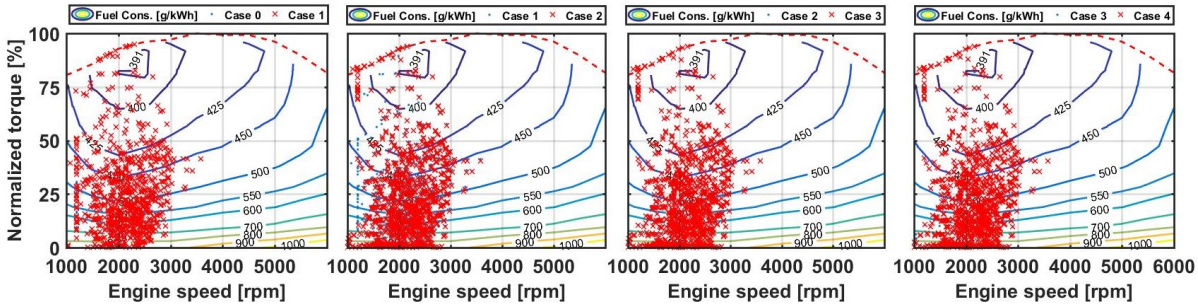

Figure 02 - Histogram of engine torque, engine speed and engine specific fuel consumption over the FTP-75 cycle for H_1.4_E100_12V

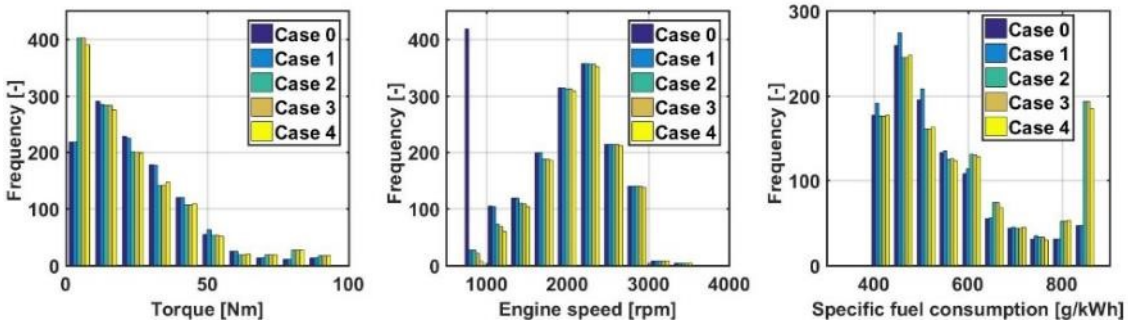

Figure 03 - Comparison of the engine operating points among the cases over the HWFET cycle for H_1.4_E100_12V

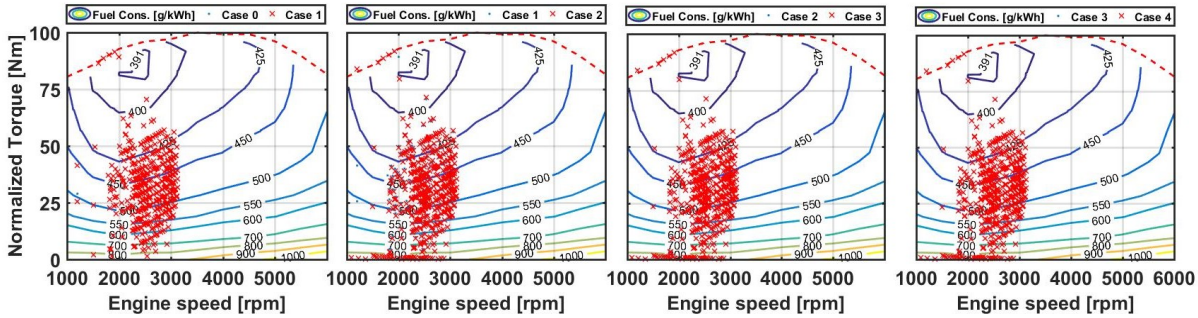

Figure 04 - Histogram of engine torque, engine speed and engine specific fuel consumption over the HWFET cycle for H_1.4_E100_12V

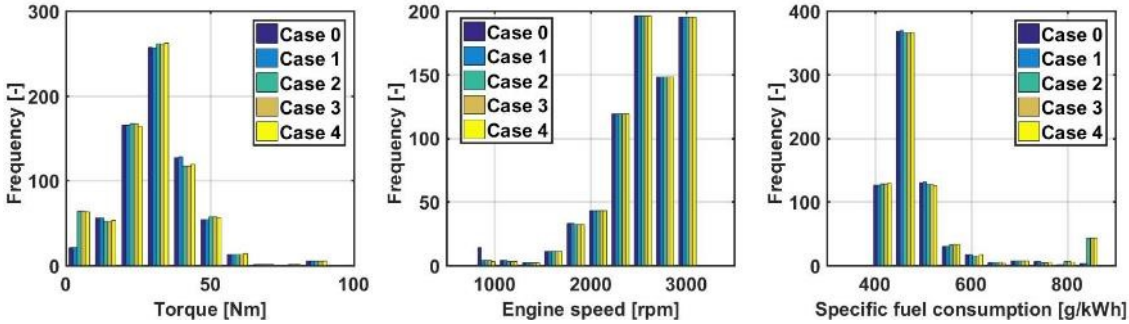

Figure 05 - Comparison of the engine operating points among the cases over the SP cycle for H_1.4_E100_12V

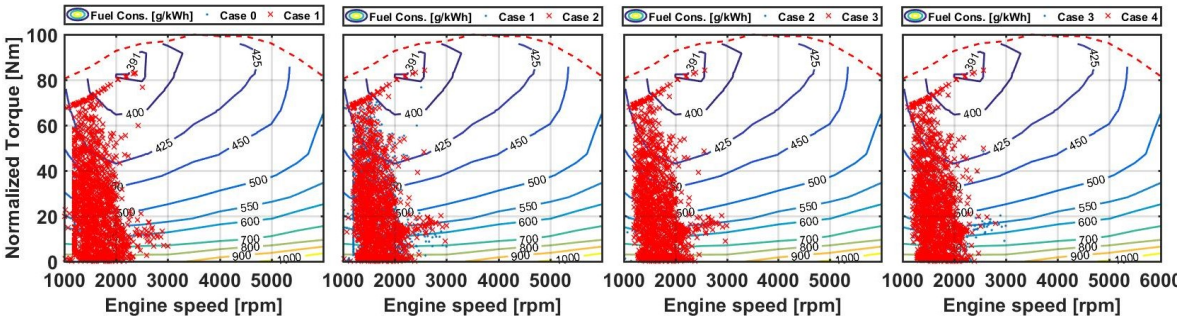

Figure 06 - Histogram of engine torque, engine speed and engine specific fuel consumption over the SP for H_1.4_E100_12V

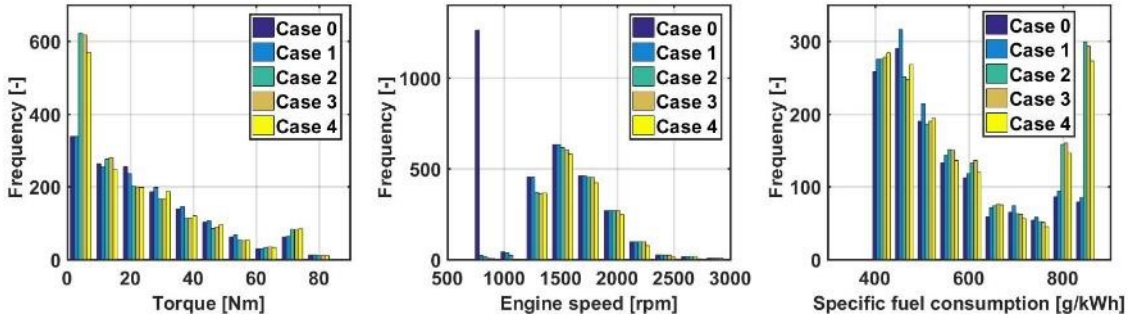

Figure 07 - Comparison of the motor operating points among the cases over the FTP-75 cycle for H_1.4_E100_12V

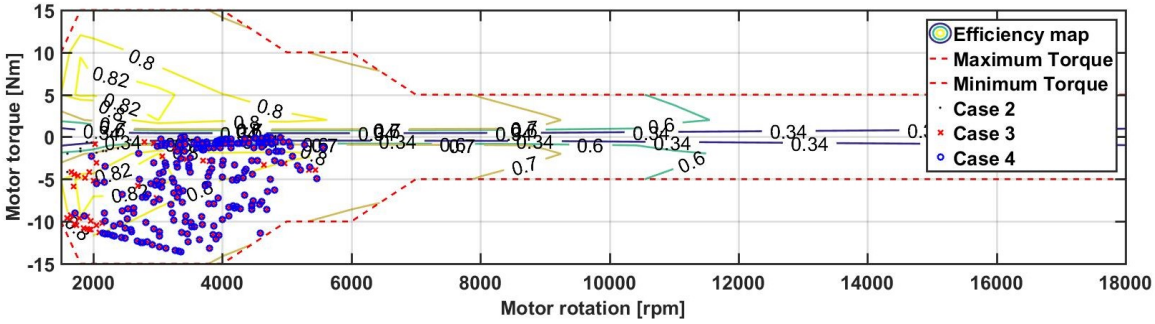

Figure 08 - Histogram of engine torque, engine speed and engine specific fuel consumption over the SP for H_1.4_E100_12V

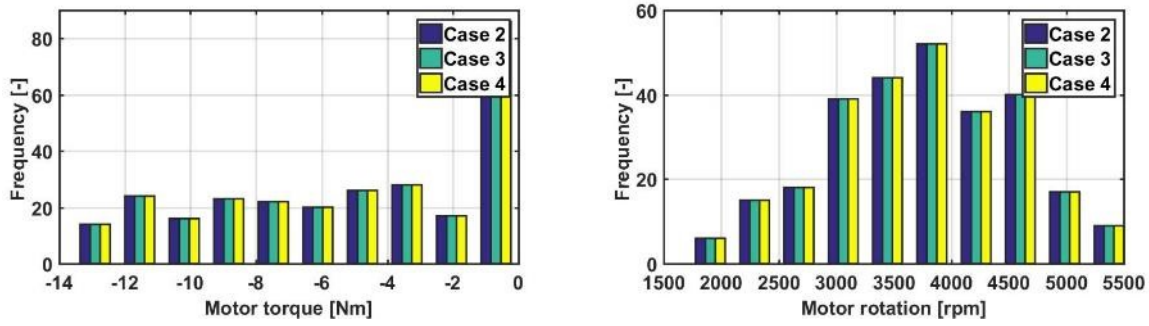

Figure 09 - Comparison of the motor operating points among the cases over the HWFET cycle for H_1.4_E100_12V

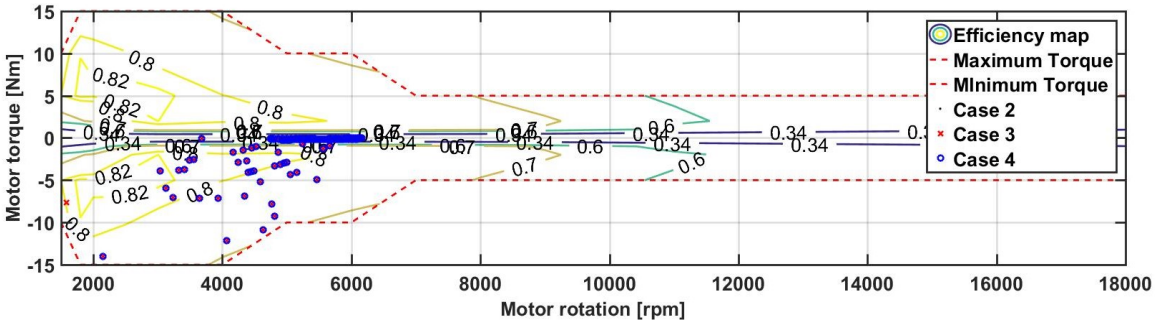

Figure 10 - Histogram of motor torque, motor speed and specific fuel consumption over the HWFET cycle for H_1.4_E100_12V

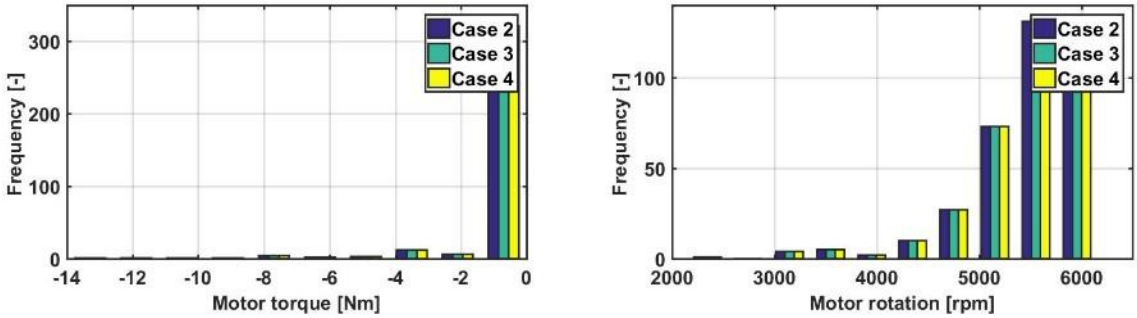

Figure 11 - Histogram of motor torque, motor speed and specific fuel consumption over the HWFET cycle for H_1.4_E100_12V

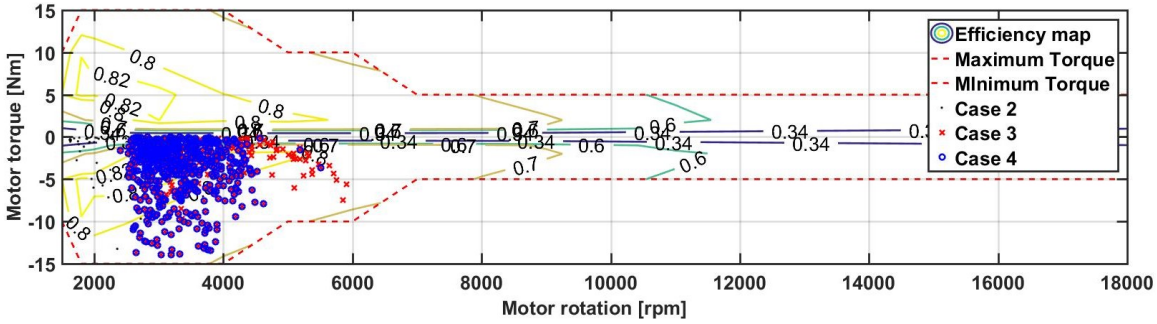

Figure 12 - Histogram of torque, engine speed and specific fuel consumption over the HWFET cycle for H_1.4_E22_12V

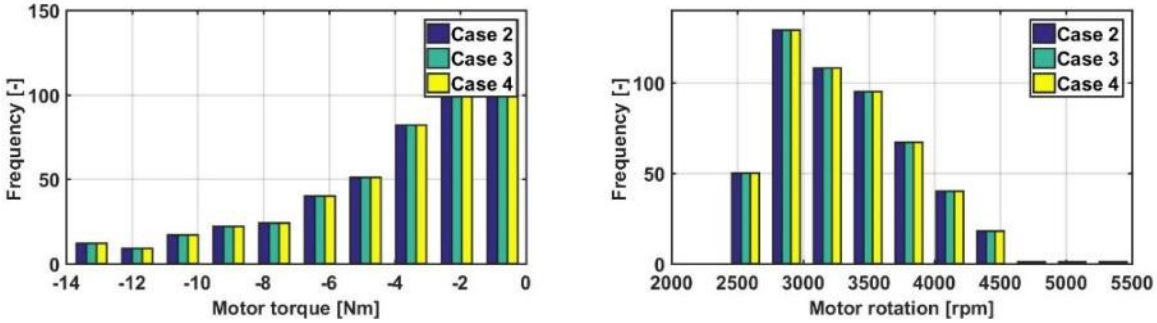

APPENDIX B – FUEL CONSUMPTION RESULTS FOR SUV_1.8_E22_12V

The autonomy Table's results for SUV_1.8_E22_12V are shown in Tables 01, 02, and 03. The charts were plotted in Figures 01, 02, 03, 04, 05, 06, 07, 08, 09, 10, 11, and 12

Table 01 - SUV_1.8_E22_12V absolute fuel autonomy results

[Km/l]	case 0	case 1	case 2	case 3	case 4
FTP	12.854	14.077	14.275	14.312	14.483
	Abs. variation→	1.223	1.421	1.458	1.629
	% variation→	9.52%	11.05%	11.34%	12.68%
HW	14.599	14.633	14.754	14.758	14.767
	Abs. variation→	0.034	0.155	0.160	0.168
	% variation→	0.24%	1.06%	1.09%	1.15%
COMB	13.585	14.322	14.486	14.509	14.610
	Abs. variation→	0.738	0.902	0.925	1.025
	% variation→	5.43%	6.64%	6.81%	7.55%
SP	7.996	10.434	10.905	11.002	11.388
	Abs. variation→	2.437	2.909	3.006	3.392
	% variation→	30.48%	36.38%	37.59%	42.42%

Table 39 - SUV_1.8_E22_12V relative fuel autonomy results

[Km/l]		case 1 - case 0	case 2 - case 1	case 3 - case 2	case 4 - case 1
FTP	**Abs. variation→**	1.223	0.197	0.037	0.172
	% variation→	9.52%	1.53%	0.29%	1.34%
HW	**Abs. variation→**	0.034	0.121	0.005	0.009
	% variation→	0.24%	0.83%	0.03%	0.06%
COMB	**Abs. variation→**	0.738	0.164	0.023	0.100
	% variation→	5.43%	1.21%	0.17%	0.74%
SP	**Abs. variation→**	2.437	0.472	0.097	0.386
	% variation→	30.48%	5.90%	1.21%	4.83%

Table 40 - SUV_1.8_E22_12V SOC delta

[%]		case 2	case 3	case 4
FTP	**SOC Initial →**	43%	43%	41%
	SOC Final →	68%	68%	65%
	% Delta→	-26%	-26%	-24%
HW	**SOC Initial →**	68%	68%	65%
	SOC Final →	43%	43%	41%
	% Delta→	26%	26%	24%
COMB	**SOC Initial →**	43%	43%	41%
	SOC Final →	43%	43%	41%
	% Delta→	0%	0%	0%
SP	**SOC Initial →**	55%	55%	50%
	SOC Final →	55%	55%	50%
	% Delta→	0%	0%	0%

Figure 01 - Comparison of the engine operating points among the cases over the FTP-75 cycle for SUV_1.8_E22_12V

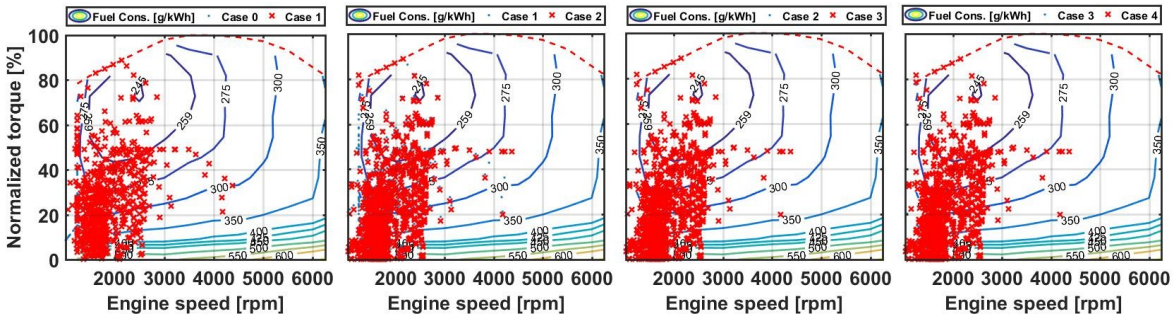

Figure 02 - Histogram of engine torque, engine speed and engine specific fuel consumption over the FTP-75 cycle for SUV_1.8_E22_12V

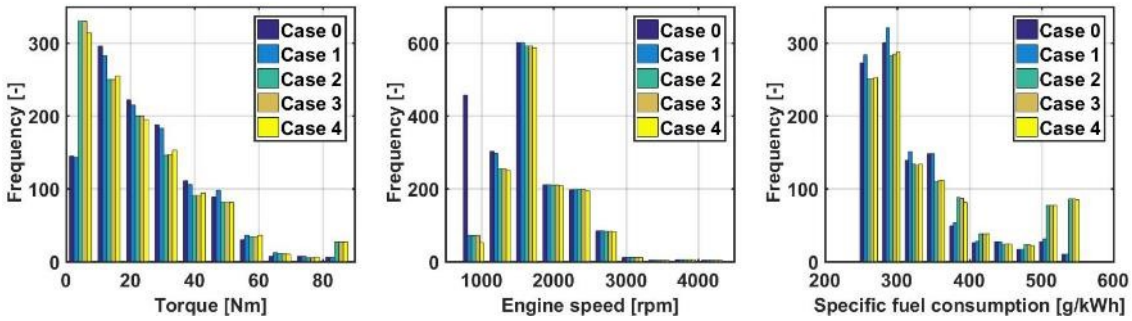

Figure 03 - Comparison of the engine operating points among the cases over the HWFET cycle for SUV_1.8_E22_12V

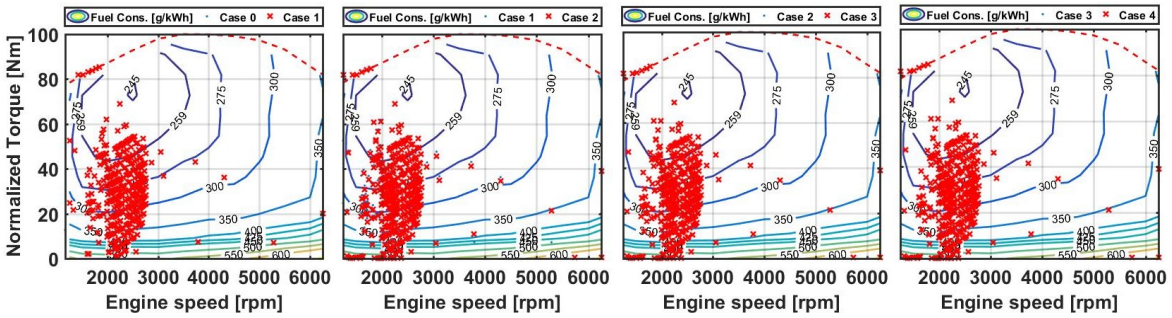

Figure 04 - Histogram of engine torque, engine speed and engine specific fuel consumption over the HWFET cycle for SUV_1.8_E22_12V

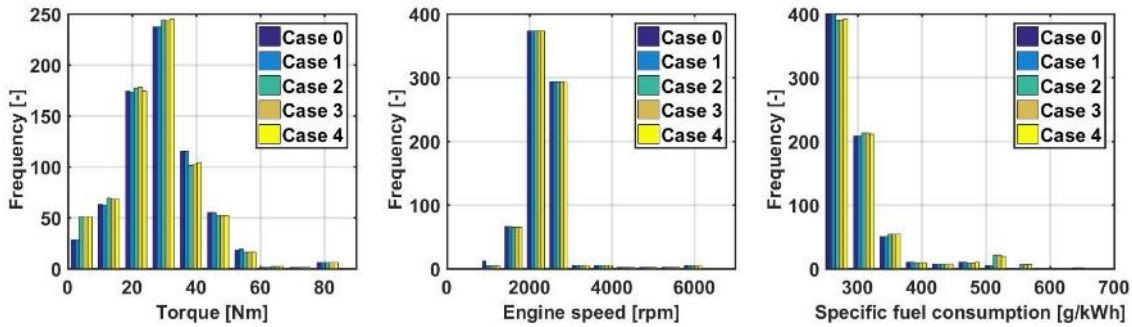

Figure 05- Comparison of the engine operating points among the cases over the SP cycle for SUV_1.8_E22_12V

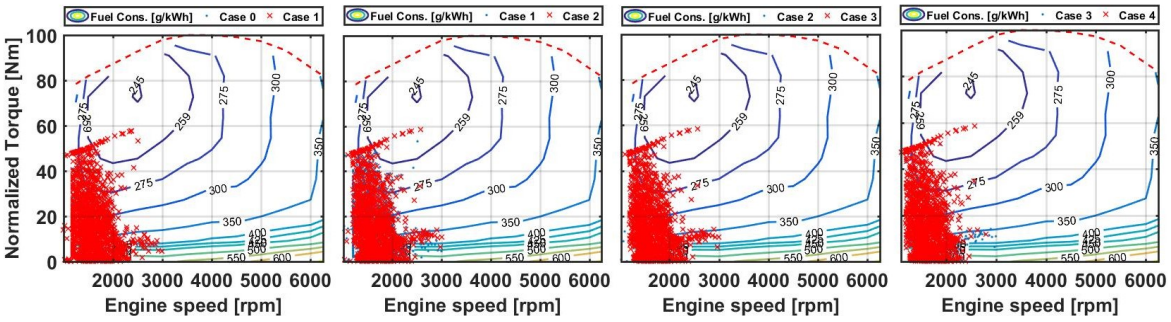

Figure 06- Histogram of engine torque, engine speed and engine specific fuel consumption over the SP for SUV_1.8_E22_12V

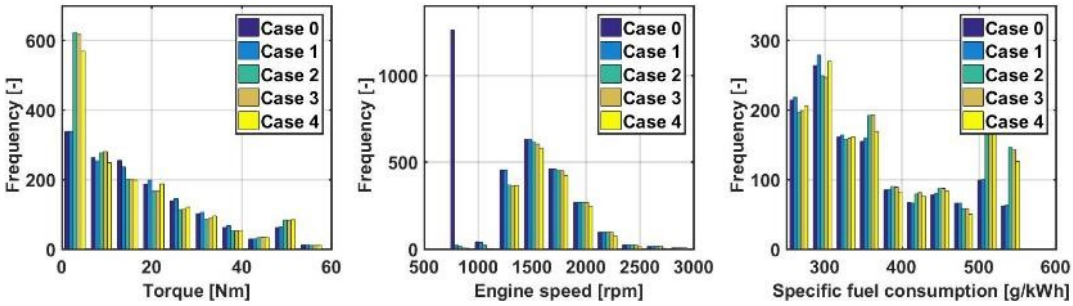

Figure 07 - Comparison of the motor operating points among the cases over the FTP-75 cycle for SUV_1.8_E22_12V

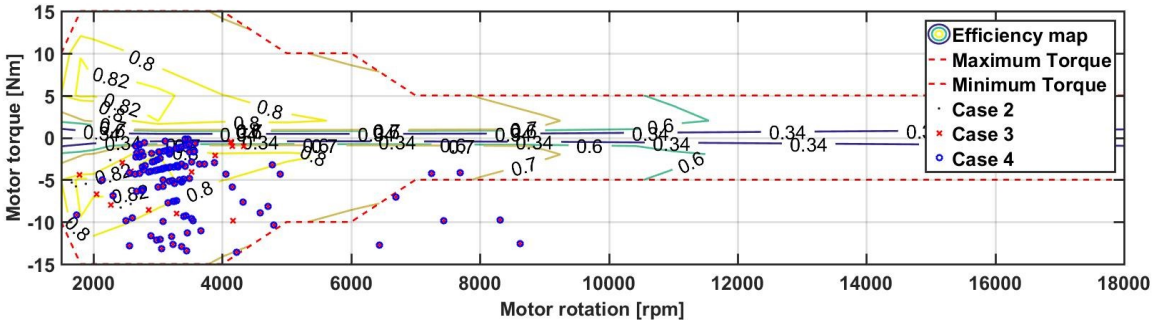

Figure 08 - Histogram of motor torque, motor speed and specific fuel consumption over the FTP-75 cycle for SUV_1.8_E22_12V

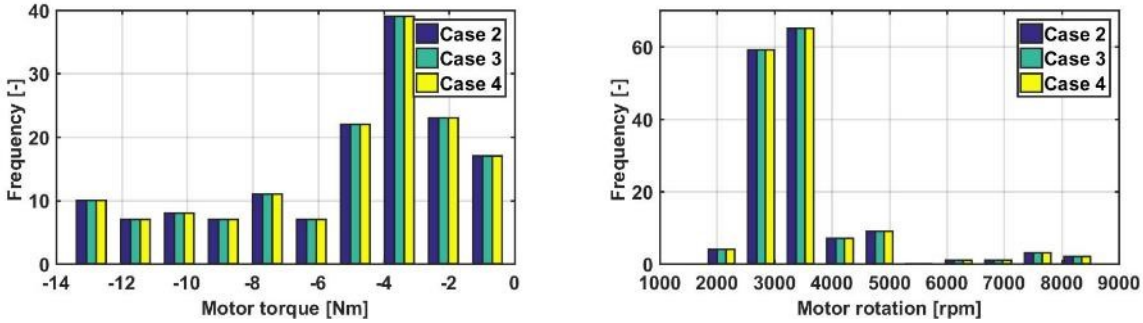

Figure 09 - Comparison of the motor operating points among the cases over the HWFET cycle for SUV_1.8_E22_12V

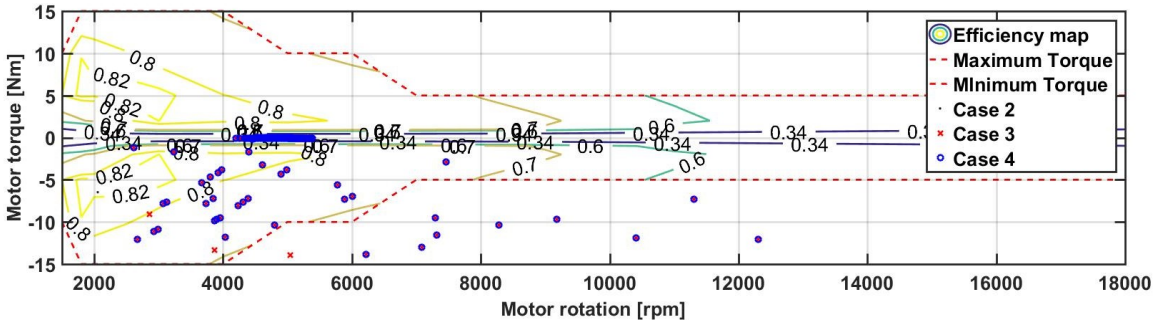

Figure 10 - Histogram of motor torque, motor speed and specific fuel consumption over the HWFET cycle for SUV_1.8_E22_12V

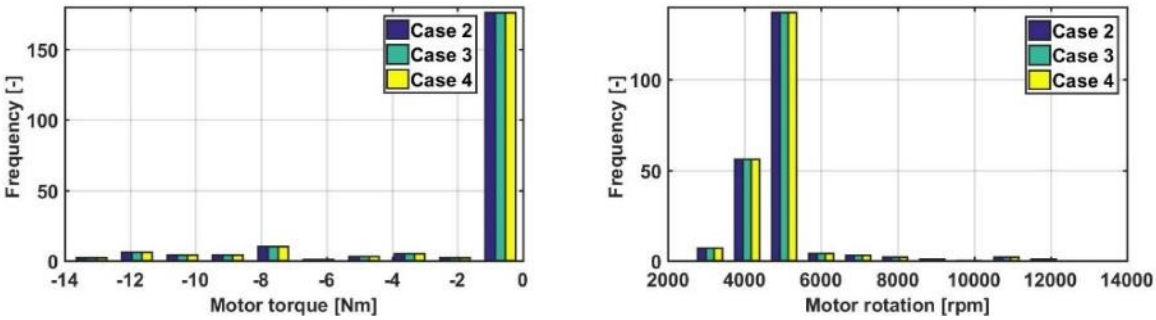

Figure 11 - Comparison of the motor operating points among the cases over the SP cycle for SUV_1.8_E22_12V

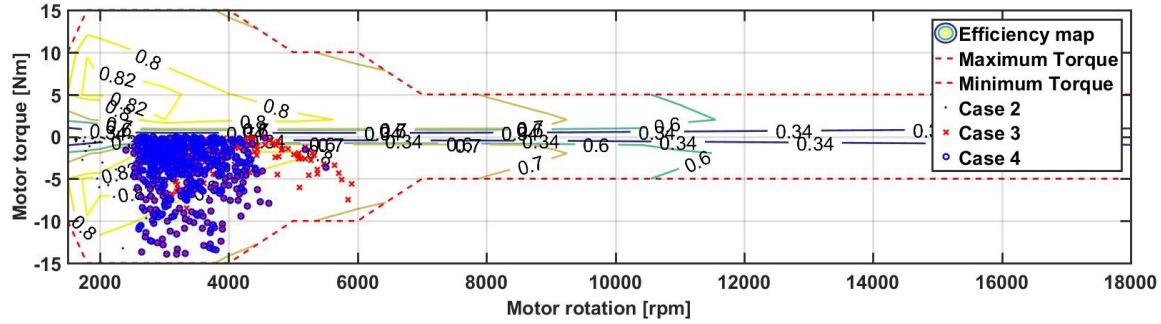

Figure 12 - Histogram of motor torque, motor speed and specific fuel consumption over the SP cycle for SUV_1.8_E22_12V

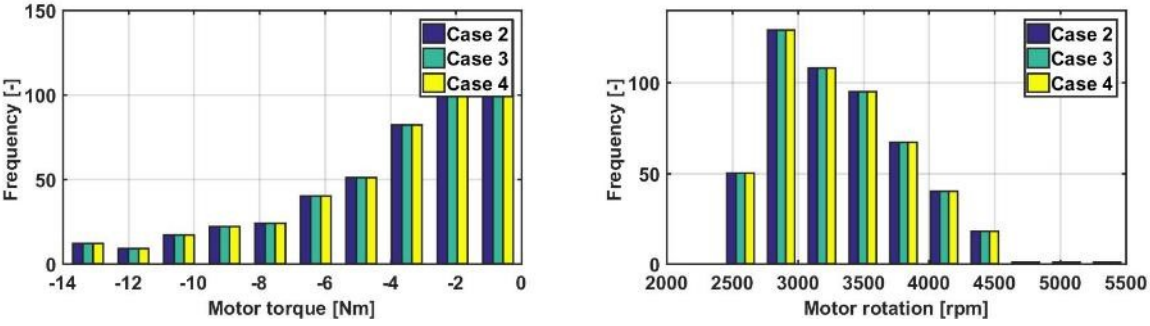

APPENDIX C – FUEL CONSUMPTION RESULTS FOR SUV_1.8_E100

The autonomy Table's results for SUV_1.8_E100_12V are shown in Tables 01, 02, and 03. The charts were plotted in Figures 01, 02, 03, 04, 05, 06, 07, 08, 09, 10, 11, and 12

Table 01 - SUV_1.8_E100_12V absolute fuel autonomy results

[Km/l]	case 0	case 1	case 2	case 3	case 4
FTP	9.870	10.769	11.007	11.034	11.158
	Abs. variation→	0.899	1.137	1.164	1.288
	% variation→	9.11%	11.52%	11.79%	13.05%
HW	10.677	10.702	10.774	10.777	10.783
	Abs. variation→	0.025	0.097	0.100	0.106
	% variation→	0.24%	0.91%	0.94%	0.99%
COMB	10.218	10.739	10.901	10.917	10.986
	Abs. variation→	0.521	0.683	0.699	0.768
	% variation→	5.10%	6.69%	6.84%	7.52%
SP	6.059	7.954	8.367	8.442	8.741
	Abs. variation→	1.895	2.308	2.383	2.682
	% variation→	31.28%	38.09%	39.34%	44.27%

Table 02 - SUV_1.8_E100_12V relative fuel autonomy results

[Km/l]		case 1 - case 0	case 2 - case 1	case 3 - case 2	case 4 - case 1
FTP	**Abs. variation→**	0.899	0.238	0.027	0.124
	% variation→	9.11%	2.41%	0.27%	1.25%
HW	**Abs. variation→**	0.025	0.072	0.003	0.006
	% variation→	0.24%	0.67%	0.03%	0.05%
COMB	**Abs. variation→**	0.521	0.162	0.016	0.069
	% variation→	5.10%	1.58%	0.16%	0.68%
SP	**Abs. variation→**	1.895	0.413	0.076	0.299
	% variation→	31.28%	6.81%	1.25%	4.93%

Table 03 - SUV_1.8_E100_12V SOC delta

[%]		case 2	case 3	case 4
FTP	**SOC Initial →**	43%	43%	41%
	SOC Final →	69%	69%	65%
	% Delta→	-26%	-26%	-24%
HW	**SOC Initial →**	69%	69%	65%
	SOC Final →	43%	43%	41%
	% Delta→	26%	26%	24%
COMB	**SOC Initial →**	43%	43%	41%
	SOC Final →	43%	43%	41%
	% Delta→	0%	0%	0%
SP	**SOC Initial →**	55%	55%	50%
	SOC Final →	55%	55%	50%
	% Delta→	0%	0%	0%

Figure 01 - Comparison of the engine operating points among the cases over the FTP-75 cycle for SUV_1.8_E100_12V

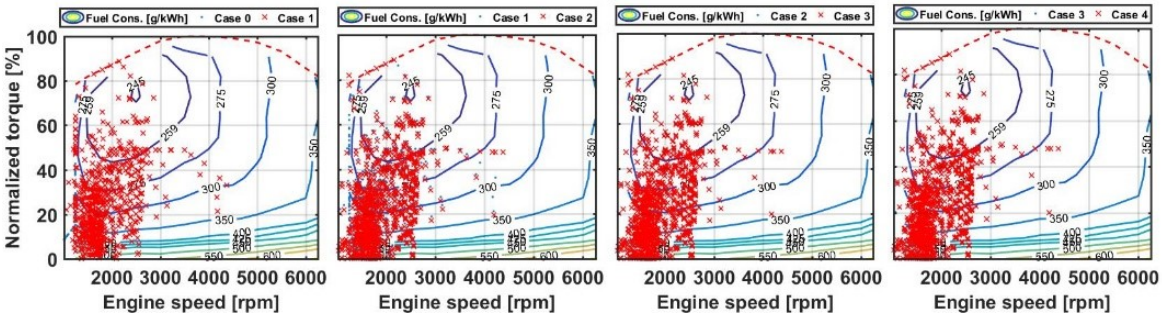

Figure 02 - Histogram of engine torque, engine speed and engine specific fuel consumption over the FTP-75 cycle for SUV_1.8_E100_12V

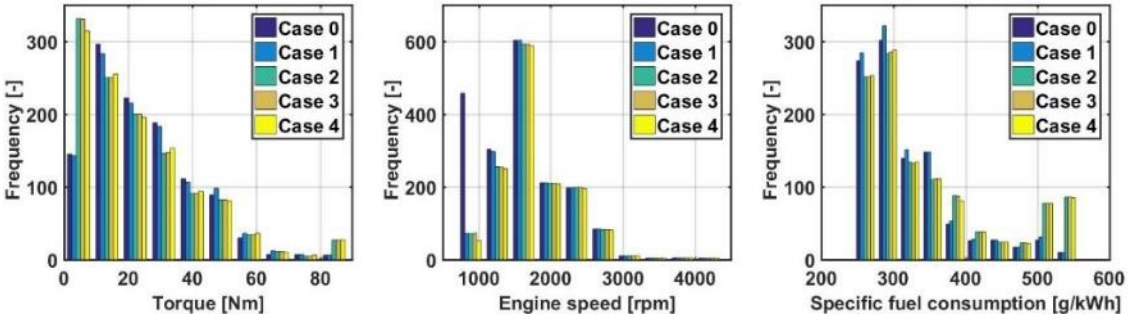

Figure 03 - Comparison of the engine operating points among the cases over the HWFET cycle for SUV_1.8_E100_12V

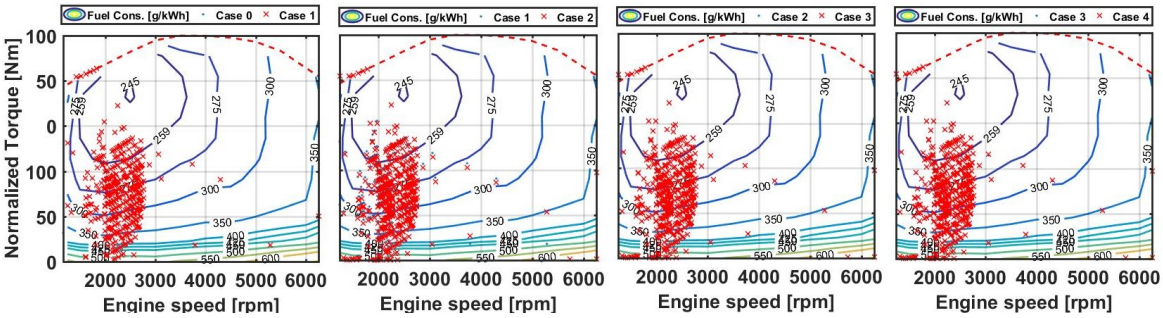

Figure 04 - Histogram of engine torque, engine speed and engine specific fuel consumption over the HWFET cycle for SUV_1.8_E100_12V

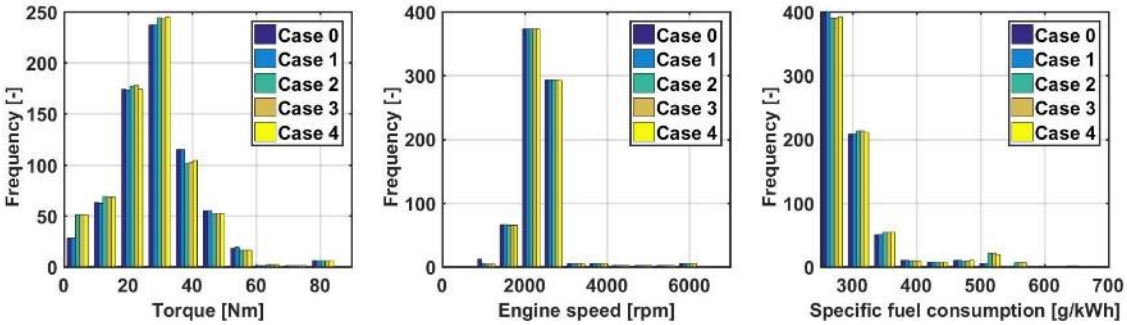

Figure 05 - Comparison of the engine operating points among the cases over the SP cycle for SUV_1.8_E100_12V

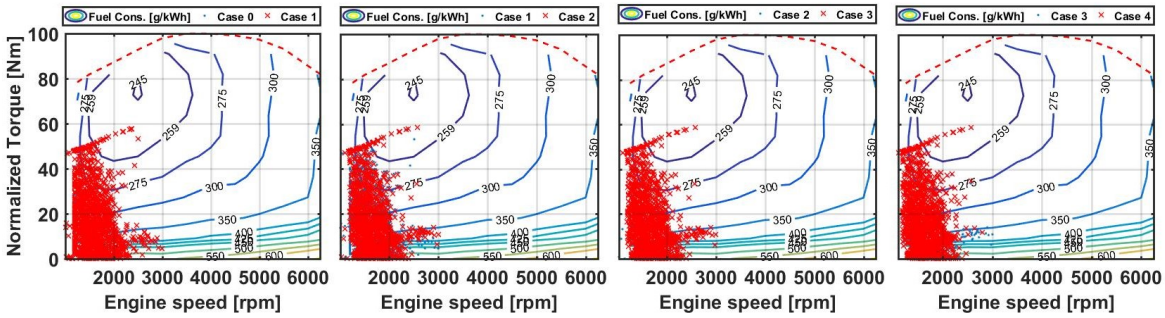

Figure 06 - Histogram of engine torque, engine speed and engine specific fuel consumption over the SP for SUV_1.8_E100_12V

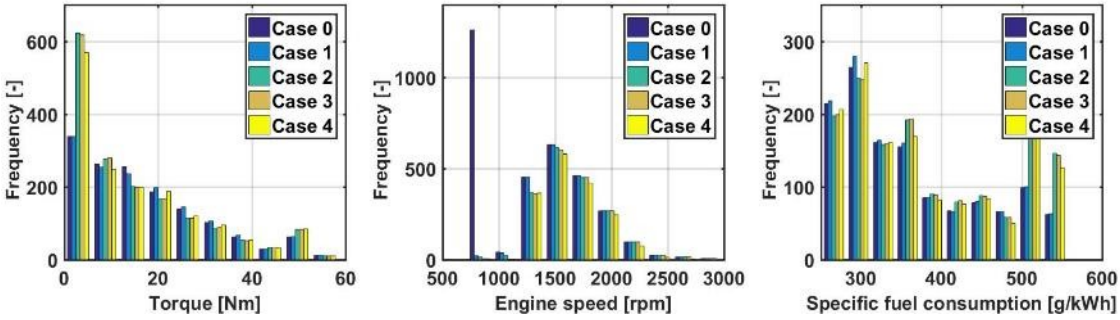

Figure 07 - Comparison of the motor operating points among the cases over the FTP-75 cycle for SUV_1.8_E100_12V

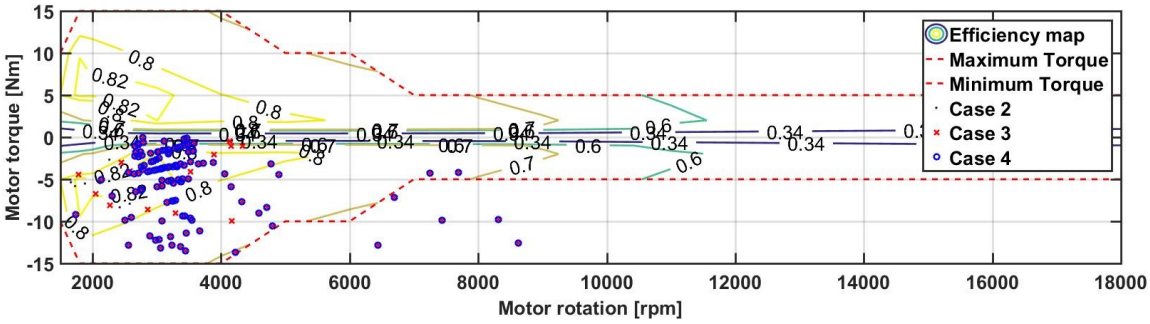

Figure 08 - Histogram of motor torque, motor speed and specific fuel consumption over the FTP-75 cycle for SUV_1.8_E100_12V

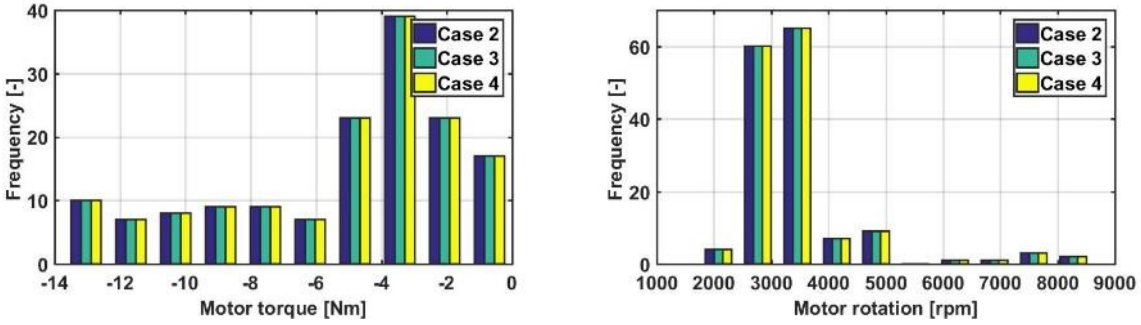

Figure 09 - Comparison of the motor operating points among the cases over the HWFET cycle for SUV_1.8_E100_12V

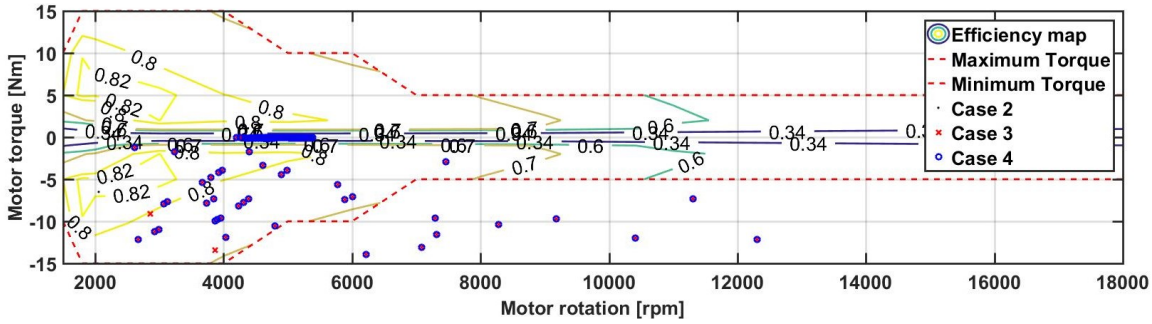

Figure 10 - Histogram of motor torque, motor speed and specific fuel consumption over the HWFET cycle for SUV_1.8_E100_12V

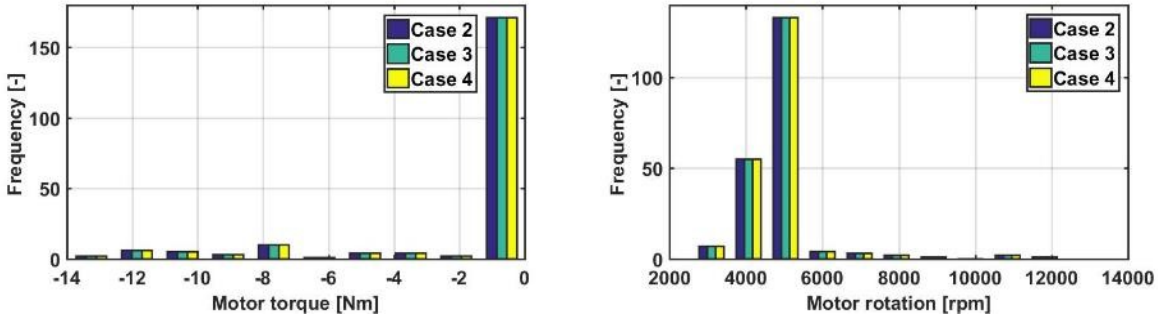

Figure 11 - Comparison of the motor operating points among the cases over the SP cycle for SUV_1.8_E100_12V

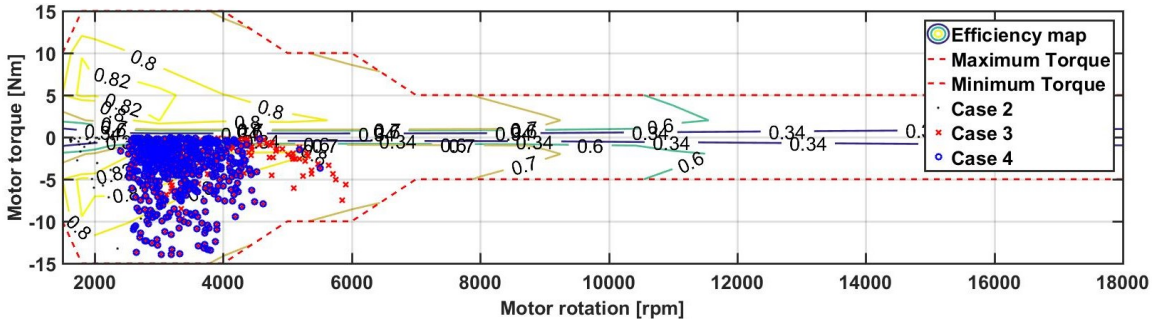

Figure 12 - Histogram of motor torque, motor speed and specific fuel consumption over the SP cycle for SUV_1.8_E100_12V

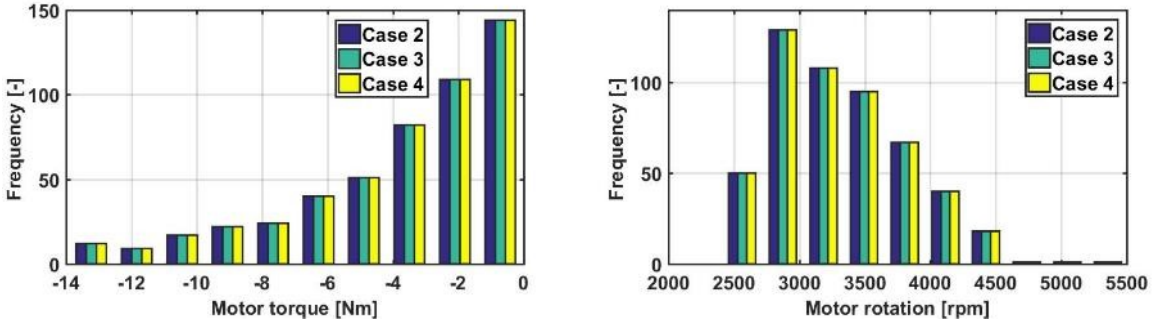

APPENDIX D – ENERGY BALANCE FOR SUV_1.8_E22_12V

The energy balance for the FTP-75 cycle with E22 for SUV_1.8_E22_12V of power and regen is shown in Tables 01 and 02, respectively. The energy balance for the HWFET cycle with the logic was presented in Tables 03 and 04.

Table 01- SUV_1.8_E22_12V energy balance over the FTP-75 for power in kW

	In_Power [kW]					out_Power [kW]					loss_Power[kW]					eff_Power[%]				
FTP E22 SUV	Case 0	Case 1	Case 2	Case 3	Case 4	Case 0	Case 1	Case 2	Case 3	Case 4	Case 0	Case 1	Case 2	Case 3	Case 4	Case 0	Case 1	Case 2	Case 3	Case 4
Fuel						41274	37104	36253	36198	35827										
Fuel Converter	41274	37104	36253	36198	35827	9185	9185	8757	8758	8784	32089	27919	27496	27440	27043	0.22	0.25	0.24	0.24	0.25
Clutch	8722	8722	8657	8657	8659	8599	8599	8598	8598	8598	123	123	59	59	61	0.99	0.99	0.99	0.99	0.99
Torque Coupling			8657	8657	8659			8657	8657	8659								1	1	1
Energy Storage			764	754	682			577	571	521			72	71	63			0.9	0.9	0.9
Energy Stored			115	113	97															
Gearbox	8599	8599	8598	8598	8598	8256	8256	8254	8254	8254	343	343	344	344	344	0.96	0.96	0.96	0.96	0.96
Final Drive	8256	8256	8254	8254	8254	8256	8256	8254	8254	8254						1	1	1	1	1
Wheel/Axle	8256	8256	8254	8254	8254	8182	8182	8175	8175	8175	73	73	79	79	79	0.99	0.99	0.99	0.99	0.99
Aux Loads	790	622	596	592	573						790	613	586	584	568					
Aero											2612	2612	2612	2612	2612					
Rolling											2550	2550	2552	2552	2552					

Table 02 - SUV_1.8_E22_12V energy balance over the FTP-75 for regen in kW

	In_Regen [kW]					out_Regen [kW]					loss_Regen [kW]					eff_Regen [%]				
FTP E22 SUV	Case 0	Case 1	Case 2	Case 3	Case 4	Case 0	Case 1	Case 2	Case 3	Case 4	Case 0	Case 1	Case 2	Case 3	Case 4	Case 0	Case 1	Case 2	Case 3	Case 4
Clutch	893	894	1111	1100	997	893	894	1111	1100	997						1	1	1	1	1
Torque Coupling			1111	1100	997			1111	1100	997								1	1	1
Motor/Controller			1128	1115	1009			764	754	682			364	361	327			0.68	0.68	0.68
Gearbox	930	931	1157	1146	1039	893	894	1111	1100	997			46	46	42	0.96	0.96	0.96	0.96	0.96
Final Drive	930	931	1157	1146	1039	930	931	1157	1146	1039						1	1	1	1	1
Wheel/Axle	3095	3095	3095	3095	3095	3098	3098	3087	3087	3088			8	8	7	1	1	1	1	1
Braking											2168	2167	1930	1941	2050					

Table 03 - SUV_1.8_E22_12V energy balance over the HWFET for power in kW

	In_Power [kW]					out_Power [kW]					loss_Power[kW]					eff_Power [%]				
HW E22 SUV	Case 0	Case 1	Case 2	Case 3	Case 4	Case 0	Case 1	Case 2	Case 3	Case 4	Case 0	Case 1	Case 2	Case 3	Case 4	Case 0	Case 1	Case 2	Case 3	Case 4
Fuel						29763	29645	29343	29343	29343										
Fuel Converter	29763	29645	29343	29343	29343	9031	9031	8904	8904	8904	20732	20614	20438	20438	20438	0.3	0.3	0.3	0.3	0.3
Clutch	8738	8738	8735	8735	8735	8733	8733	8733	8733	8733	5	5	3	3	3	1	1	1	1	1
Torque Coupling			8735	8735	8735			8735	8735	8735								1	1	1
Energy Storage			144	144	144			249	249	249			18	18	18			0.89	0.89	0.89
Energy Stored			-123	-123	-123															
Gearbox	8733	8733	8733	8733	8733	8384	8384	8383	8383	8383	349	349	349	349	349	0.96	0.96	0.96	0.96	0.96
Final Drive	8384	8384	8383	8383	8383	8384	8384	8383	8383	8383						1	1	1	1	1
Wheel/Axle	8384	8384	8383	8383	8383	8345	8345	8344	8344	8344	39	39	39	39	39	1	1	1	1	1
Aux Loads	322	318	317	317	317						322	317	316	316	316					
Aero											5015	5015	5016	5016	5016					
Rolling											2537	2537	2546	2546	2546					

Table 04 - SUV_1.8_E22_12V energy balance over the HWFET for regen in kW

	In_Regen [kW]					out_Regen [kW]					loss_Regen[kW]					eff_Regen [%]				
HW E22 SUV	Case 0	Case 1	Case 2	Case 3	Case 4	Case 0	Case 1	Case 2	Case 3	Case 4	Case 0	Case 1	Case 2	Case 3	Case 4	Case 0	Case 1	Case 2	Case 3	Case 4
Clutch	223	223	226	226	226	223	223	226	226	226						1	1	1	1	1
Torque Coupling			226	226	226			226	226	226								1	1	1
Motor/Controller			231	231	231			144	144	144			87	87	87			0.62	0.62	0.62
Gearbox	232	233	235	235	235	223	223	226	226	226			9	9	9	0.96	0.96	0.96	0.96	0.96
Final Drive	232	233	235	235	235	232	233	235	235	235						1	1	1	1	1
Wheel/Axle	594	594	594	594	594	593	593	593	593	593						1	1	1	1	1
Braking											361	360	358	358	358					

APPENDIX E – ENERGY BALANCE FOR SUV_1.8_E100_12V

The energy balance for the FTP-75 cycle with E100 for SUV_1.8_E100_12V of power and regen is shown in Tables 01 and 02, respectively. The energy balance for the HWFET cycle with the logic was presented in Tables 03 and 04.

Table 01 - SUV_1.8_E100_12V energy balance over the FTP-75 for power in kW

	In_Power [kW]					out_Power [kW]					loss_Power [kW]					eff_Power [%]				
FTP E100 SUV	Case 0	Case 1	Case 2	Case 3	Case 4	Case 0	Case 1	Case 2	Case 3	Case 4	Case 0	Case 1	Case 2	Case 3	Case 4	Case 0	Case 1	Case 2	Case 3	Case 4
Fuel						42521	38282	37059	37031	36805										
Fuel Converter	42521	38282	37059	37031	36805	9472	9472	9092	9093	9110	33049	28810	27967	27938	27695	0.22	0.25	0.25	0.25	0.25
Clutch	9009	9009	8985	8985	8986	8884	8884	8934	8934	8934	125	125	51	51	52	0.99	0.99	0.99	0.99	0.99
Torque Coupling			8985	8985	8986			8985	8985	8986								1	1	1
Energy Storage			733	729	692			573	571	540			69	69	65			0.9	0.9	0.9
Energy Stored			90	90	86			0	0	0			0	0	0			0	0	0
Gearbox	8884	8884	8934	8934	8934	8529	8529	8577	8577	8577	355	355	357	357	357	0.96	0.96	0.96	0.96	0.96
Final Drive	8529	8529	8577	8577	8577	8529	8529	8577	8577	8577						1	1	1	1	1
Wheel/Axle	8529	8529	8577	8577	8577	8457	8457	8492	8492	8492	72	72	85	85	85	0.99	0.99	0.99	0.99	0.99
Aux Loads	790	622	596	592	573						790	609	582	581	570					
Aero											2612	2612	2612	2612	2612					
Rolling											2550	2550	2552	2552	2552					

Table 02 - SUV_1.8_E100_12V energy balance over the FTP-75 for regen in kW

	In_Regen [kW]					out_Regen [kW]					loss_Regen [kW]					eff_Regen [%]				
FTP E100 SUV	Case 0	Case 1	Case 2	Case 3	Case 4	Case 0	Case 1	Case 2	Case 3	Case 4	Case 0	Case 1	Case 2	Case 3	Case 4	Case 0	Case 1	Case 2	Case 3	Case 4
Clutch	857	859	1072	1067	1016	857	859	1072	1067	1016						1	1	1	1	1
Torque Coupling			1072	1067	1016			1072	1067	1016								1	1	1
Motor/Controller			1087	1082	1030			733	729	692			354	353	339			0.67	0.67	0.67
Gearbox	893	895	1116	1111	1058	857	859	1072	1067	1016			45	44	42	0.96	0.96	0.96	0.96	0.96
Final Drive	893	895	1116	1111	1058	893	895	1116	1111	1058						1	1	1	1	1
Wheel/Axle	3188	3188	3211	3211	3211	3188	3188	3204	3204	3205			7	7	6	1	1	1	1	1
Braking											2296	2293	2088	2093	2147					

Table 03 - SUV_1.8_E100_12V energy balance over the HWFET for power in kW

	In_Power [kW]					out_Power [kW]					loss_Power [kW]					eff_Power [%]				
HW E100 SUV	Case 0	Case 1	Case 2	Case 3	Case 4	Case 0	Case 1	Case 2	Case 3	Case 4	Case 0	Case 1	Case 2	Case 3	Case 4	Case 0	Case 1	Case 2	Case 3	Case 4
Fuel						28990	28932	28662	28652	28623										
Fuel Converter	28990	28932	28662	28652	28623	8606	8606	8503	8502	8501	20384	20326	20159	20150	20121	0.3	0.3	0.3	0.3	0.3
Clutch	8313	8313	8333	8333	8333	8307	8307	8329	8329	8329	5	5	4	4	4	1	1	1	1	1
Torque Coupling			8333	8333	8333			8333	8333	8333								1	1	1
Energy Storage			160	158	152			249	249	249			19	19	18			0.89	0.89	0.89
Energy Stored			-109	-110	-116															
Gearbox	8307	8307	8329	8329	8329	7975	7975	7996	7996	7996	332	332	333	333	333	0.96	0.96	0.96	0.96	0.96
Final Drive	7975	7975	7996	7996	7996	7975	7975	7996	7996	7996						1	1	1	1	1
Wheel/Axle	7975	7975	7996	7996	7996	7939	7939	7960	7960	7960	36	36	36	36	36	1	1	1	1	1
Aux Loads	322	318	317	317	317						322	319	318	317	317					
Aero											5015	5015	5016	5016	5016					
Rolling											2537	2537	2546	2546	2546					

Table 04 - SUV_1.8_E100_12V energy balance over the HWFET for regen in kW

	In_Regen [kW]					out_Regen [kW]					loss_Regen [kW]					eff_Regen [%]				
HW E100 SUV	Case 0	Case 1	Case 2	Case 3	Case 4	Case 0	Case 1	Case 2	Case 3	Case 4	Case 0	Case 1	Case 2	Case 3	Case 4	Case 0	Case 1	Case 2	Case 3	Case 4
Clutch	239	239	250	247	239	239	239	250	247	239						1	1	1	1	1
Torque Coupling			250	247	239			250	247	239								1	1	1
Motor/Controller			253	251	242			160	158	152			94	93	90			0.63	0.63	0.63
Gearbox	248	248	260	258	249	239	239	250	247	239			10	10	10	0.96	0.96	0.96	0.96	0.96
Final Drive	248	248	260	258	249	248	248	260	258	249						1	1	1	1	1
Wheel/Axle	584	584	589	589	589	583	583	588	588	588						1	1	1	1	1
Braking											335	335	328	330	339					

ANNEX A – FTP-75 CYCLE

	0	1	2	3	4	5	6	7	8	9
0	0,0	0,0	0,0	0,0	0,0	0,0	0,0	0,0	0,0	0,0
10	0,0	0,0	0,0	0,0	0,0	0,0	0,0	0,0	0,0	0,0
20	0,0	4,8	9,5	13,8	18,5	23,0	27,2	27,8	29,1	33,3
30	34,9	36,0	36,2	35,6	34,6	33,6	32,8	31,9	27,4	24,0
40	24,0	24,5	24,9	25,7	27,5	30,7	34,0	36,5	36,9	36,5
50	36,4	34,3	30,6	27,5	25,4	25,4	28,5	31,9	34,8	37,3
60	38,9	39,6	40,1	40,2	39,6	39,4	39,8	39,9	39,8	39,6
70	39,6	40,4	41,2	41,4	40,9	40,1	40,2	40,9	41,8	41,8
80	41,4	42,0	43,0	44,3	46,0	47,2	48,0	48,4	48,9	49,4
90	49,4	49,1	48,9	48,8	48,9	49,6	48,9	48,1	47,5	48,0
100	48,8	49,4	49,7	49,9	49,7	48,9	48,0	48,1	48,6	49,4
110	50,2	51,2	51,8	52,1	51,8	51,0	46,0	40,7	35,4	30,1
120	24,8	19,5	14,2	8,9	3,5	0,0	0,0	0,0	0,0	0,0
130	0,0	0,0	0,0	0,0	0,0	0,0	0,0	0,0	0,0	0,0
140	0,0	0,0	0,0	0,0	0,0	0,0	0,0	0,0	0,0	0,0
150	0,0	0,0	0,0	0,0	0,0	0,0	0,0	0,0	0,0	0,0
160	0,0	0,0	0,0	0,0	5,3	10,6	15,9	21,2	26,6	31,9
170	35,7	39,1	41,5	42,5	41,4	40,4	39,8	40,2	40,6	40,9
180	41,5	43,8	42,6	38,6	36,5	31,2	28,5	27,7	29,1	29,9
190	32,2	35,7	39,4	43,9	49,1	53,9	58,3	60,0	63,2	65,2
200	67,8	70,0	72,6	74,0	75,3	76,4	76,4	76,1	76,0	75,6
210	75,6	75,6	75,6	75,6	76,0	76,3	77,1	78,1	79,0	79,7
220	80,5	81,4	82,1	82,9	84,0	85,6	87,1	87,9	88,4	88,5
230	88,4	87,9	87,9	88,2	88,7	89,3	89,6	90,3	90,6	91,1
240	91,2	91,2	90,9	90,9	90,9	90,9	90,9	90,9	90,8	90,3
250	89,8	88,7	87,9	87,2	86,9	86,4	86,3	86,7	86,9	87,1
260	87,1	86,6	85,9	85,3	84,7	83,8	84,3	83,7	83,5	83,2
270	82,9	83,0	83,4	83,8	84,5	85,3	86,1	86,9	88,4	89,2
280	89,5	90,1	90,1	89,8	88,8	87,7	86,3	84,5	82,9	82,9
290	82,9	82,2	80,6	80,5	80,6	80,5	79,8	79,7	79,7	79,7
300	79,0	78,2	77,4	76,0	74,2	72,4	70,5	68,6	66,8	64,9
310	62,0	59,5	56,6	54,4	52,3	50,7	49,2	49,1	48,3	46,7
320	44,3	39,9	34,6	32,3	30,7	29,8	27,4	24,9	20,1	17,4
330	12,9	7,6	2,3	0,0	0,0	0,0	0,0	0,0	0,0	0,0
340	0,0	0,0	0,0	0,0	0,0	0,0	0,0	1,6	6,9	12,2
350	17,5	22,9	27,8	32,2	36,2	38,1	40,6	42,8	45,2	48,3
360	49,6	50,9	51,7	52,8	54,1	55,5	55,7	56,2	56,0	55,5
370	55,8	57,1	57,9	57,9	57,9	57,9	57,9	57,9	58,1	58,6
380	58,7	58,6	57,9	56,5	54,9	53,9	50,5	46,7	41,4	37,0
390	32,7	28,2	23,3	19,3	14,0	8,7	3,4	0,0	0,0	0,0

400	0,0	0,0	0,0	4,2	9,5	14,8	20,1	25,4	30,7	36,0
410	40,2	41,2	44,3	46,7	48,3	48,4	48,3	47,8	47,2	46,3
420	45,1	40,2	34,9	29,6	24,3	19,0	13,7	8,4	3,1	0,0
430	0,0	0,0	0,0	0,0	0,0	0,0	0,0	0,0	0,0	0,0
440	0,0	0,0	0,0	0,0	0,0	0,0	0,0	0,0	5,3	10,6
450	15,9	21,2	26,6	31,9	37,2	42,5	44,7	46,8	50,7	53,1
460	54,1	56,0	56,5	57,3	58,1	57,9	58,1	58,3	57,9	57,5
470	57,9	57,9	57,3	57,1	57,0	56,6	56,6	56,6	56,6	56,6
480	56,6	56,3	56,5	56,6	57,1	56,6	56,3	56,3	56,3	56,0
490	55,7	55,5	53,9	51,5	48,4	45,1	41,0	36,2	31,9	26,6
500	21,2	16,6	11,6	6,4	1,6	0,0	0,0	0,0	0,0	0,0
510	0,0	1,9	5,6	8,9	10,5	13,7	15,4	16,9	19,2	22,5
520	25,7	28,5	30,6	32,3	33,8	35,4	37,0	38,3	39,4	40,1
530	40,2	40,2	40,2	40,2	40,2	40,2	41,2	41,5	41,8	41,2
540	40,6	40,2	40,2	40,2	39,3	37,2	31,9	26,6	21,2	15,9
550	10,6	5,3	0,0	0,0	0,0	0,0	0,0	0,0	0,0	0,0
560	0,0	0,0	0,0	0,0	0,0	0,0	0,0	0,0	0,0	5,3
570	10,6	15,9	20,9	23,5	25,7	27,4	27,4	27,4	28,2	28,5
580	28,5	28,2	27,4	27,2	26,7	27,4	27,5	27,4	26,7	26,6
590	26,6	26,7	27,4	28,3	29,8	30,9	32,5	33,8	34,0	34,1
600	34,8	35,4	36,0	36,2	36,2	36,2	36,5	38,1	40,4	41,8
610	42,6	43,5	42,0	36,7	31,4	26,1	20,8	15,4	10,1	4,8
620	0,0	0,0	0,0	0,0	0,0	0,0	0,0	0,0	0,0	0,0
630	0,0	0,0	0,0	0,0	0,0	0,0	0,0	0,0	0,0	0,0
640	0,0	0,0	0,0	0,0	0,0	0,0	3,2	7,2	12,6	16,4
650	20,1	22,5	24,6	28,2	31,5	33,8	35,7	37,5	39,4	40,7
660	41,2	41,8	42,0	42,2	42,2	42,5	42,6	42,6	41,8	41,0
670	38,0	34,4	29,8	26,4	23,3	18,7	14,0	9,3	5,6	3,2
680	0,0	0,0	0,0	0,0	0,0	0,0	0,0	0,0	0,0	0,0
690	0,0	0,0	0,0	0,0	2,3	5,3	7,1	10,5	14,8	18,2
700	21,7	23,5	26,4	26,9	26,6	26,6	29,3	30,9	32,3	34,6
710	36,2	36,2	35,6	36,5	37,5	37,8	36,2	34,8	33,0	29,0
720	24,1	19,3	14,5	10,0	7,2	4,8	3,4	0,8	0,8	5,1
730	10,5	15,4	20,1	22,5	25,7	29,0	31,5	34,6	37,2	39,4
740	41,0	42,6	43,6	44,4	44,9	45,5	46,0	46,0	45,5	45,4
750	45,1	44,3	43,1	41,0	37,8	34,6	30,6	26,6	24,0	20,1
760	15,1	10,0	4,8	2,4	2,4	0,8	0,0	4,8	10,1	15,4
770	20,8	25,4	28,2	29,6	31,4	33,3	35,4	37,3	40,2	42,6
780	44,3	45,1	45,5	46,5	46,5	46,5	46,3	45,9	45,5	45,5
790	45,5	45,4	44,4	44,3	44,3	44,3	44,3	44,3	44,3	44,4
800	45,1	45,9	48,3	49,9	51,5	53,1	53,1	54,1	54,7	55,2
810	55,0	54,7	54,7	54,6	54,1	53,3	53,1	52,3	51,5	51,3
820	50,9	50,7	49,2	48,3	48,1	48,1	48,1	48,1	47,6	47,5
830	47,5	47,2	46,5	45,4	44,6	43,5	41,0	38,1	35,4	33,0

840	30,9	30,9	32,3	33,6	34,4	35,4	36,4	37,3	38,6	40,2
850	41,8	42,8	42,8	43,1	43,5	43,8	44,7	45,2	46,3	46,5
860	46,7	46,8	46,7	45,2	44,3	43,5	41,5	40,2	39,4	39,9
870	40,4	41,0	41,4	42,2	43,3	44,3	44,7	45,7	46,7	47,0
880	46,8	46,7	46,5	45,9	45,2	45,1	45,1	44,4	43,8	42,8
890	43,5	44,3	44,7	45,1	44,7	45,1	45,1	45,1	44,6	44,1
900	43,3	42,8	42,6	42,6	42,6	42,3	42,2	42,2	41,7	41,2
910	41,2	41,7	41,5	41,0	39,6	37,8	35,7	34,8	34,8	34,9
920	36,4	37,7	38,6	38,9	39,3	40,1	40,4	40,6	40,7	41,0
930	40,6	40,2	40,2	40,2	39,8	39,4	39,1	39,1	39,4	40,2
940	40,2	39,6	39,6	38,8	39,4	40,4	41,2	40,4	38,6	35,4
950	32,3	27,2	21,9	16,6	11,3	6,0	0,6	0,0	0,0	0,0
960	3,2	8,5	13,8	19,2	24,5	28,2	29,9	32,2	34,0	35,4
970	37,0	39,4	42,3	44,3	45,2	45,7	45,9	45,9	45,9	44,6
980	44,3	43,8	43,1	42,6	41,8	41,4	40,6	38,6	35,4	34,6
990	34,6	35,1	36,2	37,0	36,7	36,7	37,0	36,5	36,5	36,5
1000	37,8	38,6	39,6	39,9	40,4	41,0	41,2	41,0	40,2	38,8
1010	38,1	37,3	36,9	36,2	35,4	34,8	33,0	28,2	22,9	17,5
1020	12,2	6,9	1,6	0,0	0,0	0,0	0,0	0,0	0,0	0,0
1030	0,0	0,0	0,0	0,0	0,0	0,0	0,0	0,0	0,0	0,0
1040	0,0	0,0	0,0	0,0	0,0	0,0	0,0	0,0	0,0	0,0
1050	0,0	0,0	0,0	1,9	6,4	11,7	17,1	22,4	27,4	29,8
1060	32,2	35,1	37,0	38,6	39,9	41,2	42,6	43,1	44,1	44,9
1070	45,5	45,1	44,3	43,5	43,5	42,3	39,4	36,2	34,6	33,2
1080	29,0	24,1	19,8	17,9	17,1	16,1	15,3	14,6	14,0	13,8
1090	14,2	14,5	14,0	13,8	12,9	11,3	8,0	6,8	4,2	1,6
1100	0,0	0,2	1,0	2,6	5,8	11,1	16,1	20,6	22,5	23,3
1110	25,7	29,1	32,2	33,8	34,1	34,3	34,4	34,9	36,2	37,0
1120	38,3	39,4	40,2	40,1	39,9	40,2	40,9	41,5	41,8	42,5
1130	42,8	43,3	43,5	43,5	43,5	43,3	43,1	43,1	42,6	42,5
1140	41,8	41,0	39,6	37,8	34,6	32,2	28,2	25,7	22,5	17,2
1150	11,9	6,6	1,3	0,0	0,0	0,0	0,0	0,0	0,0	0,0
1160	0,0	0,0	0,0	0,0	0,0	0,0	0,0	0,0	0,0	3,4
1170	8,7	14,0	19,3	24,6	29,9	34,0	37,0	37,8	37,0	36,2
1180	32,2	26,9	21,6	16,3	10,9	5,6	0,3	0,0	0,0	0,0
1190	0,0	0,0	0,0	0,0	0,0	0,0	0,0	0,3	2,4	5,6
1200	10,5	15,8	19,3	20,8	20,9	20,3	20,6	21,1	21,1	22,5
1210	24,9	27,4	29,9	31,7	33,8	34,6	35,1	35,1	34,6	34,1
1220	34,6	35,1	35,4	35,2	34,9	34,6	34,6	34,4	32,3	31,4
1230	30,9	31,5	31,9	32,2	31,4	28,2	24,9	20,9	16,1	12,9
1240	9,7	6,4	4,0	1,1	0,0	0,0	0,0	0,0	0,0	0,0
1250	0,0	0,0	1,6	1,6	1,6	1,6	1,6	2,6	4,8	6,4
1260	8,0	10,1	12,9	16,1	16,9	15,3	13,7	12,2	14,2	17,7
1270	22,5	27,4	31,4	33,8	35,1	35,7	37,0	38,0	38,8	39,4
1280	39,4	38,6	37,8	37,8	37,8	37,8	37,8	37,8	38,6	38,8

1290	39,4	39,8	40,2	40,9	41,2	41,4	41,8	42,2	43,5	44,7
1300	45,5	46,7	46,8	46,7	45,1	39,8	34,4	29,1	23,8	18,5
1310	13,2	7,9	2,6	0,0	0,0	0,0	0,0	0,0	0,0	0,0
1320	0,0	0,0	0,0	0,0	0,0	0,0	0,0	0,0	0,0	0,0
1330	0,0	0,0	0,0	0,0	0,0	0,0	0,0	0,0	2,4	7,7
1340	13,0	18,3	21,2	24,3	27,0	29,5	31,4	32,7	34,3	35,2
1350	35,6	36,0	35,4	34,8	34,0	33,0	32,2	31,5	29,8	28,2
1360	26,6	24,9	22,5	17,7	12,9	8,4	4,0	0,0	0,0	0,0
1370	0,0	0,0	0,0	0,0	0,0	0,0	0,0	0,0	0,0	0,0
1380	0,0	0,0	0,0	0,0	0,0	0,0	0,0	0,0	0,0	0,0
1390	0,0	0,0	0,0	0,0	0,0	0,0	0,0	0,0	0,0	0,0
1400	0,0	0,0	0,0	0,0	0,0	0,0	0,0	0,0	0,0	0,0
1410	0,0	0,0	0,0	0,0	0,0	0,0	0,0	0,0	0,0	0,0
1420	0,0	0,0	0,0	0,0	0,0	0,0	0,0	0,0	0,0	0,0
1430	0,0	0,0	0,0	0,0	0,0	0,0	0,0	0,0	0,0	0,0
1440	0,0	0,0	0,0	0,0	0,0	0,0	0,0	0,0	0,0	0,0
1450	0,0	0,0	0,0	0,0	0,0	0,0	0,0	0,0	0,0	0,0
1460	0,0	0,0	0,0	0,0	0,0	0,0	0,0	0,0	0,0	0,0
1470	0,0	0,0	0,0	0,0	0,0	0,0	0,0	0,0	0,0	0,0
1480	0,0	0,0	0,0	0,0	0,0	0,0	0,0	0,0	0,0	0,0
1490	0,0	0,0	0,0	0,0	0,0	0,0	0,0	0,0	0,0	0,0
1500	0,0	0,0	0,0	0,0	0,0	0,0	0,0	0,0	0,0	0,0
1510	0,0	0,0	0,0	0,0	0,0	0,0	0,0	0,0	0,0	0,0
1520	0,0	0,0	0,0	0,0	0,0	0,0	0,0	0,0	0,0	0,0
1530	0,0	0,0	0,0	0,0	0,0	0,0	0,0	0,0	0,0	0,0
1540	0,0	0,0	0,0	0,0	0,0	0,0	0,0	0,0	0,0	0,0
1550	0,0	0,0	0,0	0,0	0,0	0,0	0,0	0,0	0,0	0,0
1560	0,0	0,0	0,0	0,0	0,0	0,0	0,0	0,0	0,0	0,0
1570	0,0	0,0	0,0	0,0	0,0	0,0	0,0	0,0	0,0	0,0
1580	0,0	0,0	0,0	0,0	0,0	0,0	0,0	0,0	0,0	0,0
1590	0,0	0,0	0,0	0,0	0,0	0,0	0,0	0,0	0,0	0,0
1600	0,0	0,0	0,0	0,0	0,0	0,0	0,0	0,0	0,0	0,0
1610	0,0	0,0	0,0	0,0	0,0	0,0	0,0	0,0	0,0	0,0
1620	0,0	0,0	0,0	0,0	0,0	0,0	0,0	0,0	0,0	0,0
1630	0,0	0,0	0,0	0,0	0,0	0,0	0,0	0,0	0,0	0,0
1640	0,0	0,0	0,0	0,0	0,0	0,0	0,0	0,0	0,0	0,0
1650	0,0	0,0	0,0	0,0	0,0	0,0	0,0	0,0	0,0	0,0
1660	0,0	0,0	0,0	0,0	0,0	0,0	0,0	0,0	0,0	0,0
1670	0,0	0,0	0,0	0,0	0,0	0,0	0,0	0,0	0,0	0,0
1680	0,0	0,0	0,0	0,0	0,0	0,0	0,0	0,0	0,0	0,0
1690	0,0	0,0	0,0	0,0	0,0	0,0	0,0	0,0	0,0	0,0
1700	0,0	0,0	0,0	0,0	0,0	0,0	0,0	0,0	0,0	0,0
1710	0,0	0,0	0,0	0,0	0,0	0,0	0,0	0,0	0,0	0,0
1720	0,0	0,0	0,0	0,0	0,0	0,0	0,0	0,0	0,0	0,0
1730	0,0	0,0	0,0	0,0	0,0	0,0	0,0	0,0	0,0	0,0

1740	0,0	0,0	0,0	0,0	0,0	0,0	0,0	0,0	0,0	0,0
1750	0,0	0,0	0,0	0,0	0,0	0,0	0,0	0,0	0,0	0,0
1760	0,0	0,0	0,0	0,0	0,0	0,0	0,0	0,0	0,0	0,0
1770	0,0	0,0	0,0	0,0	0,0	0,0	0,0	0,0	0,0	0,0
1780	0,0	0,0	0,0	0,0	0,0	0,0	0,0	0,0	0,0	0,0
1790	0,0	0,0	0,0	0,0	0,0	0,0	0,0	0,0	0,0	0,0
1800	0,0	0,0	0,0	0,0	0,0	0,0	0,0	0,0	0,0	0,0
1810	0,0	0,0	0,0	0,0	0,0	0,0	0,0	0,0	0,0	0,0
1820	0,0	0,0	0,0	0,0	0,0	0,0	0,0	0,0	0,0	0,0
1830	0,0	0,0	0,0	0,0	0,0	0,0	0,0	0,0	0,0	0,0
1840	0,0	0,0	0,0	0,0	0,0	0,0	0,0	0,0	0,0	0,0
1850	0,0	0,0	0,0	0,0	0,0	0,0	0,0	0,0	0,0	0,0
1860	0,0	0,0	0,0	0,0	0,0	0,0	0,0	0,0	0,0	0,0
1870	0,0	0,0	0,0	0,0	0,0	0,0	0,0	0,0	0,0	0,0
1880	0,0	0,0	0,0	0,0	0,0	0,0	0,0	0,0	0,0	0,0
1890	0,0	0,0	0,0	0,0	0,0	0,0	0,0	0,0	0,0	0,0
1900	0,0	0,0	0,0	0,0	0,0	0,0	0,0	0,0	0,0	0,0
1910	0,0	0,0	0,0	0,0	0,0	0,0	0,0	0,0	0,0	0,0
1920	0,0	0,0	0,0	0,0	0,0	0,0	0,0	0,0	0,0	0,0
1930	0,0	0,0	0,0	0,0	0,0	0,0	0,0	0,0	0,0	0,0
1940	0,0	0,0	0,0	0,0	0,0	0,0	0,0	0,0	0,0	0,0
1950	0,0	0,0	0,0	0,0	0,0	0,0	0,0	0,0	0,0	0,0
1960	0,0	0,0	0,0	0,0	0,0	0,0	0,0	0,0	0,0	0,0
1970	0,0	0,0	0,0	0,0	0,0	0,0	0,0	0,0	0,0	0,0
1980	0,0	0,0	0,0	0,0	0,0	0,0	0,0	0,0	0,0	0,0
1990	0,0	0,0	0,0	4,8	9,5	13,8	18,5	23,0	27,2	27,8
2000	29,1	33,3	34,9	36,0	36,2	35,6	34,6	33,6	32,8	31,9
2010	27,4	24,0	24,0	24,5	24,9	25,7	27,5	30,7	34,0	36,5
2020	36,9	36,5	36,4	34,3	30,6	27,5	25,4	25,4	28,5	31,9
2030	34,8	37,3	38,9	39,6	40,1	40,2	39,6	39,4	39,8	39,9
2040	39,8	39,6	39,6	40,4	41,2	41,4	40,9	40,1	40,2	40,9
2050	41,8	41,8	41,4	42,0	43,0	44,3	46,0	47,2	48,0	48,4
2060	48,9	49,4	49,4	49,1	48,9	48,8	48,9	49,6	48,9	48,1
2070	47,5	48,0	48,8	49,4	49,7	49,9	49,7	48,9	48,0	48,1
2080	48,6	49,4	50,2	51,2	51,8	52,1	51,8	51,0	46,0	40,7
2090	35,4	30,1	24,8	19,5	14,2	8,9	3,5	0,0	0,0	0,0
2100	0,0	0,0	0,0	0,0	0,0	0,0	0,0	0,0	0,0	0,0
2110	0,0	0,0	0,0	0,0	0,0	0,0	0,0	0,0	0,0	0,0
2120	0,0	0,0	0,0	0,0	0,0	0,0	0,0	0,0	0,0	0,0
2130	0,0	0,0	0,0	0,0	0,0	0,0	5,3	10,6	15,9	21,2
2140	26,6	31,9	35,7	39,1	41,5	42,5	41,4	40,4	39,8	40,2
2150	40,6	40,9	41,5	43,8	42,6	38,6	36,5	31,2	28,5	27,7
2160	29,1	29,9	32,2	35,7	39,4	43,9	49,1	53,9	58,3	60,0
2170	63,2	65,2	67,8	70,0	72,6	74,0	75,3	76,4	76,4	76,1
2180	76,0	75,6	75,6	75,6	75,6	75,6	76,0	76,3	77,1	78,1

2190	79,0	79,7	80,5	81,4	82,1	82,9	84,0	85,6	87,1	87,9
2200	88,4	88,5	88,4	87,9	87,9	88,2	88,7	89,3	89,6	90,3
2210	90,6	91,1	91,2	91,2	90,9	90,9	90,9	90,9	90,9	90,9
2220	90,8	90,3	89,8	88,7	87,9	87,2	86,9	86,4	86,3	86,7
2230	86,9	87,1	87,1	86,6	85,9	85,3	84,7	83,8	84,3	83,7
2240	83,5	83,2	82,9	83,0	83,4	83,8	84,5	85,3	86,1	86,9
2250	88,4	89,2	89,5	90,1	90,1	89,8	88,8	87,7	86,3	84,5
2260	82,9	82,9	82,9	82,2	80,6	80,5	80,6	80,5	79,8	79,7
2270	79,7	79,7	79,0	78,2	77,4	76,0	74,2	72,4	70,5	68,6
2280	66,8	64,9	62,0	59,5	56,6	54,4	52,3	50,7	49,2	49,1
2290	48,3	46,7	44,3	39,9	34,6	32,3	30,7	29,8	27,4	24,9
2300	20,1	17,4	12,9	7,6	2,3	0,0	0,0	0,0	0,0	0,0
2310	0,0	0,0	0,0	0,0	0,0	0,0	0,0	0,0	0,0	1,6
2320	6,9	12,2	17,5	22,9	27,8	32,2	36,2	38,1	40,6	42,8
2330	45,2	48,3	49,6	50,9	51,7	52,8	54,1	55,5	55,7	56,2
2340	56,0	55,5	55,8	57,1	57,9	57,9	57,9	57,9	57,9	57,9
2350	58,1	58,6	58,7	58,6	57,9	56,5	54,9	53,9	50,5	46,7
2360	41,4	37,0	32,7	28,2	23,3	19,3	14,0	8,7	3,4	0,0
2370	0,0	0,0	0,0	0,0	0,0	4,2	9,5	14,8	20,1	25,4
2380	30,7	36,0	40,2	41,2	44,3	46,7	48,3	48,4	48,3	47,8
2390	47,2	46,3	45,1	40,2	34,9	29,6	24,3	19,0	13,7	8,4
2400	3,1	0,0	0,0	0,0	0,0	0,0	0,0	0,0	0,0	0,0
2410	0,0	0,0	0,0	0,0	0,0	0,0	0,0	0,0	0,0	0,0
2420	5,3	10,6	15,9	21,2	26,6	31,9	37,2	42,5	44,7	46,8
2430	50,7	53,1	54,1	56,0	56,5	57,3	58,1	57,9	58,1	58,3
2440	57,9	57,5	57,9	57,9	57,3	57,1	57,0	56,6	56,6	56,6
2450	56,6	56,6	56,6	56,3	56,5	56,6	57,1	56,6	56,3	56,3
2460	56,3	56,0	55,7	55,5	53,9	51,5	48,4	45,1	41,0	36,2
2470	31,9	26,6	21,2	16,6	11,6	6,4	1,6	0,0	0,0	0,0

ANNEX B – HWFET CYCLE

	0	1	2	3	4	5	6	7	8	9
0	0	0	0	3,2	7,9	13	18,2	23,3	27,8	31,5
10	35,1	38,6	41,5	43,6	45,1	46,7	48,3	49,4	50,7	51,8
20	52,9	53,9	54,9	55,7	56,2	56,5	57,5	57,8	57,6	56,8
30	56,2	55,5	55,7	56	56,5	57,5	58,1	58,3	58,7	59,1
40	59,4	59,5	59,5	59,5	59,5	59,5	59,5	59,7	60	60,8
50	62,1	63,2	64,4	65,5	66,6	67,9	69	70	70,8	71,3
60	71,6	72,1	72,3	72,4	72,6	73, 1	73, 5	74	74,5	74,8
70	75,3	75,5	75,6	75,8	76	76,1	76	75,8	75,6	75,5
80	75,5	75,5	75,6	75,8	75,8	76	75,8	75,6	75,5	74,8
90	74,5	74,4	74,5	74,8	75,5	75,8	76,3	76,8	77,2	77,6
100	78,1	78,5	79	79,2	79	79	78,9	78,9	79	79,2
110	79,3	79,5	79,7	79,7	79,7	79,5	79	78,7	78,2	77,9
120	77,4	76,8	76,3	76,1	76,4	76,9	77,1	77,2	77,1	77,1
130	77,1	77,2	77,2	77,2	77,1	76,1	74	69,7	66, 3	63,6
140	63,1	62,8	62,8	62,9	63,6	64,5	66	67,6	69,4	70,3
150	71	71,3	71,5	71,8	71,9	72,3	72,7	73,5	73,9	74,5
160	75,3	75,5	75,6	75,8	76,6	77,1	77,2	77,2	77,1	76,9
170	76,1	75,2	74,4	73,9	73,5	73,2	73,1	72,9	72,4	70,8
180	69,4	67,9	66,8	66,8	67,8	69	70	70,7	70,2	69,7
190	69,2	69,4	69,8	70,7	71,3	71,8	72,3	72,1	71,5	70,7
200	69,8	69,5	69,5	69,4	69,2	69,2	69,4	69,8	70,7	70,8
210	70	68,6	66,8	65,5	64,4	64,4	64,9	66	67,6	68,7
220	69,4	69,5	69,8	70,7	71,3	71,9	72,6	73,1	73,7	74,8
230	75,5	76	76,3	76,1	76,1	76	76	76	75,8	75,6
240	75,6	75,5	75,3	75,5	75,6	76	76,4	77,1	77,2	77,2
250	77,2	77,2	77,2	77,4	77,6	77,6	77,4	78,2	78,7	79
260	79	79	79	79	78,9	78,7	77,6	76,8	76,4	76
270	75,2	74,4	74	73,7	73,4	73,1	72,7	72,4	71,9	71,6
280	71,7	70	68,9	67,6	64,5	62,1	60,4	57,6	55,8	54,7
290	53,6	52,3	51	49,2	47,6	46,3	45,7	46	47,5	50,5
300	53,8	57,3	60,4	62,9	64,7	66,1	67,3	68,2	68,9	69,7
310	70,5	71,3	71,9	72,4	72,7	73,1	73,2	73,7	74	74,2
320	74, 3	75,3	75,8	76,8	77,7	78,9	80	81	82,1	83,2
330	84,3	85,5	86,6	87,7	88,8	89,8	90,8	91,6	91,7	91,9
340	92,2	92,7	93	93,3	93,5	94	95,5	94,6	94,8	95
350	95	94,8	94,6	94,3	94	93,7	93,5	93,3	93,2	92,7
360	92,4	92,1	91,9	91,7	91,7	91,6	91,6	91,6	91,7	91,7
370	91,7	91,7	91,7	91,7	91,7	91,7	91,7	91,6	91,4	90,9
380	90,4	90,1	90,1	90,1	90,3	90,8	91,2	91,6	91,6	92,2
390	92,4	92,4	92,1	91,7	91,6	91,1	90,6	90,3	90,8	91,2

400	91,9	92,5	93	93,3	93,3	93,3	93,3	93,3	93,3	93,2
410	93	92,9	92,9	93	93,2	93,3	93,5	94	94,8	95,1
420	95,6	96,2	96,4	96,4	96,2	95,9	95,6	95,3	95,1	95
430	94,8	94,5	94,3	94,1	94	94	93,8	93,7	93,5	93,3
440	93,2	93,2	93,2	93, 2	93,2	93,3	93,5	93,5	93,7	93,7
450	93,7	93,5	93,3	93,3	93,3	93,3	93,3	93,3	93,2	93,2
460	93,3	93,5	93,5	93,7	93,8	93,8	93,8	93,7	93,5	93,3
470	93	92,5	91,9	91,7	91,1	90,3	90,1	89,8	89,3	88,8
480	88,7	88,5	88,4	88,4	88,4	88,4	88,4	88,4	88,5	88,5
490	88,5	88,5	88,5	88,5	88,7	88,7	88,5	88,4	88,4	88,2
500	88	87,9	87,5	87,4	87,4	87,2	87,1	87,1	87,1	86,9
510	86,9	86,9	86,9	86,9	86,9	86,9	86,9	87,1	87,2	87,7
520	88,2	88,4	88,5	88,7	88,8	88,8	89	89,2	89,3	89,5
530	89,6	89,8	90	90,1	90,1	90,1	90,1	90,1	9,01	90,1
540	90,1	90,1	90,1	90,1	90,1	90,1	90,1	90	90	90
550	89,8	89,5	89,2	88,8	88,7	88,5	88,4	87,9	87,5	87,2
560	87,1	86,6	85,9	85,8	85,5	85,1	84,4	84,3	84	83,8
570	83,7	83,7	83,7	83,7	83,8	83,7	83,7	83,5	83	82,7
580	82,2	81,6	81	80,1	79,3	78,4	77,6	77,4	77,2	77,2
590	77,4	77,9	78,7	78,9	79	79	78,9	78,9	78,7	78,2
600	77,7	77,2	77,1	76,9	76,8	77,1	77,7	78,9	79	78,9
610	78,7	77,2	75,8	74,4	74,2	74,2	74,4	75,5	76,9	78,9
620	80	81,4	82,9	84	84,8	85,3	86,3	86,9	87,1	87,5
630	88	88,7	89,2	89,2	88,5	87,7	86,3	84,5	80,8	77,6
640	74,8	74,4	74	74	74,5	75,3	76,4	77,6	78,5	79,7
650	80,8	81,6	82,2	83,2	84	84,5	83,8	83	82,2	82,1
660	82,1	82,2	82,7	83,2	83,7	84	84,5	85	84,8	84,7
670	84,2	84,2	84,3	84,5	84,8	84,8	84,3	83,8	83,2	82,2
680	81,3	80,6	80,1	80	79,8	79,7	79,7	80	80,5	80,8
690	81,4	82,2	83	83,5	83,7	83,8	84,3	85,1	85,8	86,4
700	87,2	87,7	88,2	88,5	89,3	90	90,3	90,6	90,8	90,9
710	91,2	91,6	91,7	92,2	92,9	93,7	94,6	95,1	95,3	95,1
720	94,6	94,1	93,5	92,9	92,2	91,9	91,4	90,9	90,4	89,3
730	87,9	87,1	86,4	85,6	85,1	84,5	83,7	82,6	81,3	79,7
740	78,1	76,6	75,3	73,4	71,1	68,4	63,1	57,8	52,5	47,2
750	43,1	39,4	34,6	31,4	28	24,3	20	15,6	11,3	8
760	5,3	3,2	1,1	0	0	0	-	-	-	-

ANNEX C – SP CYCLE

	1	2	3	4	5	6	7	8	9	10
0	0	0	0	0	0	0	0	0	0	0
10	0	0	0	0	0	0	0	0	0	0
20	0	0	0	0	2	4	5,5	7	6	4,75
30	8	13	20,5	25	29	31	29	24	24	24,75
40	26	26,25	26,5	27,25	29,75	31	32	33	34,5	36
50	38	40	42	42,5	43	43,25	43	43,75	45	45
60	45	46	46	46	46	44	42	42	42	43
70	43	44	45,5	49	53,25	57	61	62	62	62
80	58	56	55,25	54	52	50	48	47	45,5	45
90	43	38	35	35	35	35	36	38	40	43
100	44	46	46	47	48	50	51	51,25	51	50
110	50	51	54	56	56	55,25	54,5	51	48	47
120	48	48	47	48	49	50	49	49,25	50	50
130	49,75	49	49	48,75	45,25	42,5	42	42	43	45
140	47	49	51,25	51	50	50,5	51	50,75	50	49
150	49,5	49,75	49	49	47,75	47	45	45	45	46,25
160	48	49	51	53	53	53	52,75	53	54	55
170	57	57	56	55	54	54	53	52	51	51
180	49	47,25	46	46,5	48	48	47,75	47	47	47,5
190	49	50	49	46	44	42,25	42,25	43	44	46
200	48	50	51	51	48	43	41,25	42	44	46
210	48,5	49	46	42	40	37	36	35,75	37	38
220	37	34	31,25	29	28	29,25	27	26	28	30
230	28,5	25	20,75	16,75	13	6	0	0	0	0
240	0	0	0	0	0	0	0	0	0	1
250	10	17	21,25	23	27	28	26	24,25	22,75	20
260	19	23	25	29	30	28,75	26,5	23	21	16
270	13,25	12	11	12	15	19	22	19	14	11,5
280	10	9	7	6	4	0	0	0	5	11,75
290	15	9	4	4	7	8	14	20	22	27
300	29,25	28	27	28	27	26	26,5	27	24,75	23
310	22	20	19	12	5	0	0	0	0	0
320	0	0	0	0	0	0	0	0	0	0
330	0	0	0	0	0	0	0	0	0	0
340	0	0	0	0	0	0	0	0	0	0
350	0	0	0	0	0	0	0	0	0	0
360	0	0	0	0	0	0	0	0	0	0
370	0	0	0	0	0	0	0	0	0	0
380	4	12,75	19	23	25	29	34	37	38	40
390	42	46	46,75	46	44	45	46,5	46	48	48,25

400	46	49	54	59	63,75	69	66	58	47	37
410	34	32	29,25	24	20	18,75	13	9	7	7
420	11,75	18	21	25	21	16	12,75	11	10,5	11,75
430	16,25	22	28	30,25	30	31,5	34	37	39,75	43,25
440	44	44	45	43	42,25	42	41	40	39	38
450	39	39	39	40	38	35	34	35	36	36
460	36	33,75	32,5	33	31	25,75	21	16	4,75	0
470	0	0	0	0	0	0	0	0	0	0
480	0	0	0	0	0	0	0	0	0	0
490	0	0	0	0	0	0	0	0	0	0
500	0	0	0	0	0	0	0	0	0	0
510	0	0	0	0	0	2	4	12	18	20
520	24	28,75	32,75	36	37	37,75	39	39	38,25	37
530	36	35	37	40	42	43,5	45	46	46	46
540	47	47	47	48	49	50	48	46	45	45
550	46	45	44	40	37	33	25	17	13	9,5
560	6	4	3,5	2,5	1	0	0	0	0	0
570	0	0	0	0	0	0	0	0	0	0
580	0	0	0	0	0	0	0	0	0	0
590	0	0	0	0	0	0	0	5	10	16
600	21	21	26	30	30	30	30	31	32	32
610	32	32	32	33	36	38	40	42	41	41
620	41	40	39	38	37	36	34,75	34	36	36
630	35	33	25	16	12	10	8,25	1	0	0
640	0	0	0	0	0	0	0	0	0	0
650	0	0	0	0	0	0	0	0	0	0
660	0	0	0	0	0	0	0	0	0	0
670	0	0	0	0	0	0	0	0	0	0
680	0	10	17	18,5	18,75	21	22	26	31	35
690	35,5	37,25	35,75	30,75	29	25,25	22,75	23	25	26
700	28	25	22	20	19	21	24	23	23	22
710	21	21	23	26	26	27	27	25	24	23
720	19	11	3	0	0	0	0	0	0	0
730	0	0	0	0	0	0	0	0	0	0
740	0	0	0	0	0	0	0	0	0	0
750	2,75	4	7	10	12,75	17	20	24	28,5	35
760	37	38	40	42	43	42,5	41	40,25	39,25	38
770	39	39	40	39	39	39	39	40	40,25	42
780	44	46	46	45	45	46	45	46	45	44,75
790	42,25	40	40	39	37	34	29	25	22	15
800	11	5,25	1	0	0	0	0	0	0	0,5
810	2	3	4	4	4	4	5	4	5,25	5
820	3	1	1,25	3	10	11	11	11	15	19

830	21	23	21	21	23	25,75	28	28,5	29	31
840	34,25	35	33,75	33	33	34	35,5	36	36	36
850	36	35	35	34	36,5	35	31,5	30	28	25
860	23	22	21	20	18	16	14	7	0	0
870	0	0	0	0	0	0	0	0	0	0
880	0	0	0	0	0	0	0	0	0	0
890	0	0	0	0	0	0	0	0	0	0
900	0	0	0	0	0	0	0	0	0	8,75
910	15	16	19	18,75	18	18,25	22	24,5	25	25
920	27	31	32	34,5	34	34	33	34	35	36
930	37	37	37	37	37	38	39	39,25	39	41
940	42	42	41,5	43	44	44	44	42	39	38
950	39	40	40	39	38	38	37	36,25	35,25	29
960	27	29	32	36	40	44	44	39,25	42	46
970	43	37	30	23	20,5	18	13	5,5	0	0
980	0	0	0	0	0	0	0	0	0	0
990	0	0	0	0	0	0	0	0	0	0
1000	0	0	0	0	0	0	0,6875	11	17,25	20
1010	23	29	32	33	35	36	37	37	38	39
1020	39	39	40	39,5	39	40	40	41	43	44,5
1030	45	44	45	46	47	47,75	49	46	39	33
1040	26	16	9	1,75	0	0	0	0	0	0
1050	0	0	0	0	0	0	0	0	0	0
1060	0	0	0	0	0	0	0	0	0	0
1070	0	0	0	0	0	0	0	0	0	0
1080	0	0	0	0	0	0	0	0	0	0
1090	0	0	0	0	0	0	0	0	0	0
1100	0	0	0	0	7	15	17,25	18,25	21	24
1110	25	22	24	29	31	34	33	32,5	34	36
1120	36	36	38	39	40,5	42	40	37,75	37	37,25
1130	36	34	35	35	37	37	36,5	37,5	40	41
1140	41	41	41	44	44	40	38	37	37,25	36
1150	37,25	38	39	41	43,75	45	45	46,5	47	47
1160	46,5	46	45,75	46	46	45	44	44	44	44
1170	43,75	43	44	44	45	45	45	45	46,75	48
1180	47	46	45,5	45	45	45	45	45,5	45	46
1190	47	47	47	47	46,25	46	45	44	42	41
1200	40	40	40	40	39,75	41	42	42,5	42	40
1210	39	40	39,25	38	38	37	36	35	34	34
1220	35	34	30	26,25	24	21,25	17	13	7	5,25
1230	3	0	0	0	0	0	0	0	0	0
1240	0	0	0	0	0	0	0	7	14	19
1250	21	26	30	33	32	31	31	29,25	29	34

1260	37	39	41,75	41	40	38,75	38	37	35	34,25
1270	30,5	25	22	22	22	21	22,25	20	15	15
1280	18	22	22	23	25	30,5	31	32	31	30
1290	28	25	24	26	27	30	33	35	35	35
1300	32,25	30	31	32	32,75	34	36	36	36	35
1310	35	34	33,75	31	24	20	18	18	18	21
1320	26,5	33	35,5	38	41,25	43	40,75	38	35	34,25
1330	35	38	41	44,75	44,25	43	42	40,75	40	39
1340	37,5	36,25	36	38	41	43	44	41	39	37
1350	35	32,75	32	35	36	35	33	31	32	34
1360	36	35	29	26	27	29	30	31	31	30
1370	33	36,25	40	44	45	43	41	39	37	36
1380	37	36	34	34	33	34	37	38	39	40
1390	39	37,5	37	37	33	30	29	28,25	28,75	30
1400	31,5	34	34	33	34,25	36	38	40	42	43
1410	42	44	48	48	49	45,75	40	31	25,5	21
1420	19	18	16	14,25	12	15	19	21	21,25	22
1430	24	27	30,25	34	36,5	39	40	39	38,5	37
1440	35	35	36	36	37	38	39	37,25	37	36,75
1450	36	34	30,25	29,25	29	30,75	33	35	36,75	38
1460	37,75	36,75	35	32	29,25	28,25	28	29,25	29	28
1470	29	28	29	30	31	30	28	26	25	24
1480	23	22	15	6,5	0	0	0	0	0	0
1490	0	0	0	0	0	0	0	0	0	0
1500	0	0	0	0	0	0	0	0	0	0
1510	0	0	0	0	0	0	0	0	0	0
1520	0	0	4	13	18	18	17,75	17,75	16	13
1530	13,25	16,25	21	23	22,5	24	23	19	15	13
1540	11	9	8	13	17	18	18	17	15	17
1550	20	21,75	18,25	17	17	17	20	22	20,25	21
1560	24,75	24	25	28	29,25	29	27	27	29,25	32
1570	36	39	39	39,75	41	42	40,75	40	39	38
1580	35	32	28	25	21	13,5	12	11	10	5
1590	3	0	0	0	0	0	0	0	0	5,5
1600	14	17	10	8,75	11	10	8	9	12,25	19
1610	19	20	23	25	28,25	30	30,75	32	32	31
1620	30	29	28	27	22,5	19,75	17	13	10,75	9,75
1630	9	7	3	0	0	0	0	0	0	0
1640	0	0	0	0	0	0	0	0	0	0
1650	0	0	0	0	0	0	0	0	0	0
1660	0	0	0	0	0	0	0	0	0	0
1670	0	0	0	0	0	0	0	0	0	0
1680	0	0	0	0	1,25	2	2	6	12,5	15

1690	16	19	22	25	27,5	30,75	31,25	32	33	34
1700	35	38	40	43	44	43	42	41	41	40,75
1710	41	41	41	42	40,75	39,25	38	36	35	34
1720	35	37	38	36,5	35	35	34,75	34,5	34	32
1730	31	32	33	33,75	34	34	35	36	36	36
1740	37,25	37	37	38	38	38	39	38,5	39	31
1750	24,5	17	9	2	0	0	0	0	0	0
1760	0	0	0	0	0	0	0	0	0	0
1770	0	0	0	0	0	0	0	0	0	0
1780	0	0	0	0	0	0	2	3	7	12,25
1790	14	13	13	14	15	17,75	21	21	23	22
1800	20	14	12	10,5	11	11	11	11	12	10
1810	6	3	0	0	0	0	0	0	0	0
1820	0	0	0	0	0	0	0	0	0	0
1830	0	0	0	0	0	0	0	0	0	0
1840	0	0	0	0	0	0	0	0	0	0
1850	0	0	0	0	0	0	0	0	0	0
1860	0	0	0	0	0	0	0	0	0	0
1870	0	0	0	0	0	0	0	0	0	0
1880	0	0	0	0	0	0	0	0	0	0
1890	0	0	0	0	0	0	0	0	0	1
1900	9	14	19	20	22	26,25	28	26	24	21
1910	19	18	16	12	7	4	4	7,25	11	13
1920	12	10	9	8,25	7	6	4	3	2	3
1930	1	0	0	0	0	0	0	0	0	0
1940	0	0	0	0	0	0	0	0	0	0
1950	0	0	0	0	0	0	0	0	0	0
1960	0	0	0	0	0	0	0	0	0	0
1970	0	0	0	0	0	0	0	0	0	0
1980	0	0	0	0	0	0	0	0	0	0
1990	0	0	0	0	0	0	0	0	0	0
2000	0	0	0	0	0	0	0	0	0	0
2010	0	0	0	0	0	0	0	0	0	2
2020	2	3	8	12	14	14	16	16	16	17
2030	18	19	18,75	17	14	11	9	9,25	8	6
2040	5	4,25	3	3	2	0,9375	0	0	0	0
2050	0	0	0	0	0	0	0	0	0	0
2060	0	0	0	0	0	0	0	0	0	0
2070	0	0	0	0	0	0	0,625	4	5	5
2080	4	1,75	0	0	0	0	0	0	0	0
2090	0	0	0	0	0	0	0	0	0	0
2100	0	0	0	0	0	0	0	0	0	0
2110	0	0	0	0	0	0	0	0	0	0

2120	0	0	0	0	0	0	0	0	0	0
2130	0	0	0	0	0	0	0	0	0	0
2140	0	0	0	0	0	2	2	4	3	7
2150	5	4	7	11	14	18	18	20	22	26
2160	28	24	19	13	11	15	18,75	20,25	21	23
2170	25	26	27	27,75	28	27	26	26	27	30
2180	31	33	35	36	38	39	39	38	39	40
2190	41	40,5	41	42	42	42	42	43	41	35
2200	30	25	21	14	7	2	0	0	0	0
2210	0	0	0	0	0	0	0	0	0	0
2220	0	0	0	0	0	0	0	0	0	0
2230	0	0	0	0	0	0	0	0	0	0
2240	0	0	0	0	0	0	0	0	0	0
2250	0	0	0	0	0	0	0	0	0	0
2260	0	0	0	4	10	17	17	19	22	25
2270	28	29	29	27,75	26	26,5	27	25	21	19
2280	17	14	13	12	13	10,5	9	9	12	15
2290	17	17,75	22	28	33	33	35,25	35	34,5	33
2300	33	33	33,5	32	32	34	35	35,75	35	34
2310	35	33,75	34	36	37	37	36	34,25	34	35
2320	36,5	39	41	40	38	37	35	33	32	33
2330	35	35	34,75	34	35	31	23,25	20	15	7
2340	1	0	0	0	0	0	0	0	0	0
2350	0	0	0	0	0	0	0	0	0	0
2360	0	0	0	0	0	0	0	0	0	0
2370	0	0	0	0	0	0	0	0	0	0
2380	0	0	0	0	2	7	7	7	6	2,5
2390	0	0	0	0	0	0	0	0	0	0
2400	0	0	0	0	0	0	0	0	7,25	12
2410	17	17,25	19	22	26	29	31,75	33	33,75	33
2420	34	35	37	40	41	41	42	43	43,75	43
2430	41	37	31	25	20	15	10	3	0	0
2440	0	0	0	1	8	14,5	18	18,5	22	23
2450	25	29	29,5	30	31	36	36	35	35,75	37
2460	38	38	37,75	36	32	28	26	25	25	27
2470	26,5	20	15	9	2	0	0	0	0	0
2480	0	0	0	0	0	0	0	0	0	0
2490	0	0	0	0	0	0	0	0	0	0
2500	0	0	0	0	0	0	0	0	0	0
2510	0	0	0	0	0	0	0	0	0	0
2520	0	0	0	0	0	0	0	0	0	5,5
2530	13	17	17	19	22	25	26	25	22	17
2540	13	10,5	10	4	0,5625	0	0	0	6	9

2550	11	16	17	17	14	12	12	14	17	20,5
2560	23	22	20	19	18	20	21	20	19	19
2570	20	21	21,75	23	24	23	24,5	25,75	25	23
2580	21	19	19	21	20,75	19	18	18	18	17
2590	16,25	17	20	22	25	28	29	27,75	27	27
2600	30	32	27,5	27	28	28,75	30,25	32	33	32
2610	35	34	34	33	31,25	28,5	25,5	21	18	18
2620	20	21	20,25	18	20	20	22	21	22	26
2630	25	27	26,75	29	29	27,25	25,75	17	5	0
2640	0	0	0	3	7,5	6	5,25	8	8	1
2650	0	0	0	0	0	0	2	6,25	6	4
2660	2	2	7	12	10	7,25	9,75	12	17	24
2670	31	37	41	44,75	47	48	49	50	50	49
2680	45	33	22,5	12,25	3	0	0	0	0,875	2
2690	7	6	7	3,5	1	3	0	0	0	0
2700	0,4375	4,25	8	4	1	0,6875	0	2,5	7	5
2710	2,5	2	0,6875	0	1,5	0	0	0,4375	4,5	12
2720	17	22	22	25	27,75	31	32	31	30	29
2730	28	27	26	23	19,5	19	19	19,25	18,75	18,5
2740	19	17	14,5	11	11	12	10	11	8	5
2750	4,75	7	4	6	3	6	7	0,6875	0	0
2760	0	0	0	0	0	0	0	0	0	0
2770	0	0	0	0	0	0	0	0	0	0
2780	6	7	5	3	0	3	9	12	12	9
2790	7	5	4	2,75	0	0	0	0,5625	0	0
2800	0	0	0	0,75	5,25	5,5	5	2	0	0
2810	0	0	0	0	0	0	0	0	0	0
2820	0	0	0	0	0	0	0	0	0	0
2830	0	0	0	0	0	0	0	0	0	0
2840	0	0	0	0	0	0	0	0	0	0
2850	0	0	0	0	0	0	0	0	0	0
2860	0	0	0	0	0	2	2	0	0	1
2870	2	0,5	4	5	5,5	8	11	11,75	12	13
2880	15	19	18	21	23	23	20	19	19	23
2890	30	31,5	32,75	31	25	21	20	19,25	18,75	18
2900	15	15	15	13	13,5	13	11,25	11	12,5	13
2910	12	12	13	13	12	11	9	7,25	2	0
2920	0	0	0	0	0	0	6,25	12	19	21
2930	22	23	21	17	14	8	2,5	1	4	3
2940	6	6,75	9	11	14,5	15	17	21	25	31
2950	32,25	34,25	34,75	34	32	28	23	20	18,5	17,5
2960	10	2	0	0	0	0	0	0	0	0
2970	0	0	0	0	0	0	0	0	0	0

2980	0	0	0	0	0	4	9	11,75	12	15
2990	18	21	24	23,75	22	19	14	12	11	13
3000	15	18	20	22	21	15	13	10	8	6,5
3010	5,75	5	3,25	0,75	0	0	0	0	0	0
3020	0	0	0	0	0	0	0	0	0	0
3030	0	0	0	0	0	0	0	0	0	0
3040	0	0	0	0	0	0	0	0	0	0
3050	0	0	0	0	0	0	0	0	0	0
3060	0	0	0	0	0	0	0	0	0	0
3070	0	0	0	0	0	0	0	0	0	0
3080	0	0	0	0	0	0	0	0	0	0
3090	0	0	0	0	0	0	0	0	0	0
3100	0	0	0	0	0	0	0	3	8	16
3110	17	19	22	25	26	29	31	33	31	29
3120	27	23,75	23	25,25	27	26,75	29,75	34	35	35
3130	35	37	37	37,5	37	37	37	38	37	34
3140	31	29	28	26	24	22	22	25,25	28	26
3150	23	20	21	25	25	24,25	26	30	32	34
3160	33	34	34	32	29	29	30	31,25	32	34
3170	36	33	27	21	14,5	13	12,25	13	17	21,5
3180	26	28	30	29,25	29	29	30,75	33	34	35
3190	35,75	36	36	36	37	37	36	34,75	34	34
3200	36	37	38	37	37	36	36	35	35	35,25
3210	36	36	35	34	33	34,5	36	38	38	35
3220	33	32	30	24	19	14,25	14	18	23	29
3230	33	34	34,25	34	33	31	26,25	25	24	25
3240	25	25	26,25	27	28,5	29	29	26	23	21
3250	18	14,75	16	18	18	17	19	20	14	0

ANNEX D – DRIVE CYCLE MODEL

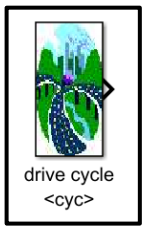

Drive cycle <cyc>

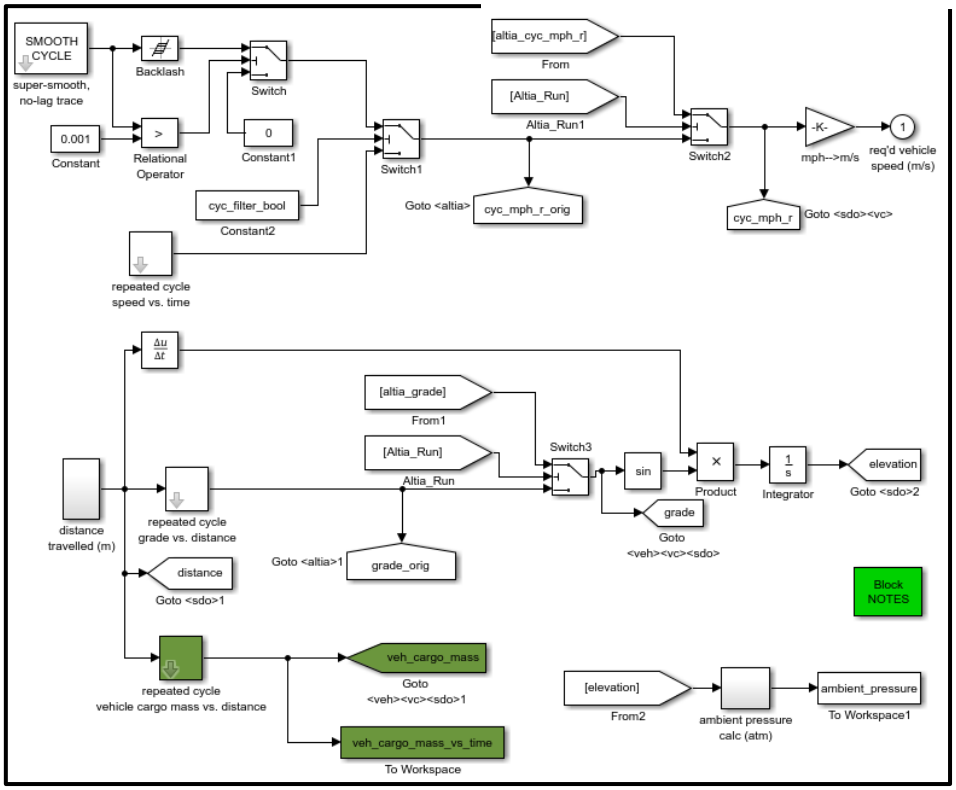

Distance travelled (m)

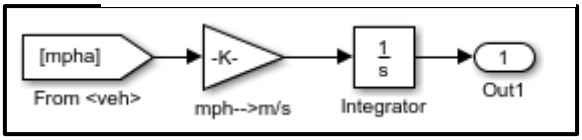

Ambient pressure Cal (atm)

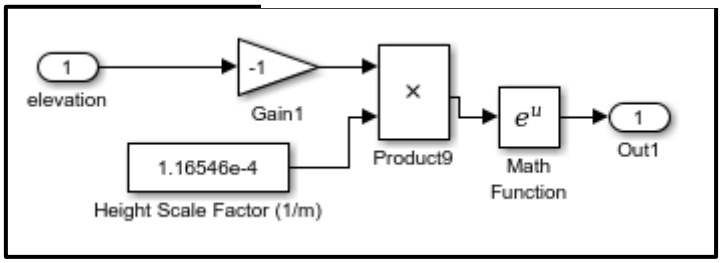

ANNEX E – VEHICLE CYCLE MODEL

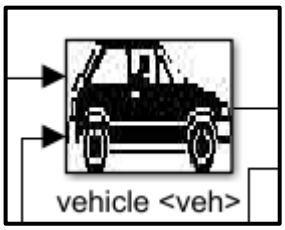

VEHICLE <veh>

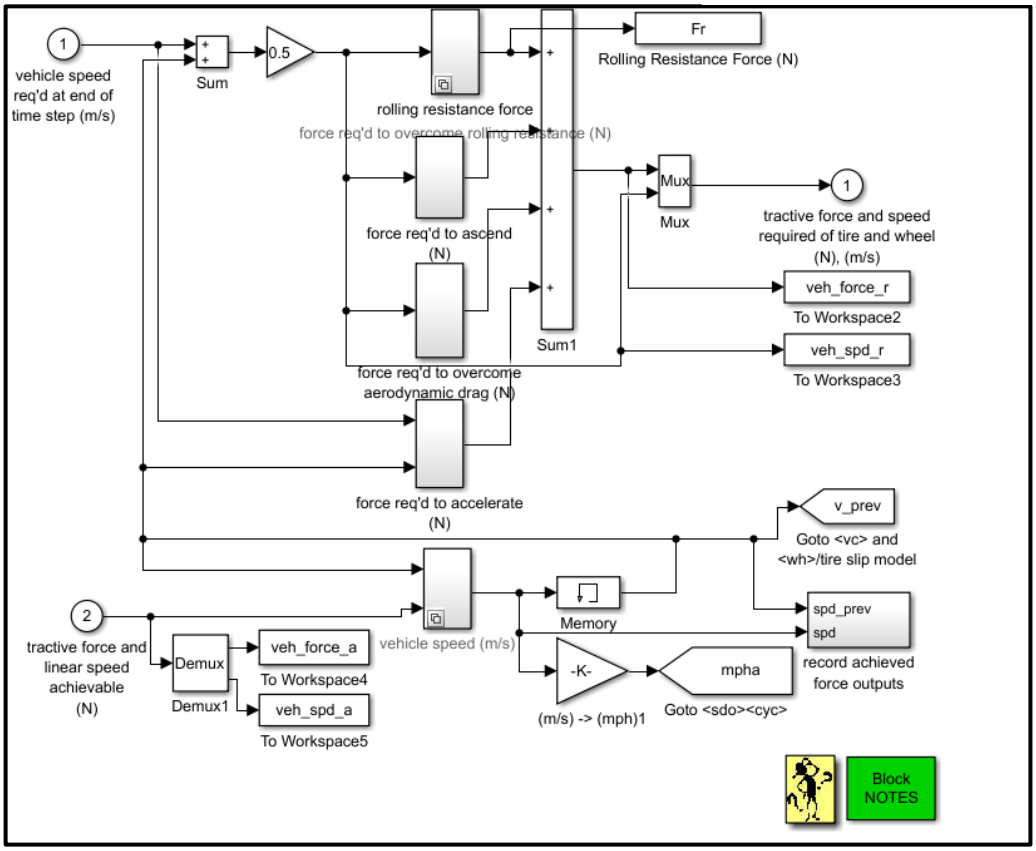

rolling resistance force

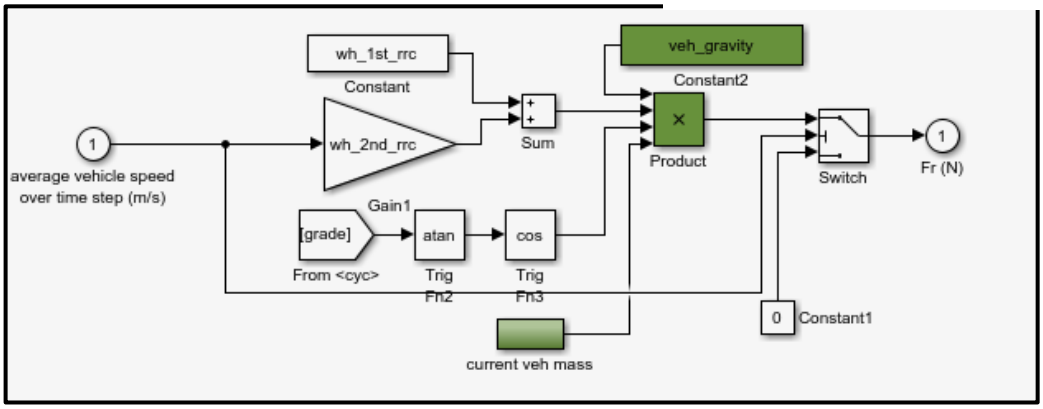

Force req d to ascend (N)

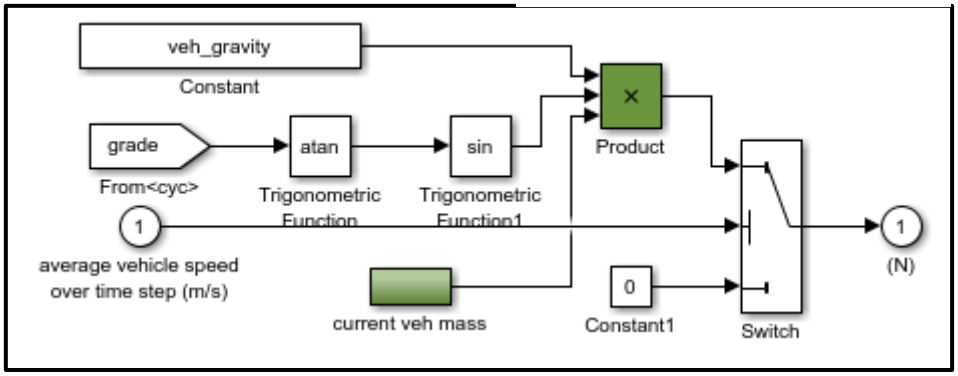

force req'd to overcome aerodynamic drag (N)

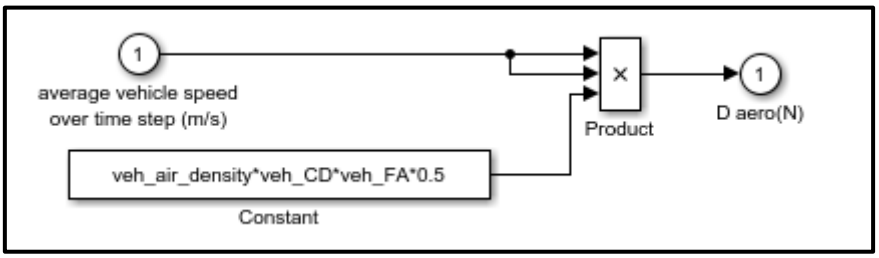

force req'd to accelerate (N)

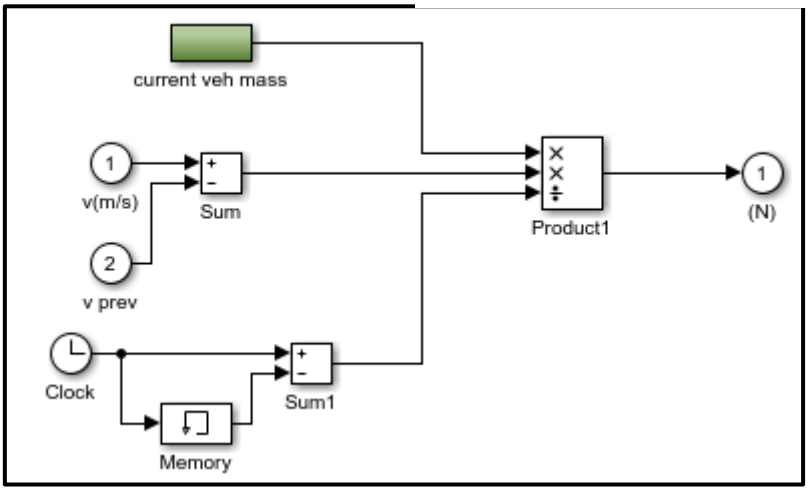

current veh mass

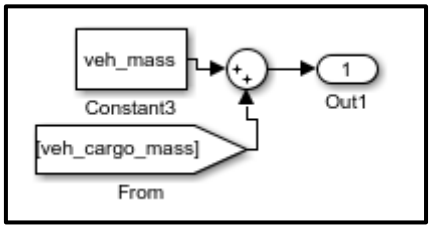

record achieved force outputs

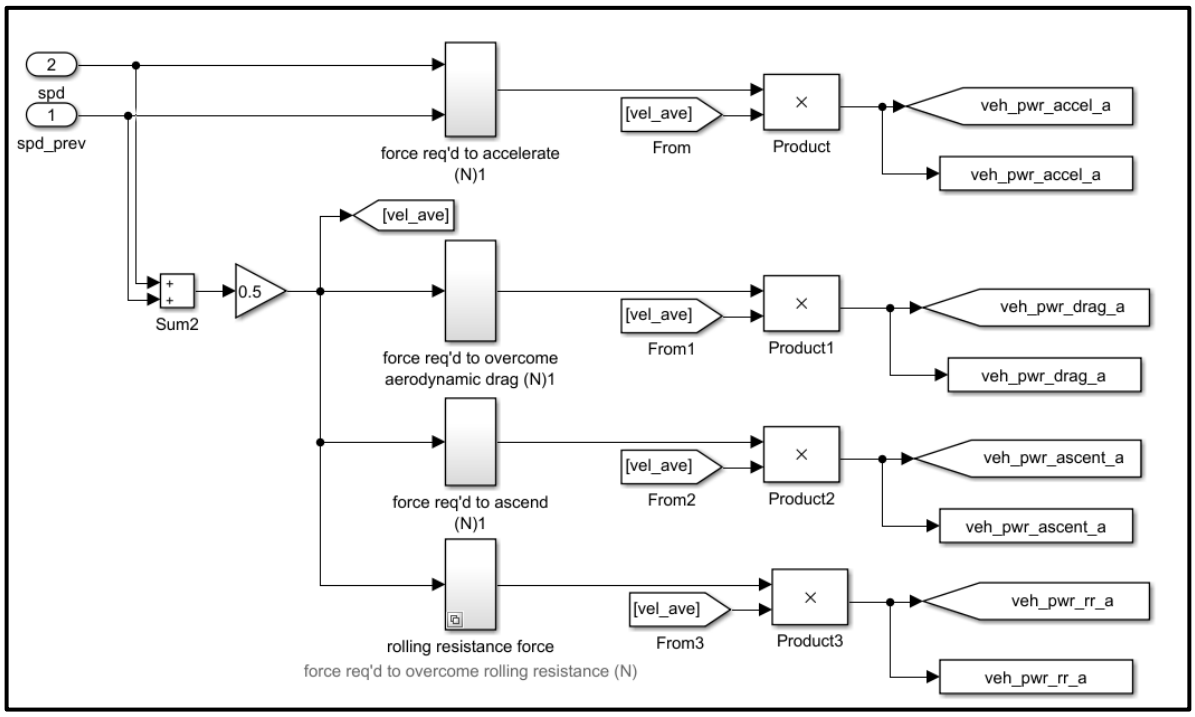

Vehicle speed (m/s)

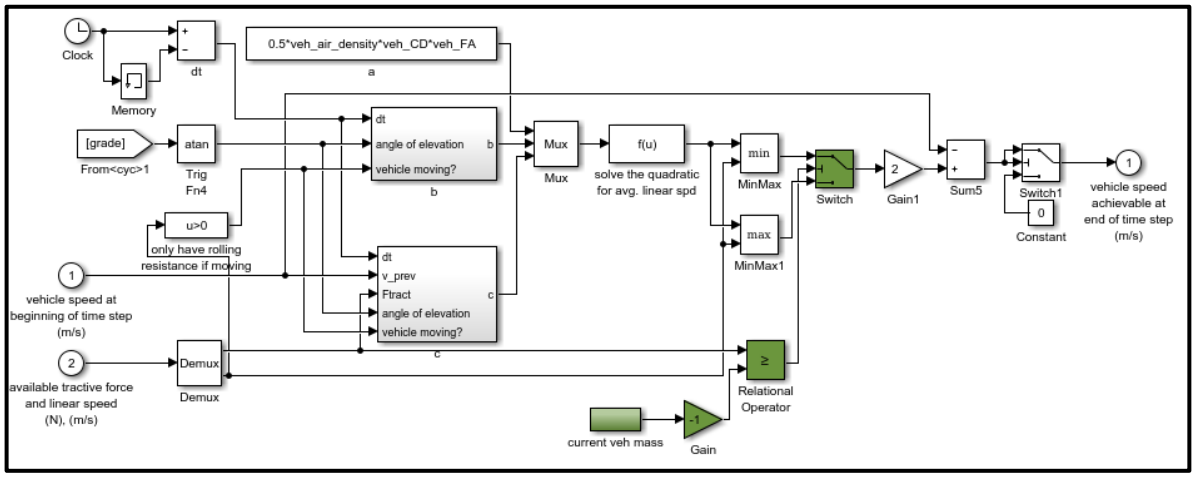

ANNEX F– WHEEL AND AXLE FORM/REAR MODEL

Wheel and axle front/rear

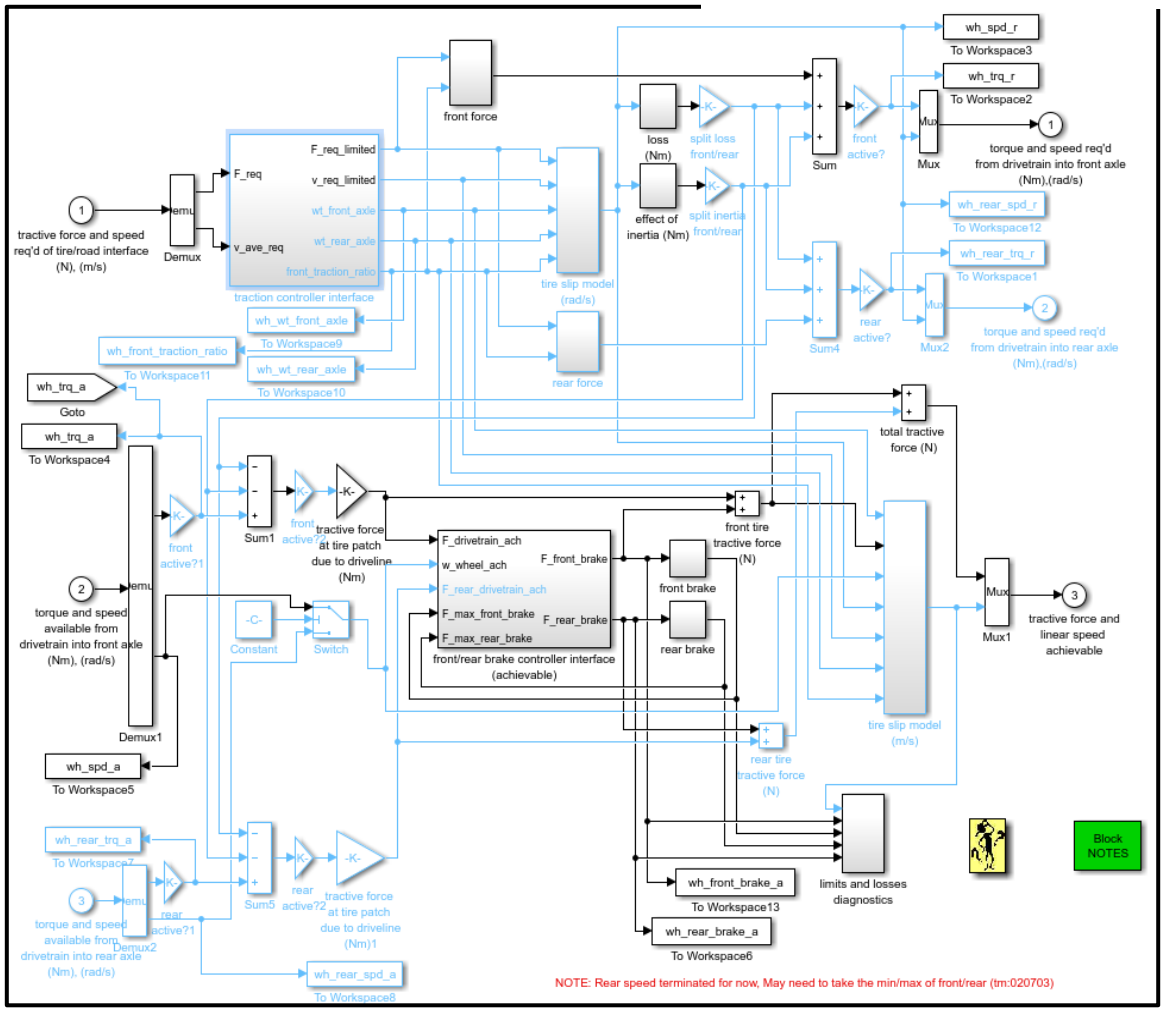

Loss (Nm)

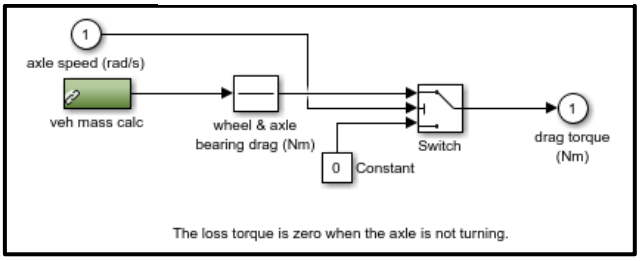

Effet of inertia (Nm)

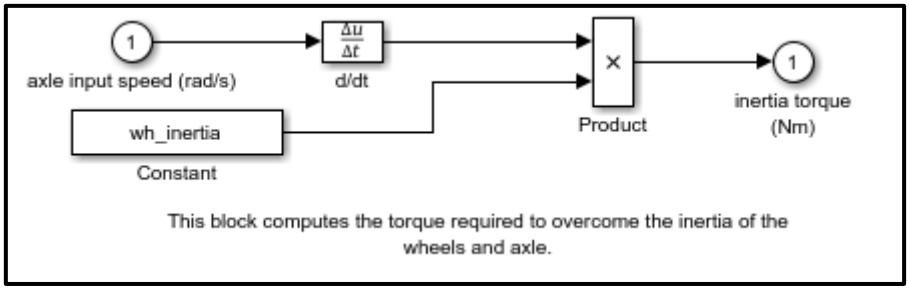

Tire slip model (rad/s)

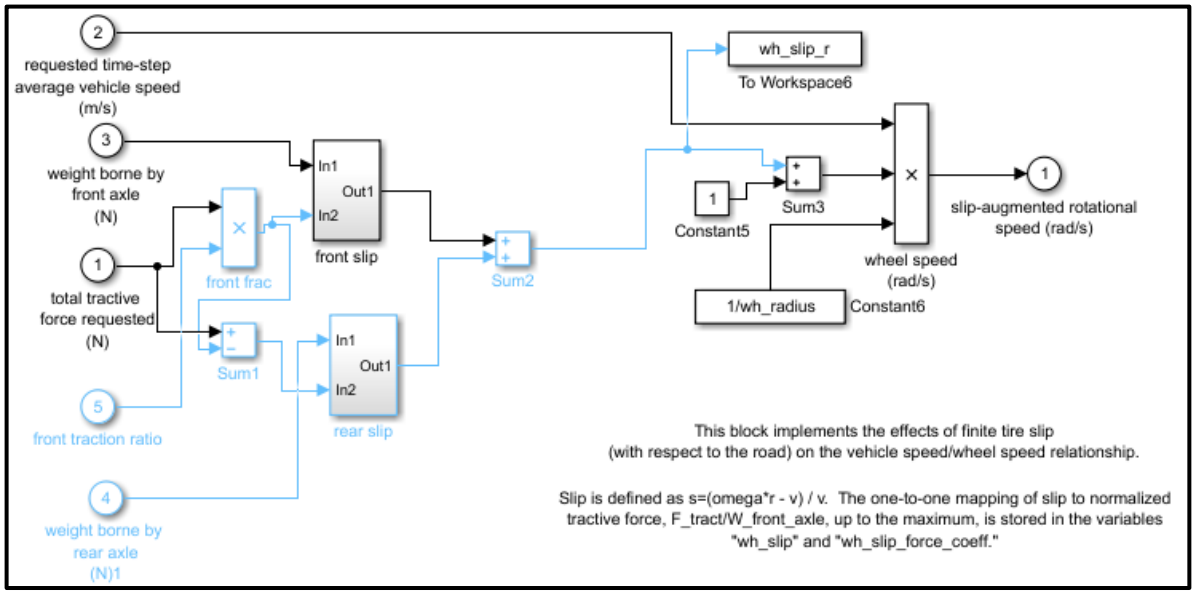

Rear force

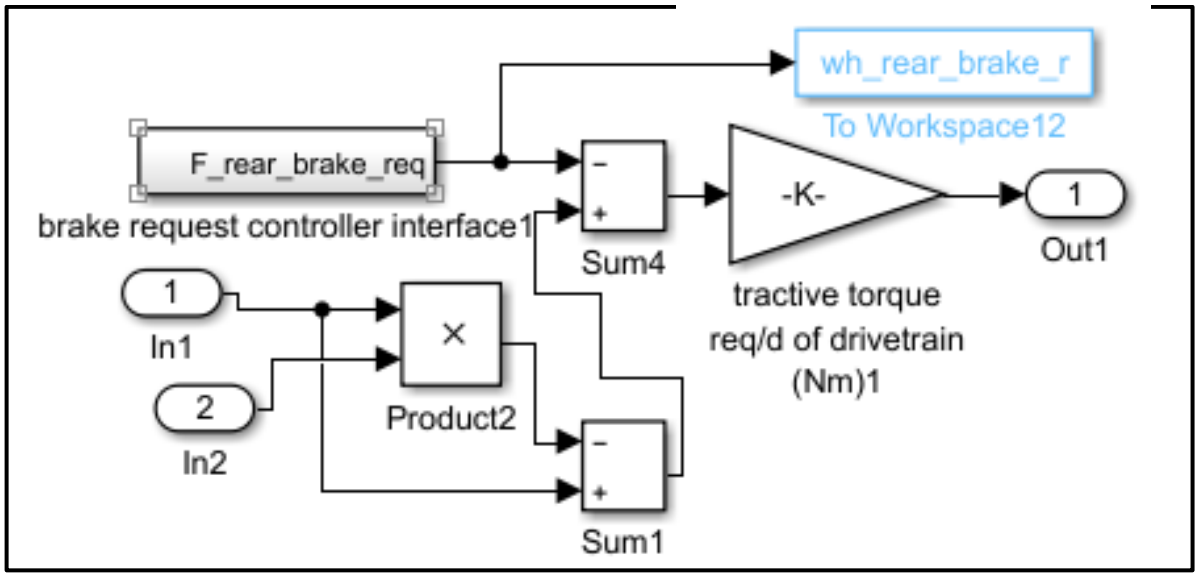

front force

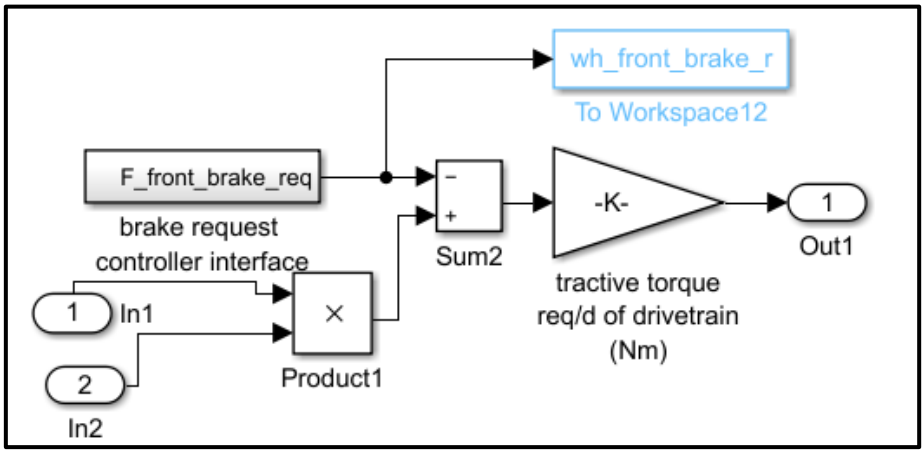

Limits and losses diafnostics

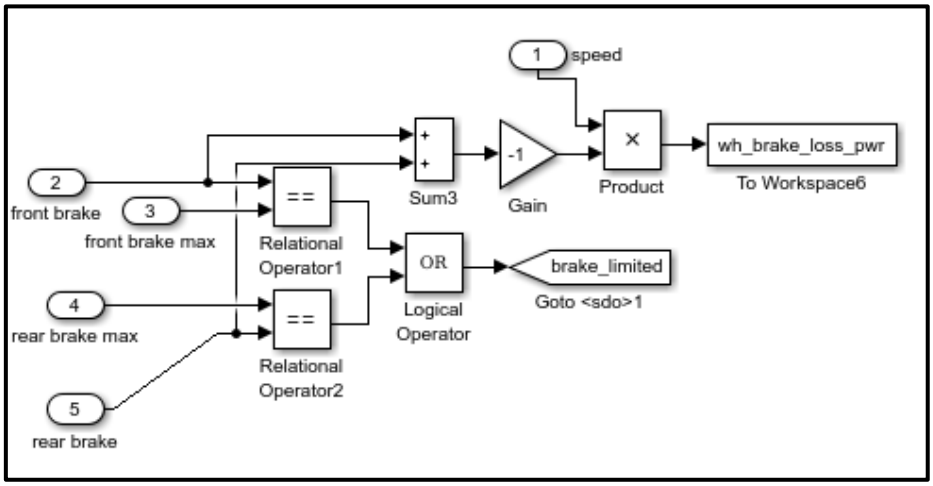

Tire slip model (m/s)

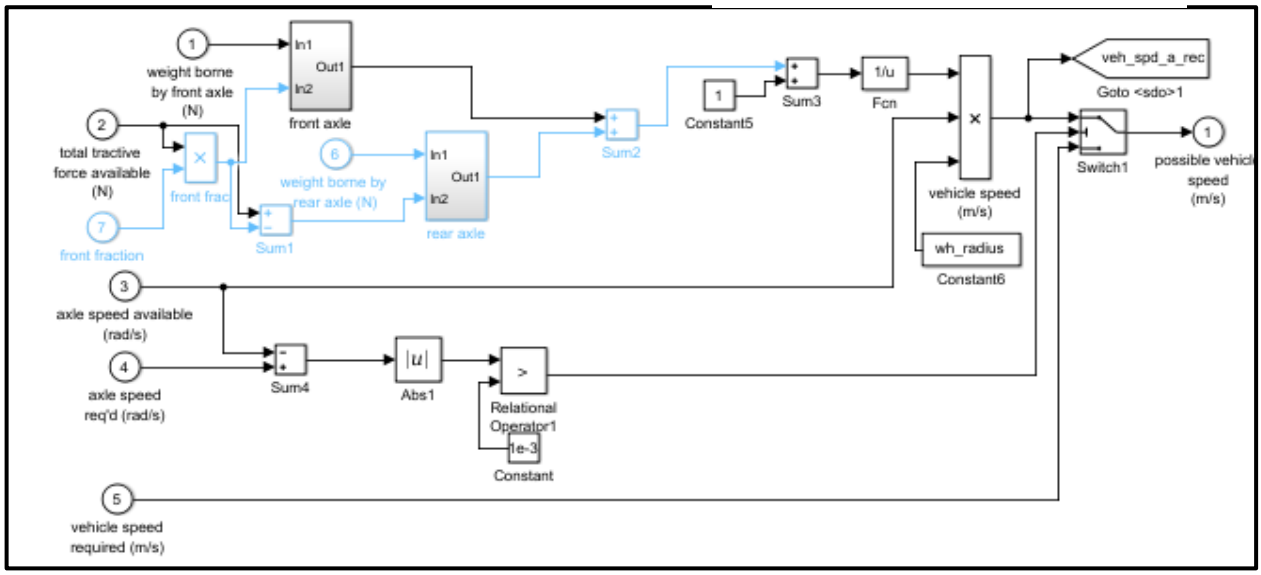

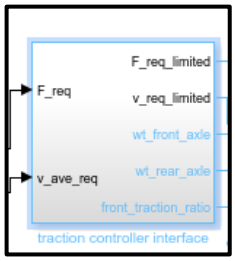

Traction controller interface

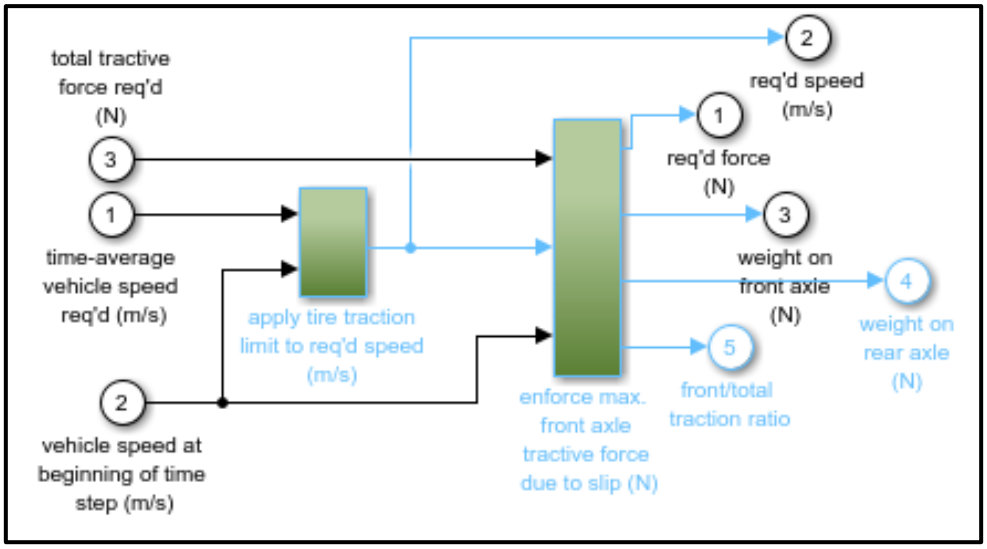

Enforce max front axle tractive force due to slip (N)

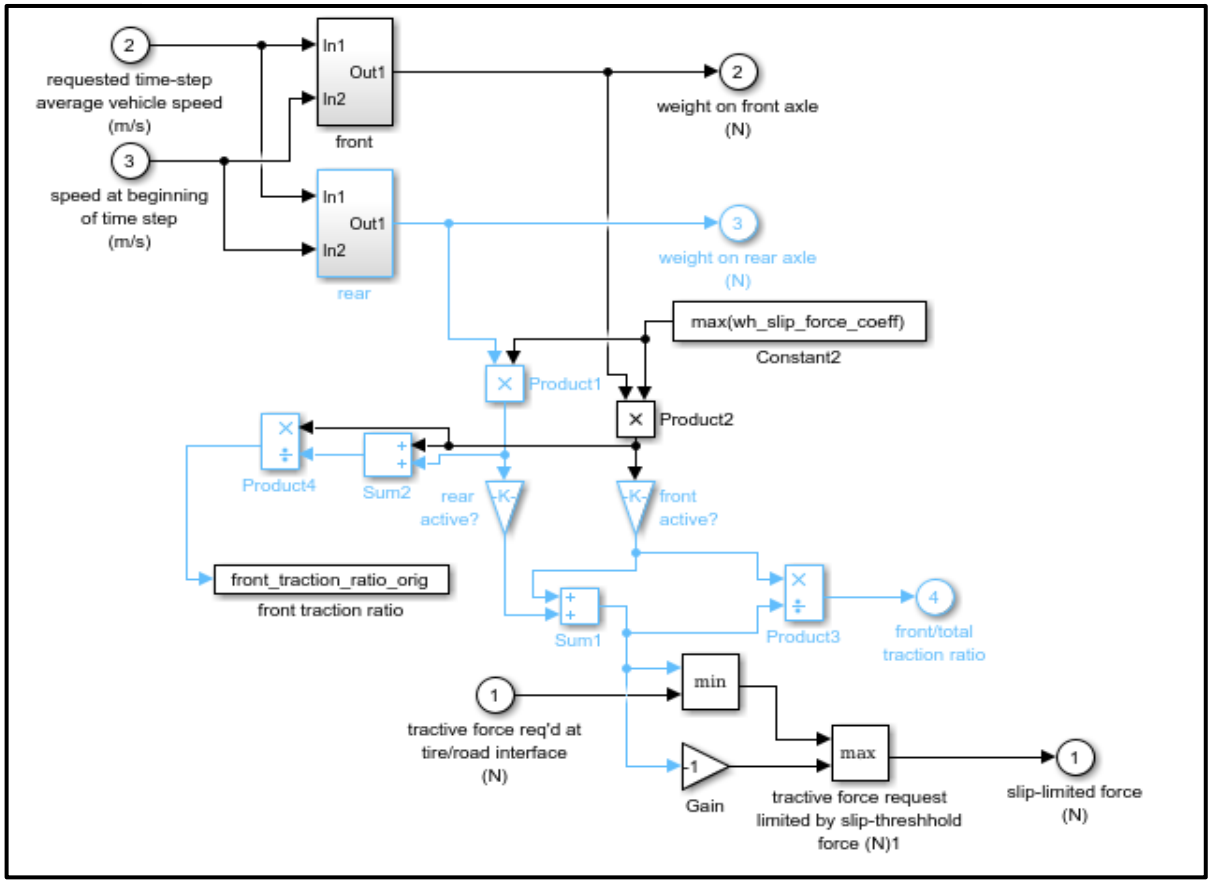

Apply tire traction limit to req d speed (m/s)

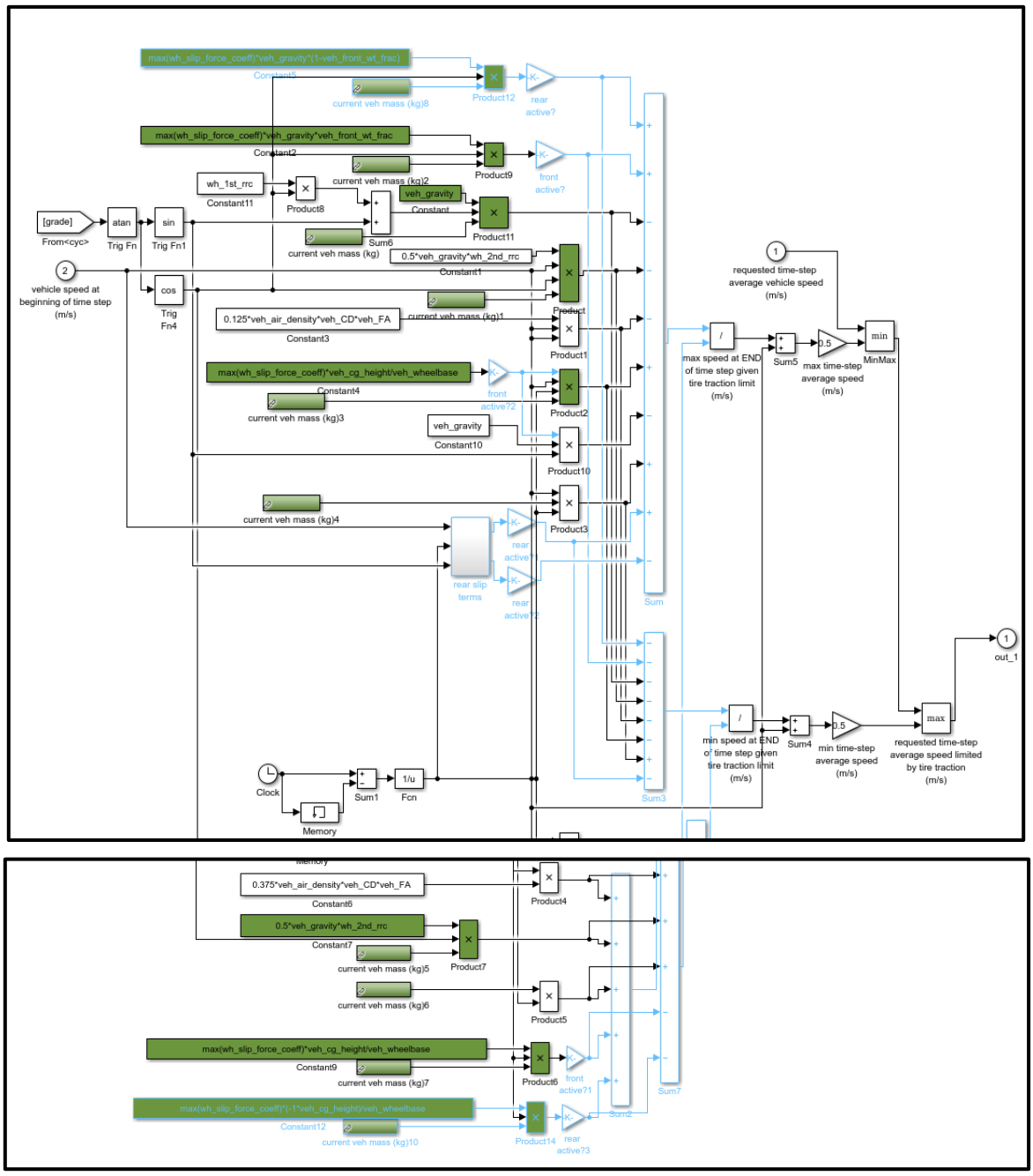

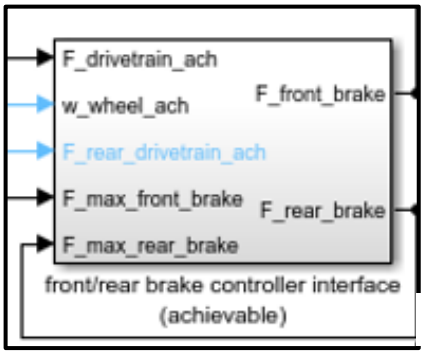

Front and rear brake controller (achievable)

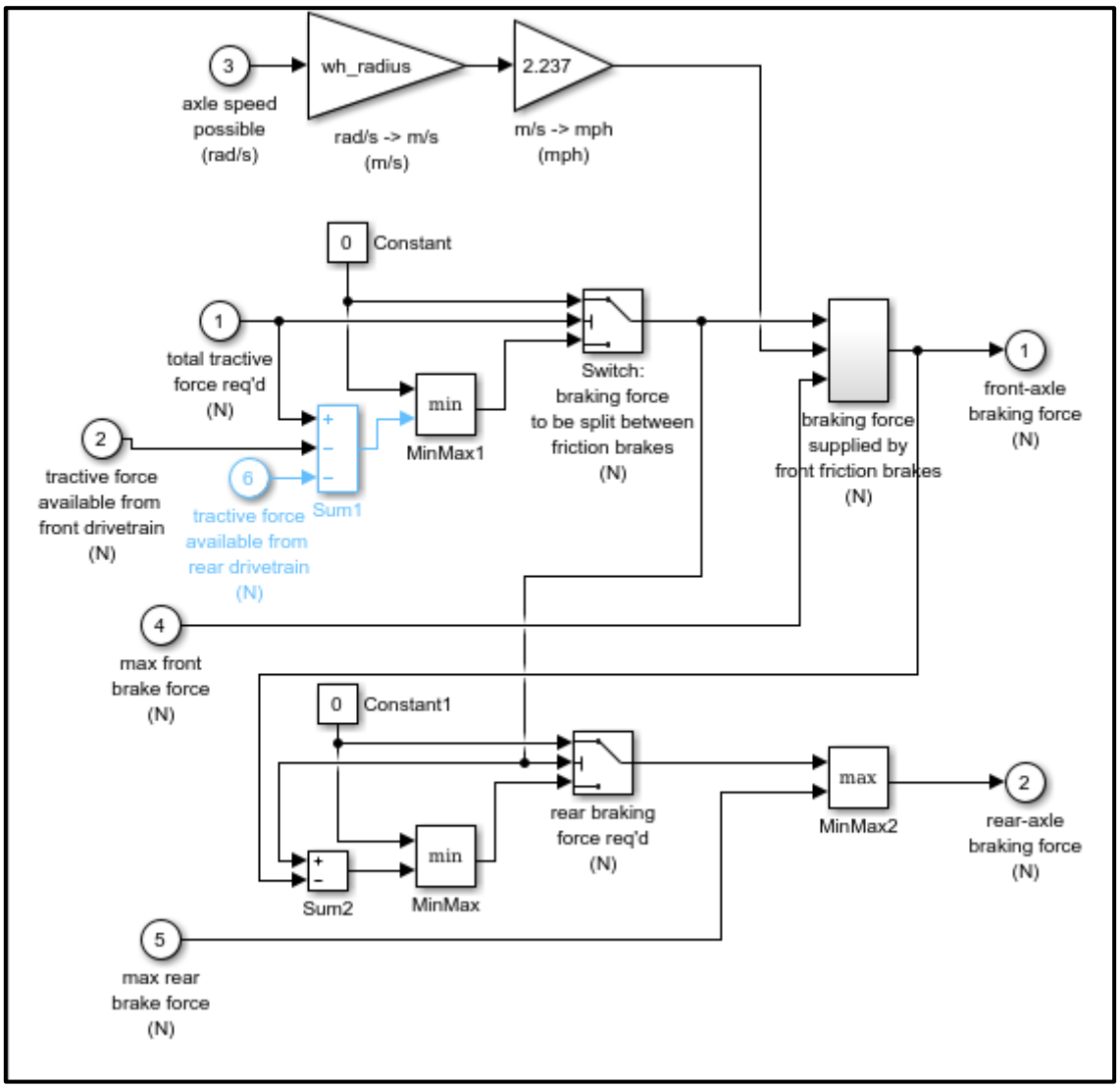

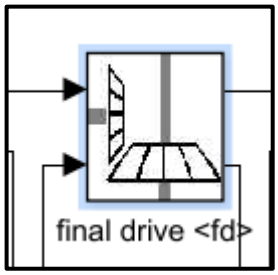

Final drive <fd>

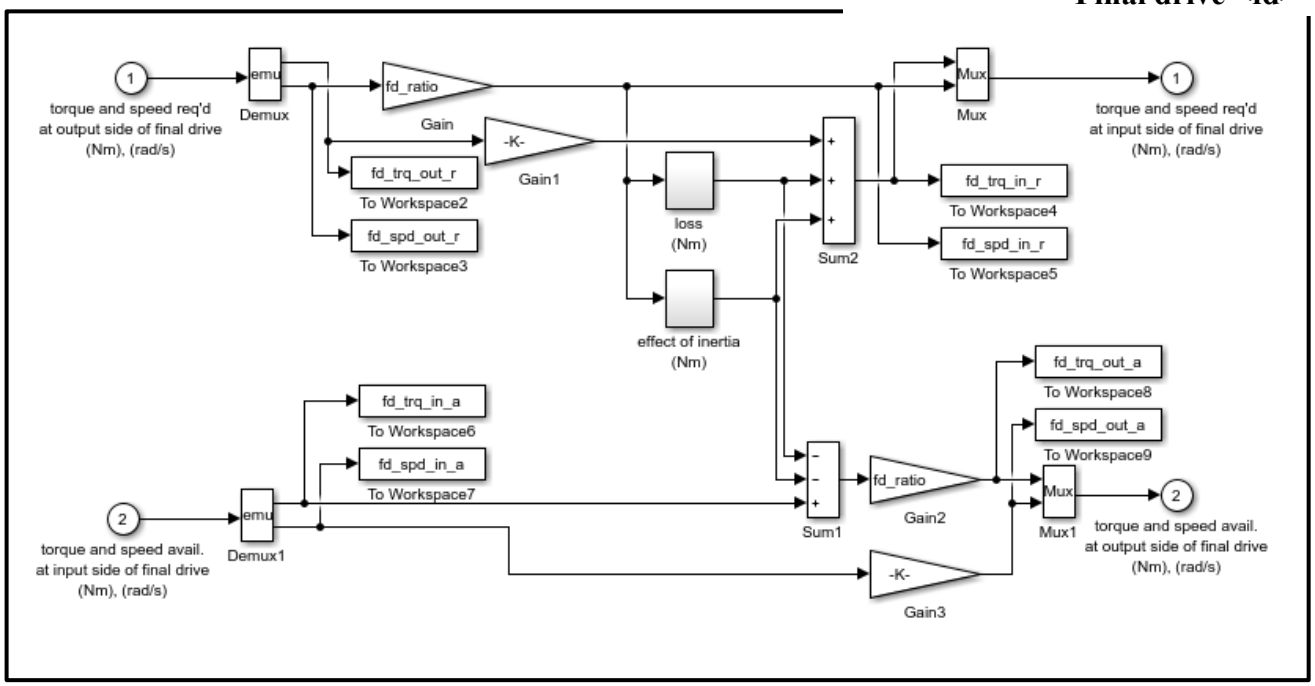

ANNEX G – GEAR SHIFT INDICATOR

Gear Shift indicator for BL_ H_1.4_E22_NoHybrid, H_1.4_E22_12V, and H_1.4_E100_12V configurations over the FTP – 75 + HWFET cycles

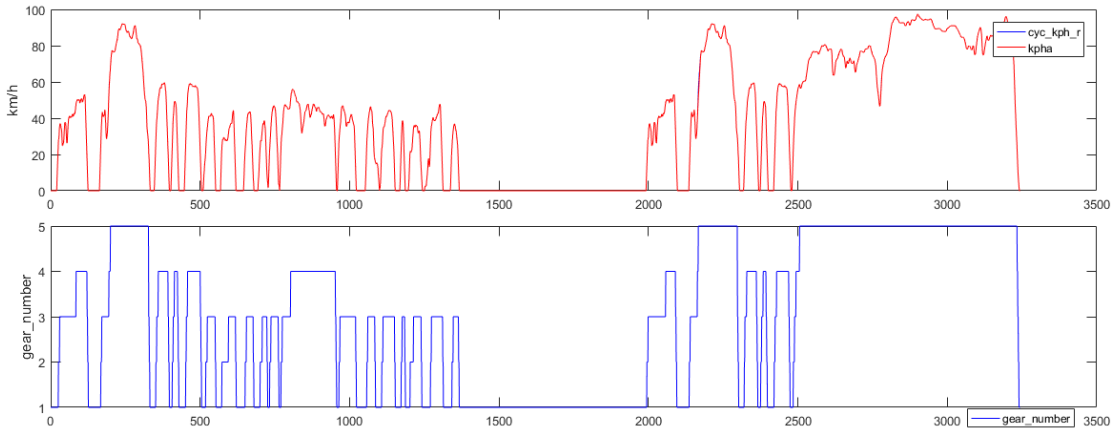

Gear Shift indicator for BL_ H_1.4_E22_NoHybrid, H_1.4_E22_12V, and H_1.4_E100_12V configurations over the SP cycle

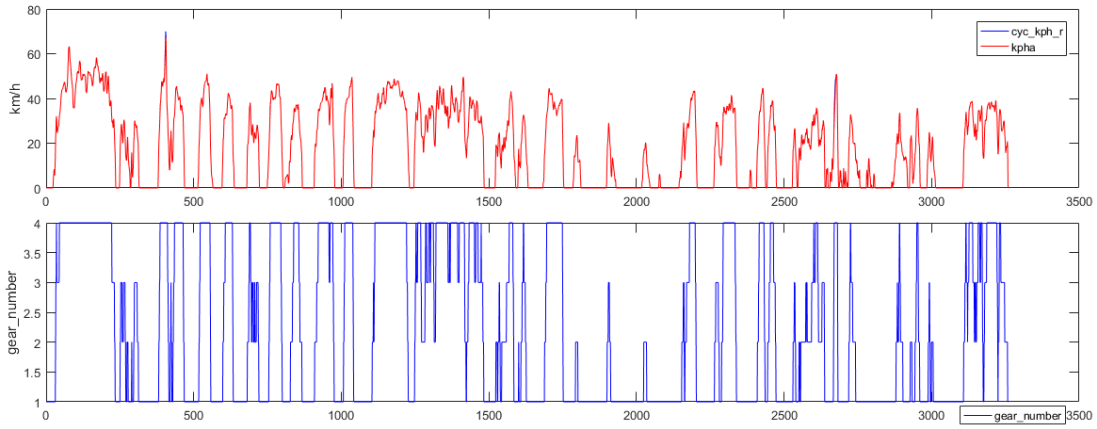

Gear Shift indicator for BL_SUV_1.8_E100_NoHybrid, SUV_1.8_E22_12V, and SUV_1.8_E100_12V configurations over the FTP – 75 + HWFET cycles

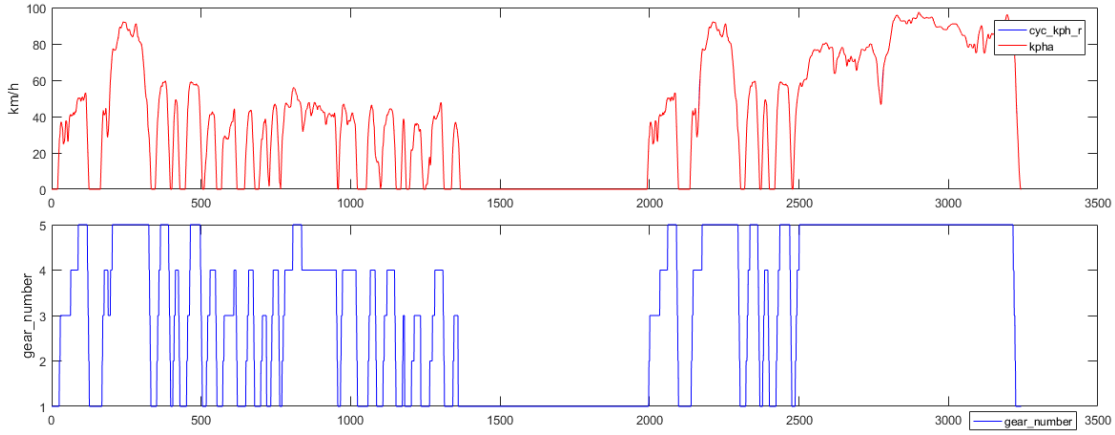

Gear Shift indicator for BL_SUV_1.8_E100_NoHybrid, SUV_1.8_E22_12V, and SUV_1.8_E100_12V configurations over the SP cycle

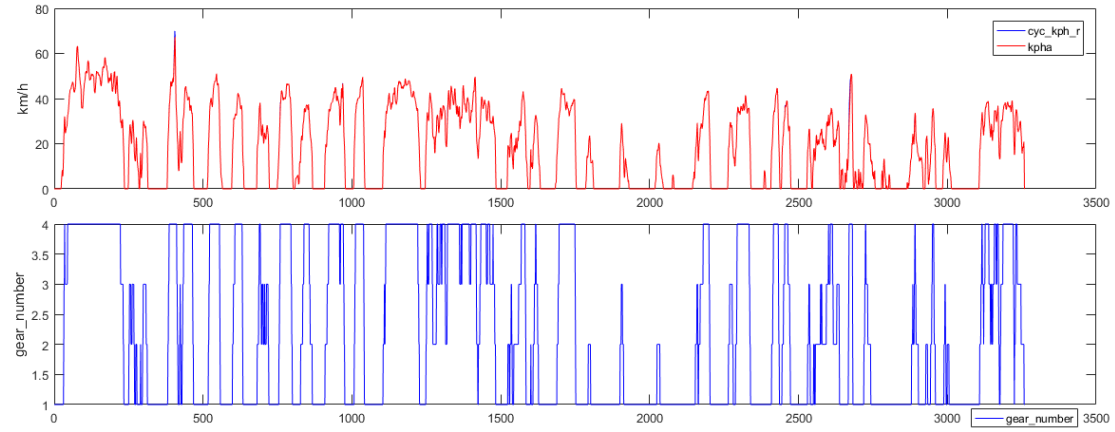

ANNEX H – GEARBOX MODEL

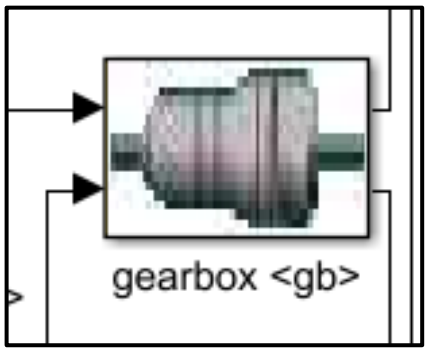

Gearbox <gb>

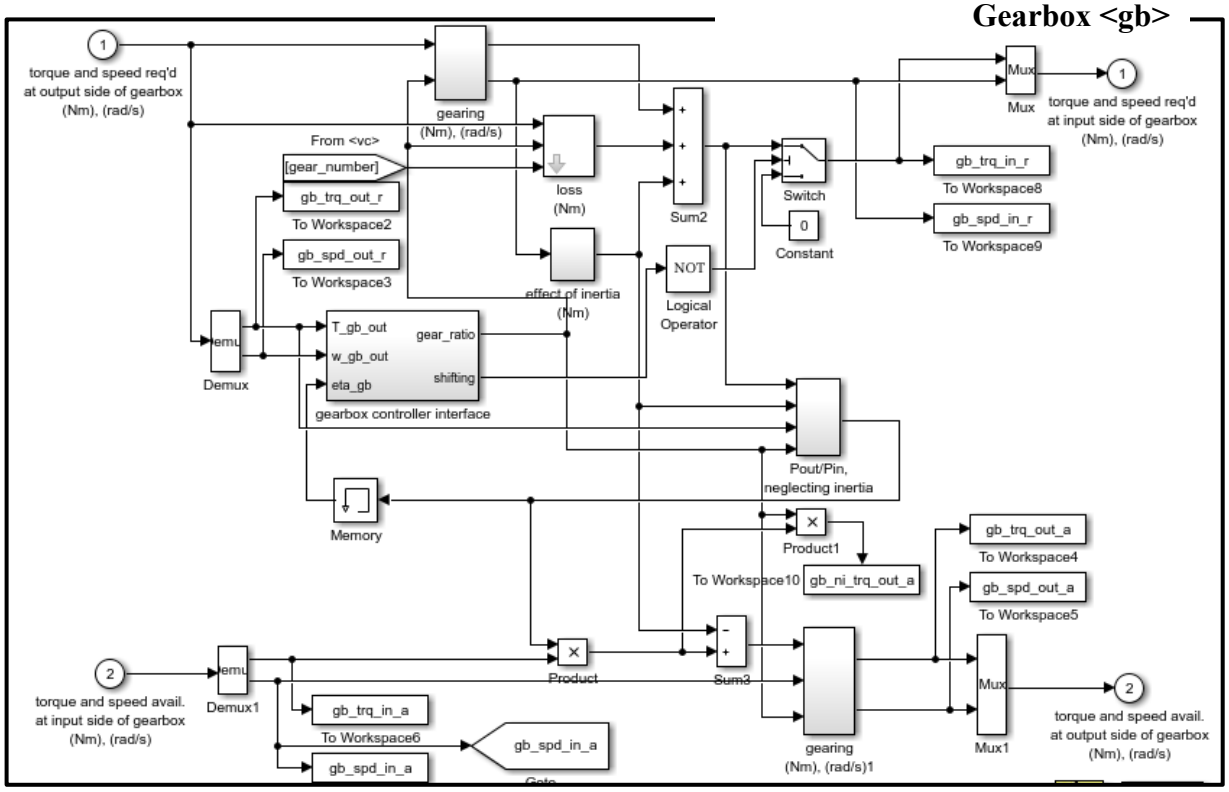

Gearing (Nm), (rad/s)

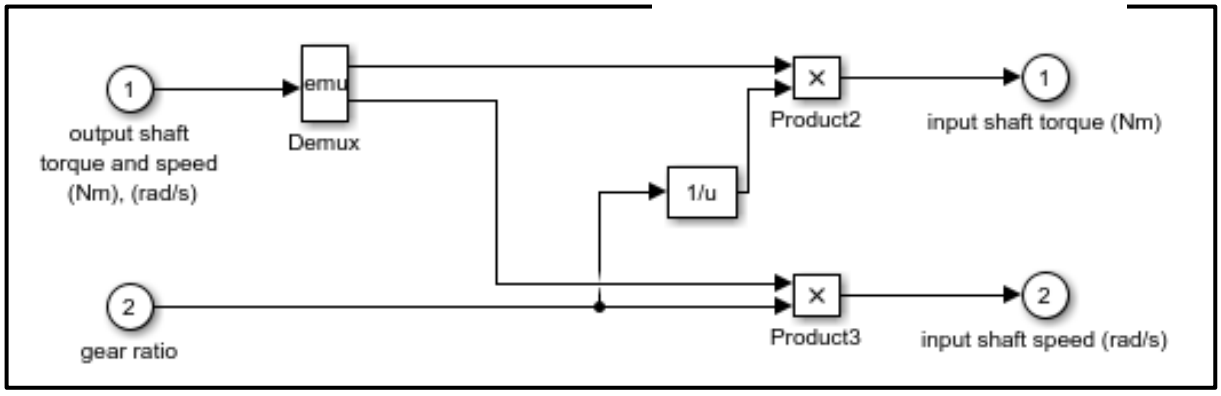

Pout/Pin, neglecting inertia

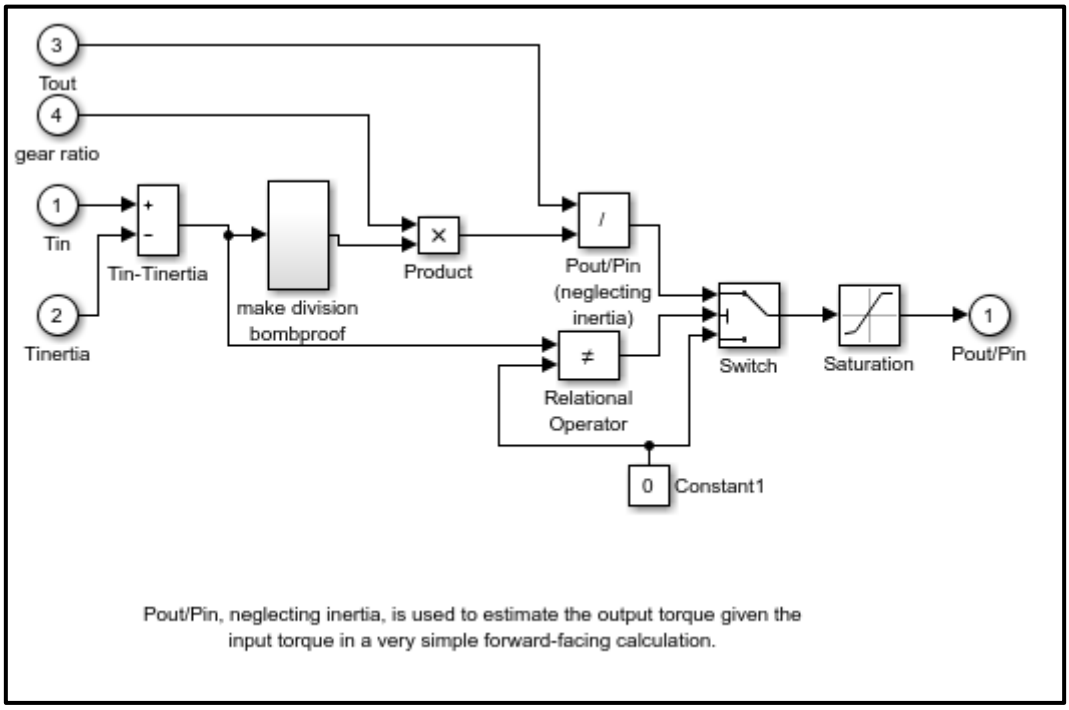

Effect of inertia (Nm)

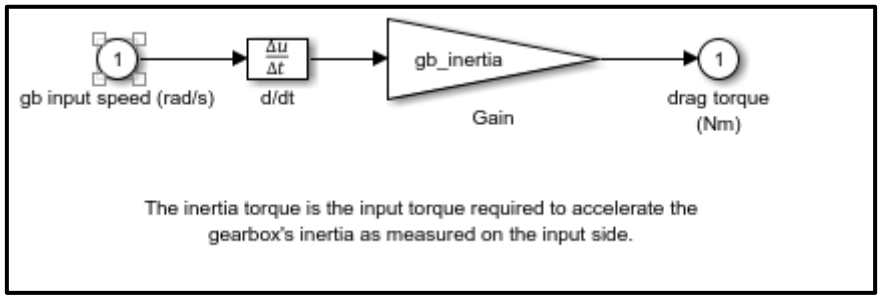

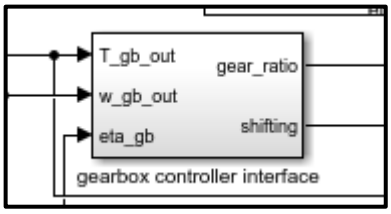

Gearbox controller interface

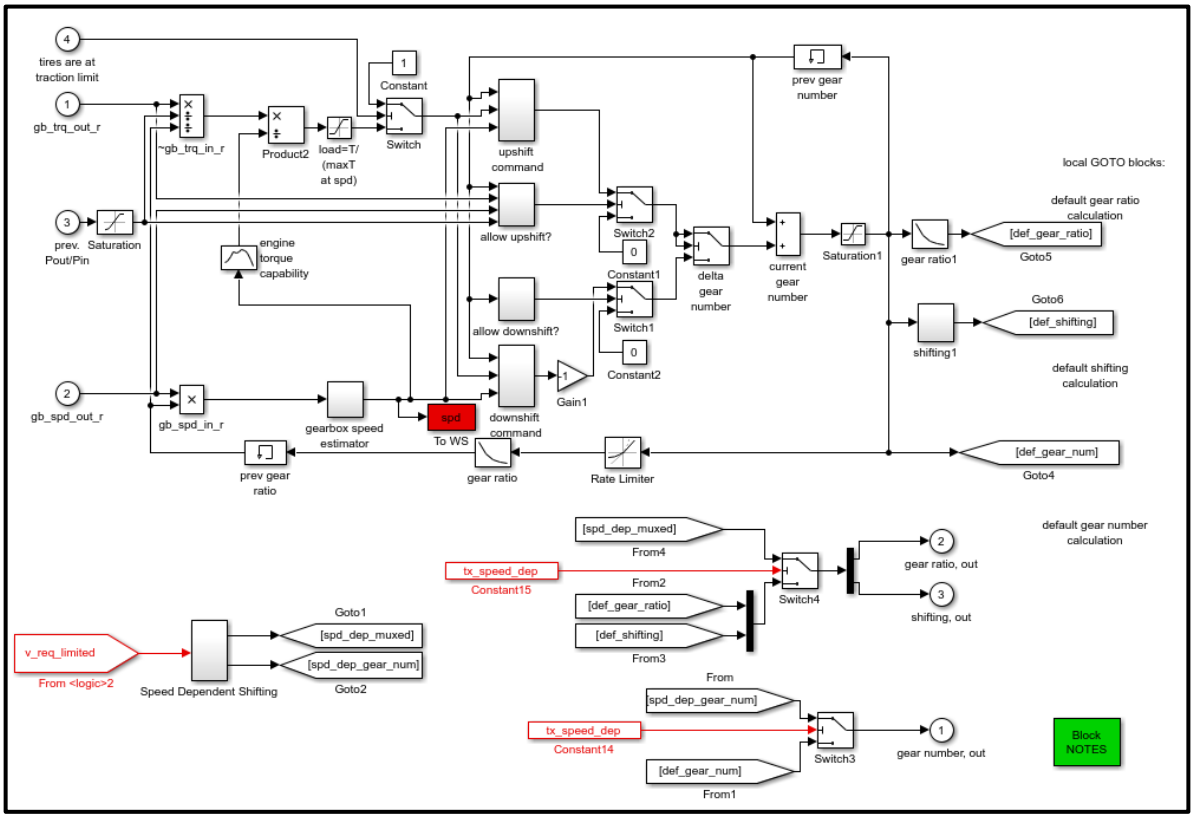

ANNEX I – TORQUE COUPLER MODEL

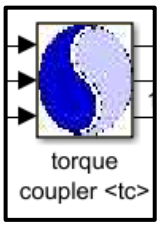

Torque coupler <tc>

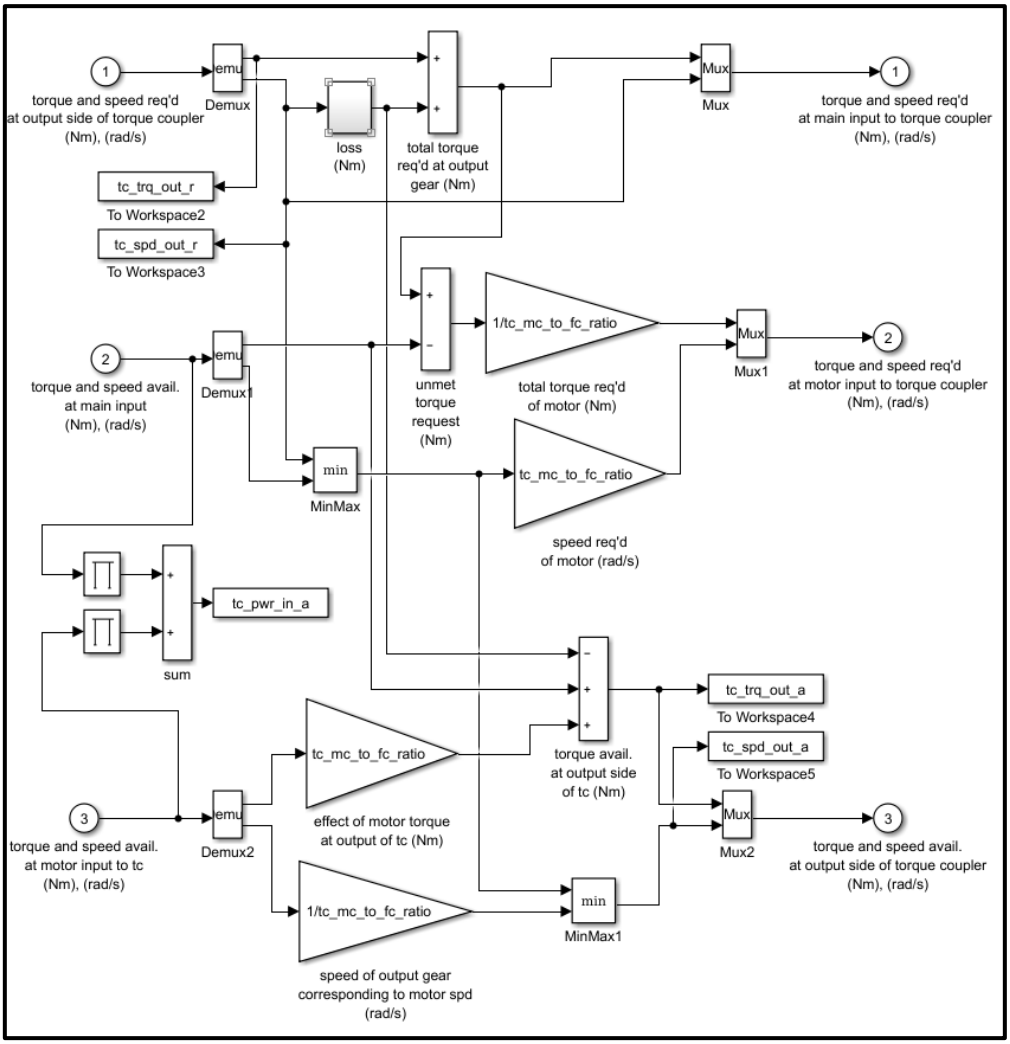

Loss (Nm)

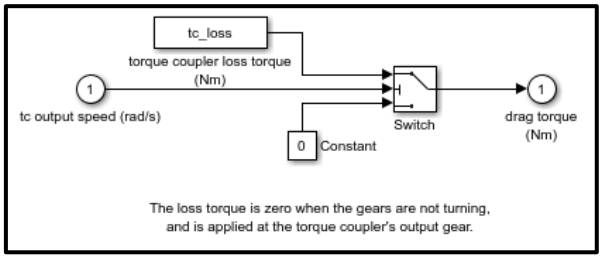

ANNEX J – MOTOR CONTROLLER MODEL

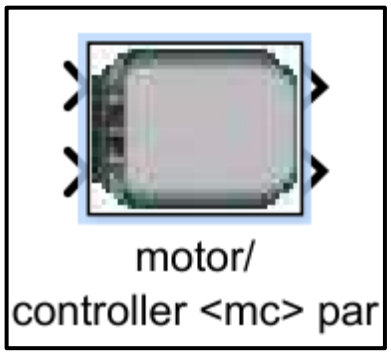

Motor/controller <mc> par

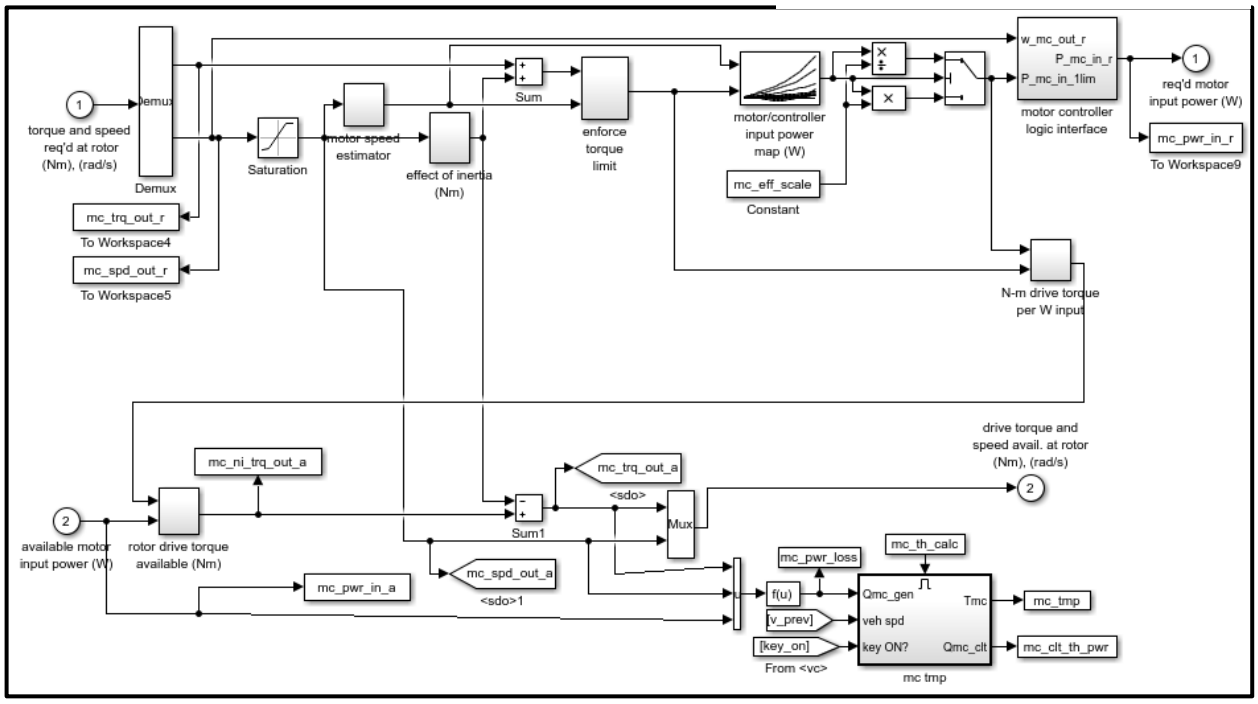

Motor speed estimator

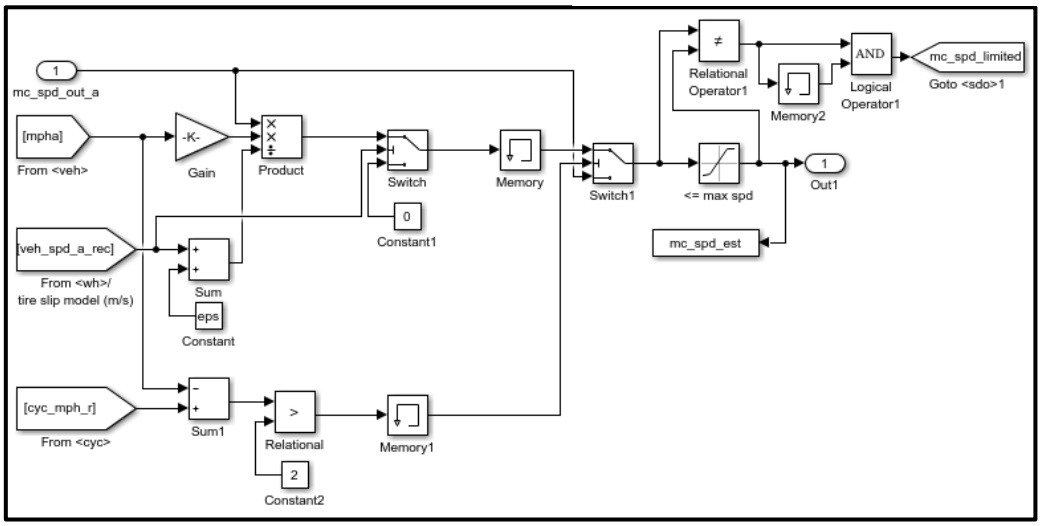

Effect of inertia (Nm)

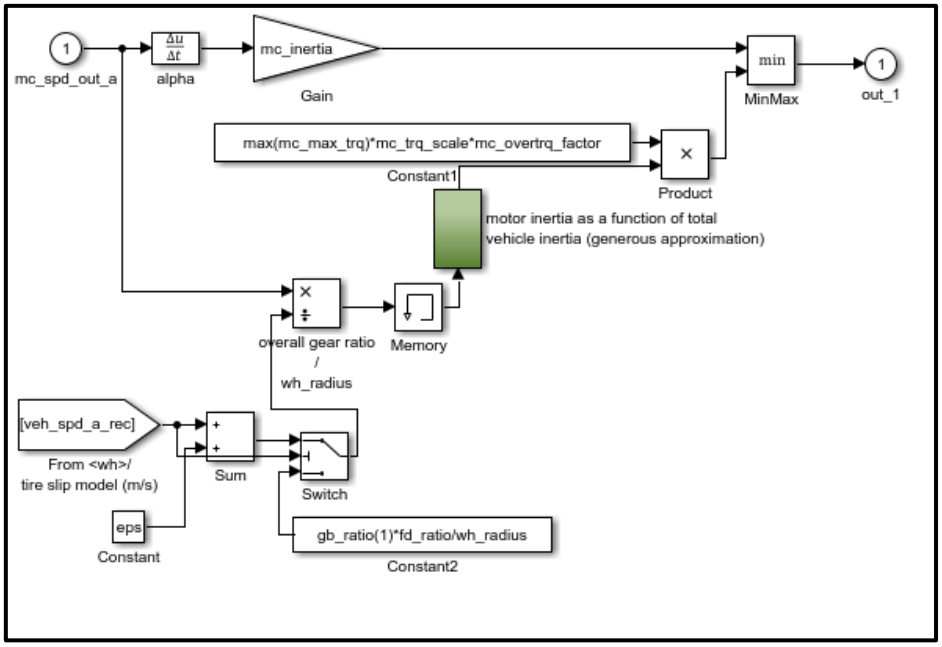

Enforce torque limit

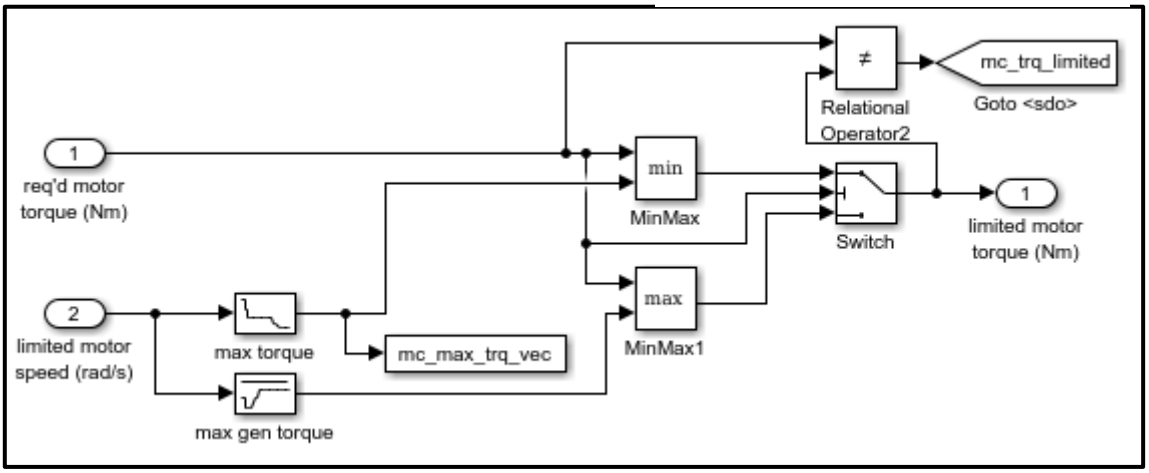

N-m drive torque per W input

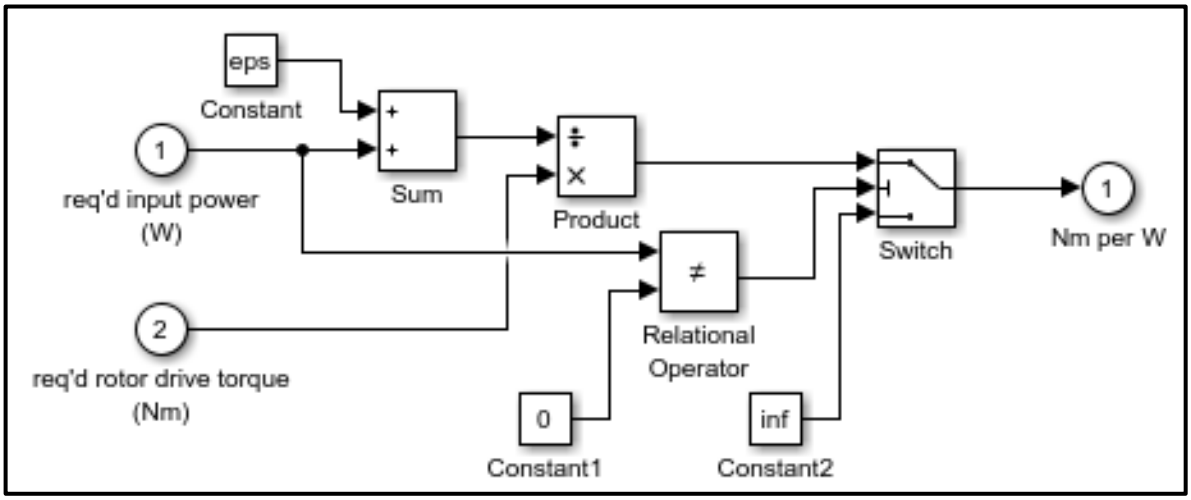

Rotor drive torque available (Nm)

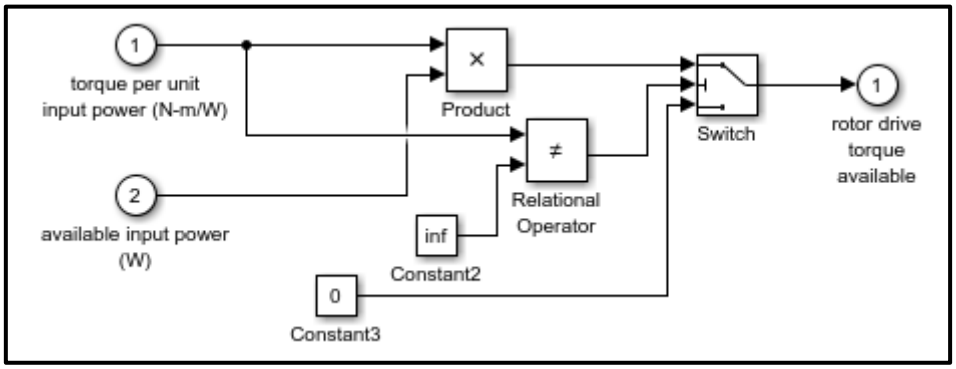

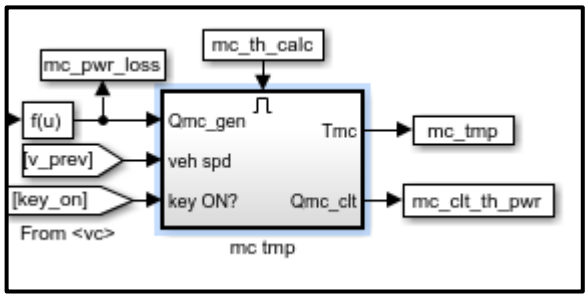

mc tmp

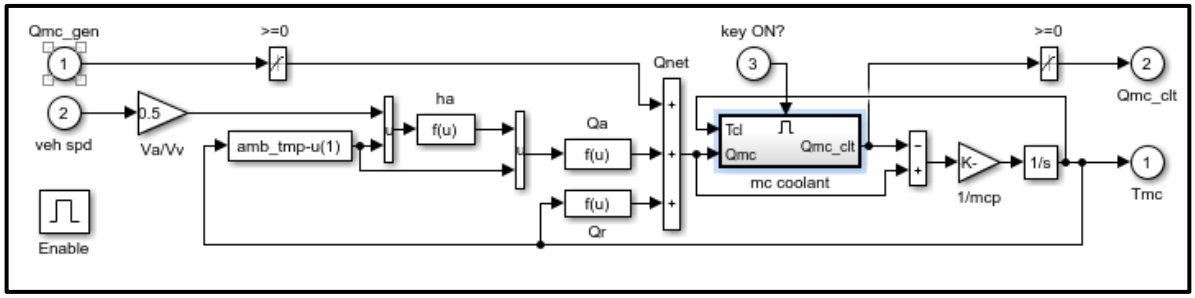

Motor controller logic interface

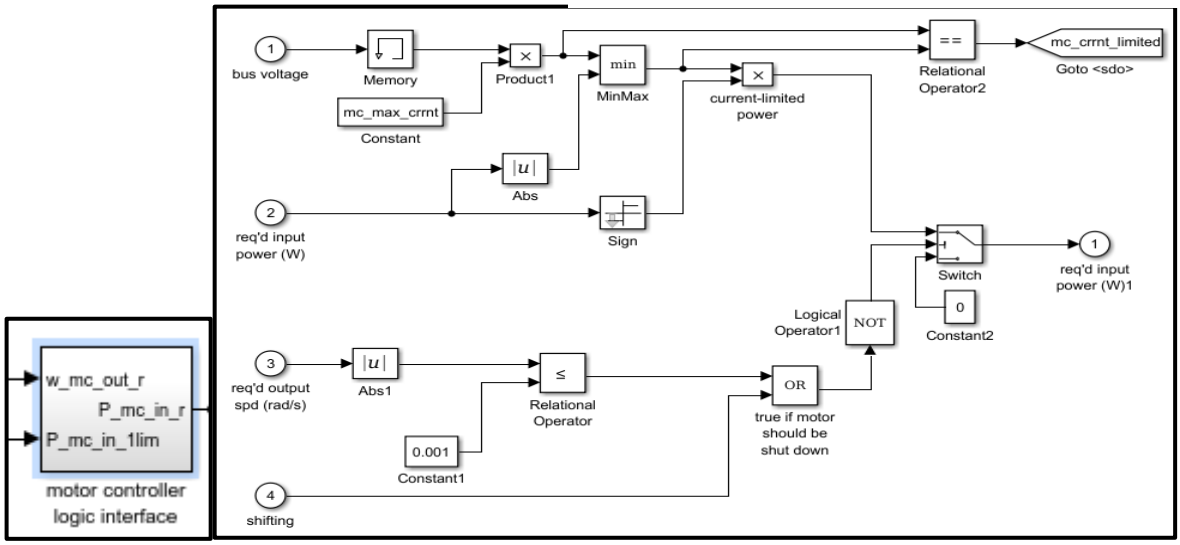

ANNEX K – ELECTRIC ASSIST CONTROL STRATEGY MODEL

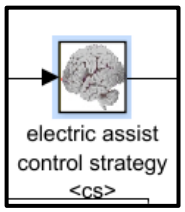

Electric assist control strategy <cs>

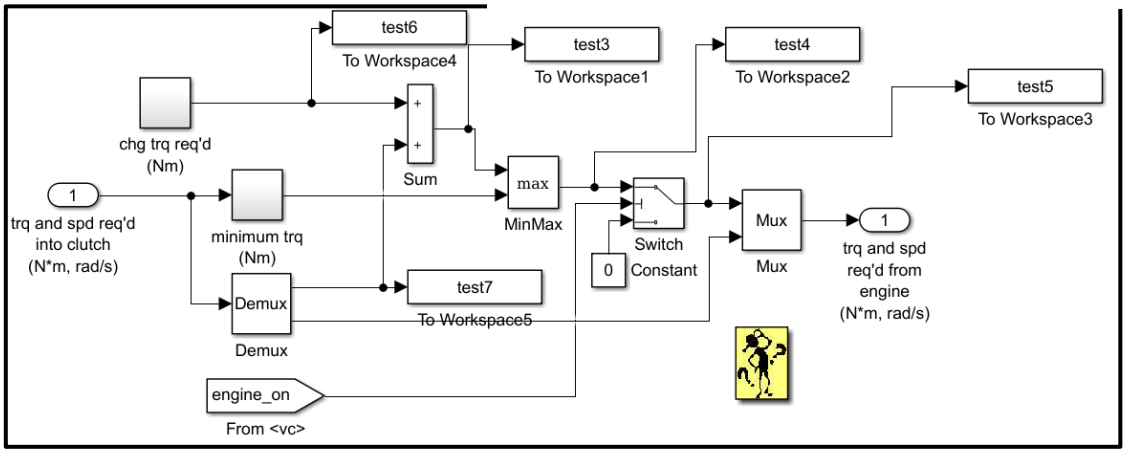

Chg trq req'd (Nm)

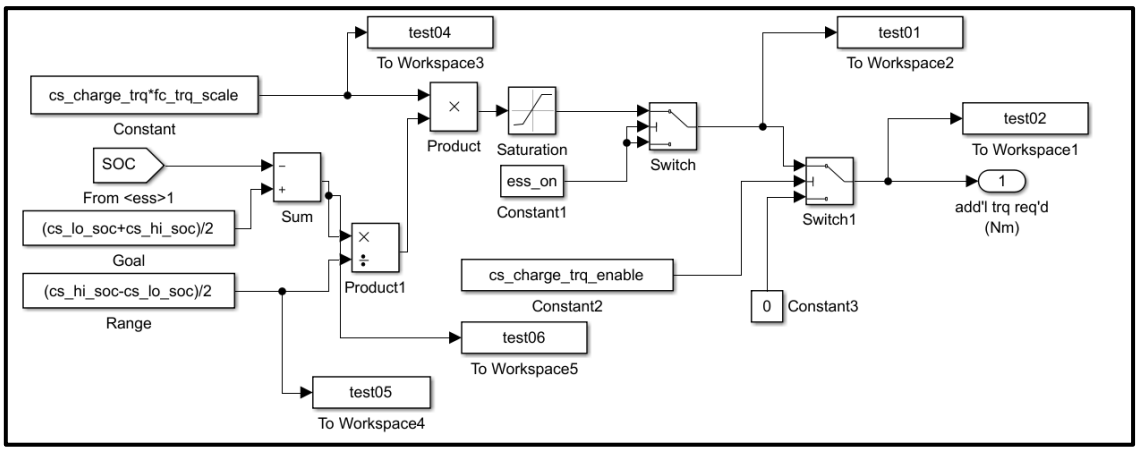

Minimum trq (Nm)

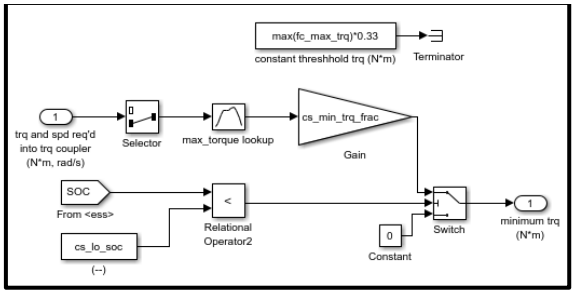

ANNEX L – MECHANICAL ACCESSORY LOADS MODEL

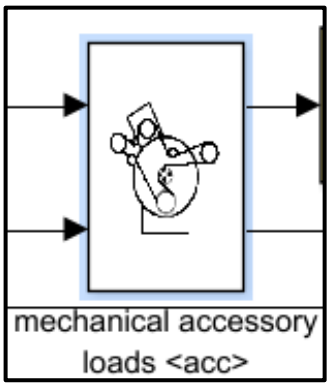

Mechanical accessory loads <acc>

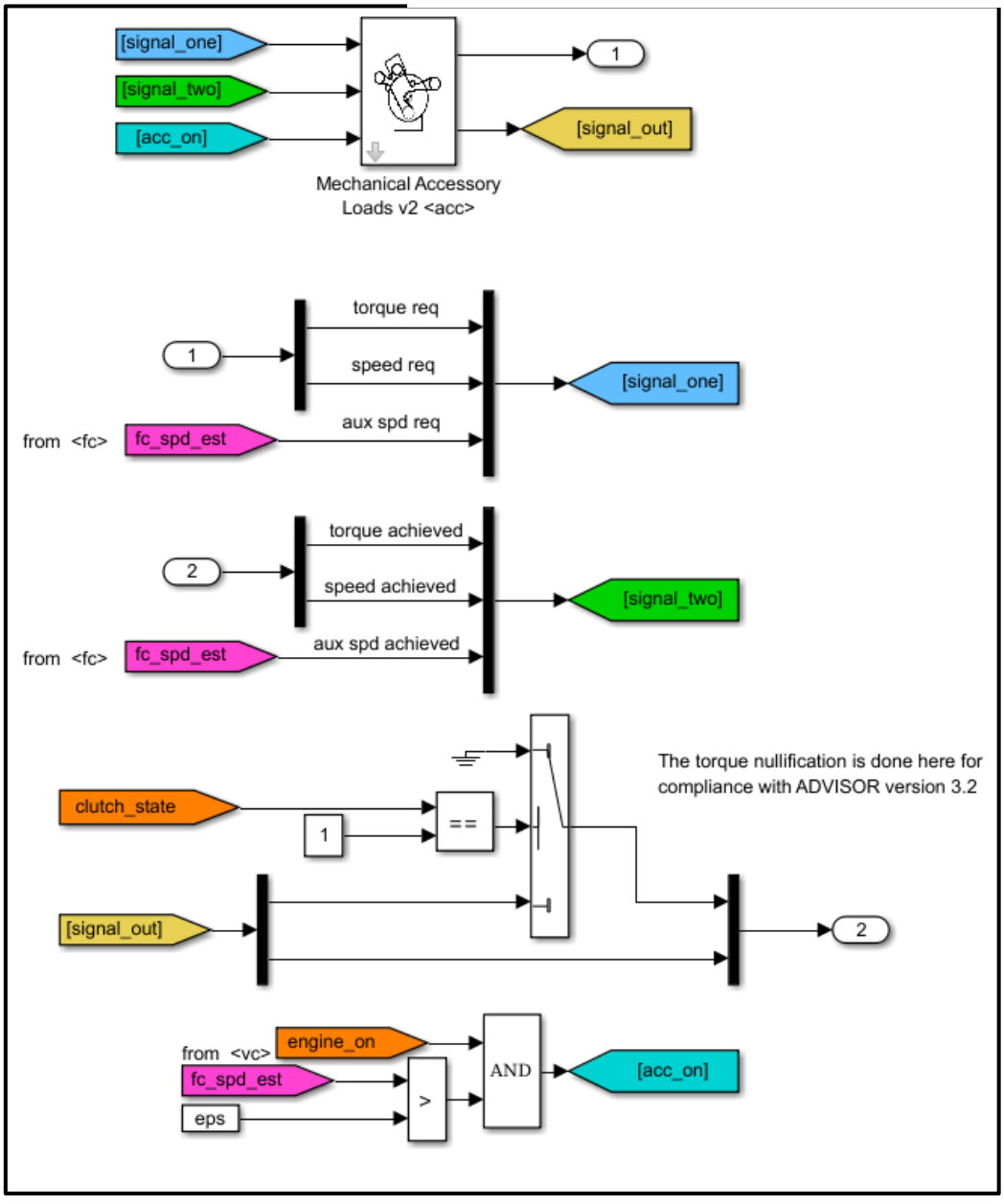

Mechanical Accessory Loads v2 <acc>

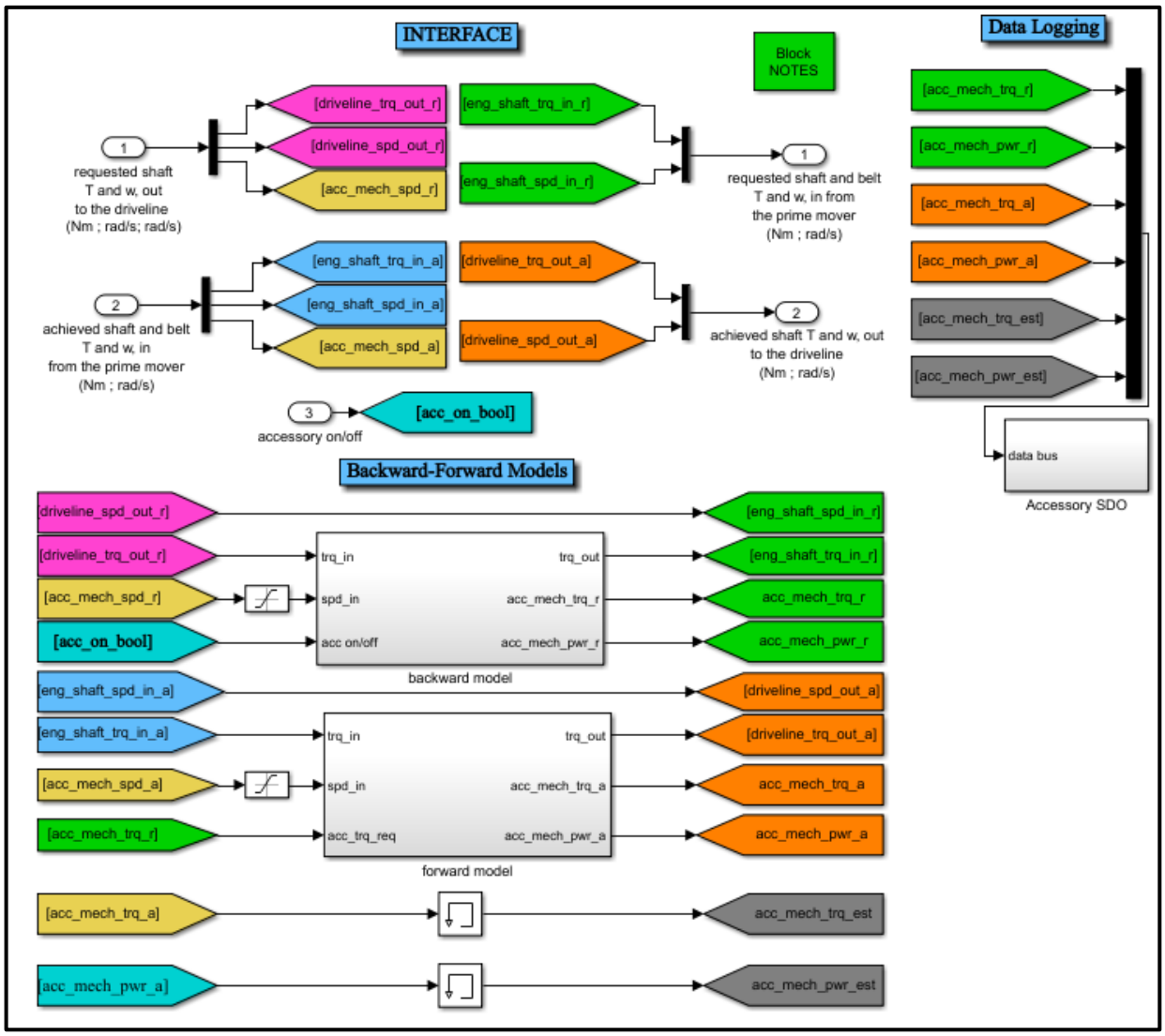

Forward model

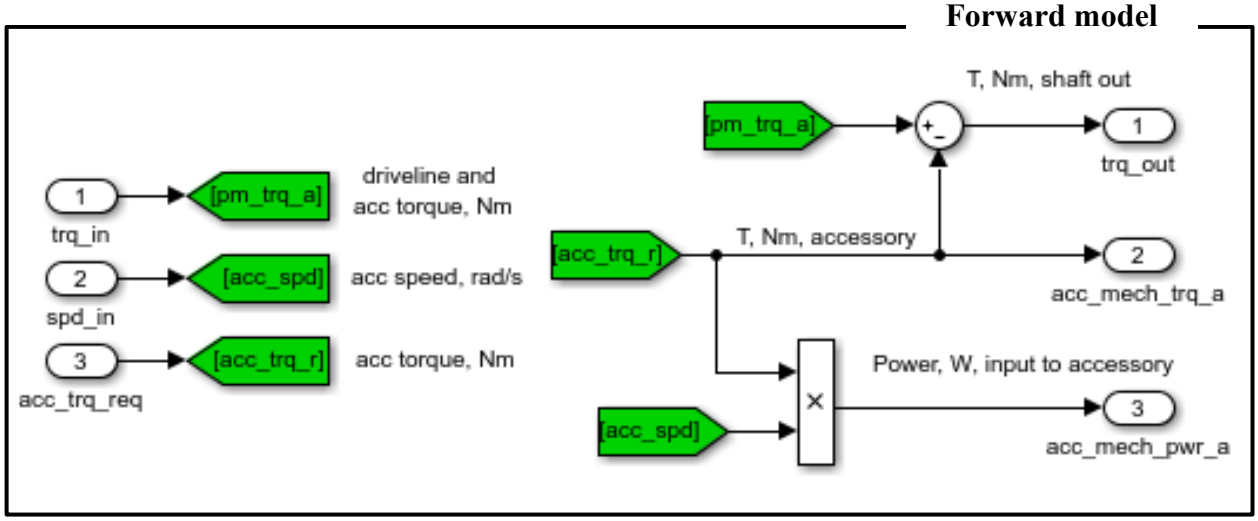

backward model

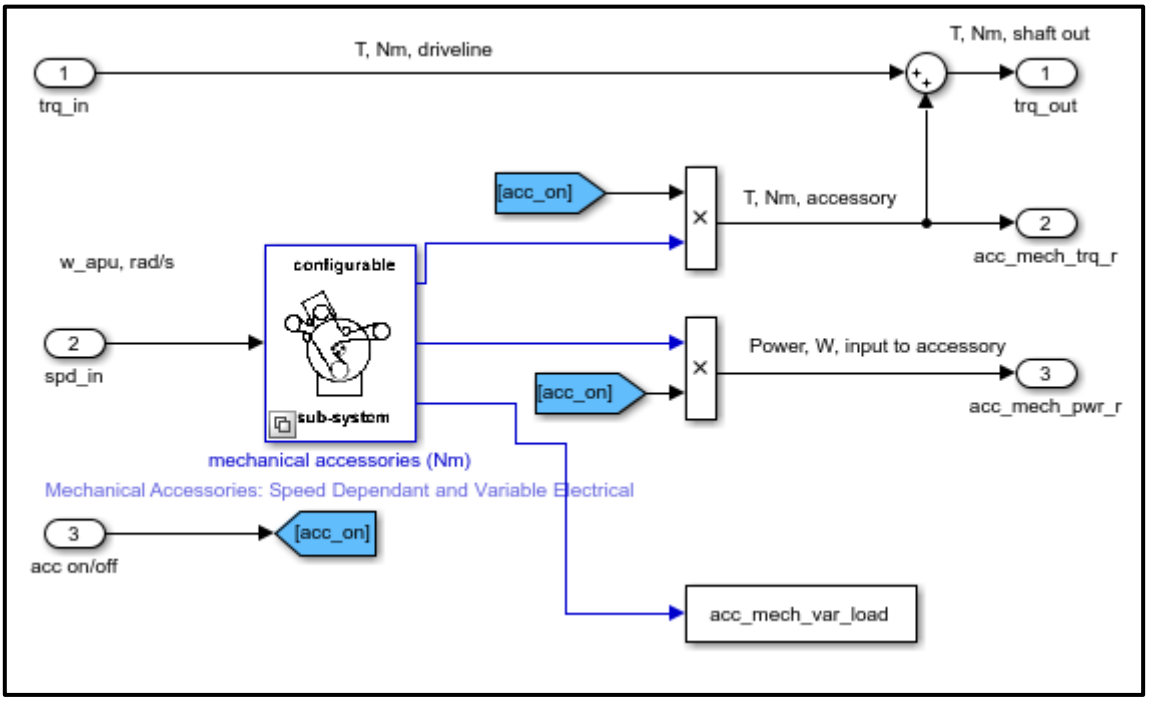
T, Nm, driveline
T, Nm, shaft out
1
trq_in
1
trq_out
[acc_on]
T, Nm, accessory
2
acc_mech_trq_r
w_apu, rad/s
configurable
2
spd_in
sub-system
Power, W, input to accessory
[acc_on]
3
acc_mech_pwr_r
mechanical accessories (Nm)
Mechanical Accessories: Speed Dependant and Variable Electrical
3
acc on/off
[acc_on]
acc_mech_var_load

ANNEX M – ENERGY STORAGE MODEL

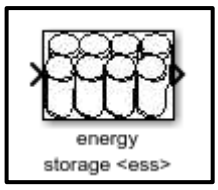

Energy storage <ess>

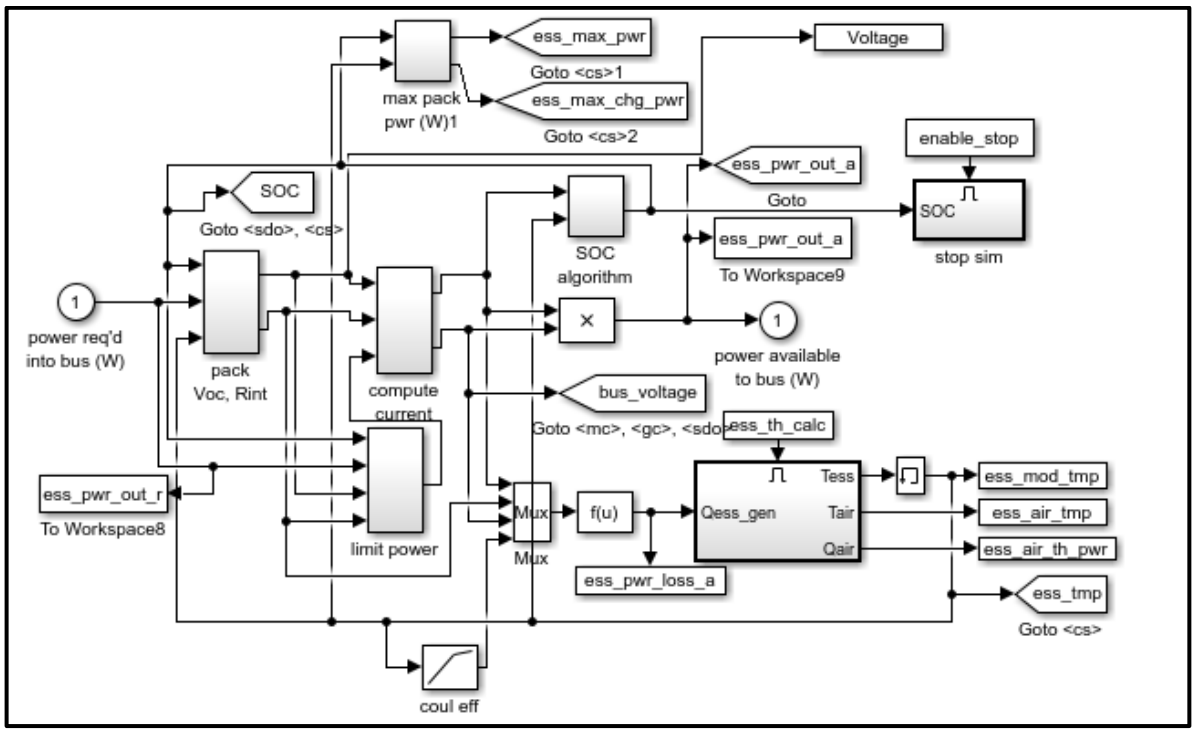

Pack Voc, Rint

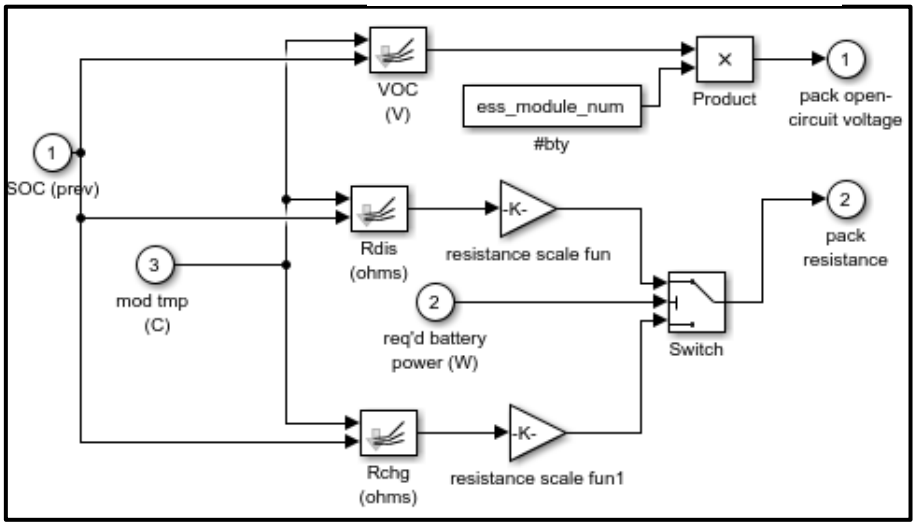

Max pack pwr (W)

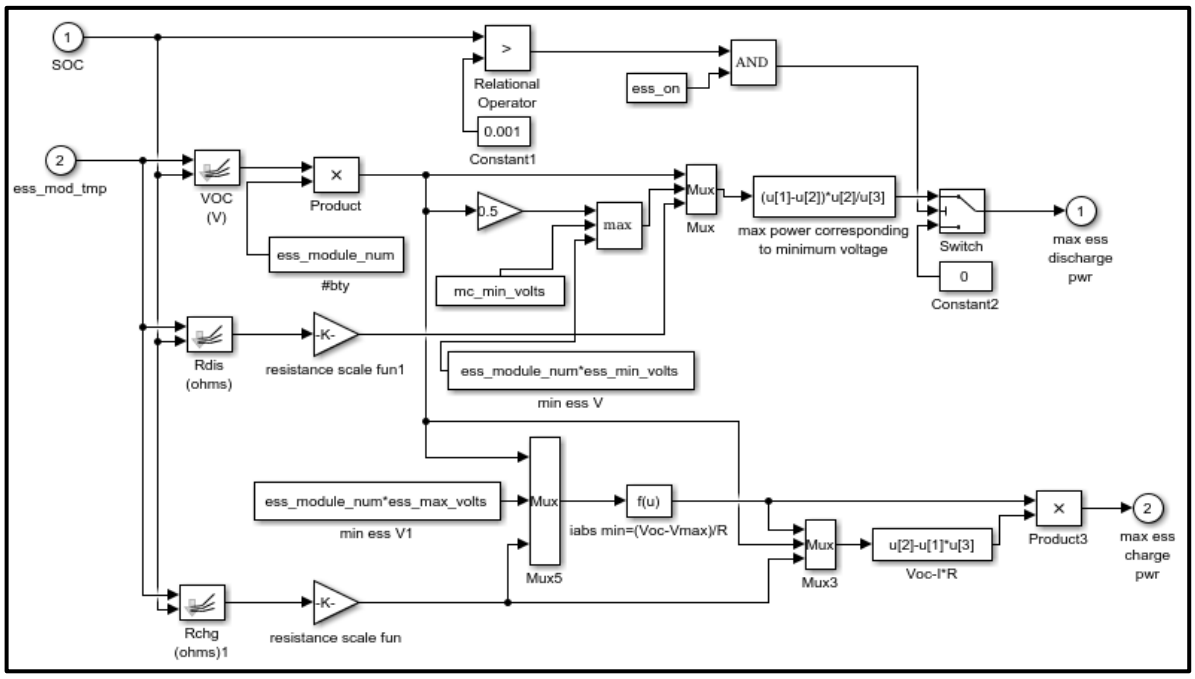

Compute current

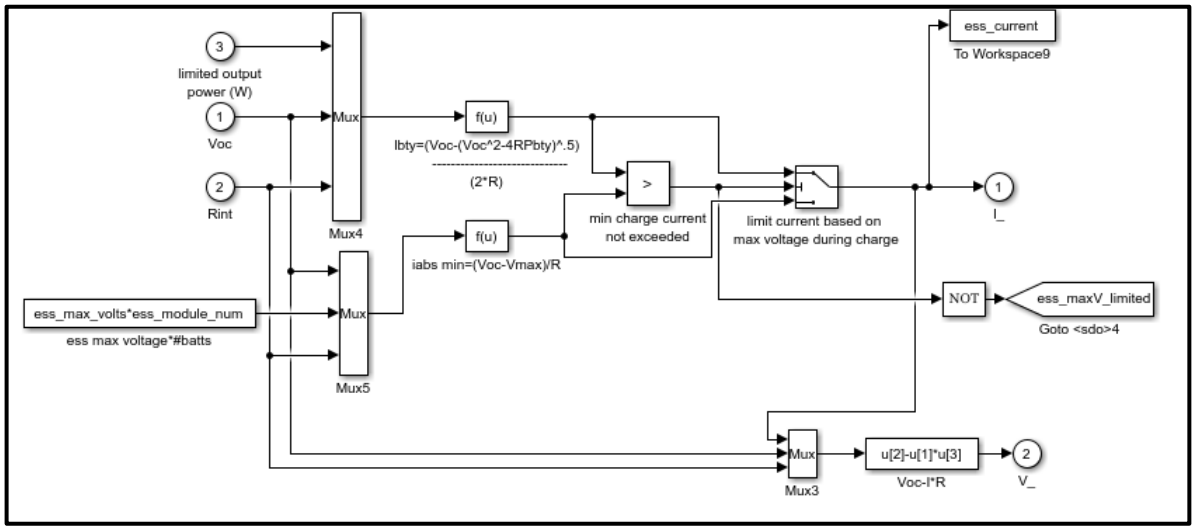

Stop sim

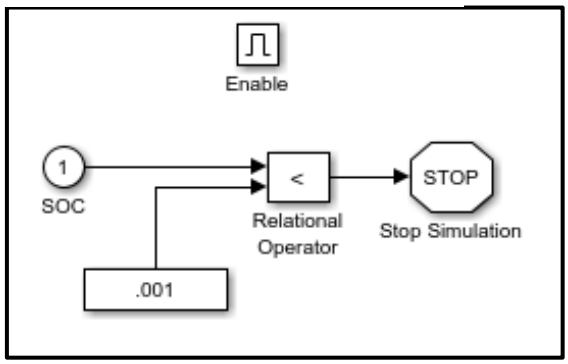

SOC algorithm

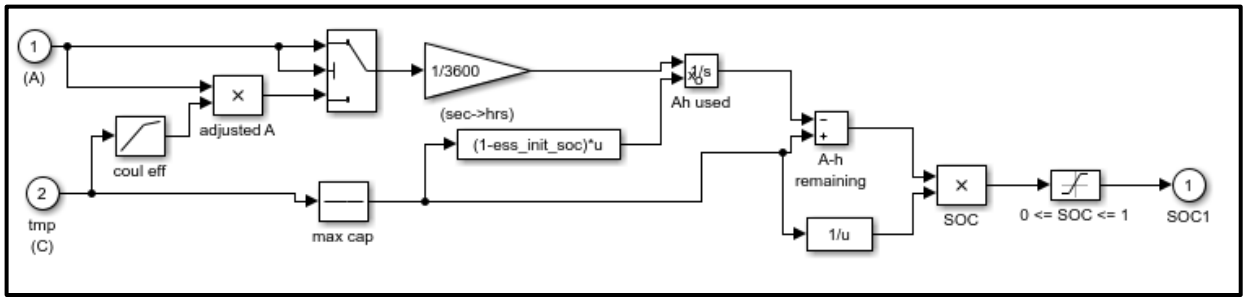

Ess tmp

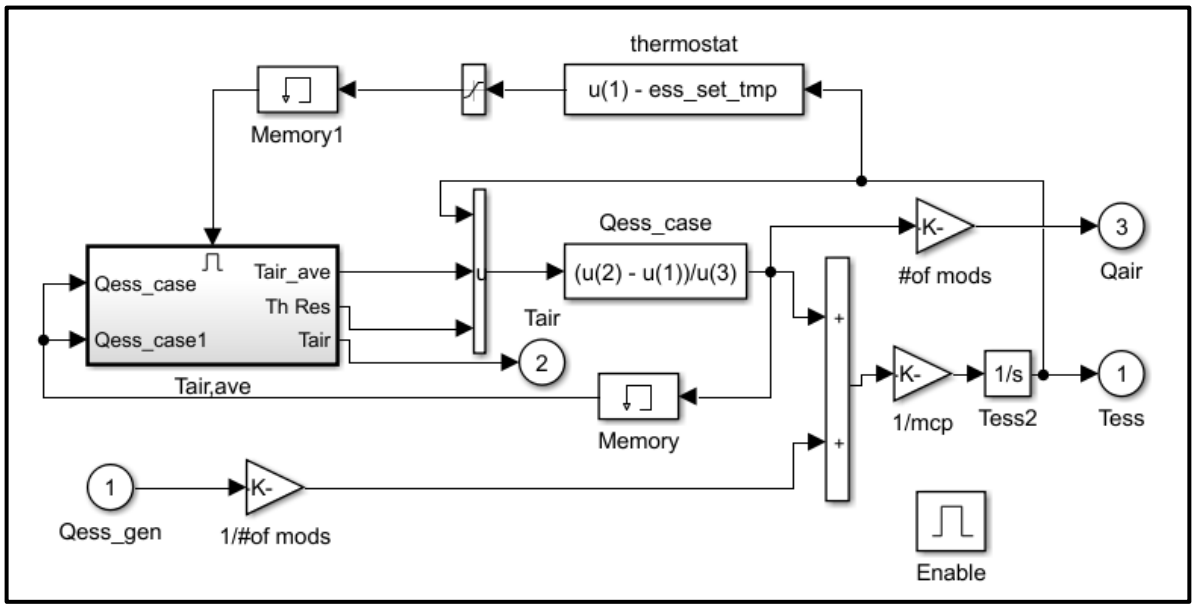

Tair,ave

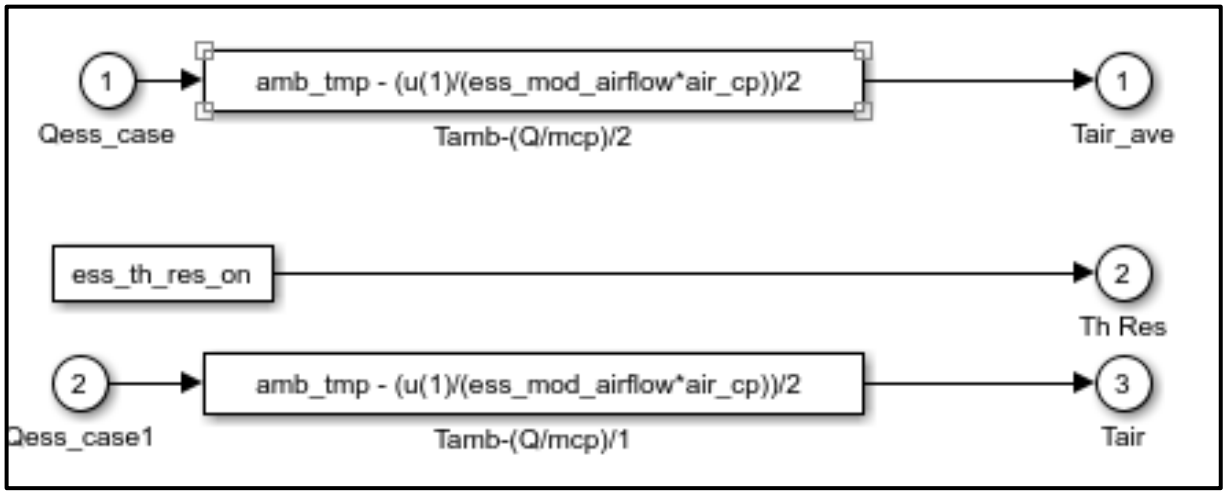

Limit power

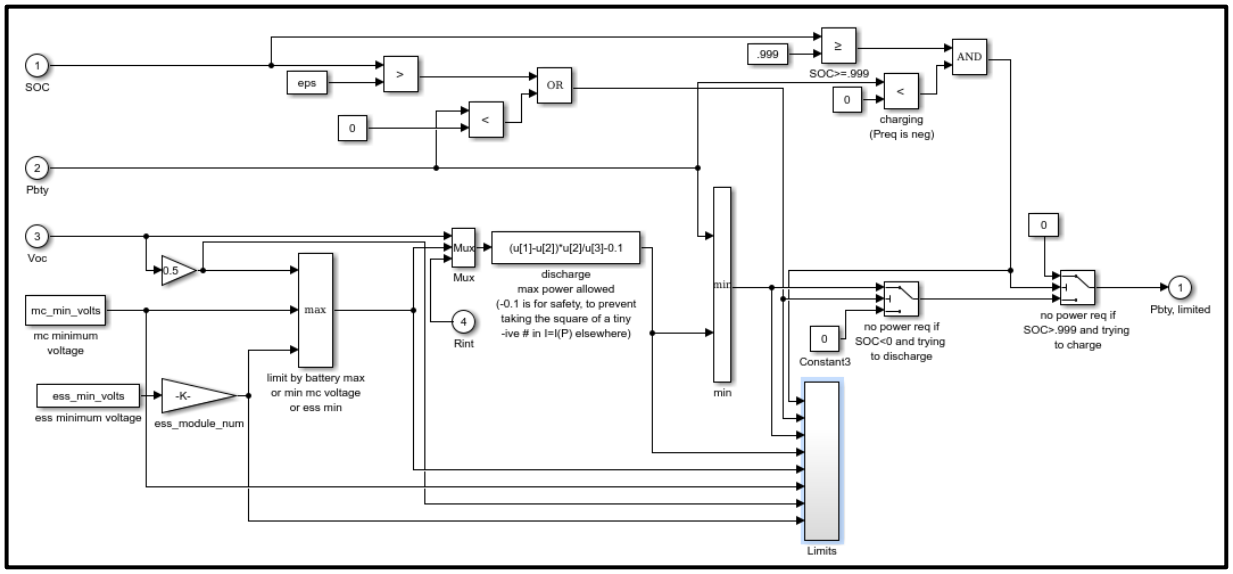
1
SOC
2
Pbty
3
Voc
mc_min_volts
mc minimum voltage
ess_min_volts
ess minimum voltage
-K-
ess_module_num
0.5
max
limit by battery max or min mc voltage or ess min
eps
>
0
<
OR
.999
≥
SOC>=.999
AND
charging (Preq is neg)
Mux
Mux
(u[1]-u[2])*u[2]/u[3]-0.1
discharge max power allowed (-0.1 is for safety, to prevent taking the square of a tiny -ive # in I=I(P) elsewhere)
4
Rint
min
min
Constant3
no power req if SOC<0 and trying to discharge
no power req if SOC>.999 and trying to charge
Pbty, limited
Limits

Limit

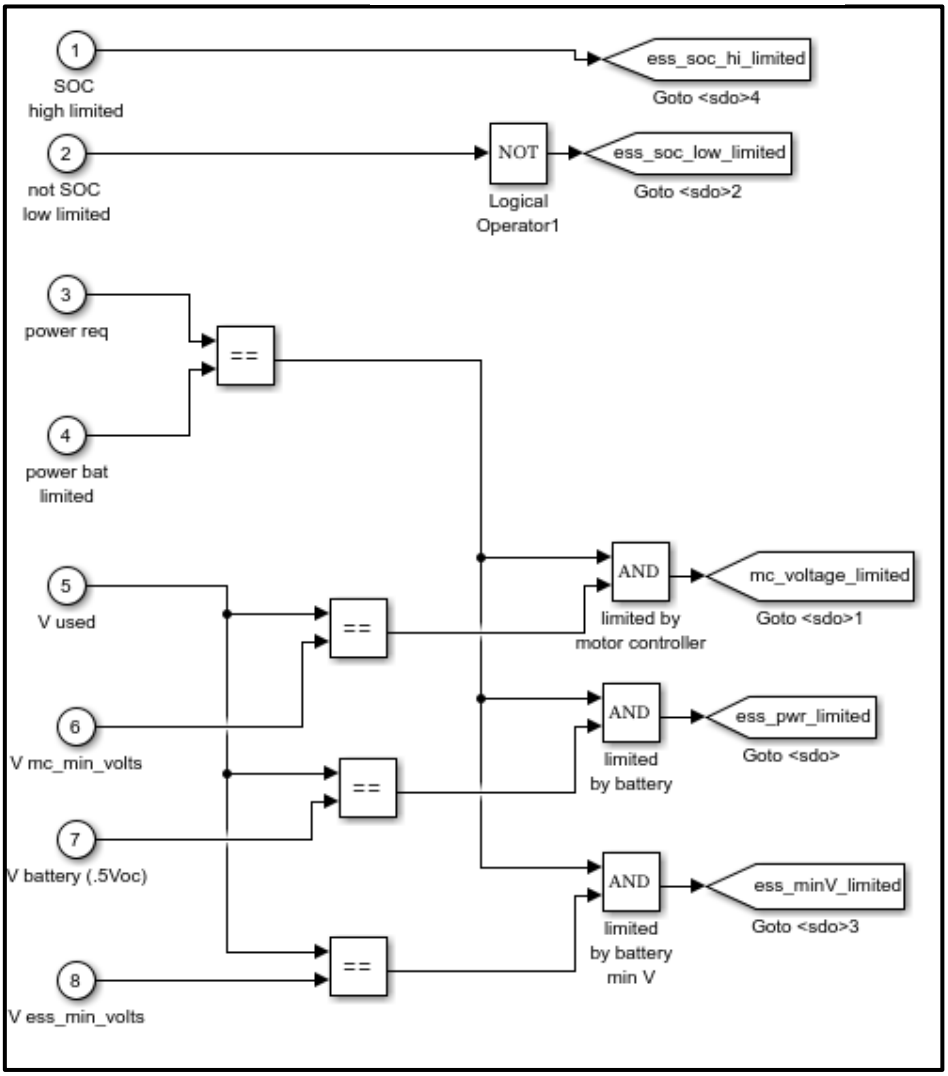
1
SOC high limited
ess_soc_hi_limited
Goto <sdo>4
2
not SOC low limited
NOT
Logical Operator1
ess_soc_low_limited
Goto <sdo>2
3
power req
==
4
power bat limited
5
V used
==
AND
limited by motor controller
mc_voltage_limited
Goto <sdo>1
6
V mc_min_volts
==
AND
limited by battery
ess_pwr_limited
Goto <sdo>
7
V battery (.5Voc)
==
AND
limited by battery min V
ess_minV_limited
Goto <sdo>3
8
V ess_min_volts
==

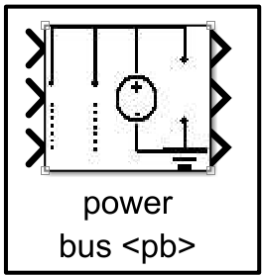
power
bus <pb>

Power bus <pb>

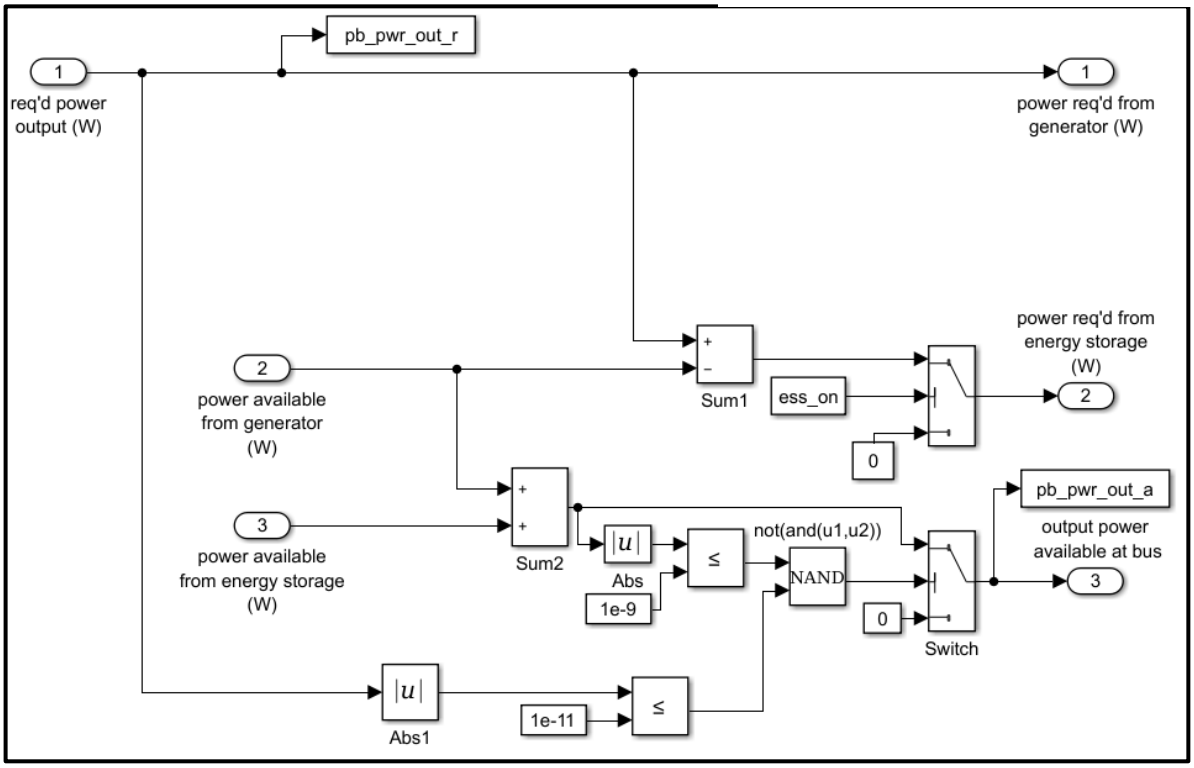
pb_pwr_out_r
1
req'd power output (W)
1
power req'd from generator (W)
2
power available from generator (W)
Sum1
ess_on
0
power req'd from energy storage (W)
2
3
power available from energy storage (W)
Sum2
|u|
Abs
1e-9
≤
not(and(u1,u2))
NAND
0
Switch
pb_pwr_out_a
output power available at bus
3
|u|
Abs1
1e-11
≤

ANNEX N – ADVISOR BATTERY THERMAL MODEL

There is available only one option of cooling option which considering a parallel-flow air cooling, in addition, is assuming that the airflow is the same for each module assuming no turbulences on airflow, also the temperature is assuming the same to all battery. Figure 1 illustrates the thermal model, as can been seen this is a single-node lumped-parameter where internal battery temperature and exiting air temperature are predicted as a function of time, during soak periods and while the vehicle is driven.

Figure – Schematic of ESS thermal model

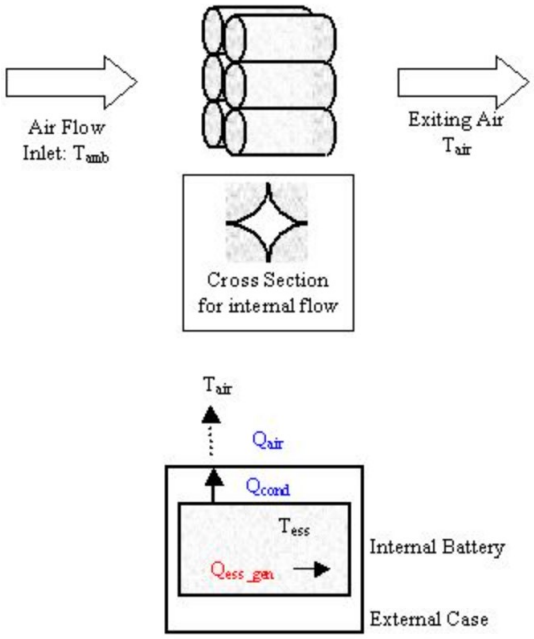

Fonte: adapted from the advisor Simulink model

The flux heat combination of conduction and convection from the internal battery to the air is called here Q_{ess_case} and it is calculated by the internal battery temperature T_{ess} minus the air temperature divided by the effective thermal resistance equation 1.

$$Q_{ess\_case} = \frac{(T_{ess} - T_{air})}{R_{eff}} \quad (1)$$

Equation 2 calculate the effective thermal resistance consider the convection portion first part of the equation, and the conduction second part of the equation. The A is the surface area, the h is the convective heat transfer coefficient, the k is the conductive heat transfer

$$where\ h = \begin{cases} h_{forced} = 30\left(\frac{\dot{m}/\rho A}{5}\right)^{0,8} & T_{ess} > ess\_set\_tmp \\ h_{natl} = 4\,T_{ess} \leq ess\_set\_tmp \end{cases} \quad (3)$$

coefficient and t is the temperature of the surface.

$$R_{eff} = \frac{1}{hA} + \frac{t}{kA} \quad (2)$$

The convective heat transfer coefficient can be subdivided into two, the h_{forced} that is forced by the air flux which is applied when the temperature has exceeded a setpoint , ess_set_tmp.

The effective air temperature T_{air} is slightly warmer than ambient temperature T_{amb} and it is the temperature which the battery convicts, besides the temperatures the m means the airflow over the battery and $C_{p,air}$ is the specific heat at constant pressure for the air in equ 4.

$$T_{air} = T_{amb} + \frac{Q_{ess\_case}}{2\,\dot{m}C_{p,air}} \quad (4)$$

Finally, the temperature of the battery is calculate by the following integral on decency of the heat generated by the battery and the flux of heat.

$$T_{ess} = \int_0^t \frac{Q_{ess\_gen} - Q_{ess\_case}}{m_{ess}C_{p,air}} \quad (5)$$

ANNEX O – FUEL CONVERTER MODEL

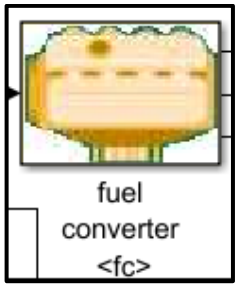

Fuel converter <fc>

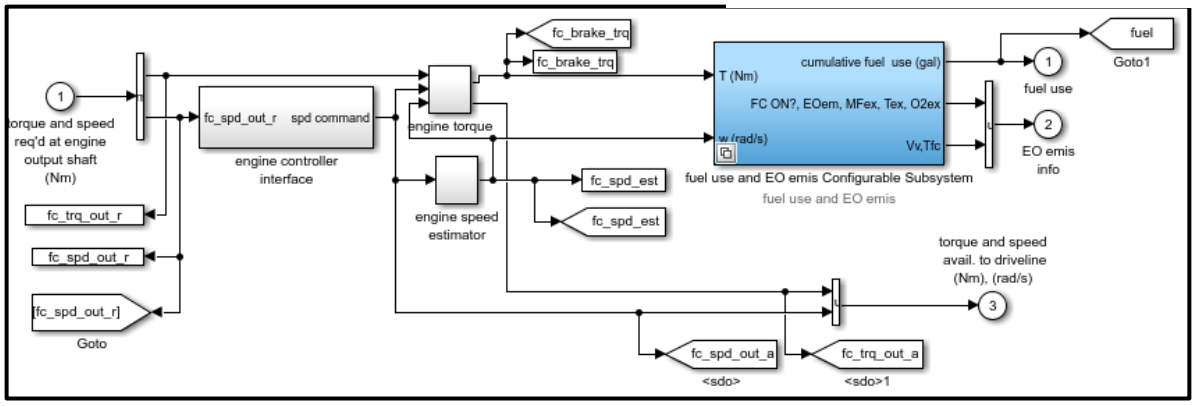

Fuel use and EO emis Configurable Subsytem

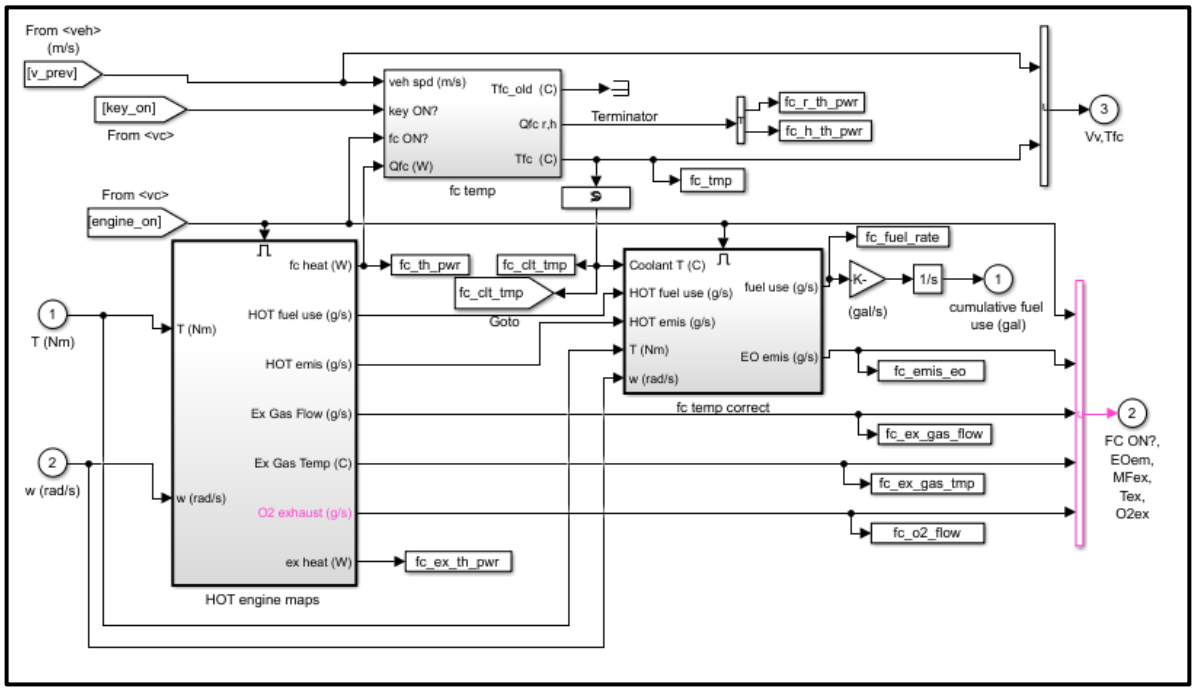

Hot engine maps

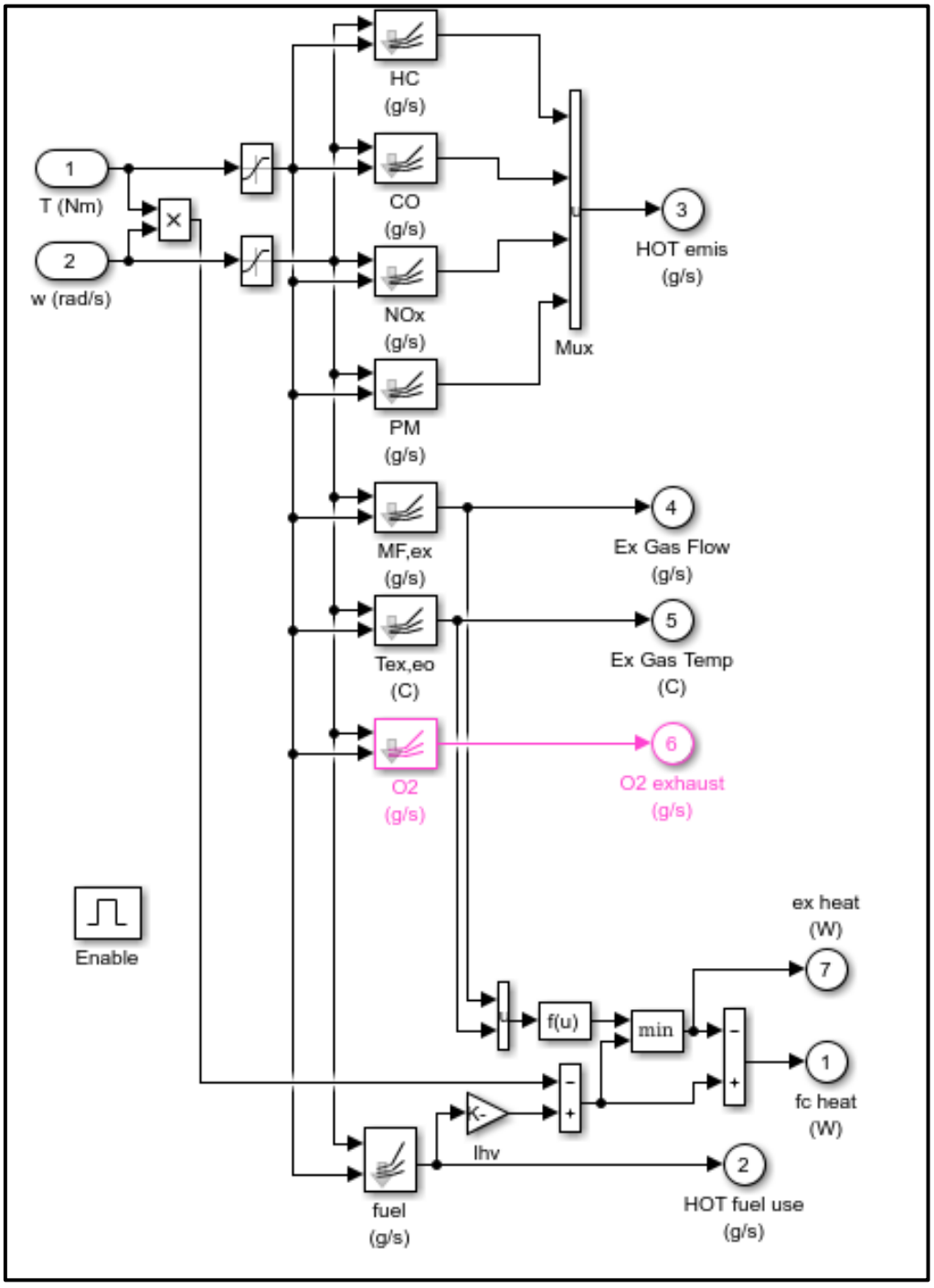

Engine controller

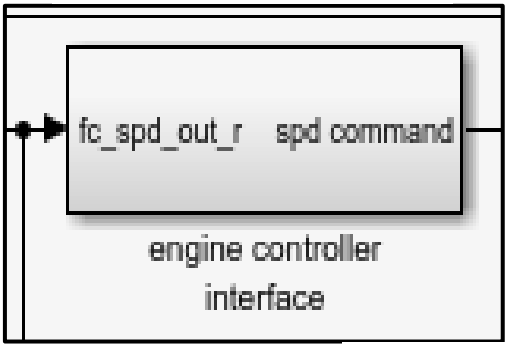

Engine controller

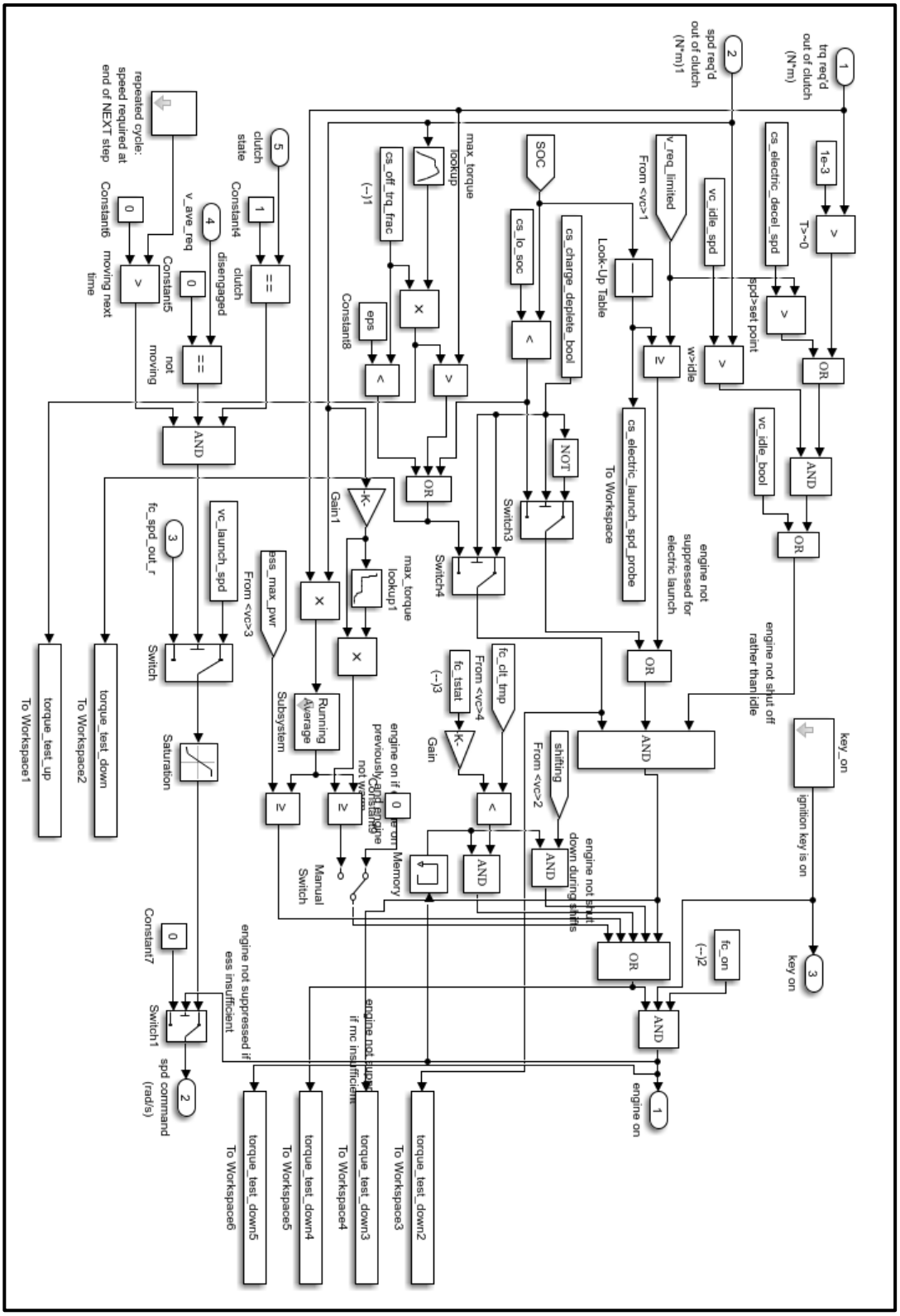
trq req'd out of clutch (N*m)
spd req'd out of clutch (N*m)1
1e-3
T>0
cs_electric_decel_spd
spd>set point
vc_idle_spd
w>idle
v_req_limited
From <vc>1
Look-Up Table
SOC
cs_lo_soc
cs_charge_deplete_bool
To Workspace
cs_electric_launch_spd_probe
vc_idle_bool
OR
AND
engine not shut off rather than idle
engine not suppressed for electric launch
key_on
ignition key is on
key on
fc_on
(-)2
engine on
torque_test_down2
To Workspace3
torque_test_down3
To Workspace4
torque_test_down4
To Workspace5
torque_test_down5
To Workspace6
engine not suppressed if ess insufficient
spd command (rad/s)
Switch1
Constant7
engine not suppressed if mc insufficient
Memory
Manual Switch
engine on if previously on and engine not w...
shifting
From <vc>2
engine not shut down during shifts
fc_clt_tmp
From <vc>4
fc_tstat
(-)3
Gain
Switch3
Switch4
max_torque lookup1
Gain1
ess_max_pwr
From <vc>3
Subsystem
Running Average
vc_launch_spd
fc_spd_out_r
Switch
Saturation
torque_test_up
To Workspace1
torque_test_down
To Workspace2
clutch state
Constant4
clutch disengaged
v_ave_req
Constant5
not moving
Constant6
moving next time
repeated cycle: speed required at end of NEXT step
max_torque lookup
cs_off_trq_frac
(-)1
Constant8
eps
NOT

ANNEX P – NOVO UNO SPORTING 1.4 FLEX TECHNICAL REPORT

ENGINE	1368cc 8V EVO flex				
characteristics	Number of cylinders		04 in line		
	Position		cross		
	Total / unit displacement		1368,3 cc	/ 342,1 cc	
	Diameter x Stroke		72 x 84 mm		
	Cycle - Times		OTTO - 04		
	Compression ratio		12,35 + 0,15-0,2 :1 :1		
	Aspiration		natural		
	Block (material)		Cast iron		
	Head (material)		aluminum		
performance	Gasoline (E22)				
	Maximum power	ABNT	85,0 CV	62,6 KW	@ 5750 rpm
	Maximum Torque	ABNT	12,4 kgfm	121,6 Nm	@ 3500 rpm
	Idling regime		780 ± 50 rpm		
	Ethanol (E100)				
	Maximum power	ABNT	88,0 CV	64,8 KW	@ 5750 rpm
		ABNT	12,5 kgfm	122,6 Nm	@ 3500 rpm
	Maximum Torque		780 ± 50 rpm		
distribution	Number of valves per cylinder		02 in the head		
	Valve reference diameter		32,7 mm	(inlet valve)	
			26,5 mm	(outlet valve)	
	camshaft		01 no in the head		
	Distribution trigger		Toothed belt		
		desliga:	94 ± 2° (1ª vel.) ; 100 ± 2° (2ª vel.)		

Gear	Number of gears		05 the front and 01 a ré		
	Gear ratios	1ª	4,273	(47 / 11)	
		2ª	2,316	(44 / 19)	
		3ª	1,520	(38 / 25)	
		4ª	1,029	(35 / 34)	
		5ª	0,872	(34 / 39)	
		RÉ	3,909	(43 / 11)	
	differential		4,067	(63 / 15	)

Tires	Type		185/60 R15 88H 185/60 R15 84H	
	Filling pressure		*Kg/cm²*	*lb/pol²*
	On medium load	front wheels::	1,9	28
		Rear wheels:	1,9	28
	Fully loaded	front wheels: :	2,2	32
		Rear wheels:	2,2	32
MEDIDAS	**external**			
	Length (L103)		3810,4 mm	
	Body width (W103)		1673,0 mm	

Width between mirrors (W104+ W105)		1907,5 mm
Height	Empty vehicle (H100)	1487,0 mm
	Loaded vehicle	1441,0 mm
Wheelbase (L101)		2376,0 mm
Front balance (L104)		795,1 mm
Rear swing (L105)		639,3 mm
Input angle		20,4 °
Output angle		19,3°
Front gauge (W101)		1430,0 mm
Rear gauge (W102)		1420,0 mm
Minimum height from the ground	empty vehicle	170,0 mm
	loaded vehicle	137,0 mm
Height in previous seats (H61-1)		996,0 mm
Rear seat height (H61-2)		955,0 mm
Width at shoulder height anterior (W3-1)		1350,0 mm
Back shoulder width (W3-2)		1320,0 mm

share. of luggage

Rear seat capacity in normal position	Standard ISO 3632	280 l / 290 l	
Capacity with bank back folded / to the glass	Standard ISO 3632	690,0 l	(Total)
	Standard ISO 3632	422,0 l	(hit 1/3)
	Standard ISO 3632	550,0 l	(hit 2/3)

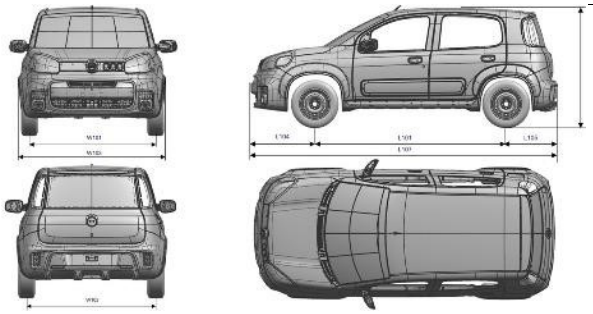

WEIGHTS		**previous**	**later**	**total**
NOVO UNO SPORTING 1.4 FLEX				
	std A	595,0 Kg	422,0 Kg	1017,0 Kg
	std C	689,0 Kg	728,0 Kg	1417,0 Kg
	std D	637,0 Kg	780,0 Kg	1417,0 Kg
	std A	601,0 Kg	422,0 Kg	1023,0 Kg
	std C	695,0 Kg	728,0 Kg	1423,0 Kg
	std D	643,0 Kg	780,0 Kg	1423,0 Kg

Charge capacity	400,0 Kg		
Maximum allowable load per axle	front	730,0 Kg	
	rear	780,0 Kg	
Maximum towable load			
	trailer without brake	400,0 Kg	

weight / power ratio

Gasoline E22			
NOVO UNO SPORTING 1.4 FLEX	11,96 kg/CV	16,2 kg/KW	ABNT
NOVO UNO SPORTING 1.4 FLEX DUALOGIC	12,04 kg/CV	16,3 kg/KW	ABNT
Etanol			
NOVO UNO SPORTING 1.4 FLEX	11,56 kg/CV	15,7 kg/KW	ABNT
NOVO UNO SPORTING 1.4 FLEX DUALOGIC	11,63 kg/CV	15,8 kg/KW	ABNT

ANNEX Q – 1.8 E-TorQ EVO FLEX MT5 SPORT FWD TECHNICAL REPORT

ENGINE	1.8 E-TorQ EVO FLEX MT5				
characteristics	Number of cylinders		04 in line		
	Position		cross		
	Total / unit displacement		1.747,0 cm³	436,75 cc	
	Diameter x Stroke		80,5 x 85,8 mm		
	Cycle - Times		OTTO - 4		
	Compression ratio		12,35 + 0,15-0,2 :1 :1		
	Aspiration		natural		
	Block (material)		Cast iron		
	Head (material)		aluminum		
performance	Gasoline (E22)				
	Maximum power				
		ABNT	130,0 CV	95,6 KW	@ 5250 rpm
	Maximum Torque	ABNT	18,6 kgfm	182,3 Nm	@ 3750 rpm
	Idling regime		850 ± 50 rpm		
	Ethanol (E100)				
	Maximum power	ABNT	132,0 CV	97,1 KW	@ 5250 rpm
		ABNT	19,1kgfm	187,2 Nm	@ 3750 rpm
	Maximum Torque		850 ± 50 rpm		
distribution	Number of valves per cylinder		04 in the head		
	Valve reference diameter		29,86 mm	(inlet valve)	
			23,76 mm	(outlet valve)	
	camshaft		01 no in the head		
	Distribution trigger		Toothed belt		

Gear	Number of gears		05 the front and 01 a ré		
	Gear ratios	1ª	4,273	(47 / 11)	
		2ª	2,316	(44 / 19)	
		3ª	1,520	(38 / 25)	
		4ª	1,156	(37 / 32)	
		5ª	0,872	(34 / 39)	
		RÉ	3,909	(43 / 11)	
	differential		4,200	(63 / 15)	

Tires	Type		215 / 65 R16	
	Filling pressure		*Kg/cm²*	*lb/pol²*
	On medium load	front wheels:	2,2	32
		Rear wheels:	2,2	32
	Fully loaded	front wheels:	2,2	32
		Rear wheels:	2,4	35
MEDIDAS	**external**			
	Length (L103)		4232,0 mm	

Body width (W103)		1798,0 mm
Width between mirrors (W104+ W105)		2018,0 mm
Height	Empty vehicle (H100)	1666,0 mm
	Loaded vehicle	1610,0 mm
Wheelbase (L101)		2570,0 mm
Front balance (L104)		883,0 mm
Rear swing (L105)		789,0 mm
Front gauge (W101)		550,0 mm
Rear gauge (W102)		1552,0 mm
Minimum height from the ground	empty vehicle	177,0 mm
	loaded vehicle	164,0 mm
Height in previous seats (H61-1)		1042,0 mm
Rear seat height (H61-2)		1036,0 mm
Width at shoulder height anterior (W3-1)		1420,0 mm
Back shoulder width (W3-2)		1431,0 mm

share. of luggage

Rear seat capacity in normal position	Standard ISO 3632	273 l / 260 l

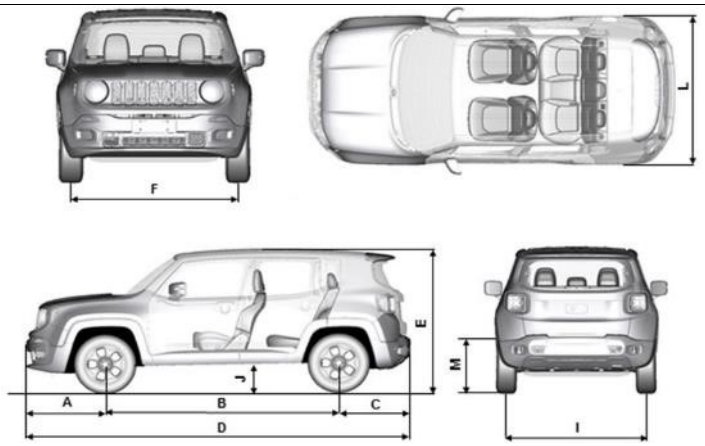

WEIGHTS		**previous**	**later**	**total**
NOVO UNO SPORTING 1.4 FLE				
	std A	832,0 Kg	561,0 Kg	1393,0 Kg
	std C	865,0 Kg	598,0 Kg	1463,0 Kg
	std D	931,0 Kg	862,0 Kg	1793,0 Kg
Charge capacity	400,0 Kg			
Maximum towable load				
	trailer without brake	400,0 Kg		